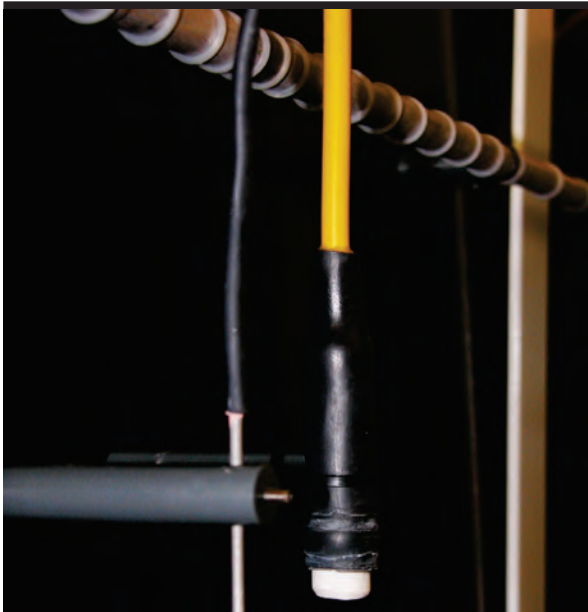


Non-destructive electrochemical monitoring of reinforcement corrosion



PhD Thesis

Department of Civil Engineering

2008

Peter Vagn Nygaard
DTU Civil Engineering-Report R-202 (UK)
ISBN: 97-8877-877-2695
ISSN: 1601-2917
July 2009

Non-destructive electrochemical monitoring of reinforcement corrosion

Peter Vagn Nygaard

Ph.D. Thesis

Department of Civil Engineering
Technical University of Denmark

2008

Non-destructive electrochemical
monitoring of reinforcement corrosion
Copyright (c), Peter Vagn Nygaard, 2008
Printed by Schultz Grafisk, Albertslund
Department of Civil Engineering
Technical University of Denmark
ISBN number: 97-8877-877-2695
ISSN number: 1601-2917

Preface

This thesis is submitted as a partial fulfilment of the requirements for the Danish Industrial PhD degree. In addition to the thesis four papers were prepared during the project period. The papers are not included in the thesis, but a list of these is given after the Table of Contents.

Lyngby the 28th of July 2008

Peter Vagn Nygaard

Acknowledgements

This PhD project was sponsored by FORCE Technology and the Danish Ministry of Science, Technology and Innovation. I gratefully acknowledge their financial contributions.

I am most grateful for the support of my supervising team - Associate Professor Mette Rica Geiker, Department of Civil Engineering, Technical University of Denmark, Head of Department Oskar Klinghoffer, FORCE Technology and Professor Per Møller, Department of Mechanical Engineering, Technical University of Denmark.

Furthermore, I would especially like to thank Professor Bernhard Elsener for my stay at ETH Zürich, Switzerland, which has been very fruitful for my work.

Finally, a great thanks to my colleges at FORCE Technology as well as my fellow PhD students at the 'PhD-office' who all contributed to some excellent years as a PhD student.

Abstract

Condition assessment of reinforced concrete structures may be facilitated by non-destructive techniques. Since the publication of the first version of the ASTM C876 standard in 1977 the use of half-cell potential mapping has been widely accepted as a non-destructive "state of the art" technique for detection of corrosion in concrete structures. And, over the last decade, the trend in corrosion monitoring has moved towards quantitative non-destructive monitoring of the corrosion rate of the steel reinforcement.

A few corrosion rate measurement instruments have been developed and are commercially available. The main features of these instruments are the combined use of an electrochemical technique for determining the corrosion rate and a so-called "confinement technique", which in principle controls the polarised surface area of the reinforcement, i.e. the measurement area.

Both on-site investigations and laboratory studies have shown that varying corrosion rates are obtained when the various commercially available instruments are used. And in the published studies, conflicting explanations are given illustrating the need for further clarification. Only by examining the effect of the confinement techniques and the electrochemical techniques separately the variations in measured corrosion rates can be explained. Such work was conducted in the present project.

A method for quantitative assessment of current confinement techniques is presented in the thesis. The method comprises monitoring of the operation of the corrosion rate instrument and the distribution of current between the electrode assembly on the concrete surface and a segmented reinforcement bar embedded in concrete. The applicability of the method was demonstrated for two commercially available corrosion rate instruments, the GECOR 6 and GalvaPulse instruments, which are based on different confinement techniques as well as different electrochemical techniques. The variations in measured corrosion rates were explained, and the instruments' performance evaluated.

On passive reinforcement neither of the instruments were able to effectively confine (or compensate for) the lateral spread-out of the counter-electrode current. As a result both instruments overestimated the corrosion rate of the passive steel. For reinforcement with one or several actively corroding areas on an otherwise passive reinforcement bar, it was found that neither of the instruments could locate the corroding areas. This was due to the lateral current flow from the electrode assembly on the concrete surface to the actively corroding areas on the reinforcement bar independent of the position of the elec-

trode assembly. In the presence of a single small corroding area with a high corrosion rate both instruments underestimated the actual corrosion rate. The underestimation was due to a combination of the constant confinement length, here much larger than the active area, and the obtained confinement. For unconfined measurements it was found that a distinction between passive and actively corroding steel with a low corrosion rate or small corroding areas is almost impossible. As was the case with the confined corrosion rate measurements, it was found that actively corroding areas could not be located. The conclusions regarding current confinement are based on investigations on concrete slabs with cover thickness of 30 and 75 mm representing most chloride exposed structures. However, the concrete had a relatively high w/c-ratio (0.5) and therefore a relatively low electrical resistivity, facilitating the distribution of current and thus proving a conservative assessment of the efficiency of the confinement techniques. For modern concretes with lower w/c-ratios and supplementary cementitious materials, which have higher resistivity, improved efficiency of the current confinement techniques may be expected.

In addition to the effect of the confinement techniques, the effect of the polarisation time and current on the measured polarisation resistance and thus the corrosion current density were investigated. The two electrochemical techniques used in the GECOR 6 and the GalvaPulse instruments were considered in the study: the galvanostatic linear polarisation resistance technique and the galvanostatic potential transient technique, respectively. Measurements were performed on 45 concrete specimens each with 10 steel bars prepared from concrete with and without admixed chloride to obtain passive and actively corroding steel bars. Varying corrosion rates were obtained by exposing the 45 specimens to 15 different climates, being a combination of five temperatures (1 to 35 °C) and three relative humidities (75 to 96 %RH). On passive reinforcement the measured polarisation resistance - and hence corrosion rate - was for both galvanostatic techniques found to be highly affected by the polarisation time and current. No plateau at either short or long polarisation times (10 to 165 seconds) or low or high currents (0.25 to 100 μ A) was identified. Nevertheless, it was found that a qualitative estimate clearly showing the passive state of steel reinforcement can be obtained with either technique even though stationary conditions are not achieved and the obtained potential response is outside the linear current-potential range around the free corrosion potential. On actively corroding reinforcement a large effect of the polarisation time but only a minor effect of the polarisation current on the measured polarisation resistance were found for both galvanostatic techniques. Also, it was found that the effect of the polarisation time is practically independent of the corrosion rate. For both galvanostatic techniques guidelines were given for polarisation times and currents for non-destructive corrosion rate measurements on reinforcement steel in concrete.

Finally, a study on the effect of temperature and relative humidity on the corrosion rate of steel in concrete was conducted. Contrary to published short-term corrosion studies the Arrhenius equation was found inadequate for describing the temperature dependency of the corrosion rate in this study where measurements were made after approximately two years of constant exposure.

Resumé

Tilstandsvurdering af armerede betonkonstruktioner kan lettes ved brug af ikke-destruktive teknikker. Brugen af elektrokemisk potentiale målinger har siden publicering af ASTM C876-77 standarden i vid udstrækning været accepteret som en 'state of the art' teknik til detektering af korrosion i betonkonstruktioner. Gennem det sidste årti har tendensen inden for korrosionsovervågning gået i retning af en øget anvendelse af kvantitative ikke-destruktive teknikker, der giver information om korrosionshastigheden af armeringen.

Nogle få instrumenter til måling af korrosionshastighed er kommercielt tilgængelige. De primære egenskaber ved disse instrumenter er den kombinerede brug af en elektrokemisk teknik til måling af korrosionshastigheden og en så kaldt 'confinement' teknik, der i princippet bestemmer det polariserede overfladeareal på armeringen, det vil sige måleområdet.

Både felt- og laboratorieundersøgelser har vist, at varierende korrosionshastigheder opnås med forskellige kommercielle instrumenter. I de publicerede studier findes modstridende forklaringer på de varierende korrosionshastigheder, hvilket illustrerer behovet for yderligere undersøgelser. I det foreliggende projekt er effekten af 'confinement' teknikkerne og de elektrokemiske teknikker undersøgt individuelt for at forklare de varierende korrosionshastigheder.

En metode til kvantitativ vurdering af 'confinement' teknikker er præsenteret i afhandlingen. Metoden er baseret på monitorering af instrumenternes funktionalitet og fordelingen af strøm mellem instrumenternes elektroder, som er placeret på betonoverfladen, og en segmenteret armeringsstang indstøbt i beton. Anvendeligheden af metoden er demonstreret ved undersøgelse af to kommercielt tilgængelige instrumenter: GECOR 6 og GalvaPulse. Variationerne af de målte korrosionshastigheder er forklaret og instrumenternes funktion vurderet.

Ved måling på passiv armering var ingen af instrumenterne i stand til effektivt at afgrænse (eller kompensere for) den vandrette spredning af strømmen fra modelelektroden med det resultat, at begge instrumenter overvurderede korrosionshastigheden af den passive armering. Ved måling på armering med et eller flere aktivt korroderende områder på en ellers passiv armeringsstang blev det observeret, at ingen af instrumenterne kunne lokalisere de aktivt korroderende områder. Dette var et resultat af, at strømmen fra instrumenternes elektroder løb gennem betonen til de aktivt korroderende områder uafhængigt af elektrodernes placering på betonoverfladen. Ved tilstedeværelsen af et enkelt lille aktivt korroderende område med høj korrosionshastighed underestimerede begge instrumenter

den faktiske korrosionshastighed. Underestimeringen skyldtes en kombination af den konstante 'confinement' længde, som var større end længden af det aktivt korroderende område, og den opnåede 'confinement'. For korrosionshastighedsmålinger uden brug af 'confinement' teknik var det ikke muligt at skelne mellem passiv og aktivt korroderende armering, hvis korrosionshastigheden var lav eller det korroderende område lille. I lighed med korrosionshastighedsmålingerne, hvor 'confinement' teknik blev anvendt, kunne de aktivt korroderende områder heller ikke lokaliseres uden 'confinement' teknik.

Konklusionerne fra undersøgelserne af 'confinement' teknikkerne er baseret på undersøgelser på betonemner med 30 og 75 mm dæklag svarende til de fleste klorid eksponerede betonkonstruktioner. Den anvendte beton havde et relativt højt vand/cement-forhold (0,5) resulterende i en relativ lav elektrisk resistivitet. Moderne betoner med lavere vand/cement-forhold og supplerende bindemidler har en højere elektrisk resistivitet, og det kan derfor forventes, at 'current confinement' teknikkerne vil have en større virkningsgrad end den i dette projekt observerede.

Foruden effekten af 'confinement' teknik blev effekten af polarisationstid og -strøm på den målte polarisationsmodstand og herved korrosionshastighed også undersøgt. De to elektrokemiske teknikker anvendt i GECOR 6 og GalvaPulse instrumenterne blev undersøgt i studiet: Den galvanostatiske lineære polarisationsteknik og den galvanostatiske potentiale-transient teknik. Der blev udført målinger på 45 beton prøveemner, hver med 10 stålstænger fremstillet af beton med og uden iblandet klorid for herved at opnå både passive og aktivt korroderende stålstænger. Forskellige korrosionshastigheder blev opnået ved at eksponere de 45 emner i 15 forskellige klimaer, værende en kombination af fem temperaturer (1 til 35 °C) og tre relative luftfugtigheder (75 til 96 %RF). For passiv armering var den målte polarisationsmodstand - og herved korrosionshastighed - for begge galvanostatiske teknikker i høj grad påvirket af polarisationstiden og -strømmen, og der blev ikke observeret konvergens, hverken ved korte eller lange polarisationstider (10 til 165 sekunder) eller lave eller høje strømme (0,25 til 100 μA). For begge teknikker blev det imidlertid fundet, at en tydelig indikation af den passive tilstand af armeringen, kan opnås på trods af, at et ligevægtspotentialerespons ikke er opnået, og at potentialeresponsen er udenfor det lineære strøm-potential område omkring det frie korrosionspotentiale. For aktivt korroderende armering blev det for begge galvanostatiske teknikker fundet, at polarisationstiden har en stor effekt på den målte polarisationsmodstand, mens kun en mindre effekt af polarisationsstrømmen blev observeret. For begge galvanostatiske teknikker blev polarisationstider og -strømme foreslået til brug for målinger på armeringsstål i beton.

Foruden de ovenfor nævnte undersøgelser blev effekten af temperatur og relativ fugtighed på korrosionshastigheden af stål i beton undersøgt. I modsætning til korttidskorrosionsstudier kunne Arrheniusligningen ikke beskrive korrosionshastighedens temperaturafhængighed for de aktuelle målinger, som blev gennemført cirka to år efter eksponeringsstart.

Table of Contents

1	Introduction	1
1.1	Background	1
1.2	Objectives	3
1.3	Research approach	4
1.3.1	Effect of confinement techniques	4
1.3.2	Effect of measurement technique and procedure	4
1.3.3	Effect of exposure on the corrosion rate	5
1.4	Organisation of the Thesis	5
2	The electrochemistry of steel in concrete	7
2.1	General	7
2.2	Thermodynamical aspects	7
2.2.1	Basic corrosion mechanism	7
2.2.2	Passive state	9
2.2.3	Active corrosion	10
	Corrosion in oxygen rich environment	10
	Corrosion in oxygen deprived environment	11
2.2.4	Intense localised corrosion	12
2.2.5	Steel potentials in concrete	13
2.3	Corrosion rate of steel in concrete	15
2.3.1	Expression of corrosion rate	15
2.3.2	Polarisation and corrosion kinetics	16
2.3.3	Corrosion rate and polarisation resistance	18
2.3.4	Corrosion rate affecting factors	21
	Temperature	21
	Electrical resistivity	24
	Moisture content	26
3	Measurement of steel corrosion in concrete	29
3.1	Half-cell potential measurement	29
3.2	Measurement of polarisation resistance	32
3.2.1	Linear polarisation resistance techniques	33
	Influence of delay time and sweep rate	34
	Ohmic drop compensation	39
3.2.2	Galvanostatic transient technique	44

Linearisation	44
CPE modified randles circuits	50
3.3 Current confinement	53
4 Experimental work	67
4.1 Effect of confinement techniques	67
4.1.1 Commercial instruments - principle of operation	69
GECOR 6	69
GalvaPulse	70
4.1.2 Manufacture of test specimens	73
Concretes	75
Segmented reinforcement bars	75
4.1.3 Test methods	78
Macro-cell current measurements	78
Half-cell potential and polarisation resistance measurements	78
Measurements with commercial corrosion rate instruments	80
4.2 Effect of measurement technique, procedure and exposure	82
4.2.1 Manufacture and conditioning of test specimens	82
4.2.2 Test methods	86
Instrumentation and measuring sequence	87
Potentiodynamic linear polarisation resistance measurements	89
Galvanostatic potential transient measurements	93
5 Experimental Results	97
5.1 Effect of confinement techniques	97
5.1.1 Macro-cell current measurements	97
5.1.2 Half-cell potential and polarisation resistance measurements	101
5.1.3 Measurements with commercial corrosion rate instruments	106
Passive reinforcement	106
Intense localised corrosion	115
Active general corrosion	137
5.2 Effect of measurement technique, procedure and exposure	151
5.2.1 Potentiodynamic linear polarisation resistance measurements	151
5.2.2 Galvanostatic potential transient measurements	158
Passive reinforcement	158
Active general corrosion	163
6 Discussion	175
6.1 Half-cell potential measurements	175
6.2 Corrosion rate measurements - effect of confinement	177
6.2.1 Unconfined corrosion rate measurements	177
Passive reinforcement	177
Active reinforcement - general and localised corrosion	180
6.2.2 Confined corrosion rate measurements, commercial instruments	184
Functionality of the tested commercial instruments	184

Assessment of confinement techniques	187
6.3 Corrosion rate measurements - effect of technique and procedure	196
6.3.1 Passive reinforcement	196
6.3.2 Actively corroding reinforcement	203
6.4 Corrosion rate - effect of exposure	207
6.4.1 Relative humidity	207
6.4.2 Temperature	209
7 Conclusion	215
8 Recommendations for further work	219
Bibliography	221
A Concrete composition	235
A.1 Constituent materials	235
A.1.1 Cement	235
A.1.2 Water	235
A.1.3 Fine aggregate	235
A.1.4 Coarse aggregate	235
A.2 Concrete	236
A.2.1 Concrete mix design	236
A.2.2 Mixing	239
B Concrete properties I	241
C Concrete properties II	243
D GECOR 6 and GalvaPulse measurements, numerical values	247
E MatLab code, Potentiodynamic polarisation resistance	253
F MatLab code, Potential transient measurements	257
G Mean values and Standard deviations for Section 5.2.2	263
List of Symbols	267
List of Figures	271
List of Tables	285

Additional work (not included in the thesis)

- [1] Nygaard P.V., Geiker M., Møller P., Sørensen H.E., Klinghoffer O.: Corrosion rate measurement, modelling and testing of the effect of a guard ring on current confinement, Presented at: *EUROCORR 2005, 4-8 September 2005, Lisbon, Portugal.*

- [2] Nygaard P.V., Geiker M.R., Klinghoffer O., Møller P.: Corrosion of steel reinforcement in concrete, Part II - Non-destructive testing, in: *Proceedings of Dansk Metallurgisk Selskab, Korrosion - mekanismer, havarier, beskyttelse, Sorø, Denmark, 2006, Somers (ed),* page 101- 115.

- [3] Nygaard P.V., Geiker M.R., Elsener B.: Corrosion rate of steel in concrete - Evaluation of confinement techniques for on-site corrosion rate measurements, *Materials and Structures*, 42(8):1059-1076.

- [4] Raupach M., Polder R., Frølund T., Nygaard P.V.: Corrosion Monitoring at Submerged Concrete Structures - Macrocell Corrosion due to Contact with Aerated Areas?, Presented at: *EUROCORR 2007, 9-13 September 2007, Freiburg im Breisgau, Germany.*

Chapter 1

Introduction

1.1 Background

Periodical condition assessments are essential to optimise the maintenance of reinforced concrete structures. Such assessments may be facilitated by the use of qualitative as well as quantitative condition indicators. In this connection, reliable non-destructive techniques for assessment of the corrosion state of reinforcement are required.

The use of half-cell potential mapping has been widely accepted as a non-destructive "state of the art" technique for detection of reinforcement corrosion in concrete structures ever since the publication of the ASTM C876 standard in 1977 (ASTM C 876-77, 1977). Since then, progress has been made with respect to corrosion detection as well as corrosion rate monitoring, see e.g. Elsener et al. (2003), Andrade et al. (2004) and literature therein. Over the last decade, the trend in corrosion monitoring has moved towards increased use of quantitative non-destructive techniques that give information on the actual corrosion rate of the reinforcement as a supplement to half-cell potential mapping (Elsener et al., 2003).

The corrosion rate, often expressed as the corrosion current density, i_{corr} , is determined by measuring the polarisation resistance, R_P , of the reinforcement and using the empirical Stern-Geary relationship (Stern and Geary, 1957) given in Equation 1.1:

$$i_{corr} = \frac{B}{R_P \times A} \quad (1.1)$$

where B is a proportionality factor that depends on the anodic and cathodic Tafel slopes and A is the polarised surface area on the reinforcement.

There are several steady and non-steady (transient) state techniques for determining the polarisation resistance of steel in concrete: the linear polarisation resistance (LPR) technique (Gonzalez et al., 1980) (Millard et al., 1992), electrochemical impedance spectroscopy (John et al., 1981) and the galvanostatic pulse technique (Elsener et al., 1997) (Elsener, 2005). Good correlation between the electrochemical weight loss calculated by integration of R_P data from LPR measurements and gravimetric measurements has been found (Andrade and Gonzalez, 1978). Furthermore, good correlation between the results

from different electrochemical techniques has been found in several comparative studies where measurements were performed on small size laboratory specimens where a uniform counter-electrode current distribution was ensured (Elsener, 1995) (Sehgal et al., 1992).

Only few techniques have been adopted in instruments for on-site corrosion rate measurements (Clear, 1989) (Rodriguez et al., 1994) (Elsener et al., 1997) (Bässler et al., 2007). The main features of the corrosion rate instruments are the combined use of an electrochemical technique for determining the polarisation resistance, R_P , and a so-called "confinement technique", which in principle controls the current distribution from the electrode assembly on the concrete surface to the embedded reinforcement and thus determines the polarised surface area, A , of the reinforcement. The non-destructive electrochemical techniques for determining the corrosion rate of steel in concrete as well as the different confinement techniques are described in e.g. Rodriguez et al. (1994), Bässler et al. (2007), Clear (1989) and Luping (2002).

Both on-site investigations and laboratory studies show that varying corrosion rates are measured when different commercially available instruments are used. A number of experimental studies have been conducted to explain these variations; instruments have been compared through measurements on a variety of field and laboratory samples and in some studies also calibrated against gravimetric measurements (Sehgal et al., 1992) (Flis et al., 1993) (Flis et al., 1995) (Elsener, 1995) (Luping, 2002) (Gepreags and Hansson, 2004) (Andrade and Martinez, 2005).

The effect of selected confinement techniques has also been numerically simulated and their efficiency under varying conditions investigated, e.g. corrosion state, concrete resistivity, cover thickness (Song, 2000) (Wojtas, 2004a) (Wojtas, 2004b) (Elsener, 1998). Alongside the experimental and numerical approaches, there has also been a lot of discussion on the problems encountered when performing on-site corrosion rate measurements (Feliu et al., 2005) (Gonzalez et al., 2004) (Gonzalez et al., 1995a) (Elsener et al., 1996b) (Videm, 1998).

Although large efforts have been invested in studies on techniques and instrument for on-site corrosion rate measurements the published studies do not supply unambiguous explanations for the variations in measured corrosion rates: In some studies the different confinement techniques, rather than different electrochemical techniques are considered the main reason for the variations (Flis et al., 1993) (Flis et al., 1995) (Gepreags and Hansson, 2004). In other studies the different polarisation times are considered the main reason (Luping, 2002). Also, in several studies and in a recent RILEM Recommendation it has been stated that: *"not all guarded techniques are efficient. Only that using a Modulated Confinement of the current, is able to efficiently confine the current within a predetermined area"*, and *"the method of modulated confinement of the current is the most suitable for cases of localized attack, because it delimitates the area polarized"* and furthermore *"it is the only method which is able to minimize the effect of macrocells or to notice active/passive region transition"* (Andrade et al., 2004) (Andrade and Martinez, 2005). In contrast, it has also been reported that: *"the modulated confinement is not able*

to confine the lateral spread of the counter-electrode current within a defined and constant area. Using the constant diameter of confined area for different test conditions leads to serious errors” and “the measuring devices using modulated confinement and automatically deliver polarisation resistance values are not suitable for on-site measurements on reinforced concrete structures” (Wojtas, 2004a) (Wojtas, 2004b).

The conflicting explanations for the variations in the measured corrosion rates and contrary statements illustrate the need for further clarification. Only by investigating the effect of the confinement techniques and the electrochemical techniques separately the variations in the measured corrosion rates can be explained. Such work is undertaken in the present project.

1.2 Objectives

The purpose of the present thesis is to provide background information for future development of instruments for on-site corrosion rate measurements and assessment of reinforced concrete structures. The thesis addresses the following objectives:

- **Corrosion rate measurement of steel in concrete**

For both passive and actively corroding reinforcement to determine the applicability of corrosion rate measurements with regard to:

- Effect of confinement techniques

Determination of the effect of the different confinement techniques used in commercially available corrosion rate instruments.

- Effect of measuring technique and procedure

Determination of the effect of polarisation time and current on the measured polarisation resistance and hence corrosion current density for two galvanostatic techniques: the linear polarisation resistance technique and the galvanostatic potential transient technique.

- **Effect of exposure on corrosion rate**

For both passive and actively corroding reinforcement to investigate the influence of environmental exposure for:

- Effect of temperature and relative humidity

Determination of the long-term combined effect of temperature and relative humidity on the corrosion rate of steel in concrete.

The short-term effect of temperature and relative humidity variations is covered in the literature and is therefore not included in the present study.

The thesis focuses on systems relevant for full scale reinforced concrete structures. Traditional corrosion studies of metals in solutions are not covered.

1.3 Research approach

1.3.1 Effect of confinement techniques

Confinement studies were undertaken on segmented reinforcement bars embedded in concrete slabs as described below. Based on a small parametric study, numerical simulations were initially not found suitable for detailed investigations of the effect of confinement (Nygaard et al., 2005). Also, the possible use of solutions for simulating concrete of varying resistivity and cover thickness was not found robust as both unwanted corrosion and varying resistivity were experienced.

To quantitatively assess the different confinement techniques and evaluate the commercially available corrosion rate instruments, GECOR 6 and GalvaPulse a test method was developed. The method was based on real-time monitoring of: a) the operation of the instrument's, and b) the distribution of current between the instruments electrode assembly on the concrete surface and an embedded segmented reinforcement bar.

The operation of the instruments was monitored by recording the current applied from the counter-electrode and guard ring together with the potential of the reinforcement bar measured versus the reference electrode(s) in the electrode assembly. The segmented reinforcement bar allowed the current distribution to be measured in specific positions, i.e. the distribution of current was measured as a number of discrete currents giving a step-wise distribution along the length of the reinforcement bar. By comparing this distribution of current with the currents applied from the electrode assembly the effect of the confinement techniques was quantified.

Three concrete slabs varying in chloride content were prepared to obtain different corrosion states and rates. Each concrete slab contained two segmented reinforcement bars. Different corrosion scenarios were obtained by manufacturing segmented reinforcement bars from carbon steel segments (passive and general corrosion) and a combination of carbon and stainless steel segments (intense localised corrosion).

Information on the actual corrosion rate of the segmented reinforcement bars was obtained from macro-cell current, half-cell potential and conventional potentiodynamic Linear Polarisation Resistance (LPR) measurements. For the LPR measurements a laboratory potentiostat and a large external counter-electrode ensuring uniform current distribution were used.

1.3.2 Effect of measurement technique and procedure

To quantify the effect of polarisation time and current on the measured polarisation resistance and hence corrosion current density at varying corrosion states and rates, 45 concrete specimens each with 10 reinforcement bars were prepared: 30 specimens with and 15 specimens without admixed chloride. Plain carbon steel bars were embedded in the 15 specimens without chloride and in 15 out of the 30 specimens with chloride. In the remaining 15 specimens with chloride partly nickel coated carbon steel bars were em-

bedded. This way test specimens with passive, active general and active intense localised corrosion should be obtained. Variation in the corrosion rates was obtained by exposing all 45 specimens in 15 different climates, being a combination of five temperatures (1, 5, 15, 25, 35 °C) and three relative humidities (75, 85, 96 %RH).

Galvanostatically induced potential transients were measured on the 10 steel bars in each specimen using nine different polarisation currents and a constant polarisation time. The measured potential transients were analysed with both the galvanostatic linear polarisation resistance technique and the galvanostatic potential transient technique. Information on the effect of the polarisation time was obtained by a step-wise analysis of the recorded transients, e.i. parts of the potential transients with increasing length (polarisation time), were analysed. In this way information on both the polarisation time and current on the measured polarisation resistance were obtained. For comparison (and as a reference) the polarisation resistance of the 10 steel bars in each specimen was also determined with the potentiodynamic Linear Polarisation Resistance (LPR) technique.

1.3.3 Effect of exposure on the corrosion rate

Assuming the actual corrosion rate to be obtained with the potentiodynamic linear polarisation resistance technique the effect of the temperature and relative humidity on the corrosion rate was obtained from the investigations described in Section 1.3.2. In this investigation different corrosion rates were obtained by exposing a number of geometrically identical test specimens with passive and actively corroding steel bars in 15 different climates being a combination of five temperatures and three relative humidities.

1.4 Organisation of the Thesis

The introductory Chapter 1 is subsequented by Chapter 2 where a general introduction to the electrochemistry of steel in concrete is given. The different corrosion states of steel in concrete, the related mechanisms and associated half-cell reactions are first described. The kinetics of the corrosion process are then considered and the concepts of polarisation and polarisation resistance introduced and briefly discussed. Finally, the effect of a number of material properties and environmental factors on the corrosion rate of steel in concrete is discussed.

Chapter 3 deals with measurement of steel corrosion in concrete. The chapter starts with a discussion of the qualitative half-cell potential technique. Subsequently, a review of the electrochemical techniques typically used for polarisation resistance measurements on steel reinforcement in concrete structures is given. This is followed by a review of current confinement techniques.

Chapter 4 describes the experimental activities in the present research project with details on materials, manufacture of test specimens, conditioning and testing. The chapter is divided in two main sections: The first section describes an experiment in which the *Effect of confinement techniques* is investigated (Section 1.3.1). The second section de-

scribes an experiment in which both the *Effect of measurement technique and procedure* and the *Effect of exposure on the corrosion rate* are investigated (Sections 1.3.2 and 1.3.3).

Chapter 5 presents the results from the experimental investigations. The chapter is similarly to Chapter 4 divided in to two main sections and follows the structure of this.

Chapter 6 discusses the results obtained in the experimental investigations. The chapter starts with a discussion of half-cell potential measurements for detection of reinforcement corrosion. Following this the effect of current confinement on corrosion rate measurements is discussed and the performance of the GECOR 6 and GalvaPulse instruments evaluated. The effect of the measurement technique and procedure on the obtained corrosion rate is then discussed. Finally, the effect of the temperature and relative humidity on the corrosion rate of steel in concrete is discussed.

Chapter 7 summarises the main conclusions from the discussion in Chapter 6. Recommendations for further work are given in Chapter 8.

A list of symbols and abbreviations is given after the appendices.

Chapter 2

The electrochemistry of steel in concrete

2.1 General

Usually, steel in concrete free of chloride and other aggressive ions is in the passive state formed by the high pH and the availability of oxygen. The term passivity denotes that although the steel is thermodynamically not stable, the corrosion rate is insignificant ($\sim 0.1\mu\text{m}/\text{year}$). This is caused by formation of an iron oxide film on the steel surface (Arup, 1983). Information on the electrochemical stability of iron and its oxides in water, in the absence of aggressive ions such as chlorides, may be found in a potential-pH diagram as shown in Figure 2.1. This type of diagram, most often referred to as a Pourbaix diagram, only indicates whether or not corrosion or passivation is thermodynamically possible. No information as to the kinetics (rate) of the reactions can be obtained from this type of diagram.

Once a carbonation front or a threshold concentration of aggressive ions reaches the embedded steel, dissolution of the passive layer will occur. In case of carbonation general dissolution of the passive layer takes place whereas ingress of aggressive ions leads to local break down (Arup, 1983). Once corrosion is initiated, the rate will be governed by the kinetics of the corrosion process (Broomfield, 1997b).

The following sections will review the thermodynamical aspects of steel in concrete and the kinetics governing the corrosion process when initiated.

2.2 Thermodynamical aspects

2.2.1 Basic corrosion mechanism

Concrete as an electrolyte is a highly heterogeneous material with local variations in the alkalinity and moisture content (Sandberg, 1998). As a result of this and combined with variations in the steel-concrete interface several randomly positioned anodic and cathodic areas will develop on corroding steel in concrete. Iron dissolves in the pore solution in the anodic areas as described by the half-cell reaction in Equation 2.1. The

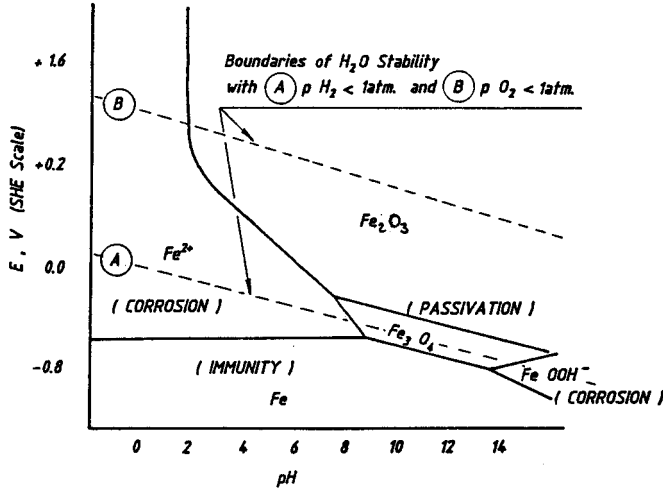
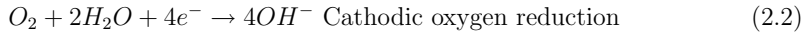
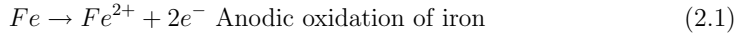
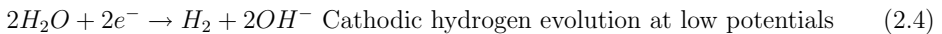


Figure 2.1 Simplified Pourbaix diagram for a Fe-H₂O system at 25 °C and iron molality of 10⁻⁶ Fe mol/kg H₂O (Page, 1988).

electrons released in the anodic reaction flow through the steel to the cathodic areas where reduction of oxygen takes place following Equation 2.2, i.e. it is not possible for large electrical charges to build up in one location on the steel; another chemical reaction must consume the electrons (Broomfield, 1997a). The basic mechanism is illustrated in Figure 2.2. The reduction of oxygen is the only half-cell reaction to consider under normal conditions when oxygen is available at the cathode (Arup, 1983).



Theoretically, hydrogen evolution is not possible unless the potential is below the reversible hydrogen electrode potential represented by line A in the Pourbaix diagram shown in Figure 2.1. In practice a hydrogen overvoltage will offset the potential to more negative values (Küter et al., 2004). Hydrogen evolution will only become the cathode reaction in the absence of oxygen or at low pH values. At low pH values the cathodic half-cell reaction given in Equation 2.3 will occur whereas the half-cell reaction in Equation 2.4 takes place at low potentials in neutral or alkaline solutions (Küter et al., 2004).



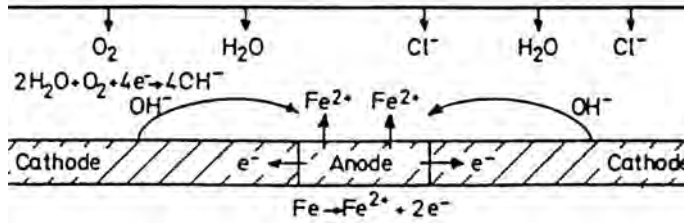


Figure 2.2 Schematic illustration of the basic corrosion mechanism, i.e. anodic dissolution of iron and cathodic reduction of oxygen (Sandberg, 1998).

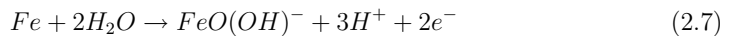
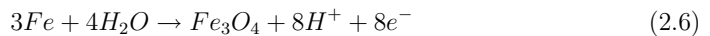
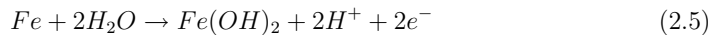
The basic anodic and cathodic reactions are the same in both the passive and active state, but in the active state the reaction rate is higher by orders of magnitude (Sandberg, 1998).

2.2.2 Passive state

The oxide layer (or film) on passive steel in concrete prevents (strongly reduces) the anodic dissolution of iron, but not the cathodic reaction which can occur on the film surface. This is due to the film being electron conducting but not ion conducting. As a consequence the steel is said to be under anodic control (Bardal, 1994).

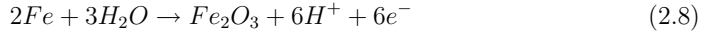
The oxide layer on passivated steel in concrete has been considered a tightly adherent iron oxide layer of hematite ($\gamma\text{-Fe}_2\text{O}_3$) (Pourbaix, 1974). However, later studies have suggested that the protective film does not only consist of hematite ($\gamma\text{-Fe}_2\text{O}_3$) but is rather a mixture of magnetite and hematite ($\text{Fe}_3\text{O}_4 - \gamma\text{-Fe}_2\text{O}_3$) (O'Grady, 1980), (Sagoe-Crentsil and Glasser, 1989), (Sagoe-Crentsil and Glasser, 1990), (Leek and Poole, 1990) and literature cited therein.

In a study by Küter et al. (2004), the mechanisms and associated half-cell reactions proposed in the literature for the oxide film formation were reviewed by comparing electrode potentials with the potential range for steel in concrete during passivation. It was found that the half-cell reactions, proposed by Sagoe-Crentsil and Glasser (1989) (Equations 2.5 to 2.7) for the oxide film formation depending on the existence of an appropriate electrochemical potential are feasible.



Also, the two half-cell reactions proposed by Alekseev (1993) describing the formation of an oxide layer with an incorporated acidification were deemed possible. The first reaction

is equivalent to the reaction proposed by Sagoe-Crentsil and Glasser (1989), given in Equation 2.6. The second proposed reaction is given in Equation 2.8.



However, the exact conditions for formation and growth of the passivating films are not fully understood and their ionic and electronic transport properties as well as their chemical and mineralogical compositions are yet to be determined (Sagoe-Crentsil and Glasser, 1989).

In a study of reinforced concrete exposed 20 years in Nordic marine environment, an oxide layer with a thickness of several hundred microns was found on passive steel (Sandberg, 1998). The layer was seen as having a duplex structure, with an inner layer of magnetite and hematite ($Fe_3O_4 - \gamma\text{-}Fe_2O_3$) and an outer layer of corrosion products interspersed with magnetite (Fe_3O_4) and calcium hydroxide ($Ca(OH)_2$). Similar observations were reported by Sagoe-Crentsil and Glasser (1989) from investigations of reinforced concrete exposed for 20 years at outdoor conditions. This *semi-passive* state is suggested to represent the actual condition of steel reinforcement in most real structures and is considered a result of considerable interaction between the steel-oxides-cement system (Sagoe-Crentsil and Glasser, 1989).

2.2.3 Active corrosion

Corrosion in oxygen rich environment

General corrosion in oxygen enriched environments, e.g. normal outdoor conditions is commonly considered to be associated with a general loss of passivity due to an overall pH decrease resulting from carbonation of the concrete surrounding the steel (Arup, 1983) (Küter et al., 2004). The mechanisms of carbonation have been well known for many years and are described in most text books, among others (Broomfield, 1997a) and (Hunkeler, 2005). The corrosion products formed on the steel surface are evenly distributed, as the anodic and cathodic sites tend to replace each other, due to the pH shift resulting from oxygen reduction at the cathodic sites (Equation 2.2) (Arup, 1983).

General corrosion may also be observed in uncarbonated concrete with excessive chloride amounts (Arup, 1983). Here, corrosion starts by formation of localised corrosion attacks, i.e. formation of corrosion pits that increase in number, expand and join up leading to the general state of corrosion (Broomfield, 1997a).

When sufficient oxygen is available at the anode solid corrosion products, frequently referred to as red rust, are formed from dissolved iron in the pore solution (the ferrous ion Fe^{2+}). In the literature, red rust in general is accepted as hydrated ferric oxide formed through the three reactions given in Equations 2.9 to 2.11 (Sandberg, 1998). From calculations of the Gibbs free energy, Küter et al. (2004) demonstrated that the three proposed reactions are thermodynamically possible.

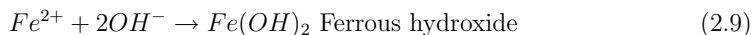
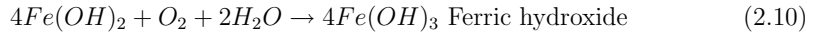




Figure 2.3 Typical example of a severe general corrosion attack in uncarbonated concrete, caused by excessive amounts of chloride.



The formation of red rust is characterised by expansion that may cause cracking and spalling of the concrete cover and brittle, flaky rust products on the exposed reinforcement, see Figure 2.3.

Corrosion in oxygen deprived environment

In concrete where the access of oxygen is so limited, that the passive film cannot be maintained, the steel becomes active in the still highly alkaline concrete. In cases where both anodes and cathodes are starved of oxygen, the corrosion rate is considered as low or even lower than in the passive state (Arup, 1983). If oxygen becomes available the steel repassivates easily.

In case where only the oxygen supply to the anode is restricted but the cathode reaction takes place in a region where the concrete has sufficient supply of oxygen, the dissolved iron (Fe^{2+}) stay in the solution as no oxygen is available for formation of the expansive ferric hydroxides (Equations 2.10 and 2.11) (Broomfield, 1997a). Thus no cracking or spalling of the concrete cover will occur and corrosion may propagate without any visible signs. The products formed in this case are often referred to as green or black rust based on the color of the liquid seen on the reinforcement when first exposed to air after excavation from the concrete (Broomfield, 1997a).

In general formation of green rust is related to the presence of chloride ions (Küter et al.,

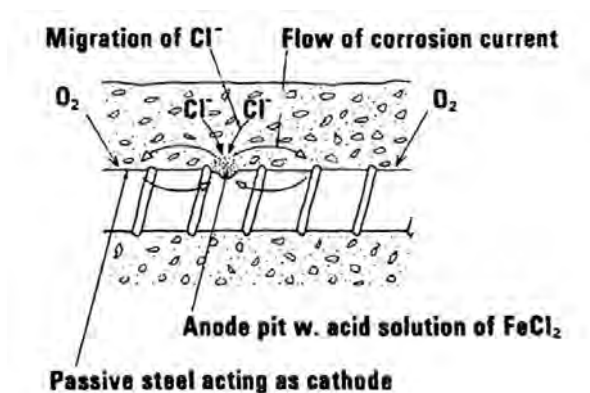


Figure 2.4 *Simplified electrochemical corrosion process around a corrosion pit on steel in concrete (Arup, 1983).*

2004). Based on experimental observations several potential mechanisms for formation of green rust have been proposed, however, the exact conditions and mechanisms are not known, see e.g. Sagoe-Crentsil and Glasser (1989), Sagoe-Crentsil and Glasser (1993b), Sagoe-Crentsil and Glasser (1993a), Sandberg (1998) and Küter et al. (2004) and literature cited therein.

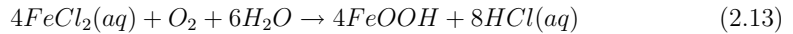
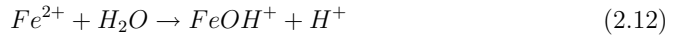
2.2.4 Intense localised corrosion

Intense localised corrosion, also referred to as pitting corrosion, is likely to develop in concrete with a low resistivity, high alkalinity, i.e. uncarbonated concrete, and a chloride concentration above the critical threshold concentration value (Arup, 1983). Thus, pitting corrosion is often considered and referred to as chloride initiated corrosion.

Pitting corrosion is considered to be initiated by local break downs of passivity in weak spots where the passive layer is more vulnerable to attacks (Broomfield, 1997a). Weak spots are suggested to be voids in the steel-concrete interface, sulphide inclusions in the steel, local pH drops or discontinuities in the oxide scale (Sandberg, 1998). Several mechanisms for local depassivation of steel in concrete as well as in alkaline solutions have been proposed, see e.g. Sato (1971), Chao et al. (1981), Yonezawa et al. (1988), Leek and Poole (1990) and Okada (1990). However, the exact conditions for initiation of pitting corrosion are not yet fully understood.

Once a pit has been created, the formation of ferric hydroxide (Equation 2.10) is believed to consume the oxygen in the emerging pit (Sandberg, 1998). A corrosion cell is formed with anodic dissolution of steel in the pit only and the adjacent passive steel acting as cathode. A simplified illustration of the electrochemical corrosion process around a corrosion pit is shown in Figure 2.4.

As the oxygen is depleted, the iron dissolved in the pit is assumed to react with water, resulting in pit acidification by the reaction in Equation 2.12 (Broomfield, 1997a) (Sandberg, 1998). In Küter et al. (2004) it was shown that this reaction is thermodynamically not possible as the Gibbs free energy is positive. However, another acidifying reaction must take place as pH values as low as one have been observed within active pits (Sandberg, 1998). As an alternative Küter et al. (2004) suggested the thermodynamically possible reaction given in Equation 2.13. Contrary to the former reaction this reaction requires some oxygen.



According to Equation 2.13 the chloride iron complexes are not stable in the presence of oxygen. Thus, acidification proceeds with a breakdown of the iron-chloride complexes, releasing the chloride, for further acidification and forming iron hydroxide. Both processes accelerate the corrosion attack. If a pH value as low as one is obtained inside a pit, the acid dissolution of the steel may be much more rapid than the electrochemical dissolution, i.e. the initial corrosion process Sandberg (1998). From the proposed reactions it is seen that the catalytic effect of chloride ions is much more extensive when oxygen is available (Küter et al., 2004).

2.2.5 Steel potentials in concrete

The potential of steel in concrete when measured versus a reference electrode is a mixed potential, referred to as the free corrosion potential, E_{corr} , representing a balance between the potential of the anodic and cathodic reactions, see Figure 2.5 (Elsener, 2005). The anodic reaction tends to increase the potential (increasing the anodic dissolution and decreasing the cathodic reduction) whereas the cathodic reaction tends to decrease the potential (decreasing the anodic dissolution and increasing the cathodic reduction). The phenomena is known as polarisation, see Section 2.3.2. At the free corrosion potential, E_{corr} , the anodic and cathodic reactions proceed at same rate, i.e. the electrons released by the anodic dissolution are consumed by the cathodic reduction and hence charge neutrality exists (Arup, 1967).

In uncarbonated concrete the passive steel potential is found in the region between the water stability lines *a* and *b* in Figure 2.6 at a pH of $\simeq 13$ (Section 2.2.1). The passive potential is largely controlled by the oxygen partial pressure in the concrete adjacent to the reinforcement and hence the moisture content (Tuutti, 1982). When oxygen is available, e.g. in structures exposed to the atmosphere, steel normally exhibits a potential in the range of +100 to -200 mV versus Cu/CuSO₄ (+177 to -133 mV versus SCE) (Arup, 1985).

However, in oxygen deprived environments, where the cathodic reaction is restricted, potentials as low as -700 mV versus Cu/CuSO₄ (-623 mV versus SCE) may be observed, as the steel potential becomes cathodically controlled (Arup, 1985). This situation is often observed in submerged structures where the concrete is water saturated and the oxygen

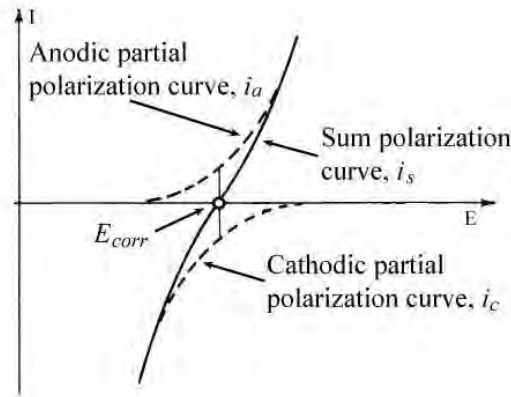
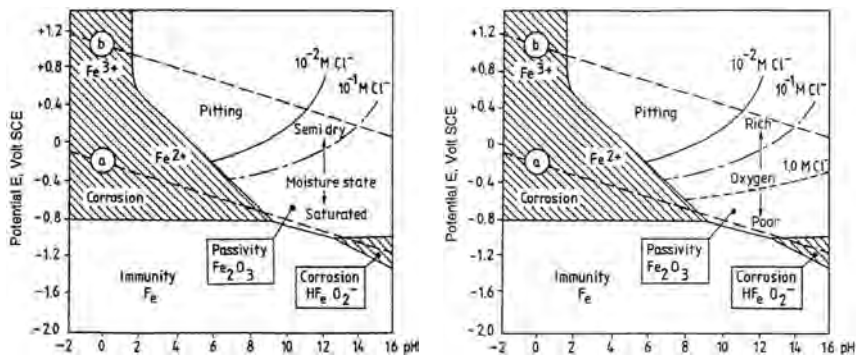


Figure 2.5 Partial and sum polarisation curves of a corroding metal (Elsener, 2005).



(a) Pourbaix diagram, relationship between moisture and steel potential. (b) Pourbaix diagram, relationship between oxygen and steel potential.

Figure 2.6 Pourbaix diagrams illustrating the effect of moisture and correlated oxygen content on the steel potential (Sandberg, 1998).

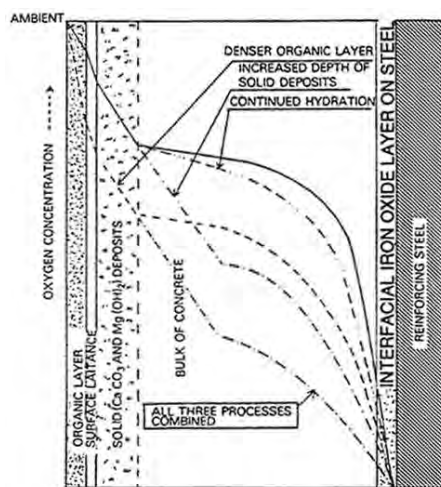


Figure 2.7 Schematic illustration of the oxygen concentration as a function of depth below the concrete cover for concrete submerged in sea water (Fidjestol and Nielsen, 1980).

diffusion coefficient low, see Figure 2.7 (Tuutti, 1982).

For steel reinforcement suffering from general corrosion, corrosion potentials are reported to be in the range of -450 to -600 mV versus Cu/CuSO₄ (-373 to -523 mV versus SCE) (Arup, 1983) (Elsener et al., 2003). In Arup (1983) it is reported that the potential of reinforcement with chloride initiated pitting corrosion typically ranges from -270 mV to -570 mV versus Cu/CuSO₄ (-193 to -493 mV versus SCE). However, no information on the effect of the chloride content on the pitting potential was given. Typical potential values for steel in concrete reported by Elsener et al. (2003) are given in Section 3.1, Table 3.3.

2.3 Corrosion rate of steel in concrete

2.3.1 Expression of corrosion rate

Corrosion rate may be expressed in three different ways:

- Thickness or cross section reduction over time
- Weight loss per unit area over time
- Corrosion current density

Of those, thickness or cross section reduction is of largest relevance for practical engineering, e.g. for estimation of residual service life or load bearing capacity of a reinforced concrete structure. Weight loss per unit area over time has previously been used within

the field of corrosion testing, i.e. for gravimetric measurements as described in e.g. ASTM G 1-90 (1990). Within the field of electrochemical testing, the corrosion rate is often expressed by the corrosion current density, i_{corr} : The corrosion current density, i_{corr} , is the amount of metal ions that leaves the metal substrate, given as an electrical current, per unit area and time. The relation between thickness reduction over time, ds/dt and corrosion current density, i_{corr} , is given by Faradays law (Bardal, 1994):

$$\frac{ds}{dt} = \frac{i_{corr} \cdot M}{z \cdot F \cdot \rho} [cm/s] \quad (2.14)$$

or

$$\frac{\Delta s}{\Delta t} = 3268 \cdot \frac{i_{corr} \cdot M}{z \cdot \rho} [mm/year] \quad (2.15)$$

where i_{corr} is given in A/cm^2 , z is the number of ionic charges ($z=2$ for Fe), M is the molecular weight ($M=56$ g/mol for Fe), F is the Faraday constant ($F = 96480$ C/mol) and ρ the specific density of the metal ($\rho=7.85$ g/cm³ for Fe). The corrosion current density, i_{corr} , is most often expressed in $\mu A/cm^2$. Thus, a corrosion current density of $1 \mu A/cm^2$ equals a thickness reduction of $11.5 \mu m/year$.

2.3.2 Polarisation and corrosion kinetics

The concept of polarisation is briefly described due to its importance for the corrosion reactions and kinetics. A detailed and quantitative discussion of the topic is outside the scope of the thesis but may be found in text books like Koryta et al. (1970), Fontana and Greene (1978) and Bardal (1994).

The rate of the electrochemical reaction, i.e. the corrosion rate, is limited by various physical and chemical factors: The electrochemical reaction is said to be polarised or retarded by these factors. Polarisation can be divided into three different types which may act separately or simultaneously: *activation*, *concentration* and *resistance* polarisation (Fontana and Greene, 1978).

Activation polarisation may be considered as a resistance against the reaction in the metal-electrolyte interface: The atoms or ions must overcome a certain energy barrier in order to reach another state. The factor limiting the reaction may be the rate at which ions or electrons are transported through the interface or the rate at which reactants are transformed. For completeness it should be mentioned that for activation polarisation the relationship between current density, i , and overpotential, η , is given by the Tafel equations (Page, 1988):

$$\eta_a = \beta_a \cdot \log \frac{i_a}{i_0} \text{ Anodic overpotential} \quad (2.16)$$

$$\eta_c = \beta_c \cdot \log \frac{i_c}{i_0} \text{ Cathodic overpotential} \quad (2.17)$$

where the Tafel coefficients, β_a and β_c are constant for the reaction at a fixed temperatures, see also Figure 2.8:

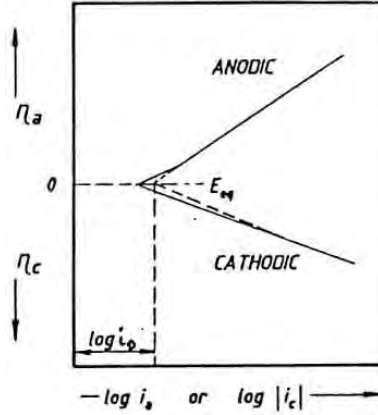


Figure 2.8 Polarisation curves for an electrode process. The relationship between polarisation potential, η , and current density, i , is given by the Tafel equations (Equations 2.16 and 2.17) (Page, 1988).

Concentration polarisation refers to the situation where the diffusion rate of the reactants through the electrolyte controls the rate of the reaction (Bardal, 1994). In most cases concentration polarisation is seen as a lack of reactants at the electrode surface, e.g. oxygen for the cathodic reduction, however, accumulation of reaction products may also occur. In case of *lack of reactants* the diffusion rate and hence the reaction rate, may be described by Fick's first law, assuming steady state (Fontana and Greene, 1978).

Resistance polarisation is caused by the ohmic resistance of the electrolyte or an electrode surface oxide film. For steel in concrete resistance polarisation relates to the resistance in the electrolyte, i.e. the concrete resistivity. In several studies relationships between concrete resistivity and the corrosion rate of steel in concrete have been demonstrated, see e.g. Alonso et al. (1988). The effect of the concrete resistivity on the corrosion rate of steel in concrete is discussed in Section 2.3.4.

For reinforced concrete structures, the free corrosion potential, E_{corr} , and the correlated corrosion current density, i_{corr} , are in most cases seen to be governed by concentration polarisation. Examples of polarisation curves for the anode and cathode reactions are illustrated in Figure 2.9. The intersection point between the anode and cathode curves defines the free corrosion potential, E_{corr} , and the corrosion current density, i_{corr} , for a given corrosion state. As illustrated in Figure 2.9 passive reinforcement exhibits a steep anodic polarisation curve (a_1). This is caused by concentration polarisation as the passive layer restricts the transport of dissolved Fe^{2+} ions away from the steel surface (Bardal, 1994). When oxygen is available the cathode curve (c_2) intersects the passive anode curve at a relatively high potential (initial potential). In oxygen deprived environments, the

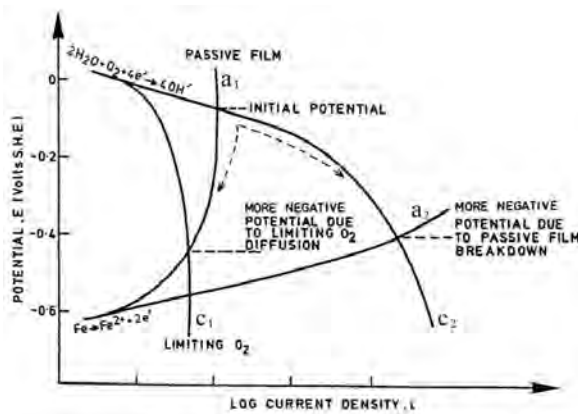


Figure 2.9 Stern diagram for active and passive polarisation curves (Sandberg, 1998).

steep cathode curve results in a much more negative free corrosion potential, E_{corr} , of the passive steel. This is seen to be caused by concentration polarisation, i.e. a restricted transport of oxygen to the cathode. In both situations a low corrosion current density, i_{corr} , is seen.

When the passive layer disrupts, e.g. due to carbonation or chloride ingress, and steel dissolution is no longer restricted by concentration polarisation (curve a_2) a much higher corrosion current density, i_{corr} , is obtained - given by the intersect of curves a_2 - c_2 (assuming oxygen to be available). From Figure 2.9 it should also be noticed that the free corrosion potential, E_{corr} , alone does not give a definite indication of the corrosion rate although these are often seen to plotted as a function of each other, see e.g. Elsener (2005).

In the active corrosion state, activation and resistance polarisation, i.e. the rate at which steel dissolve and oxygen is reduced, and the concrete resistivity, respectively, may be considered the main factors controlling the corrosion rate. The rates of the anode and cathode reactions are closely related to the temperature, and the concrete resistivity to the moisture and ion contents. The effects of these parameters on the corrosion rate are discussed in Section 2.3.4.

2.3.3 Corrosion rate and polarisation resistance

Nearly all electrochemical techniques for determining the corrosion rate rely on the empirical relation between the corrosion current, I_{corr} and the slope of the polarisation curve around the free corrosion potential, dE/dI . For a corroding electrode this relation, derived by Stern and Geary (1957), is given by:

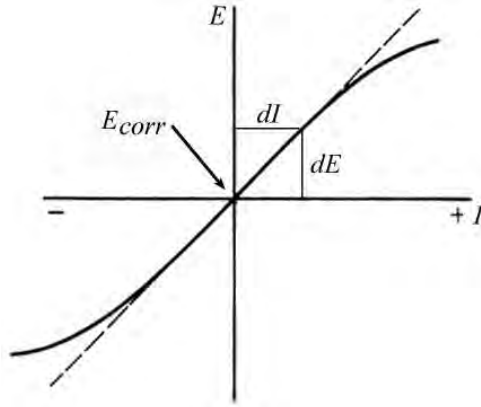


Figure 2.10 Linear correlation between polarising potential and current around the free corrosion potential, E_{corr} (Bardal, 1994).

$$\frac{dE}{dI_{x \rightarrow 0}} = -\frac{\beta_a \cdot \beta_c}{2.3 \cdot I_{corr} \cdot (\beta_a + \beta_c)} \quad (2.18)$$

where dE is the potential shift from the free corrosion potential, E_{corr} , dI the applied current, and β_a and β_c the anodic and cathodic Tafel constants, respectively. The slope of the polarisation curve, dE/dI was first referred to as the polarisation resistance, R_P , by Bonhoeffer and Jena (1951). This term is commonly used today and will also be used in the following.

Equation 2.18, often referred to as the Stern-Geary equation, was derived from theoretical considerations on the Tafel equations and the linear relation between current and potential near the free corrosion potential, E_{corr} - demonstrated in the work by Butler and Armstrong (1934), see Figure 2.10. The Stern-Geary equation is of great value as it relates the corrosion rate and the Tafel slopes to polarisation measurements close to the corrosion potential, E_{corr} , thus eliminating major disturbances from high current polarisation measurements (e.g. full polarisation curves).

Rearranging Equation 2.18 and considering the corrosion current density, i_{corr} , the form of the Stern-Geary equation seen in most textbooks and papers appears:

$$i_{corr} = \frac{B}{R_P \cdot A} \quad (2.19)$$

where A is the polarised steel area and B a constant composed of the anodic and cathodic Tafel constants:

$$B = \frac{\beta_a \cdot \beta_c}{2.3 \cdot (\beta_a + \beta_c)} \quad (2.20)$$

If the parameters A and B are, or are assumed, known the corrosion current density, i_{corr} , may be determined from measurements of the polarisation resistance, R_P . Despite widespread use of the Stern-Geary equation for determining the corrosion current density, i_{corr} , for steel-concrete systems, only few data on Tafel slopes for steel embedded in concrete have been published (Andrade et al., 2004).

For steel in neutral to acidic solutions, simulating neutralised and chloride containing steel-concrete systems anodic Tafel slopes, β_a , between 73 and 98 mV/dec were reported by Garces et al. (2005), in good agreement with 75 mV/dec at a pH of 1 found by Jäggi (2001). Cathodic Tafel slopes, β_c , of 230 mV/dec were reported by Jäggi et al. (2000) for steel in neutral and alkaline solutions.

For steel in mortar, exposed up to 12 months at 93 % relative humidity, Brem (2004) reported cathodic Tafel slopes of 200-230 mV/dec, decreasing at increasing temperatures and increasing in time, similar to the observations by Jäggi et al. (2000) for steel in alkaline solutions. However, no Tafel behaviour was found for anodic polarisation curves for steel in mortar (Brem, 2004).

From electrochemical and gravimetric measurements on steel in reinforced mortar specimens and calcium hydroxide ($\text{Ca}(\text{OH})_2$) solutions Andrade and Gonzalez (1978) proposed B values of 26 mV and 52 mV for steel in the active and passive corrosion state, respectively. The proposed values were mainly based on the results from the solution experiments where good correlation between electrochemical and gravimetric measurements was found; for the reinforced mortar specimens deviations of up to two and three orders of magnitude were seen. Nevertheless, the proposed values have since the publication been used in a vast number of studies on corrosion of steel in concrete see e.g. Alonso et al. (1988), Glass et al. (1997), Andrade et al. (2004). In a more recent study Song (2000) analysed B values from four different corrosion scenarios and concluded that B can range from 8 mV to infinite. However, an infinite value of B would result in infinite corrosion rates being calculated (Equation 2.19) which can not be true.

For steel in aqueous solutions the range of linearity around the free corrosion potential, E_{corr} , was found for values up to approximately 20 mV for non-corroding, i.e. passive systems and 50 mV for corroding systems by Stern and Geary (1957), see Figure 2.11. The same values have been seen to apply for steel-concrete systems (Andrade, 1973) (Andrade and Gonzalez, 1978) (Polder et al., 1993).

Finally, it should be mentioned that the Stern-Geary equation (Equation 2.18) was derived for a corroding electrode at the free corrosion potential, E_{corr} , without influence of non-uniform distribution of anodic and cathodic reactions and polarisation effects from macro-cells. For actively corroding steel in concrete unfortunately these conditions are most often not fulfilled. Despite this, the Stern-Geary equation is widely used for determining the corrosion current density, i_{corr} , of steel in concrete, as described in Section 3.2.

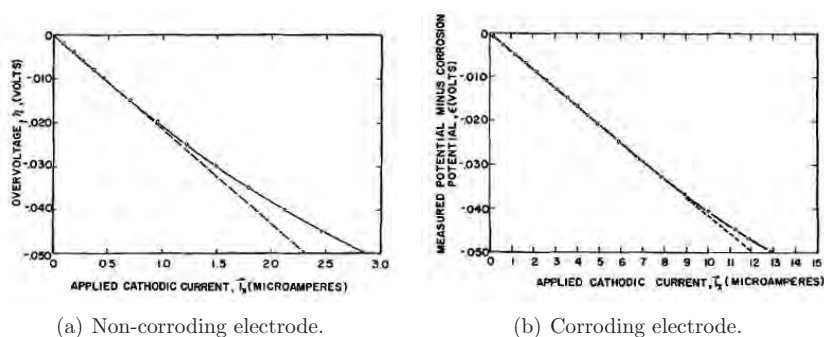


Figure 2.11 *Linear relationship between overpotential (measured potential minus the free corrosion potential) and applied current for single electrode systems (Stern and Geary, 1957).*

2.3.4 Corrosion rate affecting factors

The kinetics of the corrosion process are influenced by a number of material properties and environmental factors. Of these, temperature, concrete resistivity and moisture content seem to be the predominant factors controlling the rate of corrosion (Tuutti, 1982) (Neville, 1999). Several studies have been devoted to investigating the rate of corrosion in concrete under outdoor conditions, see e.g. Andrade et al. (2001), Andrade et al. (2002) and Andrade and Castillo (2003). However, an evaluation of the effect of the individual parameters may be difficult from such studies. Hence, the following sections will primarily be based on studies carried out under controlled laboratory conditions, where the effect of each parameter is investigated individually. In the following the effect of the various parameters is described individually, however, it should be stressed that the parameters are concurrent.

Temperature

The temperature plays an important role for the steel corrosion rate in concrete, and the subject has achieved some attention in the research community. The effect of the temperature was investigated by Tuutti (1982) on water saturated concrete specimens where corrosion initiation was obtained through accelerated carbonation. In the interval of -25 to +20 °C the corrosion current density, i_{corr} , was seen to change with a factor 100, see Figure 2.12.

Lopez et al. (1993) investigated the effect of temperature, moisture and chloride content on the corrosion current density, i_{corr} , of steel in mortar specimens. As expected, an increase of each parameter increased the corrosion current density, i_{corr} . However, Lopez et al. (1993) stated that the effect of temperature on the corrosion process cannot be separated from that of electrolytic availability (i.e. the degree of pore saturation or concrete resistivity), as both are affected by the temperature.

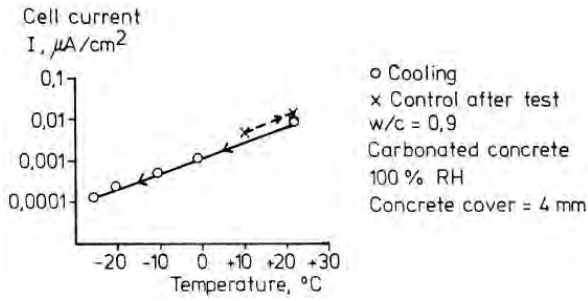


Figure 2.12 Corrosion current density as a function of the temperature for steel in carbonated concrete (Tuutti, 1982).

In more recent studies the effect of temperature on the corrosion current density, i_{corr} , is considered best described by the Arrhenius equation (Raupach, 1997a):

$$k_F = A_F \cdot e^{-\frac{E_a}{R \cdot T}} \quad (2.21)$$

where k_F is the rate constant, A_F the frequency factor (constant), E_a the activation energy, R the ideal gas constant and T the absolute temperature. In most studies a rearranged version of the Arrhenius equation, describing the relative effect of the temperature, is used:

$$i_x = \frac{i_y}{e^{a \cdot (\frac{1}{T_x} - \frac{1}{T_y})}} \quad (2.22)$$

where i_x is the corrosion current density at temperature T_x , i_y the corrosion current density at temperature T_y and a a constant combining the activation energy, E_a , and the ideal gas constant, R , ($a = E_a/R$). Although a -values are given in most studies activation energies, E_a , are used in the following.

For macro-cells with chloride induced corrosion Raupach (1997a) found that the activation energy, E_a , depended on the relative humidity. For temperatures between +20 and +60 °C, and a constant relative humidity of 70 %, an activation energy, E_a , of 32.3×10^3 J/mol was found. However, for a relative humidity of 88 %, the activation energy, E_a , increased to 40.2×10^3 J/mol. Two investigations reporting similar activation energies, E_a , are mentioned in Raupach (1997a), namely the work by Bertolini and Polder (1997) and Elsener et al. (1996a).

In the work by Bertolini and Polder (1997) an activation energy, E_a , of 29.4×10^3 J/mol was found for steel in concrete in the temperature range of +13 to +30 °C at a constant relative humidity of 80 %. From measurements in the St. Bernardino Tunnel in Switzerland Elsener et al. (1996a) showed that a temperature increase from -10 to +18 °C led to an increase of the corrosion current density, i_{corr} , of 0.5 to $2.2 \mu A/cm^2$; corresponding to an activation energy, E_a , of 31.5×10^3 J/mol, which is in agreement with the results reported from the laboratory investigations mentioned above. The value reported

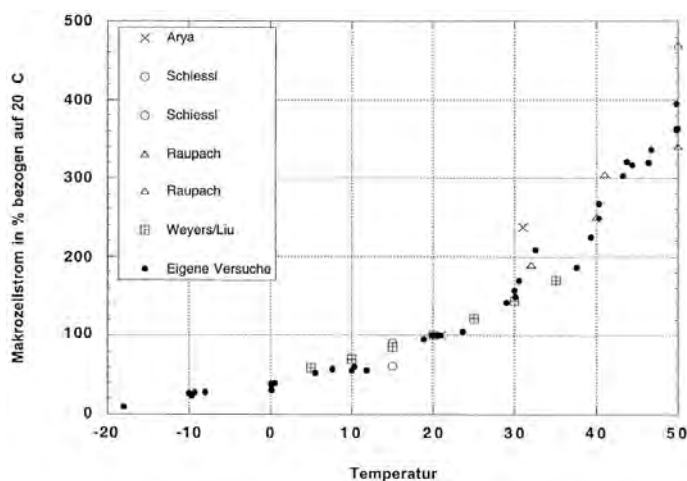


Figure 2.13 Macro-cell current as a function of the temperature for steel in mortar. The macro-cell current is given in % of the current recorded at 20 °C. Results obtained by Jäggi et al. (2001) are shown together with results reported in the literature by Schiessl and Raupach (1990), Arya and Vassie (1995), Raupach (1997b) and Liu and Weyers (1998). Reprint from (Jäggi et al., 2001).

by Elsener et al. (1996a) seems to be the only result from on-site investigations.

In the work by Jäggi et al. (2001) results from experiments on reinforced mortar specimens in a temperature range from 0 to +50 °C were compared with results presented by Schiessl and Raupach (1990), Arya and Vassie (1995), Raupach (1997b) and Liu and Weyers (1998). As shown in Figure 2.13 good correlation between all the reported data was found.

In a recent study, Baccay et al. (2006) observed that the activation energy, E_a , apart from the relative humidity, also is affected by the cement type.

Finally and for completeness it should be mentioned that contrary results have been obtained by Zivica (2002). Here, the corrosion rate was seen to increase from +20 to +40 °C. However, from +40 to +60 °C a decrease in the corrosion rate was reported. The effect was considered to be caused by a decrease in the oxygen and water content in the pore system with increasing temperature. The experiments were conducted using a sensor, based on electrical resistivity technique, that was embedded in the chloride containing mortar.

Electrical resistivity

Concrete's electrical resistivity, ρ_e , may be widely ranged - typically from 10^1 to $10^6 \Omega \times m$. The resistivity, ρ_e , is known to be a function of a number of different parameters, such as water-binder ratio, type of binder, binder content, chloride content (as well as other ions), chemical admixtures, moisture content and temperature (Tuutti, 1982) (Enevoldsen et al., 1994) (Neville, 1999) (Hunkeler, 2005). Concrete's electrical resistivity has been studied by several authors and will only be briefly discussed before the effect of the resistivity on the kinetics of the corrosion process is reviewed. A thorough review of concrete's electrical resistivity may be found in e.g. Monfore (1968), Neville (1999) and Whiting and Nagi (2003).

In concrete the electrical current is carried by ions in the pore solution. Hence, a high moisture content, a high degree of connectivity and low tortuosity (high water-cement ratio) cause low electrical resistivity (Polder et al., 1994). For a constant relative humidity, the resistivity increases with decreasing water-cement ratio, longer curing times and by addition of reactive pozzuolana such as blast furnace slag, fly ash and silica fume (Polder et al., 2000).

The concrete temperature is also seen to have a significant effect on the electrical resistivity; increasing the temperature results in a decrease of the electrical resistivity and vice versa. This is caused by changes in the ion mobility in the pore solution and by changes in the ion-solid interaction with the cement paste (Polder et al., 2000). The temperature effect on the electrical resistivity is considered described by the Arrhenius equation (Raupach, 1997a):

$$\rho_x = \rho_y \cdot e^{b \left(\frac{1}{T_x} - \frac{1}{T_y} \right)} \quad (2.23)$$

where ρ_x is the resistivity at temperature T_x , ρ_y the resistivity at temperature T_y and b a constant combining the activation energy, E_a , and the ideal gas constant, R , ($b = E_a/R$). For steady state conditions the activation energy, E_a , has been found in the range from 12.5×10^3 to 37.4×10^3 J/mol, and increase with decreasing relative humidity and decrease with decreasing water-cement ratio (Polder et al., 2000), (Hope et al., 1985) and literature cited therein.

Of the influencing factors the moisture content seems to be the predominant factor determining concrete's electrical resistivity. Based on data from Gjrv et al. (1977), Tuutti (1982) found that the conductivity (reciprocal of the resistivity) changed by several orders of magnitude when reducing the relative humidity in concrete from 100 % to 50 %. These data, as presented by Tuutti (1982), are shown in Figure 2.14. In the work by Gjrv et al. (1977) concrete's electrical resistivity was deemed only very moderately affected by the water-cement ratio and chloride content: The resistivity changed with a factor of approximately two when: a) the water-cement ratio changed from 0.70 to 0.40 and b) when the chloride content changed from 0 to 4 % CaCl_2 by mass of cement. The reason for the limited influence from the water-cement ratio and the chloride content was considered caused by the excellent conductivity of the alkali hydroxides.

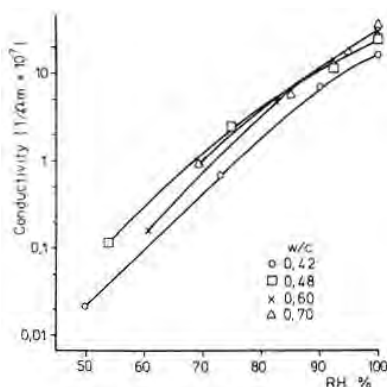


Figure 2.14 *Electrical concrete conductivity as a function of the relative humidity in the concrete (Tuutti, 1982).*

It should be stressed that concrete is not a homogenous conductor, as the current is only transported by the pore solution in the cement paste, except in the possible case of carbon from flyash. The aggregate particles are essentially isolating bodies (Hunkeler, 1996).

In the work by Tuutti (1982) it was stated that the corrosion rate is by no means directly proportional to the conductivity (reciprocal of the resistivity) although improved conductivity (lower resistivity) improve the possibility for the electrodes working. Similar considerations were stated in Hope et al. (1985) where the concrete resistivity was related to the corrosion probability.

On the contrary, an inverse proportional relationship between the corrosion rate and the electrical resistivity (linear relation between $\log(i_{corr})$ and $\log(\rho_c)$) for actively corroding steel in concrete was found by Alonso et al. (1988) and Lopez and Gonzalez (1993). They suggested that the active corrosion process is under resistance control. Their experiments were carried out on reinforced mortar specimens employing a range of different binders. Both chloride and carbonation induced corrosion were investigated. The results from the work by Alonso et al. (1988) are shown in Figure 2.15. As seen from the figure the corrosion current density, i_{corr} , is given as a function of the concrete resistance, R_Ω , and not the concrete resistivity, ρ_c . However, this makes no difference, as a constant relation between R_Ω and ρ_c exists, assuming the geometrical position of the measurement electrodes to be constant. Similar results were obtained by Gulikers (2005) from a theoretical treatment of the corrosion process. Here it was found that for a wide range of corrosion current densities, i_{corr} , the relation between $\log(i_{corr})$ and $\log(R_\Omega)$ can be approximated by an almost ideal linear relationship.

Glass et al. (1991) found a linear relationship between the corrosion current density, i_{corr} , and the inverse concrete resistance ($1/R_\Omega$), see Figure 2.16. Also, these experiments were

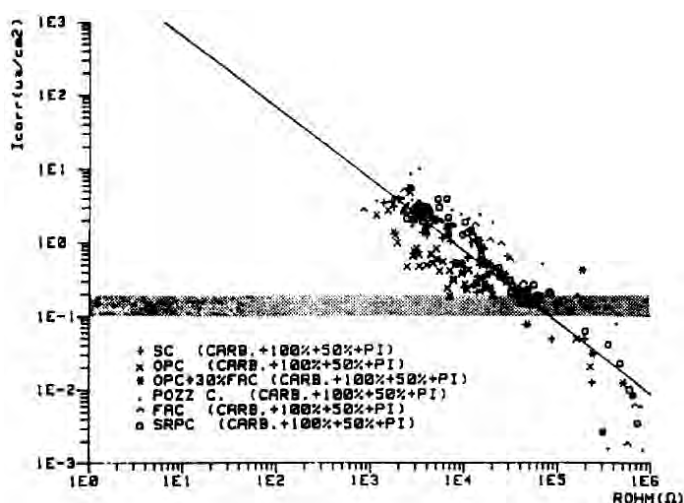


Figure 2.15 Corrosion current density, i_{corr} , as a function of ohmic resistance, R_{Ω} for steel in mortar. The slope of the straight tendency line was found to be about -1 (Alonso et al., 1988).

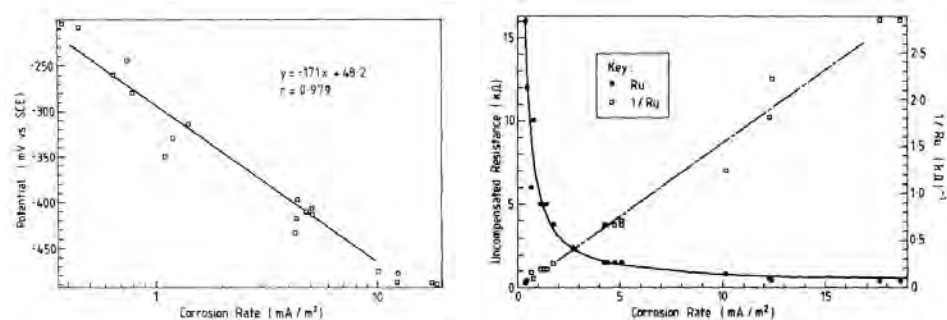
carried out with reinforced mortar specimens and, carbonation and chloride induced corrosion. In the study Glass et al. (1991) also observed that the free corrosion potential, E_{corr} , became markedly more negative as the corrosion current density, i_{corr} , increased, see Figure 2.16. Based on these observations it was suggested that the higher corrosion rate was caused by a decreased anodic polarisation. From this it was concluded that the steel corrosion rate in carbonated mortars is under anodic control with the anodic reaction being limited by the electrical resistivity. Similar results were obtained by Polder (2001) who stated that although a relation between corrosion rate and concrete resistivity was found, different relations appear to exist for different cement types.

Finally, it should be mentioned that the relationship found by Glass et al. (1991) and Polder (2001) correlates well with the mathematical formulation describing the corrosion process given in the early work by Bažant (1978).

Moisture content

With respect to the kinetics of steel corrosion in concrete the effect of the moisture content is strongly related to the concrete resistivity as described in the previous section. However, also the oxygen diffusion coefficient is affected by the moisture content. When the moisture content increases, these two factors have opposite effects on the corrosion rate: The decrease in oxygen permeability has a limiting effect while the decrease in resistivity stimulates the corrosion process (Tuutti, 1982).

In the work by Tuutti (1982) the effect of the internal relative humidity on the corro-



(a) Relationship between corrosion potential and (b) Relationship between concrete resistance and corrosion current density.

Figure 2.16 The relationship between corrosion potential, concrete resistance and corrosion current density obtained from a polarisation resistance probe in carbonated mortar with 0.4 % chloride (Glass et al., 1991).

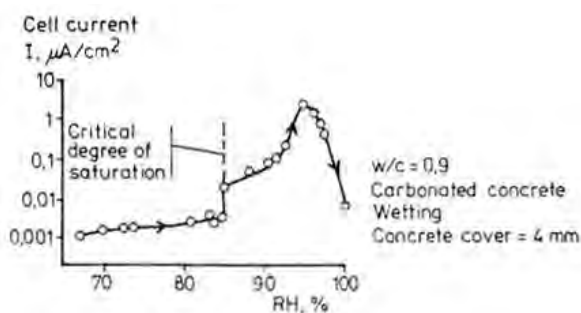


Figure 2.17 Corrosion current density as a function of the internal relative humidity (Tuttu, 1982).

sion rate was investigated on concrete specimens where corrosion was initiated by both accelerated carbonation and admixed chlorides. It was found that a critical degree of saturation exists, below which, no significant corrosion occurs, see Figure 2.17. Also, an optimum level around 90 to 95 %RH, depending on the water-cement ratio, was observed. Above the optimum, associated with an oxygen diffusion coefficient lower than $0.3 \cdot 10^{-8} \text{ m}^2/\text{s}$, cathodic control (concentration polarisation) was seen to be the limiting factor.

From similar experiments (admixed chloride and carbonated concrete) Glass et al. (1991) found the corrosion current density to increase exponentially with increasing external relative humidity in the range of approximately 40 to 90 %RH. The increase was ascribed to a decrease in the concrete resistivity.

Finally, Lopez and Gonzalez (1993) investigated the corrosion rate as a function of the

degree of pore saturation for reinforced mortar specimens with admixed chloride. For corroding reinforcement it was found that the corrosion current density, i_{corr} , increased inverse proportionally with the degree of pore saturation up till a saturation degree of 60 to 70 %. Above this, the corrosion current density, i_{corr} , decreased, similar to the observations in the work by Tuutti (1982). However, no correlation between the degree of pore saturation and the relative humidity was given.

Chapter 3

Measurement of steel corrosion in concrete

3.1 Half-cell potential measurement

The use of qualitative half-cell potential measurements for assessing the corrosion state of steel in concrete was first described in a paper by Stratfull (1957). Actively corroding areas on a bridge were located from measured half-cell potential gradients. In the following decades half-cell potential measurements were used in field and laboratory investigations for assessing the corrosion state of steel in concrete. Primarily based on the work of Spellman and Stratfull (1973), Stratfull et al. (1975) and Van Daveer (1975) the ASTM C 876-77 *Standard Test Method for Half-Cell Potentials of Uncoated Reinforced steel in concrete* was published in 1977 (ASTM C 876-77, 1977). Revised versions of the standard have later been published.

The ASTM C 876-77 (1977) standard describes the procedure to be followed and gives guidelines for interpretation of measurements. The half-cell potential, E_{corr} , of steel reinforcement in concrete is measured as a potential difference against a reference electrode (half-cell) placed at the concrete surface and over the reinforcement. The reference electrode is connected to the ground terminal on a high impedance voltmeter, and an electrical connection to the reinforcement, to the positive terminal as shown in Figure 3.1.

The numerical value of the potential difference between the embedded reinforcement steel and the reference electrode depends on the type of reference electrode used and the corrosion state of the steel. In addition, as half-cell potentials of steel in concrete can not be measured directly at the steel-concrete interface due to the concrete cover, the measured potentials are also influenced by the ohmic resistance across the concrete cover (IR drop) and possibly by macro-cell currents and junction potentials (Elsener et al., 2003).

A copper-copper sulfate (Cu/CuSO_4) half-cell is specified in the ASTM C 876-77 (1977) standard, however, various types of half-cells are used for on-site measurements. Selected half-cells often used in practical work are given in Table 3.1.

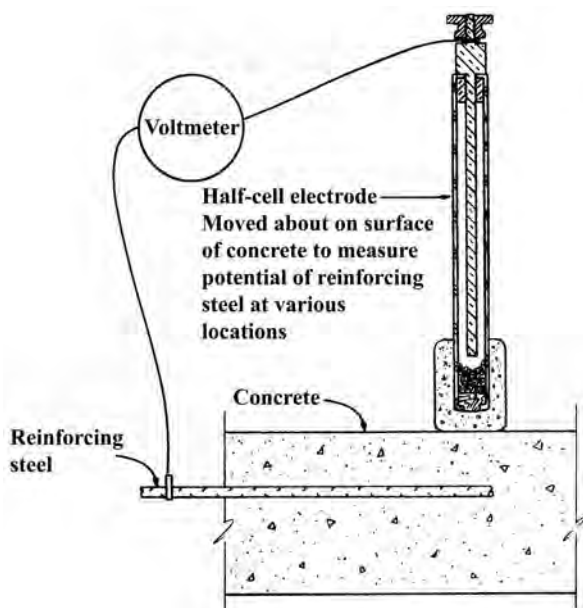


Figure 3.1 Schematic illustration of half-cell potential measurement of steel in concrete ASTM C 876-77 (1977).

Table 3.1 Selected half-cell electrodes used in practice, their potentials, given versus the Standard Hydrogen Electrode (SHE) at 25 °C and temperature coefficients (Myrdal, 2007).

Half-cell electrode	Potential [mV versus SHE]	Temperature dependency [mv/°C]
Copper/copper sulphate sat.	+318	+0.90
Calomel sat.	+241	+0.22
Silver/silver chloride sat	+199	+0.09

Half-cell potential measurements as described in ASTM C 876-77 (1977) can, in principle, be performed on any concrete structure with reinforcement that is not electrically isolated from the concrete e.g. by epoxy coating, plastic ducts, etc. However, the criteria given in the ASTM C 876-77 (1977) standard for interpretation of the measurements only apply for ordinary steel in structures exposed to the atmosphere, i.e. in oxygen enriched environments. The relationship between the measured half-cell potential values and the probability of reinforcement corrosion in such structures, as stated in the ASTM C 876-77 (1977) standard, is given in Table 3.2.

Under conditions where the potential of the embedded reinforcement steel may be influenced by a restricted oxygen availability, e.g. due to a high moisture content or carbonation (see Section 2.2.5) interpretation of half-cell potential measurements often proves to

Table 3.2 Interpretation guidelines for half-cell potentials, E_{corr} , as stated in ASTM C 876-77 (1977).

Potential		Probability of corrosion
[mV vs. Cu/CuSO ₄]	[mV vs. Ag/AgCl*]	
... > -200	... > -83	90 % probability of no corrosion
-200 > ... > -350	-83 > ... > -233	Corrosion activity is uncertain
... < -350	... < -233	90 % probability of corrosion

*: Converted from mV vs. Cu/CuSO₄ to mV vs. Ag/AgCl by adding + 117 mV.

Table 3.3 Typical range of potentials of ordinary steel in concrete (Elsener et al., 2003).

Concrete condition	Potential range [mV vs. Cu/CuSO ₄]
water saturated concrete, oxygen deprived	-900 ... -1000
wet, chloride contaminated concrete	-400 ... -600
humid, chloride free concrete	+100 ... -200
humid, carbonated concrete	+100 ... -400
dry, carbonated concrete	+200 ... 0
dry concrete	+200

be difficult. Over the years this has resulted in a vast number of papers describing field experiences, difficulties, possibilities and limitations of the half-cell potential technique, see e.g. Vassie (1978), Arup (1985), Elsener and Böhni (1990), and literature cited therein.

One of the latest and more comprehensive publications is the Rilem Technical Recommendation on half-cell potential measurements (Elsener et al., 2003). In this a thorough description of the technique, the application, the effect of concrete resistivity and cover thickness is given together with guidelines for interpretation of measurements. Typical potential ranges of ordinary reinforcing steel, as stated in the Rilem Technical Recommendation are given in Table 3.3.

For half-cell potential measurements performed on the concrete surface, the cover thickness and electrical resistivity are the two most important factors to consider: When the reinforcement suffers from general corrosion, a decrease in the concrete resistivity (e.g. by wetting the concrete surface) shifts the measured potentials to more negative values, but the potential gradients and the position of local minima do not change (Elsener and Böhni, 1990).

In case of localised corrosion, the half-cell placed on the concrete surface measures a mixed potential (anode-cathode potentials) that depends on the distance from the half-cell to the anodic and cathodic sites on the embedded reinforcement bar, respectively. When increasing the concrete cover, the potential difference, i.e the potential gradient, between two positions on the concrete surface decreases as the relative difference in dis-

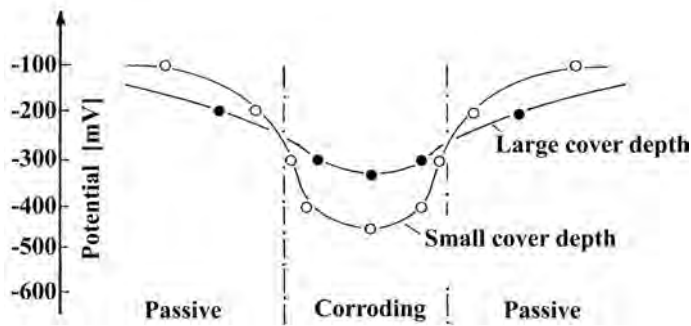


Figure 3.2 Effect of concrete cover thickness on the depth of potential field above a local anode (reference electrode type not given) (Elsener and Böhni, 1990).

tance to the anodic and cathodic sites decreases. As the potential gradients decrease, location of small corroding sites becomes more difficult (Elsener and Böhni, 1990). The phenomenon as illustrated by Elsener and Böhni (1990) is shown in Figure 3.2. The same effect is seen when the concrete resistivity increases, however, here the effect is caused by the extent of area polarised by the local anode (Elsener et al., 2003).

The major effect of cover thickness and resistivity on the measured half-cell potentials suggest that potential gradients rather than absolute values should be used for interpretation, which is also the general practice used when assessing the risk of corrosion. Also, the system resistance (and not necessarily concrete resistivity) should be measured in each location on the concrete surface where the half-cell potential is measured, as this may reveal possible sources of errors as well as provide useful information on the condition of the concrete cover.

3.2 Measurement of polarisation resistance

For electrochemical polarisation resistance measurements on reinforced concrete a conventional three electrode setup is used. Contrary to standard laboratory corrosion tests where the three electrodes are placed in a electrolyte being a solution, the counter and reference electrodes are placed on the concrete surface while the working electrode, i.e. the reinforcement is embedded in the concrete. In principle, all electrochemical techniques based on the three electrode setup can be used with this electrode arrangement. However, a number of difficulties arise due to the concrete electrolyte with more or less unknown properties, the geometry of the electrodes, and in particular the size of the embedded working electrode. In the following the electrochemical techniques often seen to be used for on-site polarisation resistance measurements are reviewed. The review will primarily focus on the practical aspects of the various techniques such as polarisation time, sweep rate, ohmic drop compensation etc.

3.2.1 Linear polarisation resistance techniques

Since its introduction the linear polarisation resistance technique has (see Section 2.3.3) been widely accepted as a standard test method for assessing the instantaneous corrosion rate in a great number of metal-electrolyte systems. The following review will focus on application of the technique on steel-concrete systems. For the interested reader a very complete review on polarisation resistance methods, not only limited to steel-concrete systems can be found in Scully (2000).

For steel-concrete systems the technique was first applied during the years 1970 to 1973 in the work by Andrade (1973). Since then the technique has been adopted in almost every study investigating the corrosion behavior of steel in concrete - for simply measuring the corrosion rate or as a reference, against which other techniques have been assessed. Despite this only very few studies have been devoted to studying the applicability of the technique and the implications met when measuring on steel-concrete systems (Feliu et al., 2005) (Elsener, 2005).

For measuring the polarisation resistance, R_P , the linear polarisation resistance technique makes use of Ohm's law on the linear relation between polarisation potential, ΔE_P , and current, ΔI , that exist for a steel electrode near the free corrosion potential, E_{corr} , see Equation 3.1 (Stern and Geary, 1957). The polarisation resistance, R_P , may also be considered as the slope of the (linear) potential-current curve around the free corrosion potential, E_{corr} , see Figure 2.10.

$$R_P = \frac{\Delta E_P}{\Delta I} \quad \Delta E_P \rightarrow 0 \quad (3.1)$$

For practical measurements polarisation of the reinforcement is usually obtained by potentiostatic, galvanostatic or potentiodynamic polarisation. With potentiostatic and galvanostatic polarisation a constant potential, ΔE , or current, ΔI , respectively, is applied to the steel-concrete system and the resulting non-controlled current or potential measured; ideally in steady state or after a given polarisation time assumed appropriate, see Figure 3.3(a). The polarisation time, being the time from initiating the static potential or current pulse to measuring the uncontrolled response, is often referred to as the *waiting* or *delay* time. In the following it will be referred to as the *delay* time. By potentiodynamic polarisation a slow potential sweep around the free corrosion potential, E_{corr} , is applied to the system while the current response is measured, see Figure 3.3(b) (Millard et al., 1992). The polarising potential at the steel-concrete interface, ΔE_P , may be very different from the potential applied to the system from a counter-electrode or the measured potential response, ΔE , due to the ohmic concrete resistance, R_Ω , between the steel bar and the reference electrode - often referred to as the IR drop. Taking the ohmic resistance, R_Ω , into account the true polarisation resistance, R_P , can be calculated from Equation 3.2:

$$R_P = \frac{\Delta E_P}{\Delta I} = R_P^{app} - R_\Omega = \frac{\Delta E}{\Delta I} - R_\Omega \quad (3.2)$$

As discussed in Section 2.3.3 the potential range of linearity around the free corrosion

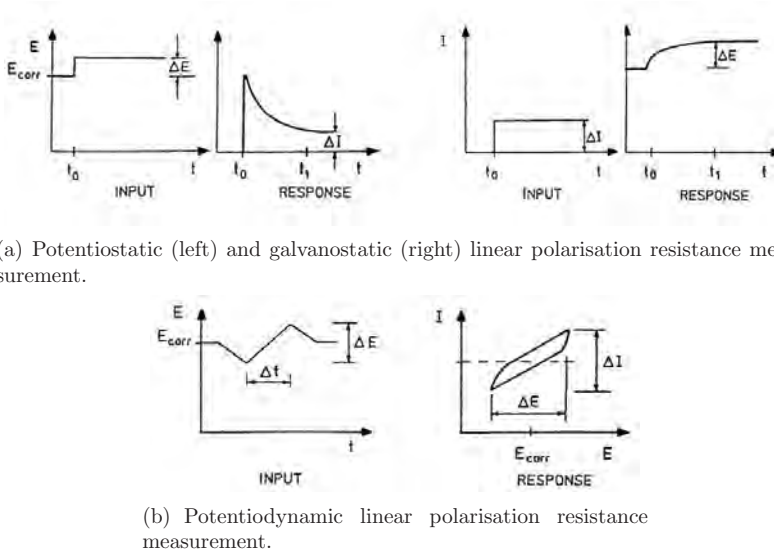


Figure 3.3 *Potentiostatic, galvanostatic and potentiodynamic polarisation methods illustrated by the applied input and response. After (Millard et al., 1992).*

potential, E_{corr} , is seen for values up to approximately 20 mV for non-corroding, i.e. passive systems and 50 mV for corroding systems (Stern and Geary, 1957) (Andrade, 1973) (Andrade and Gonzalez, 1978) (Polder et al., 1993). For measurements, where the actual corrosion state of the embedded reinforcement steel is unknown, a polarisation of 15 to 20 mV is most often used in order to stay within the linear region (Gowers and Millard, 1993) (Andrade et al., 2001) (Millard et al., 2001).

Despite the apparent simplicity of the methods a number of difficulties affecting the measured polarisation resistance, R_P , may be encountered when applying the methods to steel-concrete systems. From literature it seems as the ohmic resistance, R_Ω , and the determination of this, the delay time and the sweep rate are the factors affecting the measured polarisation resistance, R_P , most significantly (Andrade and Gonzalez, 1978) (Andrade et al., 1984) (Gonzalez et al., 1985a), (Millard et al., 1992). Hence these factors will be discussed in the following. A number of other factors also known to affect the measured polarisation resistance, R_P , such as the type of corrosion - localised or general, potential-range of anodic and cathodic partial reactions, are not discussed here.

Influence of delay time and sweep rate

In the work by Gabrielli et al. (1979) the effect of the delay time on the polarisation resistance, R_P , measured with the potentiostatic and galvanostatic methods was investigated theoretically: A simple modified Randles circuit, as shown in Figure 3.4, was assumed to describe the behaviour of a steel-electrolyte system.

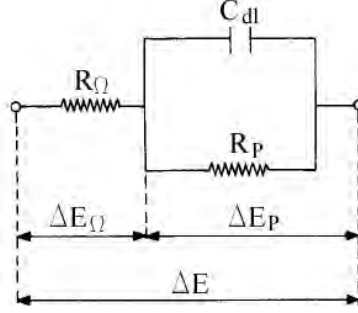


Figure 3.4 Simple modified Randles circuit over which a polarising potential, ΔE , is applied. ΔE_Ω represents the potential drop caused by the ohmic resistance, R_Ω , and ΔE_P the polarising potential over the double layer. C_{dl} is the double layer capacitance. After Gonzalez et al. (1985a).

The current response of this circuit to a constant potential, ΔE , as a function of time may be described by Equation 3.3 (Gabrielli et al., 1979):

$$I_t = \frac{\Delta E}{R_\Omega(R_\Omega + R_P)} \left[R_\Omega + R_P \exp \left(\frac{-t}{\frac{C_{dl}R_\Omega R_P}{R_\Omega + R_P}} \right) \right] \quad (3.3)$$

where the equation has a stationary component:

$$I_\infty = \frac{\Delta E}{R_\Omega + R_P} \quad (3.4)$$

and a transitory component:

$$I_{tr} = \frac{\Delta E R_P}{R_\Omega(R_\Omega + R_P)} \exp \left(\frac{-t}{\frac{C_{dl}R_\Omega R_P}{R_\Omega + R_P}} \right) \quad (3.5)$$

with a time constant, τ_E :

$$\tau_E = \frac{C_{dl}R_\Omega R_P}{R_\Omega + R_P} \quad (3.6)$$

Assuming that $R_P \gg R_\Omega$ the time constant may be reduced to:

$$\tau_E \simeq C_{dl}R_\Omega \quad (3.7)$$

In the case of applying a constant current, ΔI , to the simple modified Randles circuit, the potential response as a function of time, E_t , may be described by Equation 3.8:

$$E_t = \Delta I R_\Omega + \Delta I R_P \left(1 - \exp \left(\frac{-t}{C_{dl}R_P} \right) \right) \quad (3.8)$$

where the time constant, τ_I , is:

$$\tau_I = C_{dl}R_P \quad (3.9)$$

From the time constants in Equations 3.7 and 3.9 it is seen that determination of the polarisation resistance, R_P , with the potentiostatic method will be faster (i.e. shorter time to achieve steady state) than with the galvanostatic method due to the smaller time constant τ_E (Gabrielli et al., 1979). Hence, for passive steel in concrete where the polarisation resistance, R_P , is very high, i.e. $R_P \gg R_\Omega$, steady state should be obtained much faster with the potentiostatic method than with the galvanostatic method.

The same mathematical derivations were given in the work by Gonzalez et al. (1985a). However, in work by Gonzalez et al. (1985a) also the effect of sweep rate when using the potentiodynamic method was considered: By applying a Laplace transformation to the voltage-current behaviour of the simple Randles circuit Gonzalez et al. (1985a) showed that the current response, $I(t)$, for potentiodynamic measurements may be described by Equation 3.10:

$$I(t) = \frac{kt}{R_\Omega + R_P} + \frac{kC_{dl}R_P^2}{(R_\Omega + R_P)} \left[1 - \exp\left(\frac{-t}{\frac{C_{dl}R_\Omega R_P}{R_\Omega + R_P}}\right) \right] \quad (3.10)$$

where k is the potential sweep rate. Derivation of Equation 3.10 with $kdt = dE$ results in Equation 3.11:

$$\frac{dI}{dE} = \frac{k}{R_\Omega + R_P} + \frac{R_P k}{R_\Omega(R_\Omega + R_P)} \exp\left(\frac{-t}{\frac{C_{dl}R_\Omega R_P}{R_\Omega + R_P}}\right) \quad (3.11)$$

For $t = 0$, corresponding to very fast sweep rates, Equation 3.11 is simplified to Equation 3.12:

$$\frac{dI}{dt} = \frac{k(R_\Omega + R_P)}{R_\Omega(R_\Omega + R_P)} = \frac{k}{R_\Omega} \text{ and } \frac{dI}{dE} = \frac{1}{R_\Omega} \quad (3.12)$$

For very slow sweep rates ($t \rightarrow \infty$), i.e. for very low values of k Equation 3.11 is simplified to Equation 3.13:

$$\frac{dI}{dt} = \frac{k}{R_\Omega + R_P} \text{ and } \frac{dI}{dE} = \frac{1}{R_\Omega + R_P} \quad (3.13)$$

From Equations 3.12 and 3.13 it is seen that, depending on the sweep rate used for the potentiodynamic measurement, a value of the polarisation resistance, R_P , between R_Ω and $R_\Omega + R_P$ may be obtained. To minimise the error the sweep rate must be slower the higher the polarisation resistance, R_P . Also, as seen the true polarisation resistance, R_P , can only be calculated if R_Ω is known or if $R_\Omega \ll R_P$, and R_Ω can be neglected.

The effects of delay time and sweep rate were also demonstrated experimentally by Gonzalez et al. (1985a): Polarisation resistance measurements, from which corrosion current densities, i_{corr} , were calculated, were performed on passive steel in mortar (high R_P and C_{dl}) with the potentiostatic and potentiodynamic methods, see Figure 3.5. From the

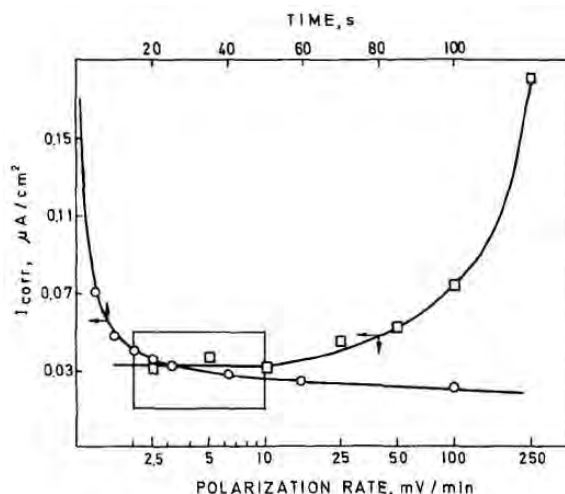


Figure 3.5 Corrosion current density, i_{corr} , as a function of sweep rate (potentiodynamic method, \square) and delay time (potentiostatic method, \circ) for passive steel in mortar exposed to $\approx 100\%$ RH (Gonzalez et al., 1985a).

results, shown in Figure 3.5, it was found that sweep rates between 2.5 and 10 mV per minute, and delay times of 15 to 60 seconds for a 10 mV potential perturbation in anodic direction, gave almost coinciding values. Similar results were obtained in an earlier study by Andrade et al. (1984) where the electrochemical measurements were also compared with gravimetric measurements. Based on the work by Andrade et al. (1984) and own results Gonzalez et al. (1985a) concluded that reliable R_P values can be obtained if a sweep rate of 10 mV per minute is used with the potentiodynamic method or a delay time of 30 seconds is used with the potentiostatic method.

Also Millard et al. (1992) investigated the effect of delay time and sweep rate on the measured polarisation resistance, R_P . In the work by Millard et al. (1992) both potentiostatic, galvanostatic and potentiodynamic measurements were performed on passive and actively corroding reinforcement bars, see Figures 3.6 and 3.7. The measurements on the passive reinforcement, shown in Figure 3.6, clearly agree with the mathematical derivations given by Gabrielli et al. (1979): The potentiostatic measurements of the polarisation resistance, R_P , approached a constant value much quicker than the galvanostatic measurements (Millard et al., 1992). For the actively corroding reinforcement, where $R_P > R_Q$, but R_P is of same magnitude as R_Q , the potentiostatic measurements approached a constant R_P only slightly faster than the galvanostatic measurements.

From the potentiodynamic measurements on passive reinforcement it was observed that the sweep rate had significant influence on the measured polarisation resistance, R_P , see Figure 3.7. However, on the actively corroding reinforcement only a limited effect was

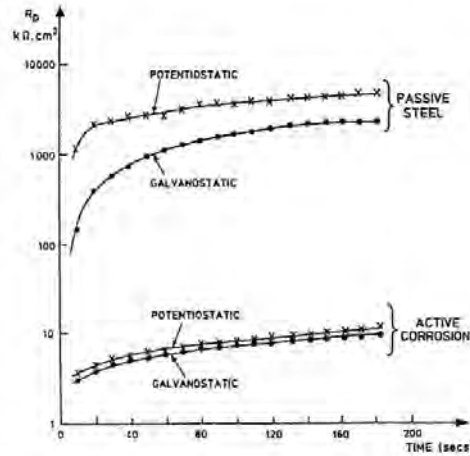


Figure 3.6 Polarisation resistance, R_p , as a function of delay time obtained with potentiostatic and galvanostatic polarisation measurements on passive and actively corroding reinforcement (Millard et al., 1992).

seen. Based on these results Millard et al. (1992) concluded that although errors are introduced when determining the polarisation resistance, R_p , the corrosion current density, i_{corr} , determined using a sweep rate of 10 mV per minute, as suggested by Gonzalez et al. (1985a), will be a good qualitative indicator for the corrosion rate. This also applied for potentiostatic measurements using a delay time of 30 seconds. Similar results and conclusions can also be found in more recent work by Gonzalez et al. (2005).

More recently, Kouřil et al. (2006) examined the potentiodynamic sweep rate's effect on the measured polarisation resistance, R_p , from measurements on stainless steel in artificial concrete pore solutions. Measurements were made in solutions with pH ranging from 8 to 13.5 and chloride content from 0.1 to 150 g per liter and with sweep rates of 60, 30, 7.5 and 2.4 mV per minute. From the measurements considerable non-linear behaviour of the polarisation curves was seen, making a determination of the polarisation resistance, R_p , difficult, see Figure 3.8. The non-linear behaviour was seen to decrease with decreasing sweep rate. Also, the *zero current potential* was seen to differ from the free corrosion potential, E_{corr} . From these observations, Kouřil et al. (2006) concluded that determination of the polarisation resistance, R_p , by the linear polarisation resistance technique is unreliable in the case of steel in the passive state. However, considering the results from the study (Figure 3.8), it can be seen that the polarisation curves obtained with sweep rates of 2.4 and 7.5 mV per minute (0.125 and 0.04 mV per second) show linear behaviour over a large part of the potential scan. Only at the start point, 9 mV lower, i.e. more negative than the free corrosion potential, E_{corr} , a highly non-linear behaviour is observed. The reason for the observed non-linear behaviour is probably a result of the very high polarisation resistance, R_p , and double-layer capacitance, C_{dl} , of the stainless

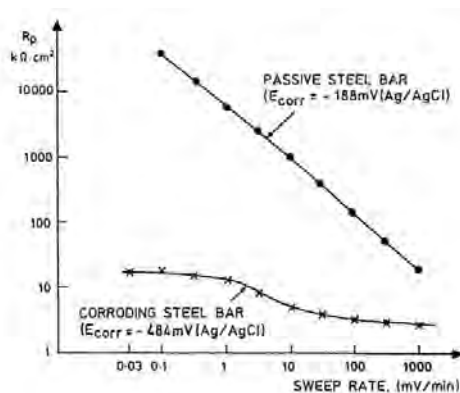


Figure 3.7 Effect of potentiodynamic sweep rate on the measured polarisation resistance, R_P , for passive and actively corroding reinforcement (Millard et al., 1992).

steel combined with the relatively high sweep rates used for the measurements (Gonzalez et al., 1985a) (Millard et al., 1992) (Scully, 2000).

Finally, it should be mentioned that most studies on steel's corrosion behaviour in concrete, performed under laboratory conditions make use of the potentiodynamic method and a sweep rate in the range of 2.5 to 10 mV per minute, see e.g. Sagoe-Crentsil et al. (1992). However, for on-site measurements the galvanostatic method seems to be preferred. The reason for this is the use of surface mounted electrodes: Most often the counter-electrode is placed on the concrete surface on a moist sponge to ensure proper electrical connection. However, due to moisture gradients and varying pressure on the electrode (often hand-held), the ohmic drop over the electrode-concrete surface interface is unknown and may vary during measurements. For the potentiostatic method this will have a direct effect on the polarising potential applied to the embedded steel, whereas a galvanostatic measurement will not be affected by variations in the system resistance as the applied potential is adjusted equivalently.

Ohmic drop compensation

For electrochemical polarisation measurements on steel-concrete systems where a conventional three electrode setup is used, concrete's high electrical resistivity may result in substantial ohmic resistance between the individual electrodes. This means that the actual polarising potential, E_P , at the steel-concrete interface differs from both the potential applied from the counter-electrode and the potential measured with the reference electrode. For accurately measuring and controlling the polarising potential at the steel-concrete interphase, the potential measured with the reference electrode should be compensated for the ohmic resistance between the steel and the reference electrode: An uncompensated measurement of the polarisation resistance will, apart from the true polarisation resistance, R_P , also contain the ohmic resistance, R_Ω , see Equation 3.2. Hence, correct

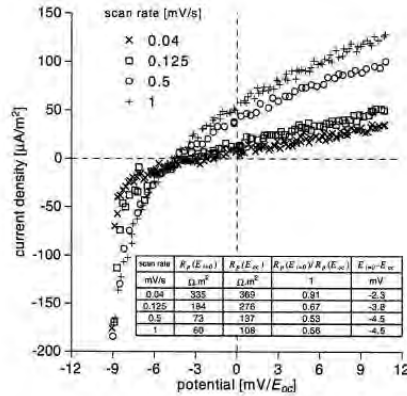


Figure 3.8 Potentiodynamic polarisation curves for stainless steel in an alkaline solution (pH 12.5) with a chloride content of 15 g/litre at various sweep rates (Kouřil et al., 2006).

determination of the true polarisation resistance, R_p , requires knowledge of the ohmic resistance, R_Ω , between the steel bar and the reference electrode. Ideally the ohmic resistance, R_Ω , should be determined continuously during polarisation resistance measurement and the recorded potential response should be continuously compensated. However, the ohmic resistance, R_Ω , can also be determined before the measurement and the constant value used for compensation during the measurement. The ohmic resistance, R_Ω , may also be determined afterwards and the uncompensated measurement then corrected.

With the potentiostatic and galvanostatic methods, an uncompensated measurement, and subsequent correction, will only result in the effective polarising potential, E_p , being smaller than anticipated during the measurement. This is of minor importance unless the ohmic resistance is very high, reducing the intended polarisation potential, E_p , to an unacceptably low value. However, for the potentiodynamic method the ohmic resistance, R_Ω , will result in an ohmic potential drop, E_Ω , that is a function of the applied current, see Figure 3.9. The changing potential drop, E_Ω , results in a changing sweep rate, meaning that the polarisation resistance that is nominally measured with a constant sweep rate will actually be measured with a varying sweep rate. As the obtained polarisation resistance, R_p , is dependent on the sweep rate, high ohmic resistance, R_Ω , may hence affect the obtained polarisation resistance, R_p , although the measurement is corrected subsequently.

At first sight the measurement and compensation for the ohmic resistance, R_Ω , seem fairly uncomplicated and straight forward. However, in the literature it can be seen to have troubled electrochemists and corrosion scientists as long electrochemical measurements have been performed, see e.g. Britz and Brocke (1975), Żakowski and Sokólski (1999), Oelssner et al. (2006) and literature cited herein. As a result of this, ohmic resistance compensation is often seen to be neglected when measurements are performed on steel-concrete systems.

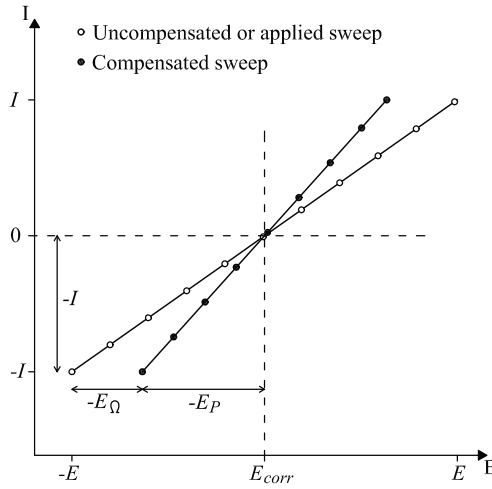


Figure 3.9 Schematic potential sweep illustrating the difference between the applied and the polarising potential due to the ohmic resistance, R_{Ω} .

In cases where the ohmic resistance, R_{Ω} , is low compared to the polarisation resistance, R_P , the introduced error is considered of minor importance (Millard et al., 1992). This may be the case for passive steel in concrete, where the polarisation resistance, R_P , is very high. However, if the steel is actively corroding and the polarisation resistance, R_P , is very low, the polarisation resistance, R_P , may be overestimated, and the calculated corrosion rate underestimated.

A very comprehensive overview of the techniques often used for ohmic resistance compensation is given in a recent work by Oelssner et al. (2006). The presented techniques are mainly used for conventional electrochemical corrosion testing in aqueous solutions, however, a few of the techniques are seen to be applicable for measurements on steel-concrete systems as well. Selected techniques are described in detail in the following.

Current interrupt method With the current interrupt method the polarisation current, I , is interrupted periodically for short time periods within the microsecond range. In these interrupt periods, t_0 , the ohmic potential drop, E_{Ω} , disappears immediately, as the system current is zero (ohms law), while the polarisation potential, E_P , of the working electrode only decreases slowly due to the (charged) capacitance of the double layer, C_{dl} , see Figure 3.10. When subtracting the polarising potential, E_P , measured at the very beginning of the interrupt period, t_0 , from the potential, E , applied during the polarisation period, t_P , the ohmic drop, E_{Ω} , is obtained. By adding this value to the applied potential, E , in the following polarisation period, t_P , the ohmic drop, E_{Ω} , is compensated. This way the applied potential is continuously corrected for the ohmic resistance, R_{Ω} , after each interrupt period, t_0 . Consequently, the interrupt method can

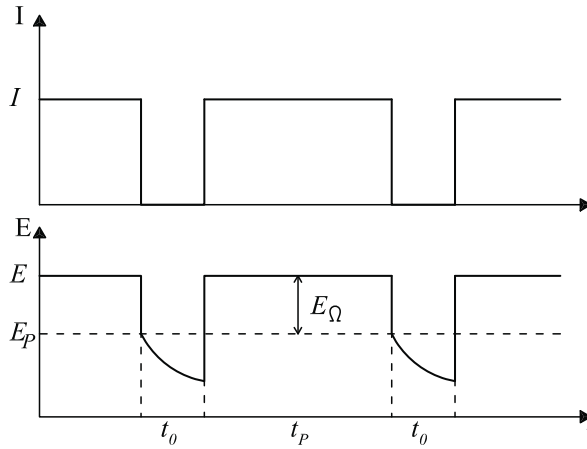


Figure 3.10 Schematic illustration of the current interrupt technique. The parameters are explained in the text. After (Oelssner et al., 2006).

also compensate continuously when the ohmic resistance, R_Ω , changes over time. Usually the ratio between the duration of the interrupt period, and the polarisation period (t_0/t_P) is chosen in the range of 1:10 to 1:1000 (Oelssner et al., 2006). As the exact point between the almost vertical potential drop and the following exponential potential decay is very difficult if not impossible to determine, some potentiostats take a few readings during the interrupt period and extrapolate the measured values to the time zero when the current was interrupted (Oelssner et al., 2006). Applications of the technique in polarisation resistance measurements on reinforced concrete can be found in the work by e.g. Elsener and Böhni (1982), Elsener and Böhni (1983) and Escalante and Ito (1990).

Positive feedback method Positive feedback has probably been the most recommended and applied technique for ohmic resistance compensation. As compensation is executed continuously, with a predetermined constant value, it can be used for fast electrochemical measurements quite suitably. For measurements on steel-concrete systems the technique has been applied in a number of studies (Andrade et al., 1984) (Gonzalez et al., 1985a) (Andrade et al., 2004).

The principle of the positive feedback system is fairly simple: The current applied to the working electrode is measured (as usual) by a so-called *current follower*, with an output potential directly proportional to the applied current. In principle the current follower can be a simple shunt-resistor over which the potential drop is measured. An amount of this potential is fed back to the input of the potentiostat and added to the applied voltage to compensate for the ohmic resistance, R_Ω . The amount of potential looped back into the potentiostat is equal to the degree of compensation.

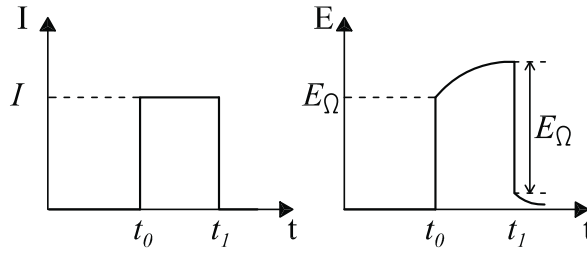


Figure 3.11 *Schematic illustration of the galvanostatic pulse ohmic resistance compensation method. Parameters are explained in the text.*

The positive feedback method for ohmic resistance compensation assumes that the ohmic resistance, R_Ω , remains constant during the measurement. This may not always be the case as the counter and reference electrodes are often placed on the concrete surface on a moist sponge. This may result in huge errors or overcompensation, resulting in the potentiostatic control circuit starting to oscillate or simply failing. The risk of oscillation or failure increases with increasing degree of compensation, but may arise even when a compensation less than 100% is used (Oelssner et al., 2006). Thus the most serious problem with positive feedback compensation is to determine the degree of compensation that should be used prior to initiating the measurement, which can be a difficult task. To find a reasonable compromise between system stability and degree of compensation, the amount of feedback potential (from the voltage follower) fed back into the potential is increased in steps. After each step the system stability is tested until an optimum value is found i.e. the highest degree of compensation that does not cause instability. Consequently, in most cases it is not possible to achieve complete compensation by the positive feedback technique (Oelssner et al., 2006).

Galvanostatic pulse methods With this method a galvanostatic pulse is applied over a very short period of time and the non-controlled potential recorded at a high frequency or after a delay time in the microsecond range, see Figure 3.11. At the very moment, t_0 , when the current, I , is applied the resistance over the double layer will be zero due to double layer capacitance, C_{dl} . The non-controlled potential response, E_Ω , will hence correspond to the ohmic resistance, R_Ω (Ohms law). During the pulse period the potential response will increase exponentially due to the charging of the double layer capacitance, C_{dl} . As for the current interrupt technique, a few measurements of the response may be recorded, though here during the charging period, and the values extrapolated back to the time zero, t_0 , when the pulse was applied. An additional measurement of the ohmic potential drop, E_Ω , can also be obtained when the current pulse is turned off, according to the principle used for the current interrupt method.

This method, which may be considered the most simple, assumes the ohmic resistance, R_Ω , to be constant during measurement of the polarisation resistance, R_P . Also, as the compensation method applies a small perturbation to the working electrode before

the actual polarisation resistance measurement, this should be delayed until the working electrode has depolarised to the initial free corrosion potential, E_{corr} .

3.2.2 Galvanostatic transient technique

Determination of the polarisation resistance, R_P , from analysis of galvanostatically induced potential transients was first investigated by Jones and Greene (1966). Assuming a simple Randles circuit, as shown in Figure 3.4, to describe the electrical behaviour of a steel-concrete system Jones and Greene (1966) derived the relation between potential response, E_t , and time, t , for a constant polarisation current, I , given in Equation 3.8. Based on this equation it was assumed that a linear relationship should exist between $\log(\Delta IR_P / (\Delta IR_P - \Delta E_t))$ and time, t . The polarisation resistance, R_P , which satisfied this relationship was determined by trial and error graphical analysis. From experiments with stainless steel (passive) in aqueous solutions the simple Randles circuit was seen to describe the potential transients accurately for overvoltages up to 5 mV and polarisation times up to 30 minutes. From a comparison with the potentiostatic linear polarisation resistance method the transient analysis technique was found to have a slightly lower accuracy. However measurements could be performed in 20 minutes or less, compared to the several hours typically used for potentiostatic linear polarisation resistance measurements (Jones and Greene, 1966).

Based on the work by Jones and Greene (1966) and Walter (1977), Ijsseling (1986) pointed out that the potential response consists of three separate parts: a quickly rising part deriving from the ohmic resistance, R_Ω , a charge transfer response related to the charging of the double layer capacitance, C_{dl} , and the corrosion process, and a slowly rising portion governed by diffusion polarisation. When the potential transient becomes dominated by diffusion the charging curve, increasing exponentially, changes to an almost linear continuously increasing response (concentration polarisation) preventing attainment of steady state (Gonzalez et al., 1985b) (Newton and Sykes, 1988).

Following the work of the above mentioned authors a number of different approaches for analysis of galvanostatically obtained potential transients have been presented in the literature. Of these, the two most dominant, and very different approaches, are reviewed in the following.

Linearisation

In an extensive experimental study, Newton and Sykes (1988) analysed galvanostatically induced potential transients obtained from steel in alkaline solutions, gels and mortar exposed to saline solutions. Regression analyses were used to divide the measured responses into contributions from diffusion and a number of resistance-capacitor pairs, with various time constants, τ , in series connections. Some attention should be given to this study, as the analysis technique used, originating from the work by Suzuki et al. (1980), has formed the basis for a number of later studies:

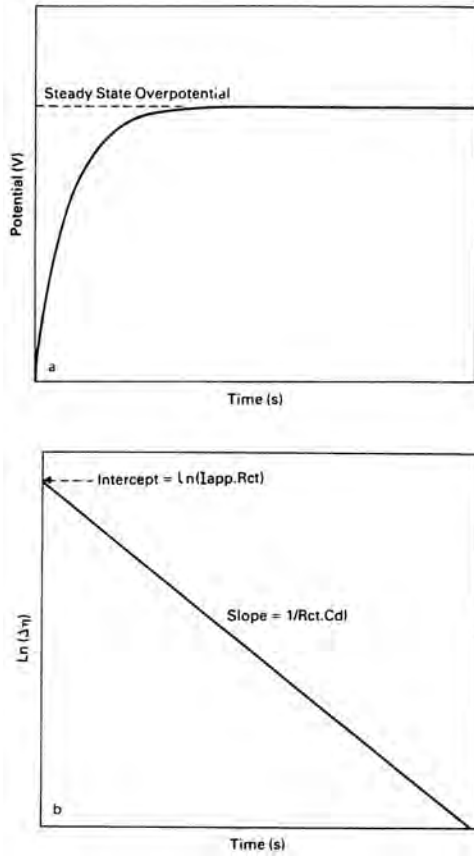


Figure 3.12 Schematic galvanostatic polarisation obtained from a simple Randles circuit.
 a: Potential transient as a function of the time, t . b: $\ln(E_{max} - E_t)$ as a function of time ($\Delta\eta = E_{max} - E_t$) Newton and Sykes (1988).

Again, considering the simple Randles circuit shown in Figure 3.4, the time dependent potential response, E_t , to a constant current, I , may as stated earlier, be described by Equation 3.8. A theoretical potential transient following this equation is illustrated in Figure 3.12, where a steady state potential response, E_{max} , is reached when:

$$\ln(E_{max} - E_t) = \ln(\Delta IR_P) - \frac{t}{R_P C_{dl}} \quad (3.14)$$

Plotting $\ln(E_{max} - E_t)$ as a function of time, t , gives a linear graph, with a slope of $1/(R_P C_{dl})$. Extrapolating the graph to $t = 0$, gives an intercept with a value of $\ln(\Delta IR_P)$, see Figure 3.12 (lower graph).

For systems including more than one resistance-capacitor pair, i.e. more than one time

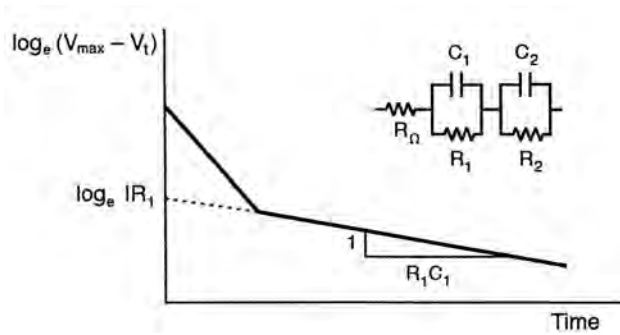


Figure 3.13 Schematic illustration of $\ln(E_{max} - E_t)$ as a function of time, t , for a system with two resistance-capacitor pairs. Note that potentials are given by V instead for E . Also, \ln is shown as \log_e . Reprint from (Law et al., 2001).

constant, τ , the plot of $\ln(E_{max} - E_t)$ as a function of time, t , will be step-wise linear, with each linear portion corresponding to a resistance-capacitor pair, see Figure 3.13. Provided the slopes of the lines are not too similar, successive stages of curve fitting will allow determination of all the circuit values in the system. This is achieved by fitting a straight line to the semi-logarithmic plot over the time period where the longest resistance-capacitor pair is dominant followed by subtraction of its calculated potential response from the curve and the semi-logarithmic plot. The same operation is repeated until all resistance-capacitor pairs have been determined (Newton and Sykes, 1988).

When diffusion effects are significant the potential transient becomes linear when plotted against $t^{\frac{1}{2}}$, with a slope, S , which can be expressed in terms of the Warburg coefficient, σ , and the applied current, I , (Newton and Sykes, 1988):

$$S = \frac{\Delta E}{t^{\frac{1}{2}}} = \left(\frac{8}{\pi}\right)^{\frac{1}{2}} \sigma I \quad (3.15)$$

It is important to remove the diffusion element of the transient by subtracting the $t^{\frac{1}{2}}$ element from the recorded potential transient before linearisation of the data to obtain the values of the existing resistance-capacitor pairs (Newton and Sykes, 1988).

From analysis of potential transients, obtained over a 4 second polarisation period, Newton and Sykes (1988) found that the impedance of active and passive steel in mortar could be separated into three resistor-capacitor pairs, whereas only two pairs could be identified for active steel in gel and solutions with chlorides, see Figure 3.14. Furthermore, it was observed that active steel in both mortar and alkaline chloride gel showed a Warburg diffusion impedance during polarisation opposite to passive steel in these electrolytes. From this it was concluded that two resistor-capacitor pairs are needed to describe the electrochemical process at the steel-electrolyte interface for steel in mortar and aqueous solutions. For steel in mortar the two resistance-capacitor pairs with the longest time

constants were considered associated with the corrosion process together with the Warburg element. Despite this Newton and Sykes (1988) pointed out that it was not entirely obvious, which of the resistance-capacitor pairs should be considered when determining the corrosion current density, i_{corr} , as contribution from the Warburg element continuously and almost linearly increased with time.

In Millard et al. (1995) and Gowers et al. (1996) the same technique was adopted for analysis of potential transients obtained from steel in aqueous solutions and mortar. In Millard et al. (1995) potential transients were measured over a period of 60 seconds at a frequency of 5 kHz: In solution four resistance-capacitor pairs were identified for actively corroding steel, whereas five and three were identified for actively corroding and passive steel embedded in concrete, respectively. In earlier investigations by the authors, resistances, related to the corrosion process, were observed to be in parallel with capacitances with values ranging from 10 to 500 $\mu F/cm^2$. Assuming this to apply for the investigated systems, two of the resistance-capacitor pairs in each system, active as well as passive, were found related to the corrosion process, similar to the observations by Newton and Sykes (1988).

Gowers et al. (1996) investigated the effect of sampling rate, polarisation time and current on the analysis results. It was found that the lowest sample rate at which all resistor-capacitor pairs could be identified was 500 Hz. For actively corroding steel a polarisation time of 10 seconds was required to identify all components, whereas a time of 40 seconds was required for passive steel where the capacitances related to the corrosion processes were higher. When increasing the applied current a higher signal-noise ratio was obtained making distinction between the individual resistance-capacitor pairs easier, however, if the response was outside the linear region the polarisation resistance, R_P , could in some cases be underestimated (Gowers et al., 1996). In the study by Newton and Sykes (1988), a lower number of resistance-capacitor pairs were generally found. This could be correlated with the use of a sampling frequency lower than the 500 Hz as suggested by Gowers et al. (1996).

For separation of the resistance-capacitor pairs related to the corrosion process and to the bulk concrete, Gowers et al. (1996) also performed a series of measurements where the distance from the counter and reference electrodes to the reinforcement bar was increased. By increasing the distance the resistances related to the corrosion process should remain constant whereas the resistances related to the bulk concrete should increase. For actively corroding and passive steel in concrete all resistances in parallel with capacitances larger than 20 and 50 $\mu F/cm^2$, respectively, were seen to increase as a function of distance. These were therefore considered to be related to the electrical properties of the bulk concrete. From this it was suggested that the resistances related to the corrosion process, as a general rule, are in parallel with and can be identified from, capacitors with values lower than 100 $\mu F/cm^2$.

Also Videm (1997) adopted the linearisation technique for analysis of potential transients: Contrary to other studies, only two resistance-capacitor pairs were needed to describe the

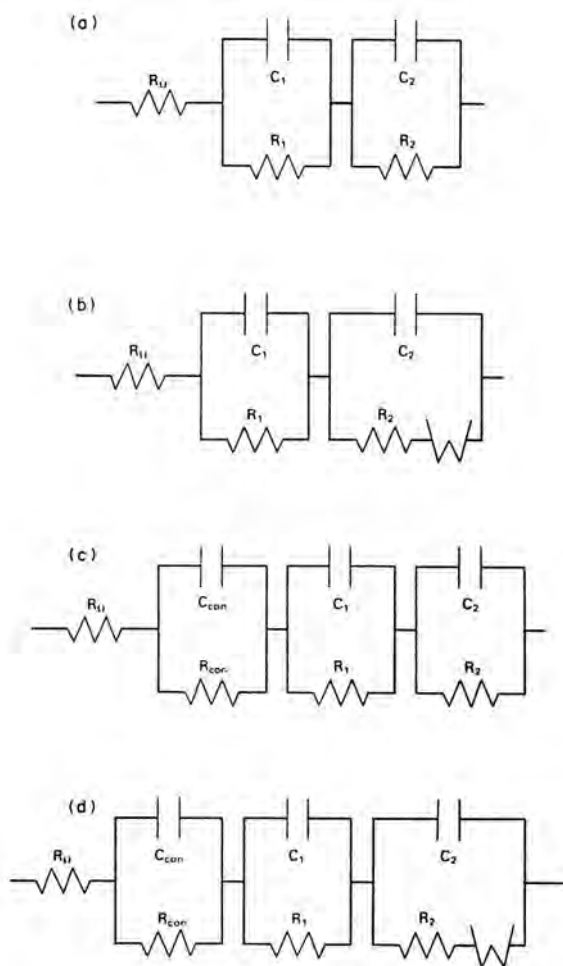


Figure 3.14 Equivalent circuits obtained from potential transient analysis. a) Steel in solution, b) steel in gel, c) passive steel in concrete, d) active steel in concrete (Newton and Sykes, 1988).

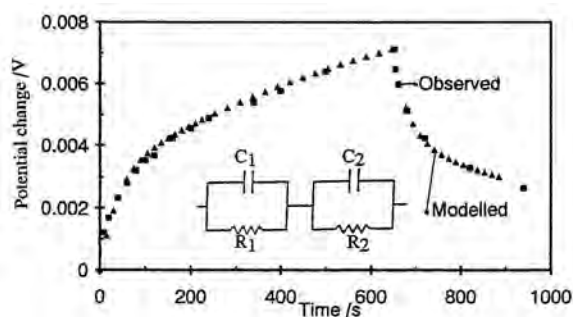


Figure 3.15 Potential transient for passive steel in mortar obtained with a galvanostatic current density of $0.022 \mu\text{A}/\text{cm}^2$. Two resistance-capacitor pairs are used to fit the recorded transient (Videm, 1997).

potential transients of both passive and actively corroding steel when a polarisation period of 600 seconds was used, see Figure 3.15. No differences between experiments performed in alkaline solutions and mortar were observed. Considering Figure 3.15, an indication of diffusion may be seen as the potential transient after approximately 300 seconds increases almost linearly. This is also commented by Videm (1997). However, the diffusion element as suggested by Newton and Sykes (1988) (see Equation 3.15) is not considered in the analysis. From the investigations, it was concluded that the corrosion current density, i_{corr} , could not be calculated from the data as the resistance-capacitor pair associated with the corrosion process could not be identified.

The most recent use of the linearisation technique seems to be the studies by Law et al. (2000b) and Law et al. (2001) who showed that it is not possible to attribute the individual resistive components to the corrosion process based solely on their associated capacitance. From the studies it was concluded that each individual system must be investigated separately. Only by taking a set of galvanostatic potential transient measurements at increasing distances from the reinforcement it is possible to determine which resistive components should be included in the calculation of the corrosion current density, i_{corr} (Law et al., 2000b).

A series of correlated potentiostatic linear polarisation resistance and galvanostatic potential transient measurements were also performed in the studies by Law et al. (2000b) and Law et al. (2001). For a direct comparison between the two techniques, all resistive components identified from the galvanostatic transient analysis were multiplied, as these would all be measured with the linear polarisation resistance technique. Corrosion current densities, i_{corr} , calculated from the linear polarisation resistance measurements were generally somewhat lower than those calculated using the potential transient technique. Differences in corrosion current densities, i_{corr} , fell within a factor of 2.5 with the largest differences observed at the highest corrosion rates. From these measurements it was determined that evaluating the magnitude of the corrosion rate seemed more meaningful

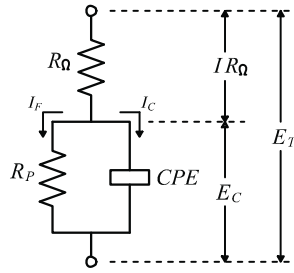


Figure 3.16 Equivalent Randles circuit modified with a Constant Phase Element (CPE). Parameters are explained in the text. After (Sagües et al., 1996).

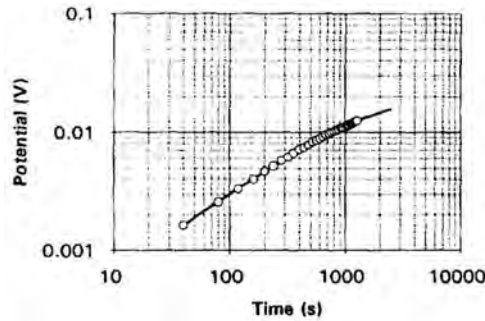


Figure 3.17 Measured (circles) and modelled (solid line) potential response (without ohmic resistance, R_Ω) to a current pulse of $0.25 \mu A$ as a function of the polarisation time (Sagües et al., 1996).

than trying to establish a high degree of precision with any of the two techniques.

CPE modified randles circuits

In Sagües et al. (1996) potential transients were analysed using a modified Randles circuit where the double layer capacitance, C_{dl} , was replaced by a Constant Phase Element (CPE) describing the non-ideal capacitive behavior, i.e. the deviation from exponential behavior, of the inhomogeneous steel-concrete interface, see Figure 3.16. Fitting of experimental data to obtain the circuit parameters was done by using a numerical procedure derived from analysis of the circuit in the time domain. A series of correlated galvanostatic potential transient and Electrochemical Impedance Spectroscopy (EIS) measurements were performed on reinforced concrete specimens with varying binder composition. The modified system, numerically fitted to the experimental data, was shown to describe the recorded potential transients well over the measurement periods of 1300 seconds, see Figure 3.17.

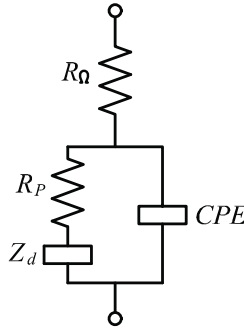


Figure 3.18 Equivalent Randles circuit modified with a Constant Phase Element (CPE) and a Warburg diffusion element (Z_d).

In a later work by Feliu et al. (1998), potential and current transients obtained from a wide range of reinforced concrete specimens, under highly varied exposure conditions were analysed. Plotting the potential transients as a function of $t^{\frac{1}{2}}$, as previously done by Newton and Sykes (1988), showed markedly straight sections after times in the range of 25 to 50 seconds, strongly suggesting diffusion control. This was observed for all specimens irrespective of their corrosion state, moisture content, age, etc. Based on these observations the effect of diffusion was included in the CPE modified Randles circuit, suggested by Sagües et al. (1996), by adding a Warburg element (Z_d) in series connection with the polarisation resistance, R_p , see Figure 3.18. However, a method for extracting the circuit parameters was first proposed in the work by Feliu et al. (2004). The proposed method was based on least squares fitting of a simulated response to the experimentally recorded potential transient. A fairly complex algorithm, based on a discretisation of the fractional differential operator, derived from the differential equation describing the equivalent system, was used for calculating the simulated response (Feliu et al., 2004).

Finally, Feliu et al. (2005) demonstrated the applicability of the Randles circuit modified with CPE and Warburg elements, as well as the applicability of the method for extracting the circuit parameter. Five potential transients obtained from steel in concrete were selected from the literature and the CPE-Warburg Randles circuit fitted to these using the proposed method (Feliu et al., 2005). The *goodness of the fits* - as mentioned in the work - was considered to serve as a parameter of the model's validity together with the obtained polarisation resistances, R_p , that should be in consonance with the corrosion state of the reinforcement. Selected results as presented by Feliu et al. (2005) are shown in Figure 3.19. As seen from the graphs in Figure 3.19 the calculated potential transients were superimposed with notable exactitude over the experimental data. Together with the calculated polarisation resistances, R_p , found to correlate well with the corrosion state of the reinforcements Feliu et al. (2005) considered these results experimental evidence for the applicability of the CPE-Warburg modified Randles circuit.

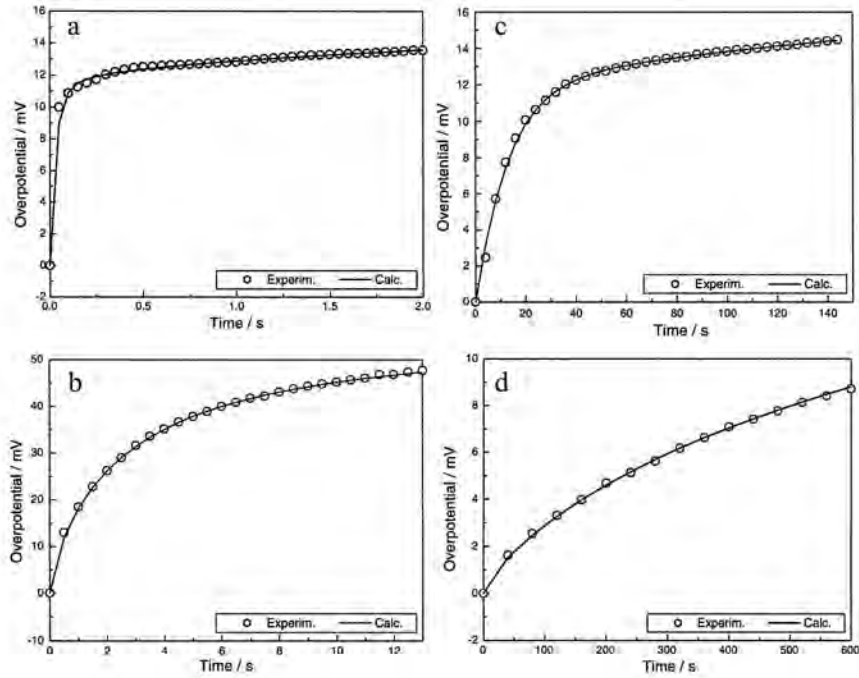


Figure 3.19 Comparison of experimental (full line) and CPE-Warburg Randles circuit model fit (circles). Reprint from (Feliu et al., 2005).

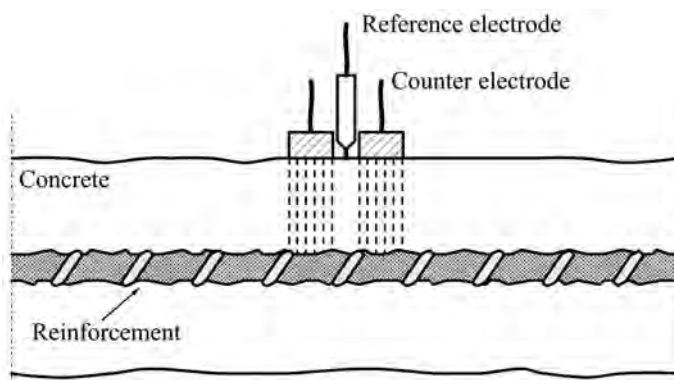


Figure 3.20 Schematic illustration of the current flow from a small counter-electrode placed on the concrete surface to a reinforcement bar with uniform general corrosion.

3.3 Current confinement

In real size concrete structures, the main difficulty when using the polarisation resistance techniques arises from the reinforcement's quasi-infinite length. As a polarisation of the entire reinforcement system is not practical and would not provide information on local conditions, counter-electrodes of much smaller dimensions than the concrete structure under test are used. Instead of distributing uniformly over the whole metallic surface, the electrical signal applied by the counter-electrode placed on the concrete surface, tends to spread laterally and vanish with increasing distance from the counter-electrode. The distance along the reinforcement over which the electrical signal spreads out is primarily a function of the polarisation resistance, R_P , of the reinforcement, i.e. the corrosion state, and the concrete resistivity, ρ_c (Feliu et al., 1987). If the reinforcement is corroding at a fast rate, the polarisation resistance, R_P , will be very low. As the applied signal follows the path of lowest resistance to the steel, the signal will only be distributed over a very small area, see Figure 3.20. On the other hand, if the steel is passive and the polarisation resistance, R_P , high, the signal will spread laterally over a much greater area of the reinforcement, see Figure 3.21. As a result, a calculation of the *true* polarisation resistance, R_P , is impossible due to the unknown polarisation area, A . Only an apparent polarisation resistance, R_P^{app} can be calculated, assuming the polarised length of the reinforcement to be equal to the diameter of the counter-electrode.

A number of approaches have been suggested in the literature to solve this problem. Of these, the current confinement technique has been the most promising and is in fact the only technique which has been adopted in commercial instruments for on-site corrosion rate measurements. This section will therefore focus on this technique. However, for completeness and to follow the development through time, a brief review of earlier approaches is also included.

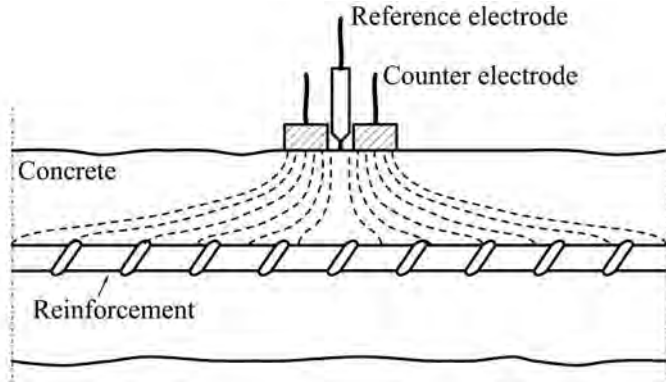


Figure 3.21 Schematic illustration of the lateral current spread occurring when a small counter-electrode is used for R_P measurements on passive steel.

In the work by Feliu et al. (1987) (identical to (Feliu et al., 1988)) an approach based on a *transmission line* model was developed. The authors proposed an approximate model providing a simple mathematical solution for modelling the spreading of an electrical signal along the reinforcement in a beam, see Figure 3.22. Two mathematical solutions were derived from the model. The first considered the relationship between the apparent polarisation resistance, R_P^{app} , the true polarisation resistance, R_P , and the concrete resistance, R_Ω , per unit length of the beam. From a mathematical treatment of the model it was shown that the true polarisation resistance, R_P , for a long beam can be determined from:

$$R_P = \frac{4 (R_P^{app})^2}{R_\Omega} \quad (3.16)$$

The second one, often referred to as the *attenuation method* was based on measuring the decrease of the applied potential with increasing distance from the counter-electrode. By taking readings of the potential, $E(x)$, at two different distances from the counter-electrode, x_1 and x_2 , it was shown, also by mathematical treatment, that the polarisation resistance, R_P , can be determined by:

$$R_P = \frac{R_\Omega}{\alpha^2} \quad (3.17)$$

where

$$\alpha = \frac{1}{x_2 - x_1} \ln \frac{E(x_1)}{E(x_2)} \quad (3.18)$$

For application of the two approaches, one must first determine, in addition to the apparent polarisation resistance, R_P^{app} , or the α value, the concrete resistance, R_Ω , per unit length of beam. As an approximate value it was suggested to measure the concrete resistivity, ρ_c , and divide this value with the cross section area of the beam, neglecting the embedded reinforcement. From correlated measurements, where a large counter-electrode

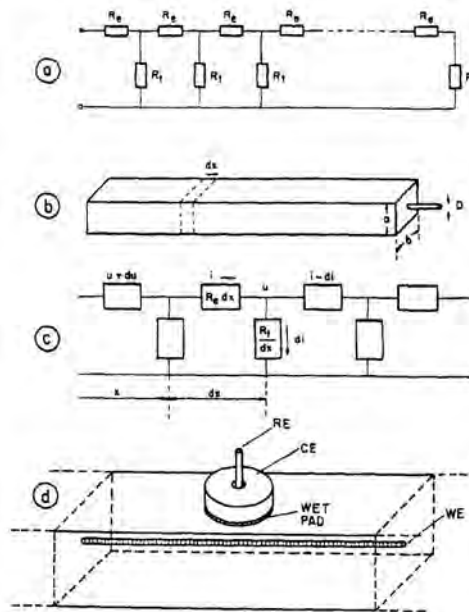


Figure 3.22 Model circuit for interpreting the lateral signal spreading. a) Transmission line model. b, c) Flow of current through an infinitesimally small element of the beam shown in d) (Andrade and Alonso, 1995).

ensuring uniform polarisation was used for reference measurements, the two approaches were shown to clearly distinguish passive ($R_P \approx 10^5 - 10^6 \Omega \text{cm}^2$) and actively corroding steel ($R_P \approx 10^3 - 10^4 \Omega \text{cm}^2$) (Feliu et al., 1987). The *transmission line* model was subsequently extended to orthogonally reinforced concrete slabs assuming radial propagation of the electrical field from the counter-electrode (Feliu et al., 1989b). Also here fairly good correlation was found between polarisation resistance values obtained with the two approaches and a large counter-electrode, giving a uniform polarisation (Feliu et al., 1989a) (Feliu et al., 1989b).

It should be noticed that the *transmission line* models assume the polarisation resistance, R_P , i.e. the corrosion rate as well as the concrete resistance, R_Ω , to be constant throughout the entire beam or slab. In Feliu et al. (1988) this was considered to be approximately true for carbonation induced corrosion, as the corrosion is usually uniform throughout the carbonated zone. Also for chloride induced corrosion this was said to be approximately true, as the attack begins locally but extends over time to cover the entire steel area. However, several studies in which gravimetric measurements have been performed have shown that ideal uniform corrosion is seldom obtained even though chlorides are admixed in the concrete (Luping, 2002) (Liu and Weyers, 2003) (Andrade and Martinez, 2005).

Another approach, based on measurements with counter-electrodes of increasing size, was later proposed by Feliu et al. (1990a). By increasing the counter-electrode size it turned out that the measured apparent polarisation resistance, R_P^{app} , approached the true polarisation resistance, R_P . By plotting the apparent polarisation resistance, R_P^{app} , as a function of the counter-electrode size in a log-log diagram, it was shown that the true polarisation resistance, R_P , could be determined by extrapolating to a counter-electrode size of 10^3cm^2 and 10^4cm^2 , for active and passive steel, respectively, see Figure 3.23. The polarisation resistance values considered to be true, i.e the reference values, were determined using the two approaches derived from the transmission line model as well as from a large counter-electrode ensuring uniform polarisation (Feliu et al., 1990a). It should be noted that this approach, similar to the transmission line model, assumes the polarisation resistance, R_P , to be constant. Also, the question arises: To which counter-electrode size should be extrapolated when performing measurements on-site where the corrosion state, chloride and moisture content are unknown?

The concept of a guard ring for confining the electrical signal from the counter-electrode to a predetermined area on the working electrode was first introduced by Escalante et al. (1980). According to this proposition, the use of a second electrode, positioned concentrically around the counter-electrode, should confine the electrical signal to a well defined area on the reinforcement in the concrete, see Figure 3.24. To obtain this, both electrodes should be maintained at the same electrical potential with respect to the working electrode: Thus, while the central-counter electrode polarises a local and well defined area of the reinforcement, the outer counter-electrode, i.e. the guard ring, polarises the surrounding reinforcement. As the current applied from the central counter-electrode is known, and the area of the reinforcement affected by it, is also known, the true polarisa-

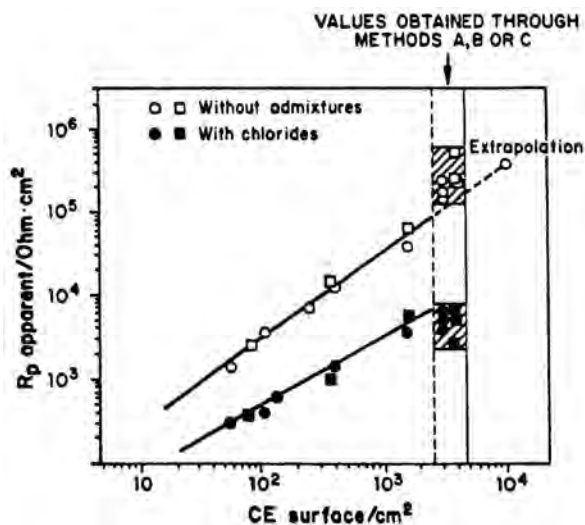


Figure 3.23 Graphical extrapolation of apparent polarisation resistances, R_p^{app} , in order to determine the true polarisation resistance, R_p . Reference values (methods A-C) were obtained using the two approaches from the transmission line model and a large counter-electrode ensuring a uniform polarisation (Feliu et al., 1990a).

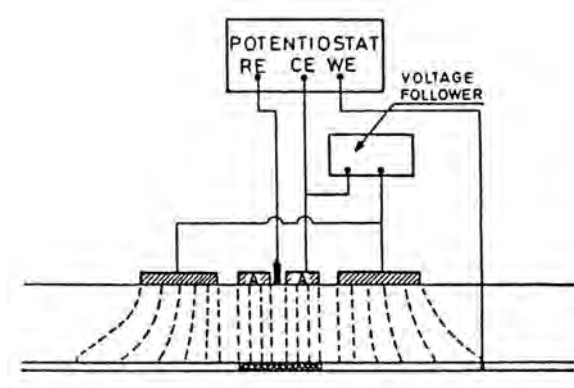


Figure 3.24 Schematic illustration of the guard ring (external CE) in the ideal case where the current lines (dashed lines) from the central counter-electrode are directed to the reinforcement directly below it (Feliu et al., 1989c).

tion resistance, R_P , can be determined immediately from the recorded potential response.

In Feliu et al. (1989c) (identical to (Feliu et al., 1990b)) the efficiency of the guard ring concept, proposed by Escalante et al. (1980), was investigated through a series of measurements on orthogonally reinforced concrete slabs with passive and actively corroding reinforcement. Polarisation resistance measurements were performed with guard rings of varying diameters (distance between rings) and widths while the geometry of the (inner) counter-electrode was kept constant. For evaluation of the measured polarisation resistance values, correlated measurements were performed using a large counter-electrode ensuring uniform polarisation of the reinforcement. From the investigations it was seen that although the geometry of the electrode assembly had some influence, the guard ring was not able to effectively confine the applied signal to a well defined area on the reinforcement when measuring on passive steel. As a result the polarisation resistance values measured on the passive steel were 3 to 10 times lower than the reference values, resulting in overestimation of the corrosion rate by a factor 3 to 10. On the other hand, polarisation resistance values measured on actively corroding reinforcement only differed 20 to 30 % from the reference values. Based on these observations it was concluded that the degree of success in the application of the guard ring technique depends on the polarisation resistance, R_P , to be measured: the higher the polarisation resistance, R_P , the less possibility there is in confining the electrical signal below the counter-electrode. Similar observations were reported by Kranc and Sagües (1993) from a numerical study where the guard ring technique was employed together with EIS for measuring the polarisation resistance, R_P . From the numerical simulations in the work by Kranc and Sagües (1993) it was found that the guard ring arrangement was only successful in measuring the polarisation resistance, R_P , when corrosion was active (low polarisation resistance, R_P), uniform and the size of the electrode assembly large compared to the concrete cover.

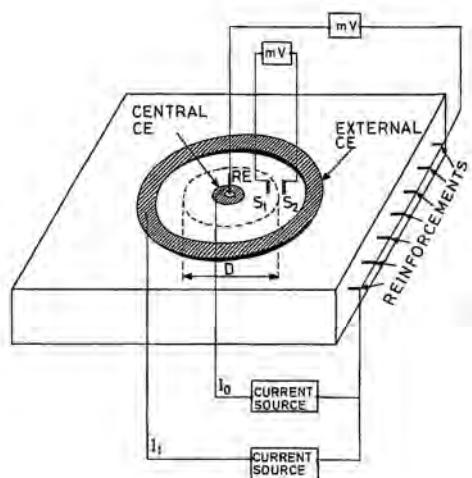


Figure 3.25 Sensorised guard ring: schematic illustration of the electrode assembly with counter-electrode (central CE), guard ring (external CE), central reference electrode (RE) and sensors (S_1 and S_2). The punctuated circle with diameter D indicate the area to which the current applied from the counter-electrode is confined (Feliu et al., 1990a).

Despite the reported difficulties and limitations of the guard ring technique using potential control the technique has been adopted, and is still used in a commercially available instrument for on-site corrosion rate measurements (GalvaPulse instrument from FORCE Technology) (Elsener et al., 1997) (Luping, 2002) (Gepreags and Hansson, 2004).

In Feliu et al. (1990a), further development of the guard ring technique was presented. As a new approach, two additional reference electrodes (often referred to as sensors) for controlling the guard ring were included in the electrode assembly, see Figure 3.25. To confine the signal from the counter-electrode to a constant and well defined area on the reinforcement, the initial potential difference between the two sensors should be maintained during a measurement: Before any electrical signals are applied from the electrode assembly, a difference in potential may exist between the two sensors, either as a result of a slight difference between the two sensors or due to macro-cells. This difference in potential is taken as reference. When a galvanostatic current is applied to the reinforcement from the counter-electrode, the difference in potential between the two sensors will change as the electrical field changes. Maintaining this current, the potential difference between the sensors is taken to the reference value, by applying an additional current from the guard ring. In order to maintain the reference value between the sensors during the entire measurement, the guard ring current is continually adjusted by feedback.

To investigate the efficiency of the sensorised guard ring Feliu et al. (1990a) performed a series of measurements almost identical to those in the earlier work where the simple guard

ring technique was investigated (Feliu et al., 1989c): Beside the diameter and the width of the guard ring, also the positioning of the two sensors was investigated. Furthermore, a series of measurements on networks of passive electrical resistors, imitating reinforced concrete slabs were also performed. The results from the reinforced concrete slabs showed that the distance between the counter-electrode and the guard ring as well as the positioning of the two sensors has little influence on the measured polarisation resistance, R_P , as long as the separation between these is not excessively little. Also, from the measurements on the electrical networks it was found that the sensorised guard ring confines the counter-electrode current to a circular area with a radius equal to the distance from the center of the electrode assembly to the central point between the two sensor electrodes. In general it was concluded that, contrary to the simple potential controlled guard ring, the accuracy of the sensorised guard ring was independent of the polarisation resistance, R_P , to be measured.

A patent on the sensorised guard ring technique was subsequently published and a commercially available instrument for on-site corrosion rate measurements developed (Feliu et al., 1993). After introduction of the instrument; GECOR from Geocisa, Spain, several studies comparing this with other commercially available instruments were published, see e.g. Flis et al. (1993) and Flis et al. (1995). In these studies the performance of the different instruments was characterised by field measurements on concrete structures in mild, moderate and aggressive climates. In general, it was found that varying corrosion current densities, i_{corr} , were obtained with the different instruments. The main reason for the varying corrosion current densities, i_{corr} , was considered a result of some instruments using current confinement and others not. Despite this, the different instruments were all deemed appropriate for inspection, monitoring and assessment of the corrosion rate of steel in concrete.

In Gonzalez et al. (1995b) the developers of the sensorised guard ring investigated the suitability of the GECOR instrument and other electrochemical techniques, for differentiating areas on embedded reinforcement bars with high and low corrosion activity. For the study a reinforced concrete beam was cast: one half of the beam length with admixed chloride and the other half without chloride. As reinforcement three deformed carbon steel bars were used: one spanning the full beam length (continuous bar) and two spanning half the length (discontinuous bar), i.e. embedded in the chloride admixed and chloride free concrete, respectively. Half-cell potential, polarisation resistance and macro-cell current measurements were performed on the concrete surface along the continuous and discontinuous reinforcement bars. Polarisation resistance measurements were performed with the GECOR instrument, and the potentiostatic linear polarisation resistance technique, using a small counter-electrode without current confinement. Macro-cell currents were measured between a small stainless steel counter-electrode placed on the concrete surface and the reinforcement connected through an ammeter. From the investigations it was found that neither the half-cell potential nor macro-cell current measurements could be used for differentiating passive and active areas on the continuous reinforcement bar. This was considered a result of the entire reinforcement bar being polarised anodically. On the contrary, the polarisation resistance technique using a small counter-electrode

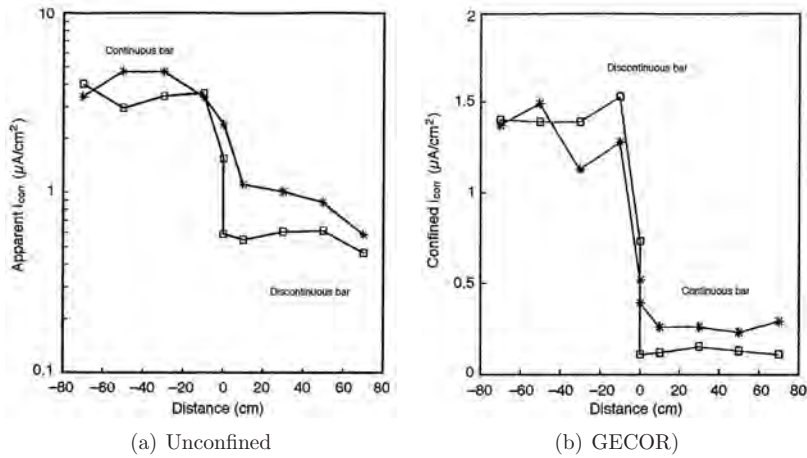


Figure 3.26 Variation of the corrosion current density, i_{corr} , along the continuous and discontinuous reinforcement bars, measured with a small unconfined counter-electrode (left), and the GECOR instrument using the sensorised guard ring (right) (Gonzalez et al., 1995b).

and no confinement was capable of distinguishing passive and active areas. However, the measurement technique led to substantial errors in the estimation of the corrosion current density, i_{corr} , for the passive areas. Here the measured values were seen to be approximately 5 to 10 times too high. On the other hand, it was found that active and passive areas were much more clearly distinguished when using the GECOR instrument. By moving the electrode assembly 10 cm to the left and the right of the boundary between the chloride containing and chloride free concrete the corrosion current density, i_{corr} , varied by a factor 10 to 30. In addition, the values obtained for the passive area were virtually identical to the corrosion current densities, i_{corr} obtained over the discontinuous bar in the chloride free concrete. The results from both types of polarisation resistance measurements, i.e. with the GECOR instrument and the unconfined electrode assembly are shown in Figure 3.26.

The remarkable precision of the GECOR instrument for differentiating passive and actively corroding areas on reinforcement in concrete was investigated further by Law et al. (2000a). From measurements on reinforced concrete slabs it was found that the orientation of the two sensor electrodes with respect to the embedded reinforcement affected the obtained polarisation resistance, R_p , when measuring over passive steel next to an actively corroding area: In the case where the sensors were orientated towards the active steel, the highest polarisation resistance, R_p , (lowest corrosion current density, i_{corr}) was obtained, consistent with passive steel. For all other orientations a significantly lower polarisation resistance, R_p , was observed. This was explained by the applied current being drawn towards the active steel, due to the lower polarisation resistance, R_p . Thus, when the sensors were orientated in the direction to which the current was drawn they detected

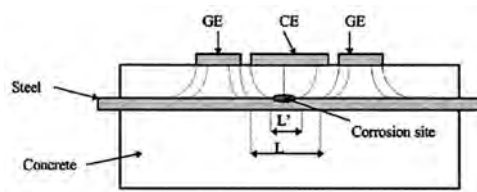


Figure 3.27 Schematic illustration of the current distribution between the GECOR electrode assembly and a reinforcement bar with a small corroding area (Liu and Weyers, 2003).

the change in steel potential being induced by this current. However, when not orientated in this direction no significant changes were detected. The current applied from the guard ring will then not be sufficient to prevent the lateral spread of the counter-electrode current towards the active steel. As a result a higher corrosion rate than that actually occurring below the electrode assembly will be indicated (Law et al., 2000a). This was also observed when measuring over passive reinforcement with numerous active areas nearby. When the electrode was directly over an actively corroding area, no effect of the orientation of the sensors was observed.

A similar phenomenon was reported by Liu and Weyers (2003) from an extensive experimental study where corrosion current densities, i_{corr} , obtained with the GECOR and 3LP instruments were compared with gravimetric measurements. Measurements were performed over a five year period on 40 reinforced concrete slabs cast with different amounts of admixed chloride, cover thickness and reinforcement diameters. From the investigations it was found that the GECOR instrument, using the sensorised guard ring underestimated the corrosion current density, i_{corr} , by a factor 4 to 6. After excavating the reinforcement bars for the gravimetric measurements, subsequent to the five year measurement period, it was seen that corrosion was non-uniform with randomly positioned corroding areas. Also, most of the corroding areas were located on the upper halves of the bars. From these observations Liu and Weyers (2003) concluded that the underestimation was a result of the sensorised guard ring not being able to properly confine the applied current when the corroding area below the electrode assembly was much smaller than the electrode assembly: In this case the actual polarisation area, to which most of the current was drawn, was much smaller than the assumed confinement area used for calculating the corrosion current density, i_{corr} , resulting in the underestimation, see Figure 3.27.

On the contrary, the 3LP instrument not using current confinement, was seen to overestimate the corrosion current density, i_{corr} , by a factor of approximately 1.5 compared to the gravimetric measurements when measuring on actively corroding reinforcement. This was suggested a result of the instrument using a too high B value (41 mV, which applies for passive steel) or an underestimation of the actual polarisation area.

The efficiency of the sensorised guard ring technique in the case of general and intense

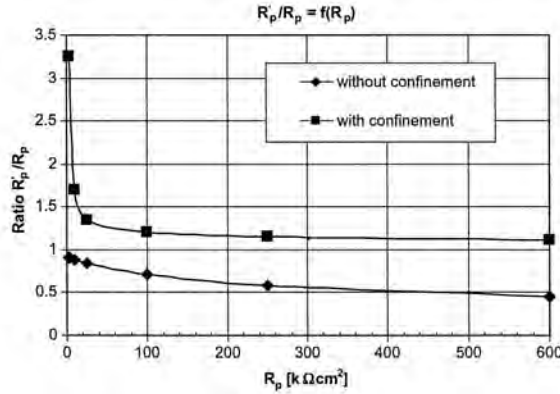


Figure 3.28 Relation between the measured and true polarisation resistance (R'_p/R_p ratio) as a function of the polarisation resistance, R_p , for measurements without confinement and with the sensorised guard ring (Wojtas, 2004a).

localised corrosion was subsequently investigated in the work by Wojtas (2004a) and Wojtas (2004b) from numerical simulations: Two and three dimensional electrical passive networks simulating a concrete beam with a single reinforcement bar and an orthogonally reinforced concrete slab were used, respectively. In the case of uniform corrosion, the effect of the polarisation resistance, R_p , to be measured and the concrete resistivity, ρ_c , was investigated. For localised corrosion, the size of the corroding area on an otherwise passive reinforcement bar was investigated. For comparison, simulations with an electrode assembly without current confinement were performed.

From the results obtained in the case of uniform corrosion, shown in Figure 3.28, it was concluded that correct determination of the polarisation resistance, R_p , over the whole range of corrosion activities (R_p values to be measured), is not possible either with the sensorised guard ring or without current confinement. At high corrosion rates (low R_p values) the sensorised guard ring was seen to deliver polarisation resistances up to 3.3 times higher than the (assumed) true values, as both the counter-electrode and guard ring currents were drawn to the reinforcement directly below the electrode assembly. For the very high corrosion rates, i.e. very low R_p values, more correct R_p values were obtained without current confinement. However, in the passive state (high R_p values) polarisation resistance values closest to the (assumed) true values were obtained with the sensorised guard ring.

From the simulations of the reinforcement with localised corrosion, too high polarisation resistance values, i.e. too low corrosion current densities, i_{corr} , were seen to be obtained from both measurements with and without current confinement. Although, too low corrosion current densities, i_{corr} , were obtained with both electrode assemblies, the errors were a factor 1.6 to 4 times greater, when the sensorised guard ring technique was used (compared to the unconfined measurements). This is seen to be in good agreement

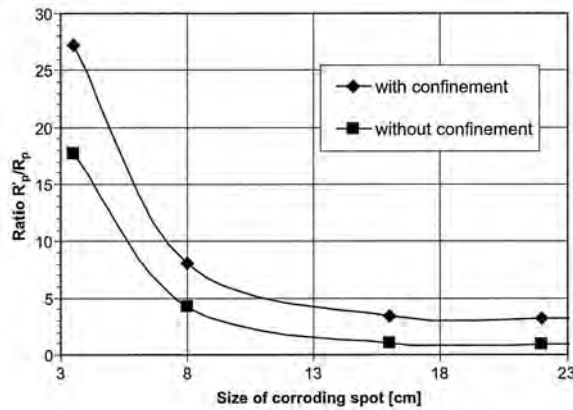


Figure 3.29 Relation between the measured and true polarisation resistance (R'_P/R_P ratio) as a function of the size of the corroding area for measurements without confinement and with the sensorised guard ring (directly over the active area) (Wojtas, 2004a).

with the observations reported earlier by Liu and Weyers (2003).

In what seems to be the most recent publication within this field, contrary results have been reported by Andrade and Martinez (2005). In their work corrosion rate measurements were performed with the GECOR instrument (version 6) on reinforced concrete slabs (400×350 mm) with varying amounts of admixed chloride. For evaluation of the measurements correlated linear polarisation resistance measurements were performed using a conventional laboratory potentiostat and a large counter-electrode ensuring uniform polarisation. Furthermore, after the test period with a duration of 100 days the reinforcement bars were excavated and gravimetric measurements performed.

On passive reinforcement with high R_P it was observed that in the case of a very low concrete resistivity (<1-4 kOhm×cm) the sensorised guard ring was not able to efficiently confine the counter-electrode current. As a result much too high corrosion current densities, i_{corr} , were obtained compared to the correlated linear polarisation resistance measurements giving values in the range of 0.01 to 0.1 $\mu A/cm^2$. Although not demonstrated, it was stated that when the concrete resistivity is higher the sensorised guard ring is able to confine the applied current correctly.

The predicted weight losses, calculated from the measurements with the GECOR instrument and the conventional laboratory potentiostat, plotted against the results from the gravimetric measurements are shown in Figure 3.30. From these results it was concluded that the GECOR instrument using the sensorised guard ring technique provides values of corrosion rate that are similar to those of the gravimetric technique, even in areas with pitting corrosion. The maximum error detected for the GECOR measurements

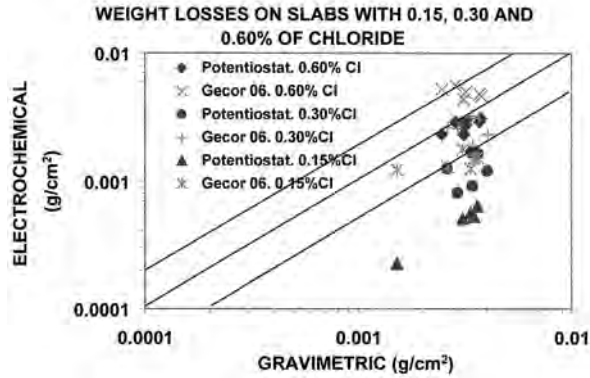


Figure 3.30 Comparison between electrochemical and gravimetric weight losses (Andrade and Martinez, 2005).

when compared to the gravimetric weight losses was stated to be within a factor 2. In contrast to this statement, it is later explained that after correction of the corrosion rate measurements, with a *pitting factor* 10 (to be multiplied), the results are even closer to the gravimetric measurements. The pitting factor 10 was earlier considered by the authors as an estimation of the relation between the total area of steel and the real size of the corroding area (Gonzalez et al., 1995a).

Chapter 4

Experimental work

This chapter will give a detailed description of the experimental work, which was performed during the research project. The chapter is divided in two main sections: The first section *Effect of confinement techniques* describes an experiment (Experiment A in Figure 4.1) where the functionality and efficiency of various current confinement techniques are investigated. The performance of selected commercial corrosion rate instruments is also investigated in this experiment. The second section *Effect of measurement technique, procedure and exposure* describes an experiment (Experiment B in Figure 4.1) where the effect of the electrochemical technique and the polarisation time and current on the measured polarisation resistance is investigated. In this experiment the effect of temperature and relative humidity on the corrosion rate of actively corroding steel in concrete is also investigated. The approach, experimental variations and the methods used in the two experiments are summarised in Figure 4.1.

4.1 Effect of confinement techniques

A new methodology for quantitative assessment of confinement techniques is presented in the following. Contrary to earlier approaches, this methodology includes: a) monitoring of the corrosion rate instrument's operation, and b) monitoring of the current distribution between the instrument's electrode assembly placed on the concrete surface and an embedded segmented reinforcement bar. Combining this with *classical* electrochemical measurements giving information on the actual corrosion rate of the segmented reinforcement bar, sound evaluation of the confinement technique as well as the performance of the corrosion rate instrument are possible. Information on the actual corrosion rate of the segmented reinforcement bar is obtained from macro-cell current, half-cell potential and conventional potentiodynamic linear polarisation resistance measurements. With the method, the two confinement techniques, i.e. the *simple guard ring* and the *sensorised guard ring* used in the GalvaPulse and the GECOR 6 instruments, respectively, have been investigated. For comparison, measurements using a small counter-electrode without confinement, and the conventional potentiodynamic linear polarisation resistance technique for determining the polarisation resistance were also performed.

Approach		Experimental variations				Method						Information obtained			
Special features	Measured	Reinforcement		Exposure	Instruments	Confinement		Technique	Analysis						
		Specimens													
			Cover [mm]	Chloride content [mass% of binder]	Relative humidity [%RH]	Temperature [°C]									
Segmented rebars allowing measurements of current distribution	Current distributions	Segmented: Passive Active: -General -Local	30	0	95	20	GECOR 6	-	-	×	-	×	-		
								GalvaPulse	×	×	×	×	-	×	(×)
								Laboratory potentiostat	×	-	-	-	×	×	-
								Laboratory potentiostat	×	-	-	×	×	-	
								Laboratory potentiostat	×	-	-	×	×	-	
Geometry giving uniform current distribution	LPR	Plain: Passive Active, gen.	-	0	75	1	Laboratory potentiostat	×	-	×	×	-			
								Laboratory potentiostat	×	-	-	×	×	-	
	Potential response curves	Ni plated: Active, loc.	4	96	35	Laboratory galvanostat	×	-	×	×	×				

Figure 4.1 Approach, experimental variations and methods used in the two experiments performed in the research project.



Figure 4.2 The GECOR 6 Corrosion Rate Meter from Geocisa, Spain (shown without connecting cables).

In the following section, detailed description of the operating principles of the two instruments selected for the investigations, i.e. the GECOR 6 and the GalvaPulse is given. Subsequently, a description of the test specimens and methods used is provided.

4.1.1 Commercial instruments - principle of operation

A detailed description of the operating principles of the GECOR 6 and the GalvaPulse is given in this section. The aim of the section is to provide the reader with detailed knowledge of two instruments, forming a background for evaluating the test methods used and the results obtained.

GECOR 6

The GECOR 6 Corrosion Rate Meter from Geocisa, Spain, shown in Figure 4.2 uses the galvanostatic linear polarisation resistance technique for measuring the polarisation resistance, R_P , (see Section 3.2.1) and the sensorised guard ring for confining the current applied from the counter-electrode (see Section 3.3). The electrode assembly consists of two circular, stainless-steel electrode rings with outer/inner diameters of 70/11 mm and 180/140 mm, respectively. The inner (smaller) electrode works as counter-electrode and the outer as guard ring. The counter-electrode and guard ring are positioned concentrically with a Cu/CuSO₄ reference electrode in the centre for recording the reinforcement potential ($E_{Ref\ 1}$ in Figure 4.3). Two auxiliary Cu/CuSO₄ reference electrodes ($E_{Ref\ 2}$ and $E_{Ref\ 3}$ in Figure 4.3) used for controlling the guard ring are positioned between the counter-electrode and the guard ring at a distance of 45 and 60 mm from the centre of the electrode assembly, respectively. Current confinement is used for all measurements and cannot be turned off.

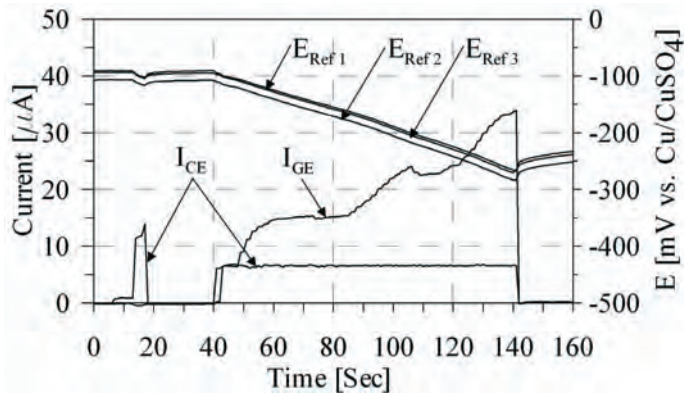


Figure 4.3 Real-time recording of a GECOR 6 measurement on passive reinforcement showing the reinforcement potential against the three reference electrodes (E_{Ref1} to E_{Ref3}) and the current applied from the counter-electrode, I_{CE} , and the guard ring, I_{GE} . The default polarisation time of 100 seconds was used for the measurement.

Figure 4.3 shows a real-time recording of the electrode currents (counter I_{CE} and guard I_{GE}) and the reinforcement potential measured against the three reference electrodes (E_{Ref1} to E_{Ref3}) during measurement on passive reinforcement with the experimental setup described in Section 4.1.3.

The instrument initiates the measurement procedure by recording the reinforcement potential against the three reference electrodes until a certain stability criterion has been reached. After this, a short current pulse is applied from the counter-electrode, see Figure 4.3. From the measured potential response, the instrument calculates an assumed optimal counter-electrode current, I_{CE} , after which the polarisation resistance measurement is started. During measuring, the I_{CE} is kept constant, polarising the reinforcement in the cathodic direction, while a secondary current is applied from the guard ring, I_{GE} , maintaining the potential difference between the auxiliary reference electrodes (E_{Ref2} and E_{Ref3}) at the initial level. A polarisation time of 100 seconds is used as default. Since the instrument operates in accordance with the galvanostatic linear polarisation resistance technique, R_P is calculated from the polarisation obtained (corrected for the ohmic potential drop, E_Ω) and the applied I_{CE} using Equation 3.1. With the electrode assembly and the confinement technique used, an area, A , corresponding to a reinforcement length of 105 mm is considered for the calculation of the corrosion current density, i_{corr} , using Equation 2.19. A value of 26 mV is used for the proportionality factor B.

GalvaPulse

The GalvaPulse from FORCE Technology, Denmark, shown in Figure 4.4 uses the galvanostatic transient technique (see Section 3.2.2) for measuring the polarisation resistance, R_P , and the simple (non-sensorised) guard ring for confining the current applied from the



Figure 4.4 The GalvaPulse instrument from FORCE Technology, Denmark.

counter-electrode (see Section 3.3). Two circular zinc electrode rings are used in the GalvaPulse electrode assembly: a counter-electrode and a guard ring with outer/inner diameters of 60/30 mm and 100/86 mm, respectively. The electrode rings are positioned concentrically with an Ag/AgCl reference electrode in the centre. Measurements can be made with or without the use of current confinement. When no current confinement is used, the guard ring is deactivated and current is only applied from the counter-electrode, i.e. the inner electrode ring.

Figure 4.5 shows a real-time recording of the instrument's operation during measurement on passive reinforcement with the experimental setup described in Section 4.1.3. The instrument initiates a measurement by recording the free corrosion potential, E_{corr} , of the reinforcement against the reference electrode, and the counter-electrode and guard ring potentials against the reinforcement. A galvanostatic current pulse, I_{CE} , polarising the reinforcement in the anodic direction with amplitude and duration preset by the user, is then applied from the counter-electrode, see Figure 4.5. A pulse time of 10 seconds and a current of 20 to 100 μA are typically used. During polarisation, the initial potential difference between the counter-electrode and guard ring is maintained, i.e. the guard ring potential or more specifically, the voltage of the guard ring, U_{GE} , is controlled by the counter-electrode voltage, U_{CE} , resulting from the current applied from the counter-electrode, I_{CE} .

A simple Randles circuit, as shown in Figure 3.4, is assumed for describing the steel-concrete system behaviour as a function of time when a galvanostatic current, I_{CE} , is applied. The polarisation resistance, R_P , is obtained from linearisation of the recorded potential transient (see Section 3.2.2). With the electrode assembly and the confinement technique used, an area, A , corresponding to a reinforcement length of 70 mm is consid-

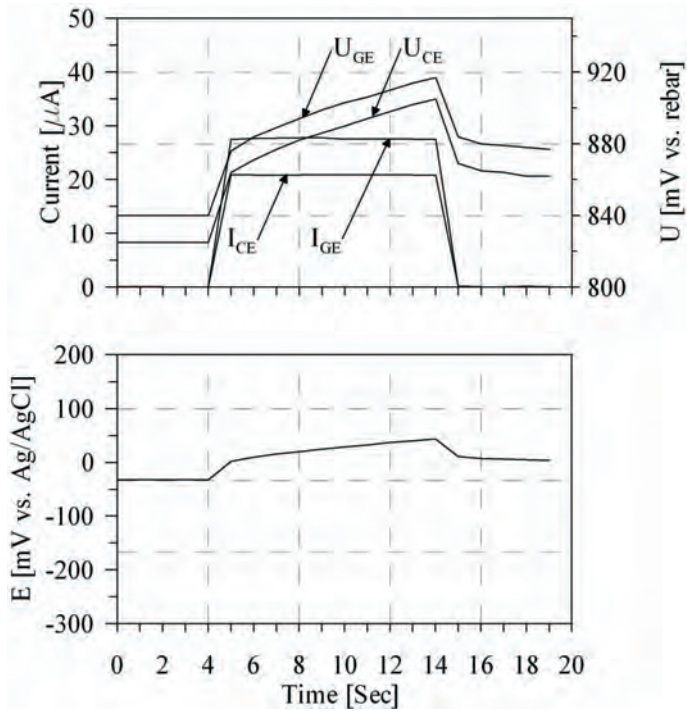


Figure 4.5 Real-time recording of a GalvaPulse measurement on passive reinforcement using current confinement. A current pulse of $20 \mu A$ and 10 second's duration was used for the measurement. The current applied from and the voltage of the counter-electrode and guard ring, I_{CE} , U_{CE} and I_{GE} , U_{GE} , respectively, are shown in the upper graph, whereas the potential of the reinforcement versus the reference electrode, E , is shown in the lower graph.

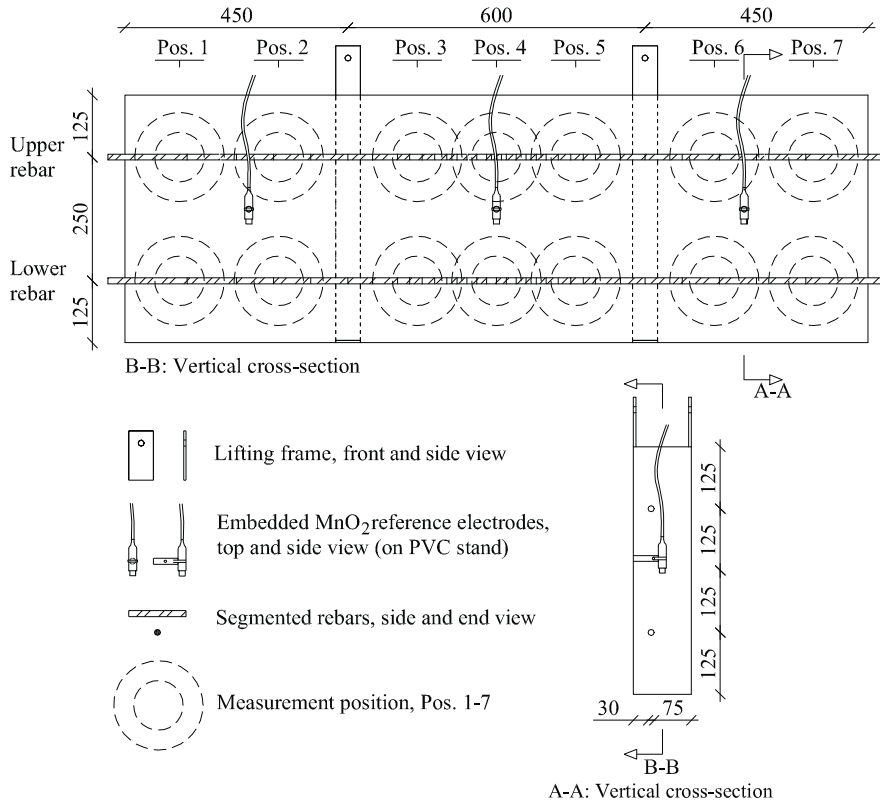


Figure 4.6 Geometry of the test slabs. Measurements positions (Positions 1-7) for the GECOR 6 and GalvaPulse are shown with large and smaller dashed circles, respectively. All measures are given in mm.

ered for calculating the corrosion current density, i_{corr} , using Equation 2.19. A value of 26 mV is used for the proportionality factor B.

4.1.2 Manufacture of test specimens

For the experiments, three test specimens (Slab I-III) with varying amounts of admixed chloride were prepared. Each test specimen consisted of a rectangular concrete slab (1.5×0.12×0.5 m) with two segmented reinforcement bars and three embedded MnO_2 reference electrodes as shown in Figure 4.6. Accurate positioning of the segmented reinforcement bars and reference electrodes was obtained by mounting these on PVC inserts fixed in the mould. For handling the slabs two stainless steel frames, coated with a non-conducting paint, were also included in each slab. The mould layout before casting is shown in Figure 4.7(a, b).



Figure 4.7 Manufacture of test slabs. a: Segmented reinforcement bars, reference electrodes, chloride sensors and lifting frames mounted in the mould (mould side removed for better view). b: All reinforcement segments are isolated with silicone rings. c: The fibreglass bar with the connecting wires and a part of the 160 mm end segment protruding from the slab. d: The three test slabs - ready for testing.

Table 4.1 Mix design of concretes.

Property	Unit	Amount
Cement	kg/m ³	325
Water	kg/m ³	162.5
Chloride	Slab I	0
	Slab II	1.5
	Slab III	4.0
Aggregate (0-4 mm)	kg/m ³	814
Aggregate (4-8 mm)	kg/m ³	1079

Table 4.2 Selected properties of the concretes used for the three slabs.

Property	Unit	Slab		
		I	II	III
Air content	Vol%	2.0	2.2	2.0
Density, hardened	kg/m ³	2370	2340	2330
Compressive strength*	MPa	36.0	36.5	35.0
Electrical resistivity**	kΩ×cm	3.4	1.6	0.8

*: At an age of 3 days.

**: Measured at the time of testing on the slabs.

Concretes

To obtain different corrosion scenarios, the three concrete slabs (Slab I-III) were cast with an addition of 0 %, 1.5 % and 4 % chloride by mass of cement, respectively. The chloride was added as calcium chloride dissolved in the mixing water. White portland cement (CEM I 52.5) and a w/c ratio of 0.5 were selected for the experiments. The mix composition and selected properties of the three concretes are given in Tables 4.1 and 4.2. A detailed description of the mix design and the constituent materials can be found in Appendix A, and a description of the fresh and hardened properties in Appendix B.

The slabs were cast by placing the fresh concrete in the mould in 150 mm layers and compacting with a poker vibrator. Each slab was cast from one batch. After casting, the slabs were stored in the mould for one day, demoulded, sealed in plastic and cured at 20 °C. At an age of 13 (Slab III), 23 (Slab II) and 34 (Slab I) days the slabs were unwrapped, and placed in a climate chamber at 20 °C and 95 % relative humidity, and kept under these conditions during the test period, see Figure 4.7(d).

Segmented reinforcement bars

The segmented reinforcement bars were prepared by mounting circular steel segments with outer and inner diameters of 12.0 and 10.2 mm, respectively, on a 10.0 mm diameter non-conducting fibreglass bar. This bar contained a slot for the connecting wires; one 0.05 mm² wire was soldered to the inside of each segment allowing external electrical



Figure 4.8 A wire is soldered to the inside of each segment, here with lengths of 20, 25 and 50 mm, respectively (from right). The silicone rings are placed between the segments when mounted on the fibreglass bar.

connection and coupling of the segments, see Figures 4.7(c) and 4.8. Silicone rings with thickness of 1 mm and, outer and inner diameter of 9 and 14 mm, respectively, were placed between the segments, electrically isolating the segments and sealing the reinforcement bar system, see Figure 4.8.

An upper and a lower segmented reinforcement bar were embedded in each slab, both with a concrete cover of 30 and 75 mm, respectively, see Figures 4.6 and 4.7. The lower segmented reinforcement bars consisted of 32 carbon steel segments with a composition as given in Table 4.3. The segments were placed symmetrically and with increasing length from the center of the bar (numbers refer to one side of the bar): five of 20 mm, four of 25 mm, two of 50 mm, three of 75 mm, one of 100 mm and one of 160 mm (of which 50 mm protruded from the end of the slab).

The upper segmented reinforcement bars were made of stainless steel (DIN 1.4301) with a composition as given in Table 4.3. The geometry was identical to the lower bars, except that the two central 20 mm segments were replaced by four 10 mm segments. Of these the two in the middle were made of carbon steel. In this way two well defined anodes should develop in the slabs cast with chloride admixed concrete (Slabs II and III).

Before the wires were soldered to the segments, all segments were cleaned: First with a water soluble degreasing agent, followed by ultrasonic cleaning. Subsequently the carbon steel segments were put in an inhibited 10 % hydrochloride acid, and the stainless segments in a 10 % nitric acid. The segments were then rinsed with distilled water and dried with hot air.

Table 4.3 *Composition of the carbon steel and stainless steel [mass%]. Tested in accordance with ASTM E415-99a (2005).*

Component	Carbon	Stainless
C	0.11	0.023
Si	0.23	0.48
Mn	0.42	1.24
P	0.01	0.039
S	0.002	0.018
Cr	0.07	18.2
Mo	0.016	0.22
Ni	0.043	11.1
Al	0.038	0.032
Co	0.004	0.079
Cu	0.059	0.23
Ti	0.003	0.011
V	0.002	0.033
Sn	0.005	0.012
Mg	0.0003	-
As	-	0.014
Se	-	0.019
N	0.015	0.066
Fe*	99	68

*: Calculated as remainder.

4.1.3 Test methods

Once the slabs had been put in the climate chamber, all segments on each reinforcement bar were connected to a switchboard. Apart from connecting the segments, the switchboard allowed the segments to be electrically separated or connected in any desired configuration for measurements on single, groups or all segments. When no measurements were being made, the segments on each bar were all kept connected so that each segmented reinforcement bar would act as an electrically continuous bar. The order in which the measurements were performed follows the order in which they are described in the following. The full series of measurements described below was repeated three times during a period of three months.

Macro-cell current measurements

Macro-cell current measurements were performed on the upper and lower segmented reinforcement bars in Slabs II and III, in order to identify the anodic and cathodic segments, and determine the currents to or from these segments. The measurements were made by inserting a zero-resistance ammeter (ZRA) in the connection on the switchboard to the individual segments. Insertion of the ZRA was performed without electrically disconnecting the segments at any time so as not to disturb the electrochemical system. The ZRA was custom-made for the experiment; with a current range of ± 1 mA and a resolution of $0.1 \mu A$.

Half-cell potential and polarisation resistance measurements

Two series of half-cell potential and polarisation resistance measurements were performed. In series one, all segments on each reinforcement bar were connected and measurements were performed on both surfaces of each slab (30 and 75 mm cover) along the upper and lower reinforcement bars with a distance of 50 mm between the measurements. As counter-electrode, a circular zinc disk with outer and inner diameters of 60 and 30 mm, respectively was used. An Ag/AgCl reference electrode was placed in the centre of the counter-electrode. A moist sponge was placed between the electrode assembly and the concrete surface. In the following this electrode assembly is referred to as the *small unconfined electrode assembly*, see Figure 4.9. By using a small counter-electrode apparent polarisation values, R_P^{app} , were obtained because of the non-uniform current distribution along the reinforcement.

In series two, measurements were performed on each reinforcement bar, with all segments, groups of segments or single segments as working electrodes. On the upper and lower reinforcement bars in Slab I, where all segments were passive, the half-cell potential, E_{corr} , and polarisation resistance, R_P , were measured with all segments connected. On the upper bars in Slabs II and III, measurements were first performed with all segments on each bar connected. The stainless steel cathodes were then divided in two groups, segments 1-16 and 19-34, respectively, and the two anodes (segments 17 and 18) disconnected. After the equilibrium potential had been reached, the half-cell potential, E_{corr} , and polarisation resistance, R_P , of the two groups of cathodes and the two anodes were measured. The equilibrium potentials of the two groups and the two single anodes were confirmed

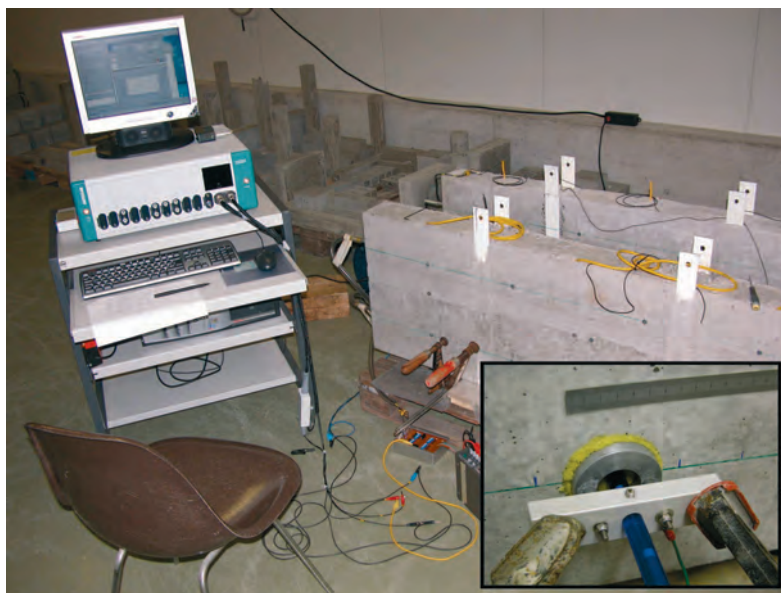


Figure 4.9 The laboratory potentiostat and the small unconfined electrode assembly consisting of a 60 mm diameter zinc counter-electrode (with a 30 mm diameter hole) with a centrally positioned Ag/AgCl reference electrode.

versus the nearest embedded MnO_2 reference electrode. On the lower reinforcement bars in Slabs II and III measurements were first performed with all segments connected. All segments were then separated. After reaching the equilibrium potential measurements were performed on the segments found as being anodic (from the macro-cell current measurements). For all measurements in Series two a 60 mm wide stainless steel bar placed on the surface and covering the full length of the test slabs was used as counter-electrode, ensuring uniform polarisation of the embedded segments. An Ag/AgCl reference electrode was placed in a 20 mm diameter hole in the counter-electrode centrally over the selected working electrode.

In both series, the polarisation resistance, R_P , was measured using the potentiodynamic linear polarisation resistance technique. Measurements were performed with a potential sweep of ± 15 mV around the free corrosion potential, E_{corr} , to ensure a potential shift in the linear Stern-Geary region. A sweep rate of 0.1 mV per second was used. After each polarisation resistance measurement, the ohmic system resistance was measured by applying stable alternating current of 40 mA at a frequency of 128 Hz between the counter-electrode and the selected working electrode.

Measurements with commercial corrosion rate instruments

Test method and setup The method used for evaluating the confinement systems was based on real-time monitoring of: a) the instruments' operation; and b) the distribution of current between the electrode assembly placed on the concrete surface and an embedded segmented reinforcement bar during the corrosion rate measurements.

As illustrated in Figures 4.3 and 4.5, the instruments' operation was monitored as follows:

- GECOR 6: The currents applied from the counter-electrode and guard ring were recorded together with the reinforcement potential measured versus the three Cu/CuSO₄ reference electrodes in the electrode assembly.
- GalvaPulse: The voltages of and the currents applied from the counter-electrode and guard ring were recorded together with the reinforcement potential measured versus the centre Ag/AgCl reference electrode in the electrode assembly.

With the setup shown in Figure 4.10 the segmented reinforcement bars allowed the current distribution to be measured as discrete currents representing the total current flowing through a given length of the reinforcement bar, i.e. through each segment. This way the current distribution was measured as a number of discrete currents (measured simultaneously) giving a step-wise distribution along the reinforcement bar. Potentials/voltages and currents were recorded with a frequency of one hertz during the corrosion rate measurements. Currents were measured with zero-resistance ammeters (ZRA) custom made for the experiment; with a current range of ± 1 mA and a resolution of 0.1 μA . Potentials/voltages were measured with a resolution of 0.1 mV. In addition to the external reference electrodes (in the instruments' electrode assemblies) the segmented reinforcement bars potentials were also recorded versus the middle embedded MnO_2 reference

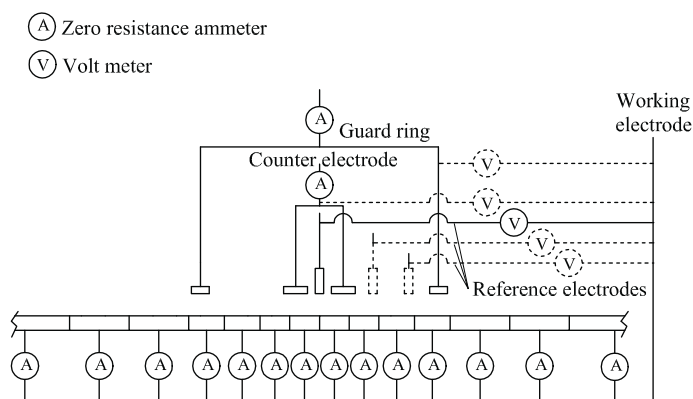


Figure 4.10 Schematic illustration of the system used for real-time monitoring of the operation of the corrosion rate instruments and current distribution. In addition to the zero-resistance ammeters and voltmeters shown with full lines, voltmeters shown with dotted lines were used with the GalvaPulse and the reference electrodes with dotted lines with the GECOR 6. Not all segments and zero-resistance ammeters used are shown.

electrode, see Figure 4.6.

Measurements Measurements were made with the GECOR 6 and the GalvaPulse on the upper and lower segmented reinforcement bars as follows: On Slab I in Position 4 only (centrally over the reinforcement bars). On Slabs II and III, in Positions 1-7, see Figure 4.6. Measurements were made on both surfaces, i.e. with a cover of 30 and 75 mm, respectively. All segments on each reinforcement bar were connected during the measurements, so that each bar acted as an electrically continuous reinforcement bar.

With the GECOR 6 the default polarisation time of 100 seconds was used for all measurements. The steel area was set to 39.6 cm², corresponding to the assumed confinement length of 105 mm. As mentioned earlier, the amplitude of the applied galvanostatic pulse was determined by the instrument. With the GalvaPulse a current of 20 μ A was used for the measurements on the upper and lower reinforcement bars in Slab I and on the upper bars in Slabs II and III. On the lower bars in Slabs II and III a current of 50 μ A was used, as active general corrosion was expected here. A polarisation time of 10 seconds was used for all measurements. The steel area was set to 26.4 cm², corresponding to the assumed confinement length of 70 mm. All GalvaPulse measurements were performed with and without current confinement, i.e. two measurements were performed in each position. A steel area of 26.4 cm² was also used for measurements without current confinement.

During all measurements, the corrosion rate instruments' operation and the current distribution between the electrode assembly and the segmented reinforcement bar were

recorded. The data logger set up for monitoring the instrument's operation and the current distribution was started and stopped approximately 30 seconds before and after each measurement. The currents recorded before each measurement (e.g. from macro-cells, off-set error, etc.) were used as off-set, to correct the current distribution recorded during the measurement.

After each corrosion rate measurement, the segmented reinforcement bar was allowed to depolarise to the initial equilibrium potential, E_{corr} , before a new measurement, i.e. in the next measurement position, was made. The depolarisation was checked by measuring the potential of the reinforcement bar versus the middle embedded MnO_2 reference electrode.

4.2 Effect of measurement technique, procedure and exposure

The present section describes the experiment in which both the *Effect of measurement technique and procedure* and the *Effect of exposure on the corrosion rate* are investigated. The section starts with a description of the manufacture and conditioning of the test specimens used. Subsequently the instrumentation and the measurements performed are described.

4.2.1 Manufacture and conditioning of test specimens

For the experiment, three series (Series I-III), each with 15 geometrically identical test specimens were manufactured, see Figure 4.11. Each specimen consisted of a rectangular concrete specimen ($760 \times 250 \times 70$ mm) with ten 10 mm diameter smooth reinforcement bars, with a length of 230 mm of which 200 mm was embedded in the concrete. Beside the reinforcement bars a mmo-titanium mesh (730×220 mm), a MnO_2 reference electrode and two pairs of resistivity sensors were embedded in each specimen. The mmo-titanium mesh was placed at a depth of approximately 5 mm below the concrete surface and the reference electrode centrally in the specimen, see Figure 4.11. An accurate positioning of the reinforcement bars and resistivity sensors was secured by fixing these in the bottom plate of the mould, whereas the reference electrode and mmo-titanium mesh were mounted on PVC inserts fixed in the mould walls. No measurements were performed on the resistivity sensors and these are therefore not considered further. The layout of the mould, in which five test specimens were cast at a time, is shown in Figure 4.12 a, b.

To obtain different corrosion environments the specimens in Series I were cast without chloride whereas the specimens in Series II and III were cast with an addition of 4 % chloride by mass of cement. The chloride was added as sodium chloride dissolved in the mixing water. The mix composition of the concretes used for the three series of test specimens is given in Table 4.4. Detailed descriptions of the mix design and constituent materials is given in Appendix A. As the test specimens were cast five at a time three batches were used for each series. The fresh and hardened properties of all nine batches used for casting the 45 test specimens (three series each with 15 test specimens) are given in Appendix C.

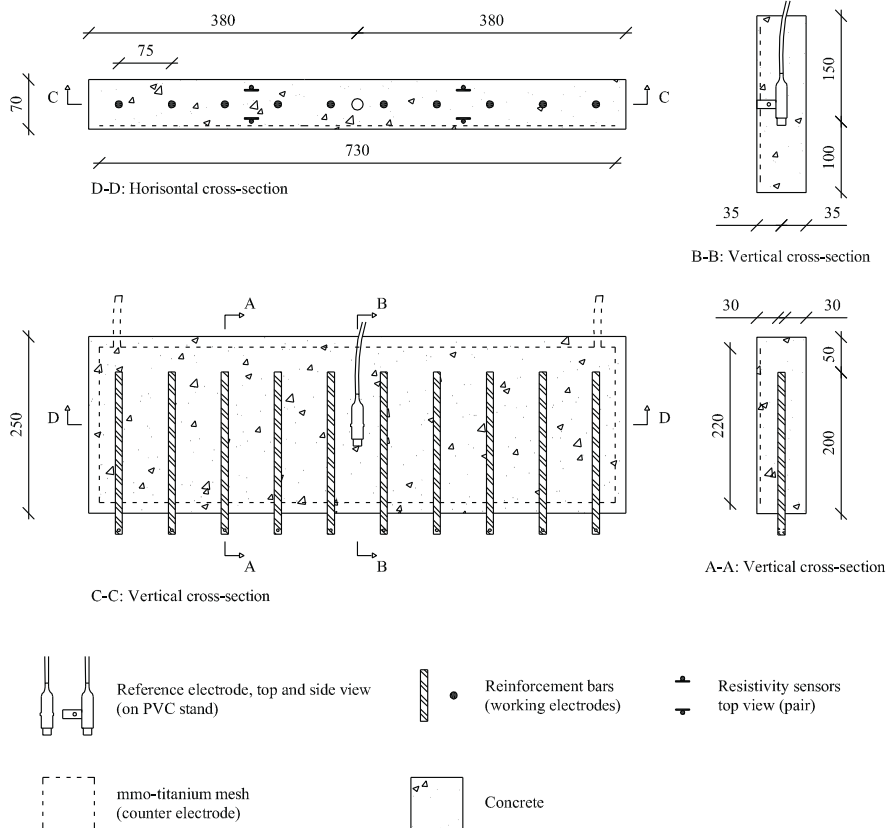


Figure 4.11 Geometry of the test specimens. All measures are given in mm.

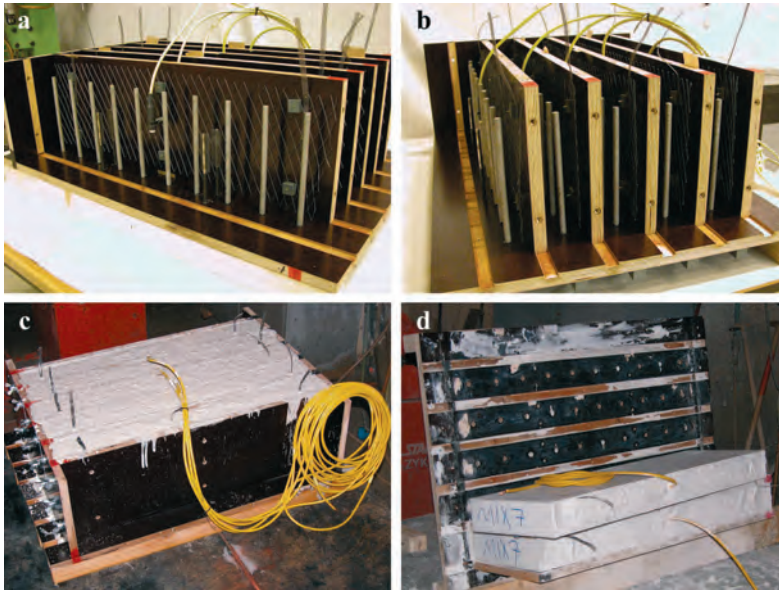


Figure 4.12 *Production of test specimens: a, b: Side and end views of the five specimen mould (side and end wall removed). c: The mould is placed on a vibration table and the specimens cast. d: The specimens are demoulded after one day.*

Table 4.5 *Composition of the carbon steel used as reinforcement [mass%]. Tested in accordance with ASTM E415-99a (2005). Only selected components are given.*

C	Si	Mn	P	S	Cr	Mo	Ni	Al
0.11	0.18	0.67	0.006	0.019	0.027	0.001	0.029	0.002
Co	Cu	Ti	V	Sn	Mg	N	Fe	
0.014	0.005	0.002	0.009	0.002	0.0002	0.0	99*	

*: Calculated as remainder.

Table 4.4 *Mix design of concretes.*

Property	Unit	Amount
Cement	kg/m ³	325
Water	kg/m ³	162.5
Chloride	Series I Series II Series III	mass% of binder 0 4.0 4.0
Aggregate (0-4 mm)	kg/m ³	814
Aggregate (4-8 mm)	kg/m ³	1079

The reinforcement bars were prepared from conventional carbon steel reinforcement with a composition as given in Table 4.5. All reinforcement bars were cleaned in a 10 % inhibited hydrochloride acid until they appeared with a uniform grey surface, rinsed with distilled water and dried with hot air. After cleaning, the steel bars for the test specimens in Series III, with 4 % chloride, were partly coated with nickel. No surface treatment was applied to the bars in the test specimens in Series I and II with 0 % and 4 % chloride, respectively. The partly nickel coated bars for Series III were prepared by masking the middle 5 mm of the 200 mm length to be embedded in the concrete. After this, a nickel coating with an average thickness of approximately 50 μm was applied electrochemically and the masking removed. After removing the masking a 5 mm wide band of carbon steel appeared on the nickel coated bar, see Figure 4.13. This way a well defined macro-cell should develop in the chloride containing concrete; with the nickel plated areas as cathode and the 5 mm carbon steel band as anode. The nickel coating was selected as nickel is (theoretically) slightly more noble than carbon steel. With the concretes and the reinforcement bars used, test specimens with passive steel (Series I), general corrosion (Series II) and intense localised corrosion (Series III) should be obtained, see Table 4.6.

After casting, the specimens were kept in the mould for one day, demoulded, sealed in plastic and cured at 20 °C. After curing for 28 days, the test specimens were unwrapped and an epoxy coating applied on the four edges and the first 30 mm of each protruding reinforcement bar. This was done in order to prevent corrosion on the protruding part of the reinforcement bars, and to obtain a unidirectional moisture transport through the two large surfaces (760×250 mm) parallel to the reinforcement bars. Prior to applying the



Figure 4.13 The two types of reinforcement bars prepared for the experiment. Lower: A cleaned and uncoated bar as used in Series I and II. Upper: A partly nickel coated bar as used in Series III. Only the length to the left of the vertical line was embedded in the test specimen.

Table 4.6 Properties of the test specimens in the three series (I-III). Each series contained 15 geometrically identical test specimens - each with 10 reinforcement bars.

	Corrosion State/type	Chloride content	Reinforcement bars
Series I	Passive	0%	Uncoated
Series II	Active/general	4%	Uncoated
Series III	Active/localised	4%	Ni coated

coating the reinforcement bars protruding from the specimens in Series II and III with 4 % chloride were sandblasted in order to remove any corrosion products formed during curing.

For conditioning the test specimens 15 climate chambers with temperatures of 1, 5, 15, 25 and 35 °C, and relative humidities of 75, 85 and 96 % (i.e. the respective combinations) were used. Saturated salt solutions were used for obtaining the relative humidities. The temperatures and relative humidities were maintained within ± 1 °C and ± 5 % relative humidity, respectively. One test specimen from each series, i.e. one specimen with passive reinforcement (Series I), one with active general corrosion (Series II) and one with active localised corrosion (Series III) were placed in each climate chamber, see Figure 4.14. The test specimens were kept under these conditions, i.e constant exposure during the entire test period.

4.2.2 Test methods

Two types of electrochemical measurements were performed for obtaining the polarisation resistance, R_P , of the 10 reinforcement bars in each of the 45 test specimens: potentiodynamic linear polarisation resistance and galvanostatic potential transient measurements. For all measurements a single reinforcement bar was used as working electrode, the mmo-titanium mesh as counter-electrode and the MnO_2 electrode as a reference (Figure 4.11). In the following the instrumentation and the measurement sequence used are described.



Figure 4.14 A test specimen from each series (I-III) is placed in each climate chamber maintained at a constant temperature and relative humidity.

After this, the measurement procedures used for the two types of measurements and the methods used for analysis of the measurements are described.

Instrumentation and measuring sequence

For the measurements a fully automatic setup, consisting of a galvano/potentiostat and a number of relay cards for switching between the individual test specimens (1 to 45) and reinforcement bars (1 to 10), was developed. A schematic illustration of the setup is shown in Figure 4.15.

Measurements were performed on the individual reinforcement bars (1 to 450) one at a time. For performing a measurement on a given reinforcement bar, all 10 reinforcement bars, the mmo-titanium mesh (counter electrode) and the MnO_2 reference electrode in the specimen containing the respective bar were first connected to the galvano/potentiostat. After this, the working electrode channel (1 to 10) to which the desired reinforcement bar was connected was activated. This way, one type of measurement (potentiodynamic or galvanostatic) was performed on all 450 reinforcement bars, before another type or another measurement parameter was used, again on all 450 reinforcement bars. The measurements were performed on all reinforcement bars in one specimen before moving on to the next specimen. Measurements were made continuously and in a loop following the sequence given in Table 4.7: Potentiodynamic linear polarisation resistance measurements were first performed on all bars. After this, galvanostatic potential transient measure-

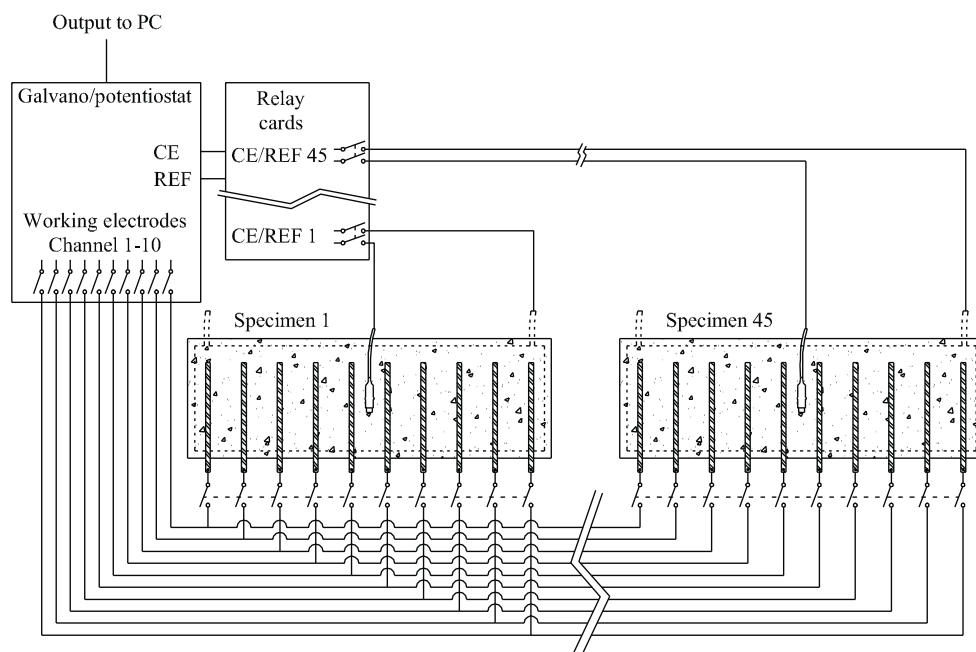


Figure 4.15 Schematic illustration of the test setup used for the potentiodynamic and galvanostatic measurements. Only two of the 45 test specimens are shown. All specimens were connected to the measurement setup as these two.

Table 4.7 Measurement sequence and parameters used for the individual measurement steps where the same type of measurements was made on all 450 reinforcement bars.

Step	Measurement type	Parameter	Unit
1	Potentiodynamic	10	mV/min
2		0.25	μA
3		0.5	μA
4		1	μA
5		2	μA
6	Galvanostatic	5	μA
7		10	μA
8		25	μA
9		50	μA
10		100	μA

ments were performed, increasing the applied current, I_{CE} , for each step. All measurement steps were initiated at noon, i.e. if a measurements step was completed after noon one day, the next step was first initiated at noon the forthcoming day.

Potentiodynamic linear polarisation resistance measurements

Each measurement was initiated by monitoring the free corrosion potential, E_{corr} , of the selected reinforcement bar versus the MnO_2 reference electrode. When a potential drift smaller than 3 mV over a 3 second period was obtained, the free corrosion potential, E_{corr} , was recorded over a period of 2 seconds, after which a current pulse of 25 μA and 4 seconds duration was applied from the counter-electrode. Before and during the current pulse the potential of the reinforcement bar was measured at a frequency of 10 hertz. After the pulse, the potential of the reinforcement bar was actively drawn to the initially measured free corrosion potential, E_{corr} . As the point between the almost vertical potential drop, E_Ω , and the potential transient could not be determined with sufficient exactitude the first second of the recorded potential transient was excluded and Equation 4.1 fitted to the remainder. By extrapolating backwards to the time zero, i.e. when the polarisation was started the ohmic potential drop, E_Ω , was determined and the ohmic system resistance, R_Ω , calculated (Ohms law).

The potentiodynamic linear polarisation resistance measurement was then started by polarising the reinforcement 15 mV in cathodic direction versus the free corrosion potential, E_{corr} , after which the reinforcement was polarised 30 mV in anodic direction, i.e. to a value 15 mV more positive than the free corrosion potential, E_{corr} . Typical polarisation curves obtained from the measurements on the passive and actively corroding reinforcement bars are shown in Figures 4.16 and 4.17, respectively. A target sweep rate of 10 mV per minute was used for all measurements corresponding to a total measurement time of 270 seconds (cathodic and anodic polarisation).

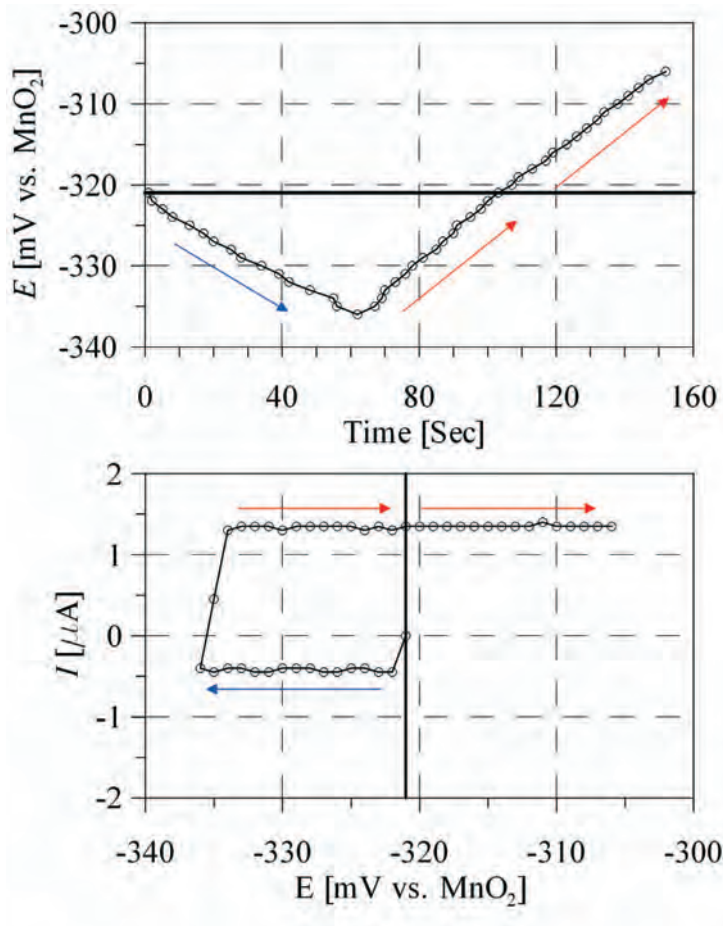


Figure 4.16 Potentiodynamic linear polarisation resistance measurement on passive steel (Series I). Upper graph: Potential as a function of time. Lower graph: The responding current as a function of the potential. The bold line indicate the free corrosion potential, E_{corr} , and the blue and red arrows the cathodic and anodic polarisation, respectively.

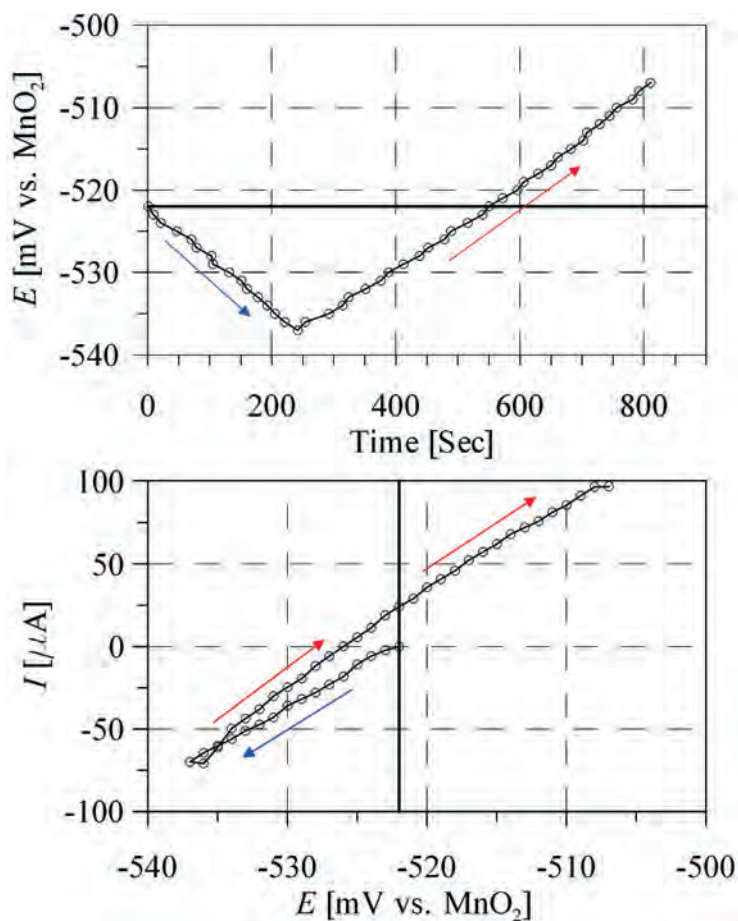


Figure 4.17 Potentiodynamic linear polarisation resistance measurement on actively corroding steel (Series II). Upper graph: Potential as a function of time. Lower graph: The responding current as a function of the potential. The bold line indicate the free corrosion potential, E_{corr} , and the blue and red arrows the cathodic and anodic polarisation, respectively.

As seen from the upper graphs in Figures 4.16 and 4.17 the actual sweep rate differed from the intended 10 mV per minute, as the measurement times deviated from 270 seconds: The sweep rate used for the measurements on the passive bars was higher whereas the sweep rate used for the measurements on the corroding bars was lower. From the lower graph in Figure 4.16 a slight hysteresis of the cathodic and anodic polarisation curves can be seen. This was observed for all measurements on the passive reinforcement bars in Series I. The phenomenon is well known and is often seen when potentiodynamic linear polarisation resistance measurements are performed on passive metals with very high polarisation resistance, R_P (Gabrielli et al., 1979) (Scully, 2000). Slight hysteresis between the cathodic and anodic polarisation curves was also observed from the measurements on the actively corroding reinforcement bars, see Figure 4.17.

For calculating the polarisation resistances, R_P , from the recorded potential sweeps a MatLab program was written. The code is available in Appendix E. For the actively corroding reinforcement bars in Series II and III, where an almost ideal linear relation between potential, E , and current, I , was observed the R_P was calculated using the data obtained from the anodic polarisation curve i.e. from -15 mV to +15 mV versus the free corrosion potential, E_{corr} , (indicated with the red arrows in Figure 4.17). After compensating the recorded potentials for the ohmic potential drop, E_Ω , determined before each measurement a straight line was fitted to the anodic polarisation curve using the MatLab Curve Fitting Toolbox. The polarisation resistance, R_P , was then determined as the slope of the fitted line multiplied with a steel area of 62.8 cm², corresponding to the reinforcement length of 200 mm and diameter of 10 mm.

The same mathematical procedure was used for the passive reinforcement bars in Series I. However, only the linear part of the anodic polarisation curve was used for the analysis, i.e. from -13 mV to +15 mV versus E_{corr} , see Figure 4.16, lower graph. This part of the polarisation curve was assumed to give the best approximation of the polarisation resistance, R_P . This assumption was based on the work by Gabrielli et al. (1979), in which the current response of a passive metal to a triangular potential sweep was considered, see Figure 4.18: In the case where $R_\Omega \ll R_P$, which is the case for the passive reinforcement, the equivalent system shown on the right side of Figure 4.18 approaches the system without ohmic resistance, R_Ω , shown on the left side of the figure. As seen from the figure the polarisation resistance, R_P , given as dE/dI , may be determined as the slope of the linear potential sweep curve, i.e. the part where the potential changes. The vertical part of the polarisation curve in Figure 4.16 may be considered a discharge and charging of the passive layer (the capacitive component) when the current is reversed and the direction of the polarisation changed, i.e. from the cathodic to anodic.

Corrosion current densities, i_{corr} , were calculated from the determined polarisation resistances, R_P , using Equation 2.19. For the passive reinforcement bars in Series I a proportionality factor B of 52 mV was used, whereas a value of 26 mV was used for the actively corroding bars in Series II and III (Andrade et al., 2004).

After analysis of all potential sweeps the mean R_P and standard deviation were cal-

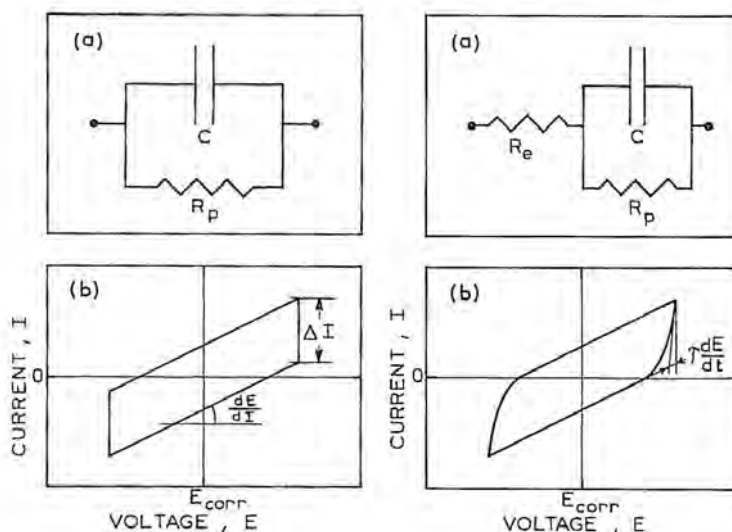


Figure 4.18 Equivalent circuits of a corroding electrode (upper) and the potential-voltage response to a triangular potential sweep (lower). Left and right figure shows the systems without and with ohmic resistance, R_Ω , respectively (shown on the figure as R_e). The polarisation resistance, R_p is equal to the slope of the parallelogram, i.e. $R_p = dE/dI$ (Gabrielli et al., 1979).

culated for the 10 reinforcement bars in each test specimen. Following this, the *outliers*, defined as R_p values more than 3 standard deviations from the mean, were identified and excluded, and a new mean R_p , i_{corr} and standard deviation calculated from the remaining values.

Galvanostatic potential transient measurements

Each galvanostatic potential transient measurement was initiated by monitoring the free corrosion potential, E_{corr} , of the selected reinforcement bar versus the MnO_2 reference electrode. When a potential drift lower than 3 mV over a 3 second period was obtained the free corrosion potential, E_{corr} , was recorded for the following two seconds. After this, a current pulse of 0.25, 0.5, 1, 2, 5, 10, 25, 50 or 100 μA (depending on the measurement step) with 170 seconds' duration was applied from the counter-electrode (Ti-mmo mesh) polarising the reinforcement in cathodic direction. Typical potential transients obtained from the passive reinforcement bars in Series I and the actively corroding bars in Series II with general corrosion are shown in Figures 4.19 and 4.20, respectively. As seen from Figure 4.20 only the potential transients obtained with current pulses from 5 to 100 μA are shown for the actively corroding reinforcement. This is because the potential shifts obtained during the measurements with current pulses from 0.25 to 2 μA were lower than

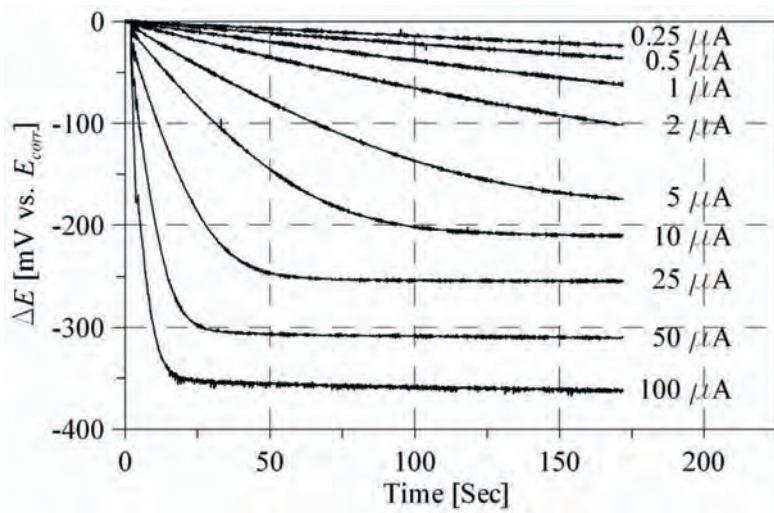


Figure 4.19 Potential transients obtained with varying counter-electrode currents from passive steel in a concrete specimen with 0 % chloride (Series I) exposed to 15 °C and 85 % relative humidity.

1 mV making a distinction between the potential transients and the noise (50 Hz) difficult. Before and during each measurement the reinforcement potential was recorded versus the MnO_2 reference electrode with a frequency of 10 hertz and a precision of 0.03 mV (16 bit resolution).

Two approaches for determining the polarisation resistance, R_P , from the recorded potential transients were used; the galvanostatic transient technique and the galvanostatic linear polarisation resistance technique (see Sections 3.2.1 and 3.2.2). For analysis of the measured potential transients, following the two approaches, a MatLab program was written. The code is available in Appendix F. To investigate the effect on the determined polarisation resistance, R_P , when exceeding the linear current-potential region near the free corrosion potential, E_{corr} , all potential transients obtained from the passive reinforcement bars were analyzed. For the actively corroding reinforcement only the potential transients obtained with current pulses of 5 μA and higher were analyzed, as the potential transients obtained with the lower current pulses (0.25 to 2 μA) could not be distinguished from the noise - as mentioned above.

For each recorded potential transient, the reinforcement bar's free corrosion potential, E_{corr} , was first determined. This was done by calculating the average value of the potential measurements recorded during the 2 second periods before the galvanostatic polarisation was initiated. After this, the recorded potential transient was offset corrected using the free corrosion potential, E_{corr} , as zero point, i.e. the determined free corrosion potential, E_{corr} was subtracted from all potential measurements (Figure 4.19 and 4.20).

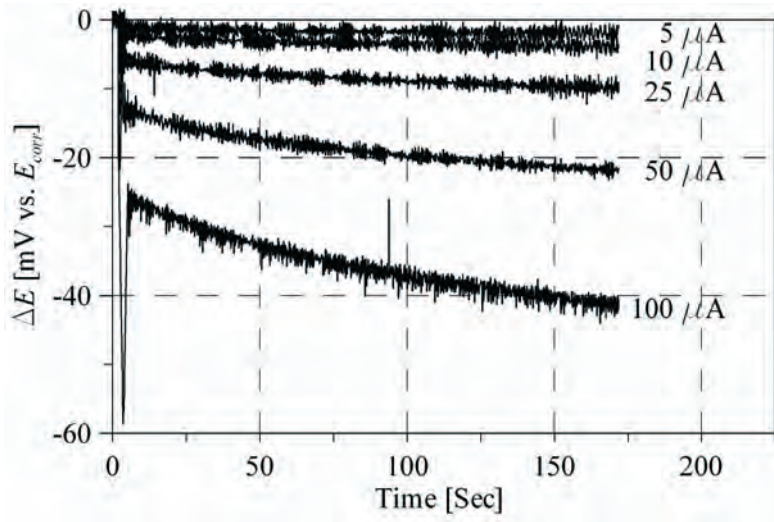


Figure 4.20 *Potential transients obtained with varying counter electrode currents from actively corroding steel (general corrosion) in a concrete specimen with 4 % chloride (Series II) exposed to 15 °C and 85 % relative humidity.*

To determine the effect of the polarisation time, t , on the obtained polarisation resistance, R_P , 32 data intervals with increasing lengths, corresponding to an increasing polarisation time, were extracted from each potential transient. The length of the extracted data intervals ranged from 10 to 165 seconds and increased in 5 seconds' steps. The polarisation resistance, R_P , was then determined for each data interval with both approaches, i.e. the galvanostatic potential transient and the galvanostatic linear polarisation resistance techniques as described in the following:

Galvanostatic potential transient technique For determining the polarisation resistance, R_P , with the galvanostatic potential transient technique, Equation 4.1 (also given in Equation 3.8) was fitted to each data interval using the MatLab Curve Fitting Toolbox and the least squares fitting Method (MathWorks, 2006). Beside the polarisation resistance, R_P , also the double layer capacitance, C_{dl} , and the ohmic resistance, R_Ω , were determined from each curve fit as all three were defined as coefficients in the fitted equation. The 32 data intervals from each potential transient were analysed in an order of decreasing length, i.e. decreasing polarisation time. This was done as the number of iterations needed for each curve fit increased with decreasing length, when constant start estimates for the coefficients were used (R_P, C_{dl}, R_Ω). To reduce the number of iterations the coefficients determined from one curve fit (R_P, C_{dl}, R_Ω) were therefore used as start values for the curve fit of the following and 5 seconds shorter data interval. Before analysis of each data interval the potential measurements recorded during the first second of

the polarisation period were excluded. This was done as the initial potential rise, caused by the ohmic resistance, R_Ω , and the initial part of the charging curve could not be clearly distinguished. This way the ohmic resistance, R_Ω , was determined by extrapolating the fitted curve backwards to the time $t = 0$, i.e. when the galvanostatic polarisation was initiated. As seen from Figure 4.20 an initial potential *overshooting* occurred when measurements were performed on the actively corroding reinforcement bars with current pulses of 25, 50 and 100 μA . The potential *overshooting*, was seen to affect the recorded potential transients up till a polarisation time of approximately 5 seconds making reasonable curve fitting difficult. The potential measurements from the first 5 seconds of these potential transients were therefore excluded from the analysis.

For calculating the polarisation resistance, R_P , the R_P -coefficient determined from each curve fit was multiplied with a steel area of 62.8 cm^2 , corresponding to the reinforcement length of 200 mm and diameter of 10 mm. The corrosion current density, i_{corr} , was calculated using Equation 2.19. For all passive reinforcement bars in Series I a proportionality factor B of 52 mV was used, whereas a value of 26 mV was used for all the actively corroding bars in Series II and III (Andrade et al., 2004).

$$E_t = I_{CE}R_\Omega + I_{CE}R_P \left(1 - \exp \left(\frac{-t}{C_{dl}R_P} \right) \right) \quad (4.1)$$

Galvanostatic linear polarisation resistance technique With this technique the polarisation resistance, R_P , was calculated for each data interval using Equation 4.2 (also given in Equation 3.2). The potential shift, ΔE , was calculated as the mean value of the potential measurements from the last second in the data interval. For the ohmic drop compensation the ohmic resistance, R_Ω , determined by the curve fit of the data interval with a length of 10 seconds was used (described in the previous section).

$$R_P = \frac{\Delta E}{I_{CE}} - R_\Omega \quad (4.2)$$

The polarisation resistance, was calculated by multiplying the determined R_P -coefficient obtained from Equation 4.2 with a steel area of 62.8 cm^2 , corresponding to the reinforcement length of 200 mm and diameter of 10 mm. The corrosion current density, i_{corr} , was calculated using Equation 2.19. For all passive reinforcement bars, i.e. all the reinforcement bars in Series I, a proportionality factor B of 52 mV was used, whereas a value of 26 mV was used for all the actively corroding bars in Series II and III.

Chapter 5

Experimental Results

5.1 Effect of confinement techniques

In this section the results from the experimental work on the effect of confinement techniques described in Section 4.1 are presented. As described in Section 4.1 the full series of measurements performed in the work were repeated three times during a period of three months. Only the results from one of the series, being representative for the three are presented below.

5.1.1 Macro-cell current measurements

The macro-cell current distributions measured on the upper segmented reinforcement bars, with stainless cathodes and two centrally positioned anodes, in Slabs II and III are shown in Figures 5.1 and 5.2, whereas the macro-cell current distributions measured on the lower segmented bars made of carbon steel segments are shown in Figures 5.3 and 5.4. The current density of each segment was calculated by dividing the measured absolute current, anodic (positive) or cathodic (negative), with the given segment's surface area. The column widths in Figures 5.1 to 5.4 correspond to the length of the individual segments. Due to the huge differences in anodic and cathodic current densities on the upper reinforcement bars these are shown in separate diagrams, i.e. a top and a bottom diagram showing the anodic and cathodic current densities, respectively (Figures 5.1 and 5.2).

On the upper segmented reinforcement bar in Slab III with 4 % chloride, both anodes (Segments 17 and 18) behaved anodically, forming a well defined macro-cell with the remaining stainless segments as cathode. A factor of approximately 10 between the current densities of the two anodes was observed, see Figure 5.2. On the upper segmented reinforcement bar in Slab II with 1.5 % chloride, only one of the carbon steel segments (Segment 17) behaved anodically. The other, i.e. Segment 18 did not start to corrode but acted as cathode, see Figure 5.1. In both Slabs II and III the cathodic macro-cell current density decreased with increasing distance from the central anodes; significantly higher current densities were found near the borders to the centrally positioned anodic segments.

On the lower segmented reinforcement bars where all segments were made of carbon steel, it was observed that local anodes with different intensities developed in random

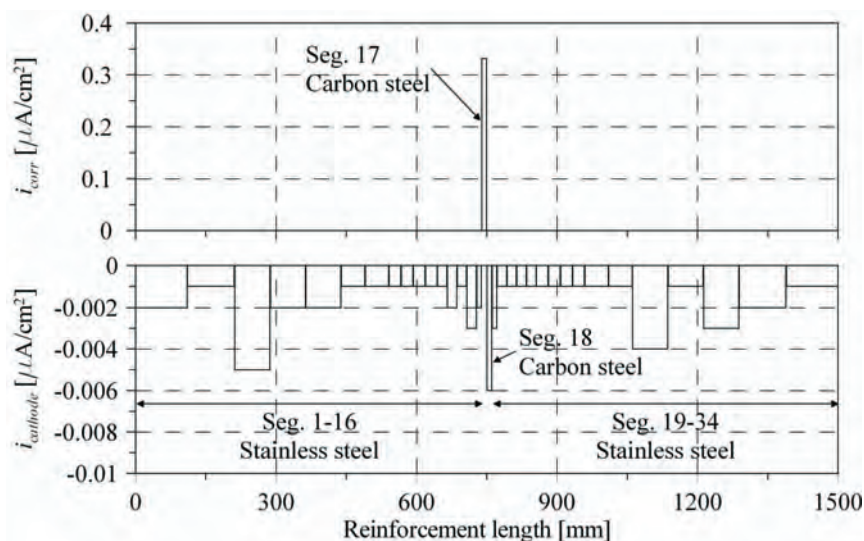


Figure 5.1 Macro-cell current density distribution on the upper segmented reinforcement bar in Slab II with 1.5 % chloride. The current densities of the anodic and cathodic segments, i.e. i_{corr} and $i_{cathode}$ are shown in the top and bottom diagrams, respectively.

positions on the bars, see Figures 5.3 and 5.4. In Slab III with 4 % chloride, the measured current densities of both the upper and lower segmented bars were approximately one order of magnitude higher than in Slab II with 1.5 % chloride. The absolute macro-cell currents, I_{corr} , and calculated current densities, i_{corr} , of the segments found to be anodic on the upper and lower reinforcement bars in Slabs II and III are summarised in Table 5.1.

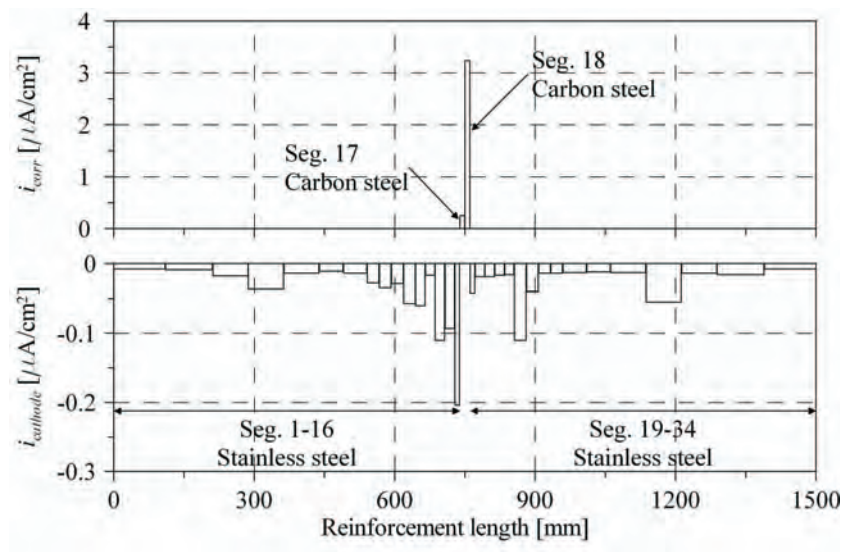


Figure 5.2 Macro-cell current density distribution on the upper segmented reinforcement bar in Slab III with 4 % chloride. The current densities of the anodic and cathodic segments, i.e. i_{corr} and $i_{cathode}$ are shown in the top and bottom diagrams, respectively.

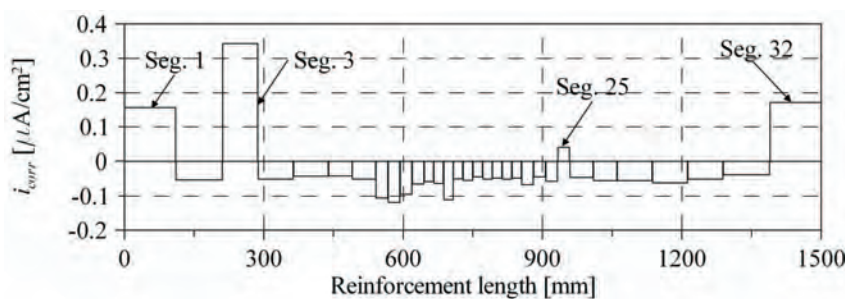


Figure 5.3 Macro-cell current density distribution on the lower reinforcement bar in Slab II with 1.5 % chloride. Segments 1, 3, 25 and 32 are seen to be anodic (positive current densities).

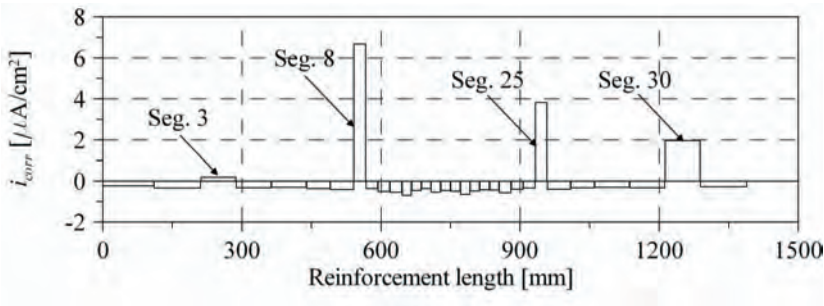


Figure 5.4 Macro-cell current density distribution on the lower reinforcement bar in Slab III with 4 % chloride. Segments 3, 8, 25 and 30 are seen to be anodic (positive current densities).

Table 5.1 Macro-cell currents, I_{corr} , and calculated current densities, i_{corr} , for the anodic segments on the upper and lower segmented reinforcement bars in Slabs II and III.

Slab	Reinforcement bar	Segment	I_{corr} μA	i_{corr} $\mu A/cm^2$
II	Upper	17	1.3	0.3
		1	6.5	0.2
	Lower	3	9.7	0.3
		25	0.4	0.1
		32	7.1	0.2
III	Upper	17	0.9	0.3
		18	12.2	3.2
	Lower	3	5.3	0.2
		8	62.9	6.7
		25	36.1	3.8
		30	55.6	2.0

5.1.2 Half-cell potential and polarisation resistance measurements

The half-cell potentials, E_{corr} , apparent polarisation resistances, R_P^{app} , and ohmic resistances, R_Ω , measured on the surfaces of Slabs I to III along each segmented reinforcement bar using the laboratory potentiostat and the *small unconfined electrode assembly* (Section 4.1.3) are shown in Figures 5.5 to 5.7. The red bold lines in the figures indicate the position and approximate anode sizes on the segmented reinforcement bars: The uppermost line represents the two central anodes on the upper segmented bar and the lower lines on the first axis represent the anodes on the lower segmented bars.

The apparent polarisation resistances, R_P^{app} , were calculated using Equation 3.1 and a steel area, A , of 22.6 cm² corresponding to a reinforcement length of 60 mm (equal to the counter-electrode diameter) and the diameter of 12 mm. By assuming a constant polarisation area an error depending on the polarisation resistance, R_P , to be measured is introduced, see Section 3.3. Despite this, such procedure is often used in practice when a small unconfined counter-electrode, resulting in non-uniform current distribution is used. To reflect this, it has therefore also been done in the present work.

For all the segmented reinforcement bars, the half-cell potentials, E_{corr} , apparent polarisation resistances, R_P^{app} , and ohmic resistances, R_Ω , were seen to be almost constant along each bar. Only on the upper segmented bar in Slab III, at the surface with a cover thickness of 30 mm, slightly more negative half-cell potentials were measured at the center of the bar directly above the corroding anodes, see Figure 5.7. On Slab I, with 0 % chloride, the half-cell potentials, E_{corr} , of the upper and lower segmented reinforcement bars were both seen to range from approximately -40 to -100 mV versus Ag/AgCl, see Figure 5.5. On Slabs II and III with 1.5 % and 4 % chloride the half-cell potentials, E_{corr} , of the lower segmented bars, made of carbon steel segments only, were much more negative than the values of the upper segmented bars with small anodes and large stainless cathodes, see Figures 5.6 and 5.7.

The half-cell potentials, E_{corr} , polarisation resistances, R_P , and ohmic resistances, R_Ω , measured on single, groups and all segments, using a large counter-electrode placed on the concrete surface ensuring uniform polarisation, are given in Tables 5.2 and 5.3. The polarisation resistance, R_P , of each segment group, i.e. a single, groups or all segments, was calculated using Equation 3.1 and the total surface area, A , of the segments in the group. Corrosion current densities, i_{corr} , were calculated for the two passive reinforcement bars in Slab I (upper and lower) and all actively corroding segments on the upper and lower bars in Slabs II and III, see Table 5.1. The corrosion current densities, i_{corr} , were calculated using the Stern-Geary equation given in Equation 2.19, the obtained polarisation resistances, R_P , and a B value of 52 mV for the passive bars in Slab I and 26 mV for the anodic segments in Slabs II and III.

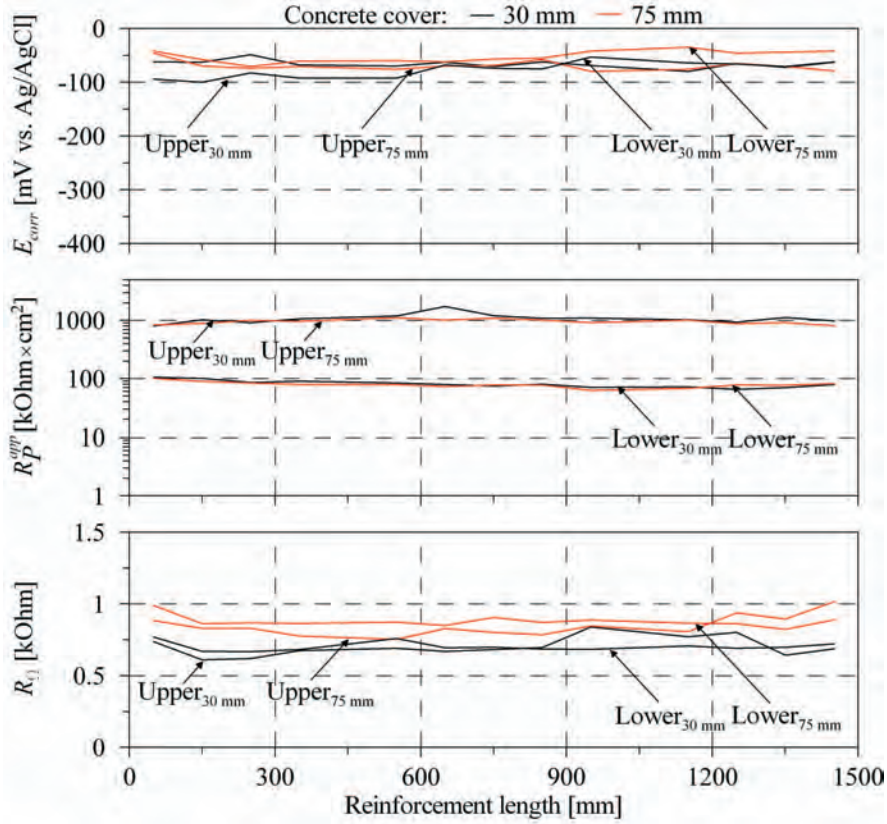


Figure 5.5 Slab I (0 % chloride): Half-cell potentials, E_{corr} , (top), apparent polarisation resistances, R_p^{app} , (middle) and ohmic resistances, R_Ω , (bottom) measured on both surfaces (30 and 75 mm cover) along the upper and lower segmented reinforcement bars at intervals of 50 mm with the small unconfined electrode assembly and the laboratory potentiostat.

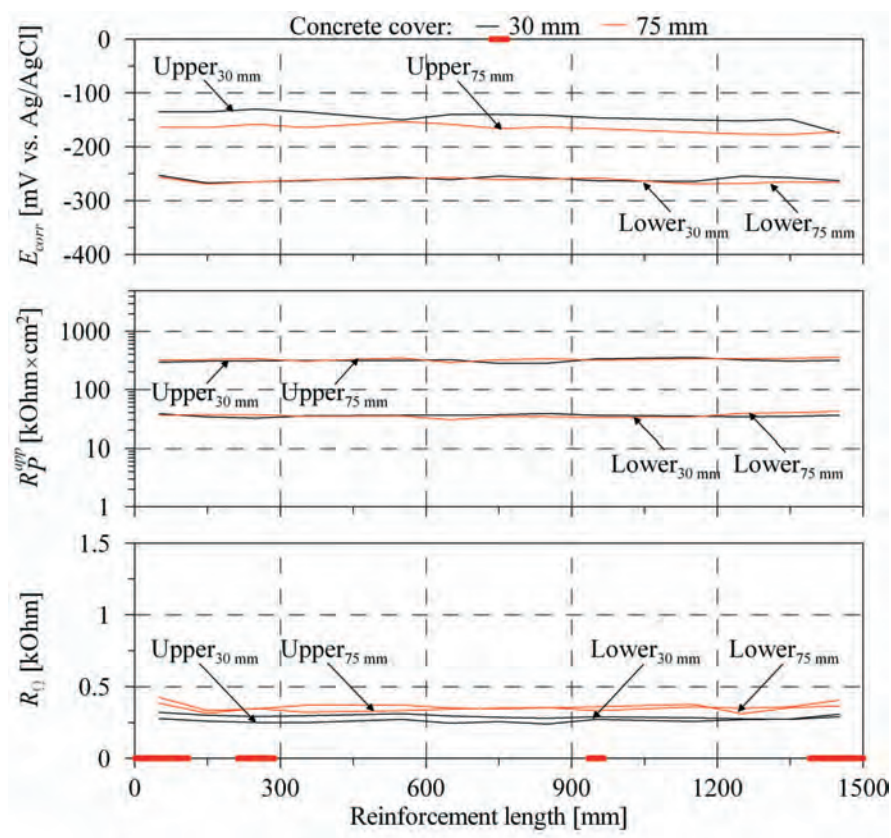


Figure 5.6 Slab II (1.5 % chloride): Half-cell potentials, E_{corr} , (top), apparent polarisation resistances, R_p^{app} , (middle) and ohmic resistances, R_Ω (bottom) measured on both surfaces (30 and 75 mm cover) along the upper and lower segmented reinforcement bars at intervals of 50 mm with the small unconfined electrode assembly and the laboratory potentiostat. The uppermost red bold line indicates the position and size of the two central anodes on the upper segmented bar, whereas the red bold lines on the first axis indicate the positions and sizes of the anodes on the lower segmented bar.

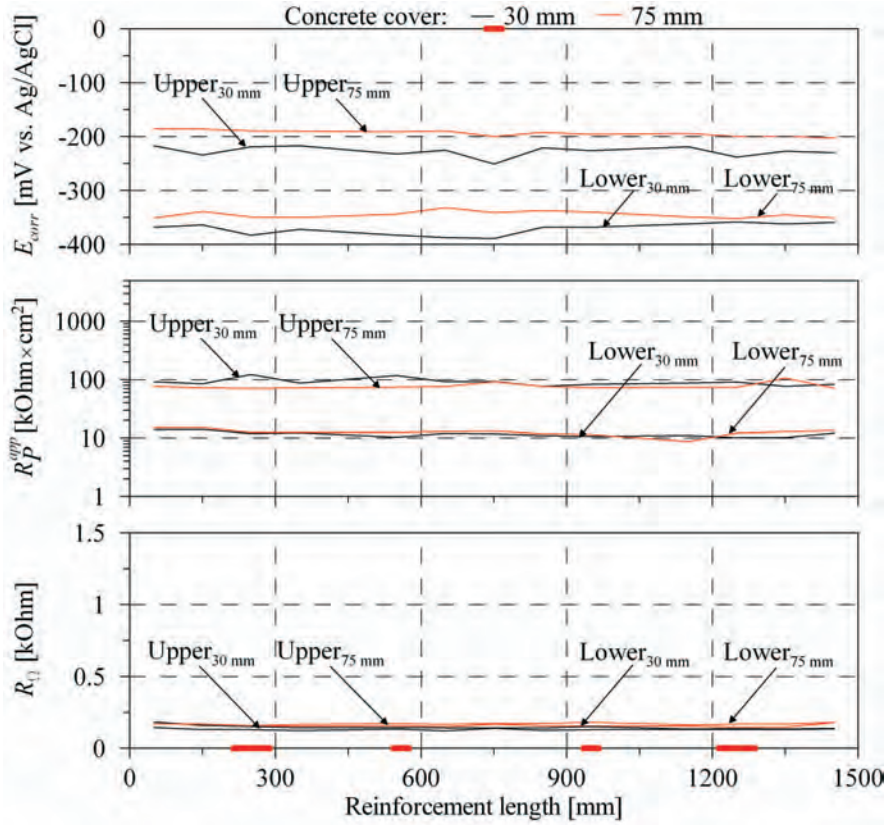


Figure 5.7 Slab III (4 % chloride): Half-cell potentials, E_{corr} , (top), apparent polarisation resistances, R_p^{app} , (middle) and ohmic resistances, R_Ω (bottom) measured on both surfaces (30 and 75 mm cover) along the upper and lower segmented reinforcement bars at intervals of 50 mm with the small unconfined electrode assembly and the laboratory potentiostat. The uppermost red bold line indicates the position and size of the two central anodes on the upper segmented bar, whereas the red bold lines on the first axis indicate the positions and sizes of the anodes on the lower segmented bar.

Table 5.2 Slabs I to III, upper bars: Half-cell potentials, E_{corr} , polarisation resistances, R_P , and ohmic resistances, R_Ω , measured with the large counter-electrode ensuring uniform polarisation and the laboratory potentiostat.

Slab	Segment	E_{corr} mV vs. Ag/AgCl	R_P kOhm \times cm ²	R_Ω kOhm	i_{corr} μ A/cm ²
I	1-34	-27	23.3×10^3	0.05	0.002
	1-34	-122	6.2×10^3	0.02	-
	1-16	-107	23.3×10^3	0.13	-
II	17	-242	122	0.69	0.21
	18	-132	269	0.68	-
	19-34	-133	66.9×10^3	0.13	-
	1-34	-282	1.2×10^3	0.01	-
III	1-16	-60	7.2×10^3	0.02	-
	17	-315	46	0.27	0.56
	18	-363	17	0.28	1.49
	19-34	-60	1.3×10^3	0.03	-

Table 5.3 Slabs I to III, lower bars: Half-cell potentials, E_{corr} , polarisation resistances, R_P , and ohmic resistances, R_Ω , measured with the large counter-electrode ensuring uniform polarisation and the laboratory potentiostat.

Slab	Segment	E_{corr} mV vs. Ag/AgCl	R_P kOhm \times cm ²	R_Ω kOhm	i_{corr} μ A/cm ²
I	1-32	-29	4.8×10^3	0.05	0.01
	1-32	-298	508	0.02	-
	1	-359	197	0.20	0.13
II	3	-375	110	0.18	0.24
	25	-270	68	0.33	0.38
	32	-375	196	0.16	0.13
	1-32	-443	79	0.01	-
	3	-413	62	0.09	0.42
III	8	-467	10	0.17	2.65
	25	-453	12	0.17	2.12
	30	-373	85	0.09	0.31

5.1.3 Measurements with commercial corrosion rate instruments

This section presents the results from the measurements with the two commercial corrosion rate instruments, and the setup allowing monitoring of the instruments' operation and the distribution of current between the instruments' electrode assemblies placed on the concrete surface and a segmented reinforcement bar during corrosion rate measurements. The results are divided into three sections after the corrosion state of the segmented reinforcement bars, on which the measurements were performed, i.e. passive reinforcement (Slab I), intense localised corrosion (upper bars in Slabs II and III) and general corrosion (lower bars in Slabs II and III).

Passive reinforcement

The half-cell potentials, E_{corr} , corrosion current densities, i_{corr} , and ohmic resistances, R_Ω , measured with the GECOR 6 and GalvaPulse on the upper and lower reinforcement bars in Position 4 on Slab I are given in Table 5.4, together with the applied counter-electrode currents, I_{CE} , used for the measurements and the potential shifts, ΔE , obtained. Real-time recordings of the GECOR 6 and GalvaPulse measurements on the upper bar are shown in Figures 5.9 to 5.11, whereas the recordings of the measurements on the lower bar are shown in Figures 5.12 to 5.14.

In the top graphs in Figures 5.9 to 5.14 the currents applied from the counter-electrode, I_{CE} , and guard ring, I_{GE} , are shown together with the measured potential response, E , as a function of time. From the measurements on the upper segmented reinforcement bar (top graphs in Figures 5.9 to 5.11), it can be observed that both instruments held the counter-electrode current, I_{CE} , constant: the GECOR 6 at 7 to 9 μA and the GalvaPulse at 20 μA , see Table 5.4. However, the guard ring currents, I_{GE} , were seen to vary: during the measurements with the GalvaPulse constant guard ring currents of 28 μA (30 mm cover) and 20 μA (75 mm cover) were observed, whereas in the experiment with the GECOR 6 the guard ring currents increased continuously to a maximum of 35 μA (30 mm cover) and 74 μA (75 mm cover) at the end of the polarisation periods. The reinforcement potential was shifted approximately 180 mV (30 mm cover) and 250 mV (75 mm cover) in cathodic direction during the GECOR 6 measurements, and 80 mV (30 mm cover) and 65 mV (75 mm cover) in anodic direction during the GalvaPulse measurements (including ohmic potential drop). A potential shift of approximately 40 mV in anodic direction was observed for both measurements with the GalvaPulse when no current confinement was used, see Table 5.4.

On the lower reinforcement bar (top graphs in Figures 5.12 to 5.14), both instruments were also seen to keep the counter-electrode current, I_{CE} , constant: the GECOR 6 at 9 μA and the GalvaPulse at 20 μA , independent of the cover thickness, see Table 5.4 and Figures 5.12 to 5.14. Constant guard ring currents, I_{GE} , were also here applied by the GalvaPulse independently of the concrete cover (Figures 5.13 and 5.14). However, the guard ring currents, I_{GE} , applied by the GECOR 6 were seen to differ significantly from the I_{GE} applied when measuring on the upper reinforcement bar, see Figure 5.12: During the measurement on the surface with a concrete cover of 30 mm, the I_{GE} increased to

approximately 20 μA within the first 10 seconds of the measurement, after which it was only slightly increasing. A more fluctuating, i.e. first increasing and later decreasing I_{GE} was recorded during the GECOR 6 measurement on the surface with a concrete cover of 75 mm. Potential shifts of approximately 70 mV (30 mm cover) and 40 mV (75 mm cover) in cathodic direction were observed during the GECOR 6 measurements. For the GalvaPulse measurements, with and without current confinement, potential shifts of approximately 70 mV (30 mm cover) and 40 mV (75 mm cover), and 25 mV (30 and 75 mm cover) in anodic direction were observed, respectively.

In the middle graphs in Figures 5.9 to 5.14 the ratios I'_{CE}/I_{CE} and lengths L_{CE} are given as a function of time for the GECOR 6 and GalvaPulse measurements. I'_{CE}/I_{CE} is the ratio between the current, I'_{CE} , flowing into the reinforcement over the assumed confinement length, L'_{CE} , and the current applied from the counter-electrode, I_{CE} . L_{CE} is the length over which the counter-electrode current, I_{CE} , is distributed, see Figure 5.8. Full confinement is achieved if a ratio I'_{CE}/I_{CE} of 1 is obtained, whereas values lower and higher than 1 correspond to under and over-confinement, respectively. Both the I'_{CE} and the L_{CE} were calculated from the current distributions measured on the segmented reinforcement bars. For the GECOR 6 and GalvaPulse the I'_{CE} was calculated by numerical integration of the current distribution over the assumed confinement lengths, L'_{CE} (105 mm and 70 mm, respectively) below the electrode assembly. L_{CE} was calculated by numerically integrating the current distribution from the center of, and symmetrically on each side of the electrode assembly, until a current equal to I_{CE} was obtained. The bold dotted line in the graphs indicate the L_{CE} , at which optimal confinement is obtained, i.e. 105 mm and 70 mm for the GECOR 6 and GalvaPulse, respectively. The L_{CE} has not been calculated for the GalvaPulse measurements where no current confinement was used (Figures 5.11 and 5.14).

Examples of the measured current distributions, from which the I'_{CE} and L_{CE} were calculated are shown in the bottom graphs in Figures 5.9 to 5.14. For the measurements with the GECOR 6 three curves are shown, illustrating the change of the current distribution over time, whereas two curves are shown for the GalvaPulse measurements due to the much shorter measurement time. The bold blue line on the first axis indicates the position and size of the assumed confinement length, L'_{CE} , on the embedded segmented reinforcement bar.

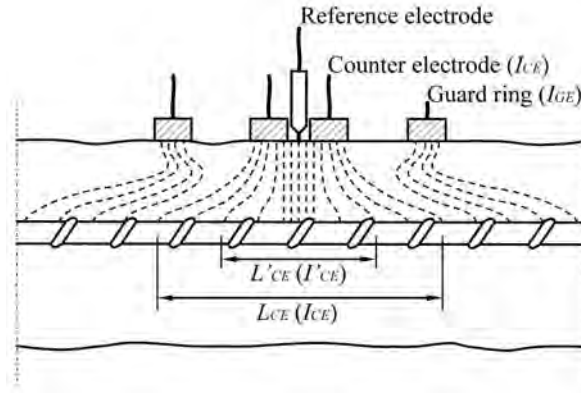


Figure 5.8 Schematic illustration of the current, I'_{CE} , flowing into the reinforcement over the assumed confinement length, L'_{CE} , and the length L_{CE} over which the applied counter-electrode current, I_{CE} , is distributed. A current I_{GE} is applied from the guard ring for confining the counter-electrode current, I_{CE} .

Table 5.4 Results from measurements with the GECOR 6 and GalvaPulse with and without current confinement (conf. on and conf. off, respectively) in Position 4 on the upper and lower segmented reinforcement bars in Slab I. The numbers in brackets are the half-cell potentials measured versus the embedded MnO_2 reference electrode (mV versus MnO_2).

	Cover mm	E_{corr} mV vs. Ag/AgCl	i_{corr} $\mu\text{A}/\text{cm}^2$	R_Ω kOhm	I_{CE} μA	ΔE mV
Upper bar						
GECOR 6	30	+25* (-285)	0.03	0.37	7	-176
	75	+25* (-262)	0.02	0.49	9	-251
GalvaPulse conf. on	30	-35 (-320)	0.31	1.0	20	76
	75	-63 (-326)	0.31	1.0	20	66
GalvaPulse conf. off	30	-20 (-342)	0.77	1.0	20	38
	75	-76 (-334)	0.77	1.0	20	36
Lower bar						
GECOR 6	30	-52* (-340)	0.09	0.48	9	-69
	75	-47* (-337)	0.16	0.59	9	-40
GalvaPulse conf. on	30	-81 (-349)	0.70	1.0	20	44
	75	-91 (-341)	0.89	2.0	20	53
GalvaPulse conf. off	30	-87 (-344)	1.46	1.0	20	24
	75	-88 (-346)	1.82	1.0	20	25

*: Converted from mV versus Cu/CuSO_4 to mV versus Ag/AgCl by adding +117 mV.

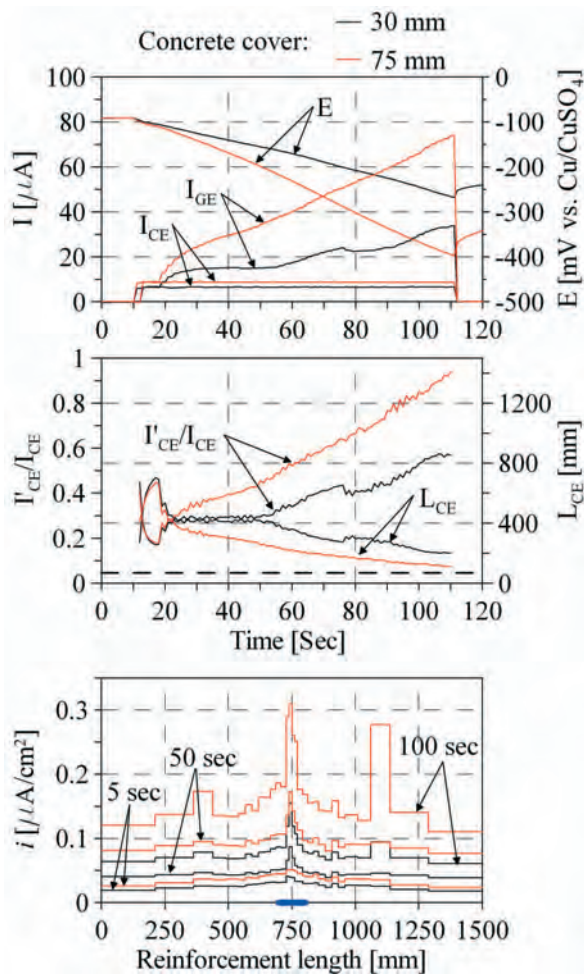


Figure 5.9 GECOR 6 measurements on the upper reinforcement bar in Slab I, Position 4. The bold blue line indicates the assumed confinement length on the segmented reinforcement bar.

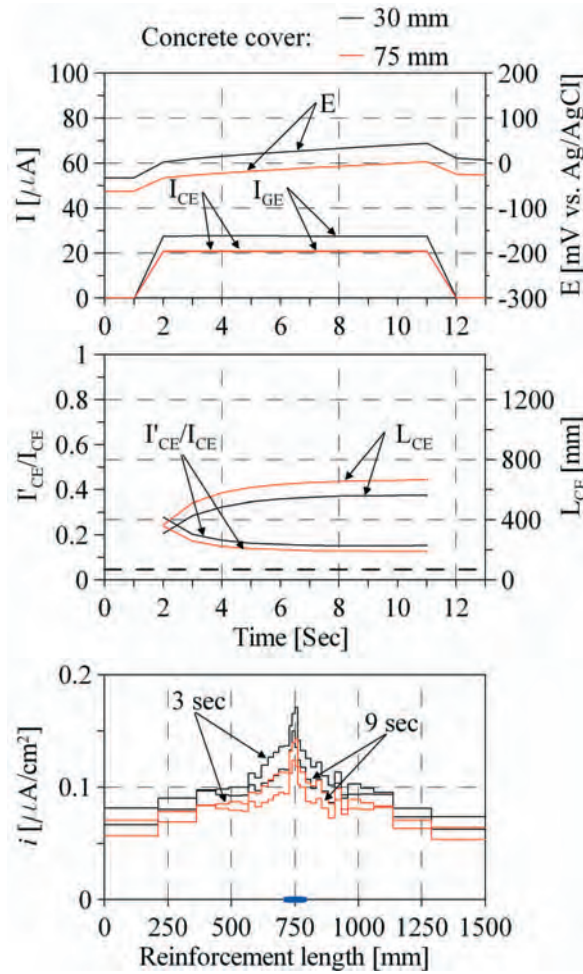


Figure 5.10 GalvaPulse measurements with use of current confinement on the upper reinforcement bar in Slab I, Position 4. The bold blue line indicates the assumed confinement length on the segmented reinforcement bar.

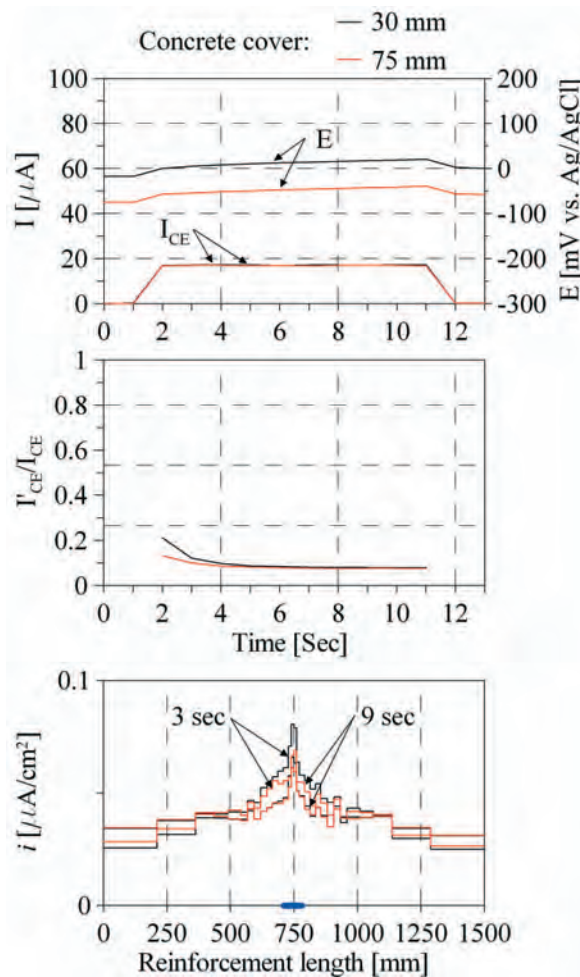


Figure 5.11 GalvaPulse measurements without use of current confinement on the upper reinforcement bar in Slab I, Position 4. The bold blue line indicates the assumed confinement length on the segmented reinforcement bar.

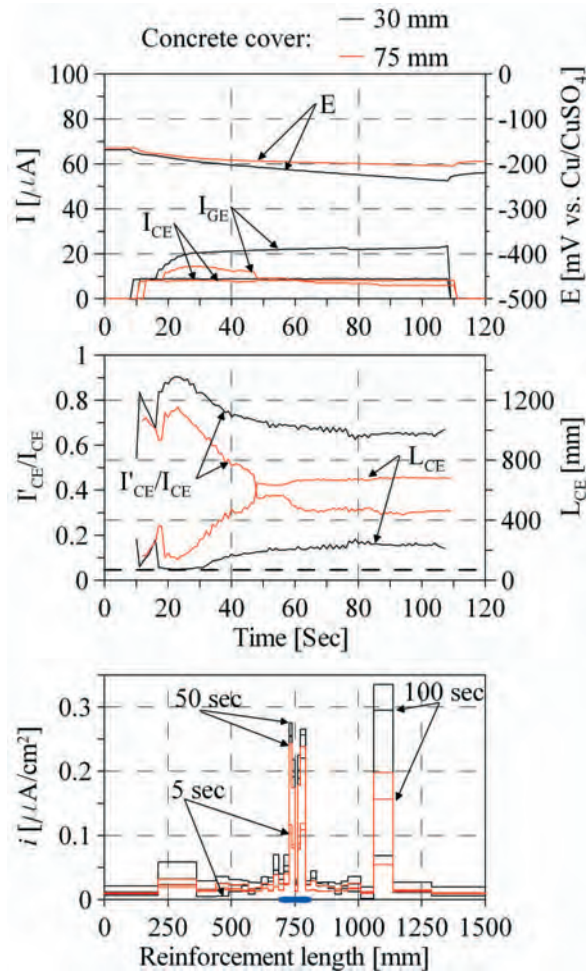


Figure 5.12 GECOR 6 measurements on the lower reinforcement bar in Slab I, Position 4. The bold blue line indicates the assumed confinement length on the segmented reinforcement bar.

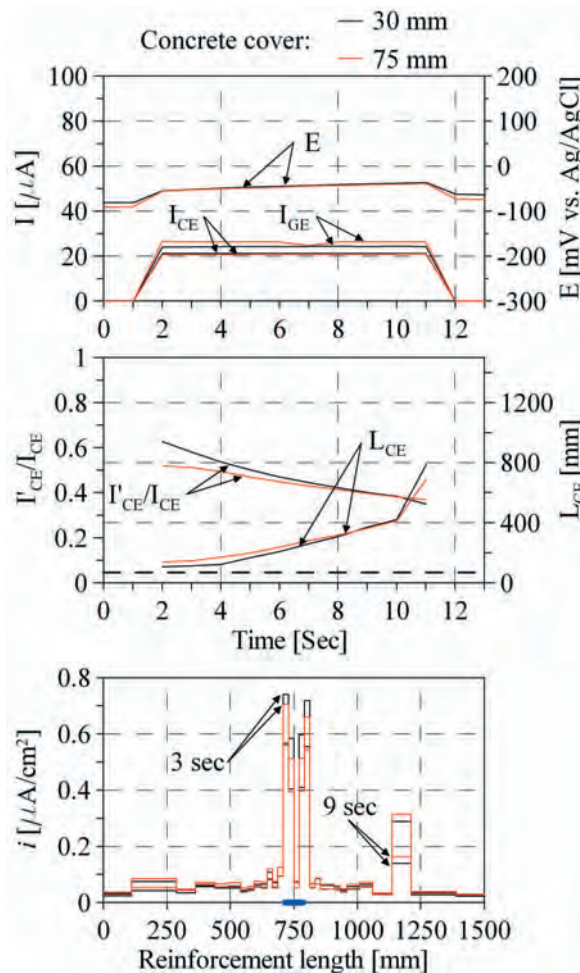


Figure 5.13 GalvaPulse measurements with use of current confinement on the lower reinforcement bar in Slab I, Position 4. The bold blue line indicates the assumed confinement length on the segmented reinforcement bar.

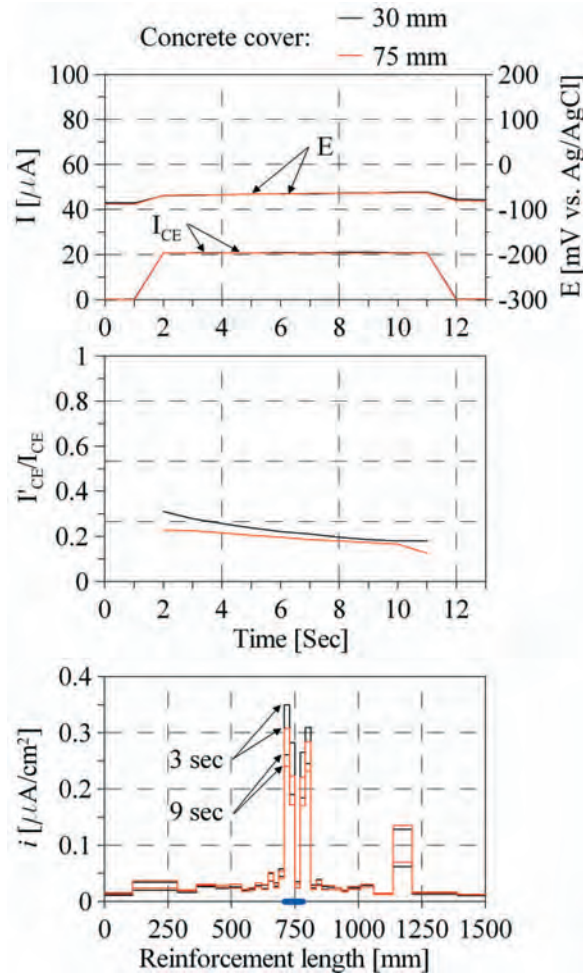


Figure 5.14 GalvaPulse measurements without use of current confinement on the lower reinforcement bar in Slab I, Position 4. The bold blue line indicates the assumed confinement length on the segmented reinforcement bar.

Intense localised corrosion

The half-cell potentials, E_{corr} , and corrosion current densities, i_{corr} , measured with the GECOR 6 and GalvaPulse instruments on the upper reinforcement bars in Positions 1 to 7 on Slabs II and III are shown in Figures 5.15 and 5.16. The half-cell potentials, E_{corr} , measured with the GECOR 6 have been converted from mV versus Cu/CuSO₄ to mV versus Ag/AgCl by adding +117 mV (Myrdal, 2007). The numeric values of the measurements shown in Figures 5.15 and 5.16 are given in Appendix D together with the measured ohmic resistances, R_{Ω} , the counter-electrode currents, I_{CE} , applied during the measurements and the potential shifts, ΔE , obtained.

No significant differences between the half-cell potentials, E_{corr} , measured with the GECOR 6 and GalvaPulse were observed (top graphs in Figures 5.15 and 5.16). As seen from the bottom graphs in Figures 5.15 and 5.16 significantly different corrosion current densities, i_{corr} , were obtained with the GECOR 6 and GalvaPulse. However, almost constant corrosion current densities, i_{corr} , were obtained with the two instruments in all 7 measurement positions, on both Slabs II and III.

Only selected and representative real-time recordings of the measurements in Figures 5.15 and 5.16 are included in the present work for explaining the differences in performance of the two instruments: The real time recordings of the measurements with the GECOR 6 and GalvaPulse instruments in Positions 2, 3 and 4, i.e. away from, near and directly over the anodes, on Slabs II and III are shown in Figures 5.17 to 5.25, and 5.26 to 5.34, respectively. A presentation of the real-time recordings and the procedure used for calculation of the parameters I'_{CE}/I_{CE} and L_{CE} can be found in the previous section. For the measurements on the upper reinforcement bars in Slabs II and III the length L_{CE} has only been calculated in Position 4 directly over the two anodes.

When considering the GECOR 6 measurements on the upper bar in Slabs II and III it can be seen that the counter-electrode current, I_{CE} , was kept constant during all measurements, see Figures 5.17 to 5.19, top graphs. A significant effect of the measurement position and cover thickness on the applied guard ring current, I_{GE} , was observed: On Slab II in Positions 2 and 3, i.e. over passive reinforcement away from the central anodes, the applied guard ring current, I_{GE} , steadily increased during the measurements, whereas the I_{GE} was almost constant or only slightly increasing when measuring in Position 4, directly over the anodes. Independent of the measurement position and cover thickness, a large part of the applied current ($I_{CE} + I_{GE}$) was seen to flow into the two central anodes, see Figures 5.17 to 5.19, bottom graphs.

On Slab III where the corrosion rate of the central anodes was higher compared to Slab II, a lower guard ring current, I_{GE} , was applied by the GECOR 6. During the measurements in Positions 2, 3 and 4 on Slab III the I_{GE} was either almost constant, slightly increasing or decreasing, see Figures 5.26 to 5.28, top graphs. As a result of the higher corrosion rate of the local anodes a larger part of the applied current ($I_{CE} + I_{GE}$), compared with the measurements on Slab II, flowed into the corroding anodes. A clear effect of this was

seen from the calculated I'_{CE}/I_{CE} ratios: In Positions 2 and 3, over passive reinforcement, I'_{CE}/I_{CE} ratios of only approximately 0.2 were obtained, whereas I'_{CE}/I_{CE} ratios of approximately 1.9 (30 mm cover) and 1.2 (75 mm cover) were obtained in Position 4 at the end of the measurements, when measuring directly over the anodes, see Figures 5.26 to 5.28, middle graphs.

From the GalvaPulse measurements on the upper reinforcement bar in Slabs II and III, both the counter-electrode and guard ring currents were seen to be constant during all measurements, see Figures 5.20 to 5.22 and 5.29 to 5.30, top graphs. During the measurements a large part of the applied current ($I_{CE} + I_{GE}$) was seen to flow into the two central anodes, independent of the electrode assembly position and the cover thickness. Despite this I'_{CE}/I_{CE} ratios of 0.1 to 0.2 were only obtained on Slab II in both Positions 2 and 3, over passive steel and in Position 4 directly over the anodes. On the contrary, on Slab III the large current flow through the central anodes, resulted in I'_{CE}/I_{CE} ratios of approximately 0.1 when measuring over passive steel (Positions 2 and 3) while I'_{CE}/I_{CE} ratios of 0.4 to 0.6 were obtained when measuring directly over the anodes in Position 4.

From the real-time recordings of the GalvaPulse measurements without current confinement it was observed that the I'_{CE}/I_{CE} ratios and the current distributions obtained were almost identical to those obtained with use of current confinement, see Figures 5.23 to 5.25 and 5.32 to 5.34, middle and bottom graphs. However, as the I_{CE} was not accompanied by the constant I_{GE} lower current densities, i , were recorded along the segmented reinforcement bars, resulting in a smaller potential shift.

A thorough discussion of the results, i.e. the measured corrosion current densities, i_{corr} , and the real-time recordings is given in Chapter 6. Before reading Chapter 6, the reader is encouraged to study Figures 5.17 to 5.34 in detail.

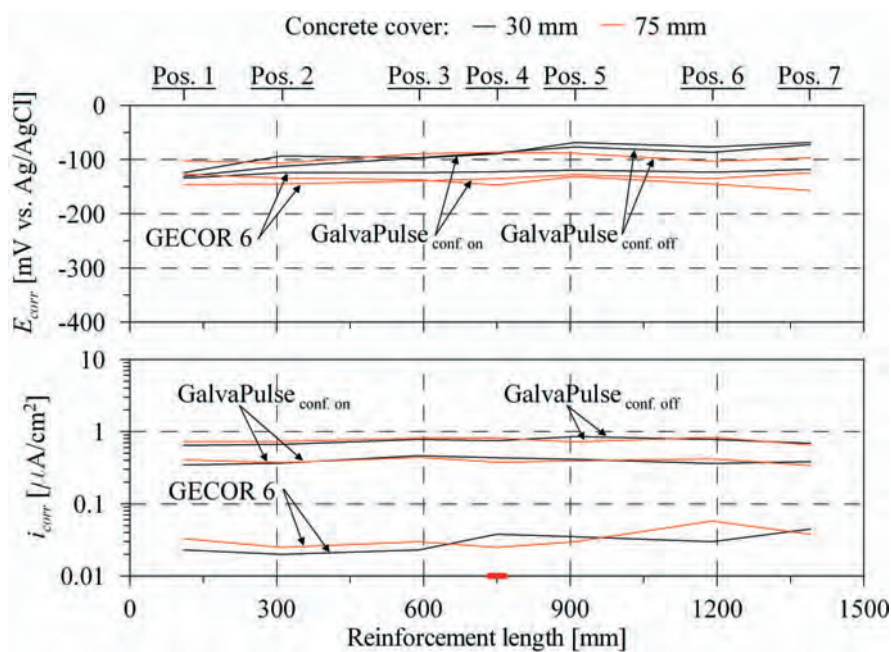


Figure 5.15 Half-cell potentials, E_{corr} , (top) and corrosion current densities, i_{corr} , (bottom) measured with the GECOR 6 and GalvaPulse instruments along the upper segmented reinforcement bar in Slab II. The position and size of the two central anodes is indicated by the red bold line on the first axis.

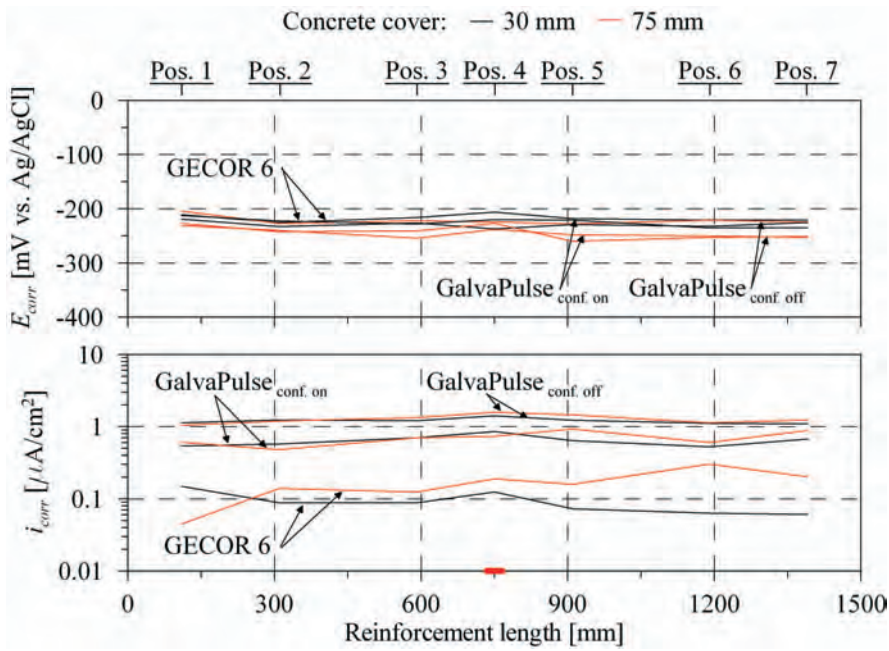


Figure 5.16 Half-cell potentials, E_{corr} , (top) and corrosion current densities, i_{corr} , (bottom) measured with the GECOR 6 and GalvaPulse instruments along the upper segmented reinforcement bar in Slab III. The position and size of the two central anodes is indicated by the red bold line on the first axis.

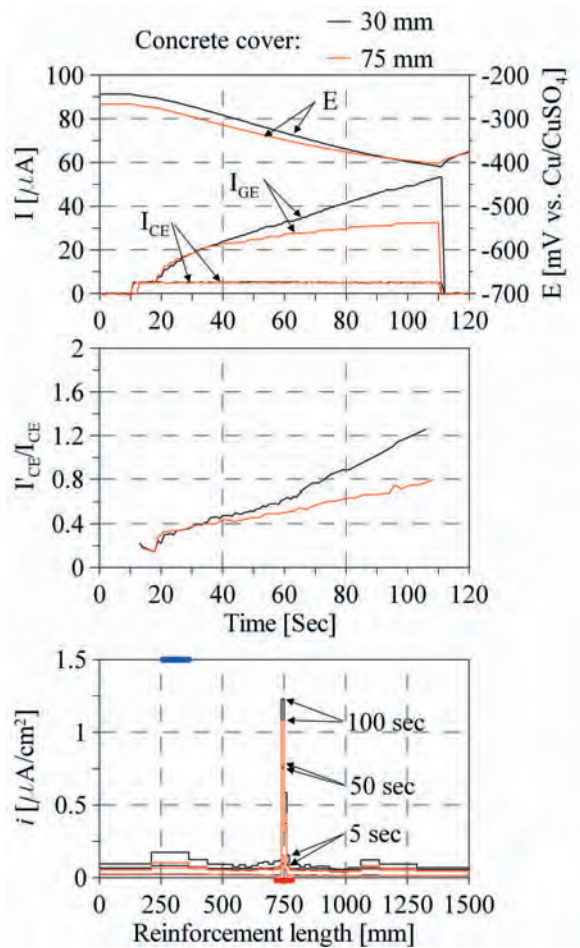


Figure 5.17 GECOR 6 measurements in Position 2 on the upper reinforcement bar in Slab II. The bold blue line indicates the assumed confinement length on the segmented reinforcement bar and the red bold line the position and size of the two central anodes.

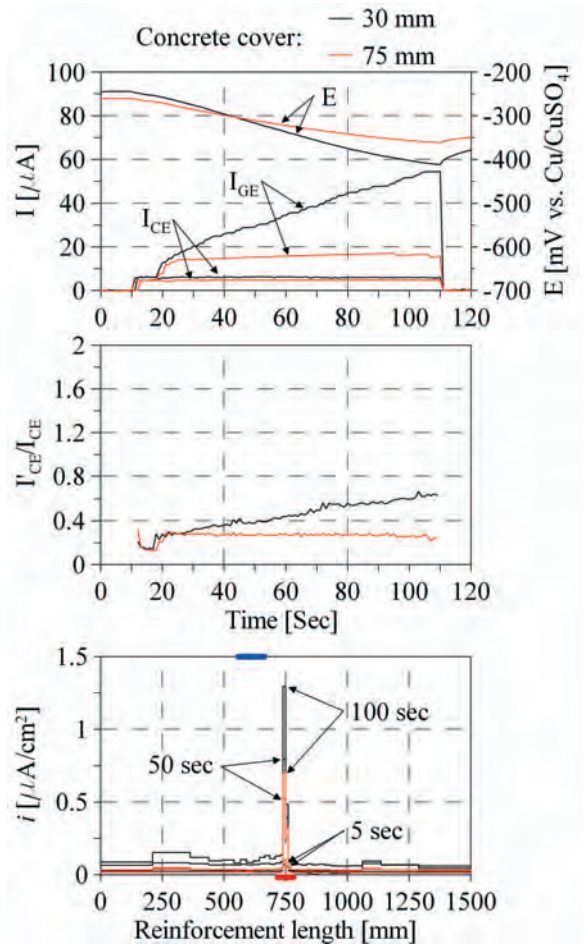


Figure 5.18 GECOR 6 measurements in Position 3 on the upper reinforcement bar in Slab II. The bold blue line indicates the assumed confinement length on the segmented reinforcement bar and the red bold line the position and size of the two central anodes.

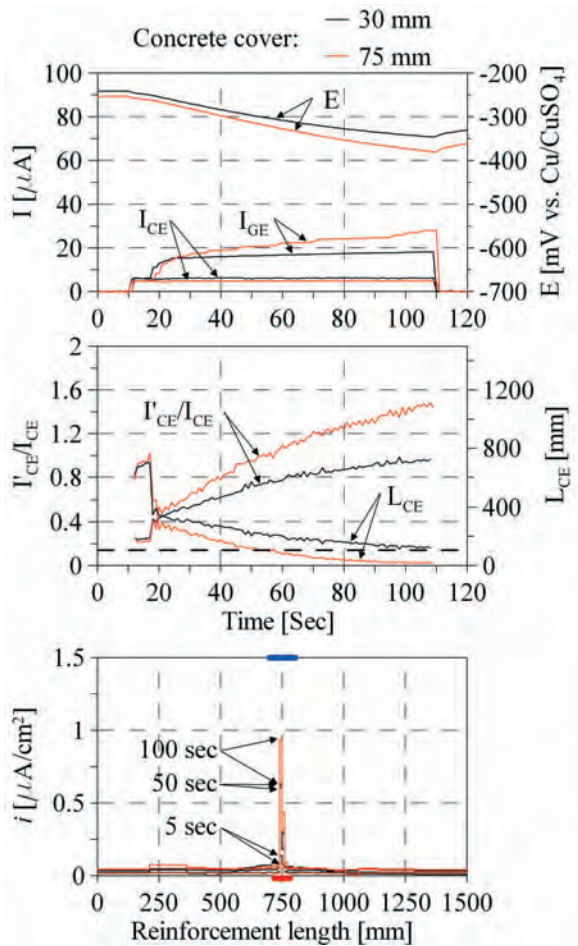


Figure 5.19 GECOR 6 measurements in Position 4 on the upper reinforcement bar in Slab II. The bold blue line indicates the assumed confinement length on the segmented reinforcement bar and the red bold line the position and size of the two central anodes.

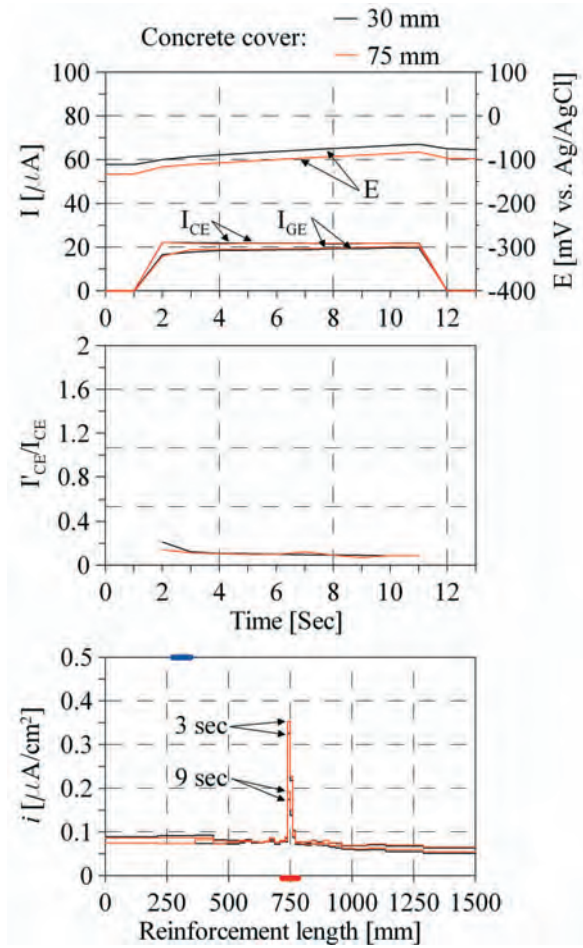


Figure 5.20 GalvaPulse measurements with use of current confinement in Position 2 on the upper reinforcement bar in Slab II. The bold blue line indicates the assumed confinement length on the segmented reinforcement bar and the red bold line the position and size of the two central anodes.

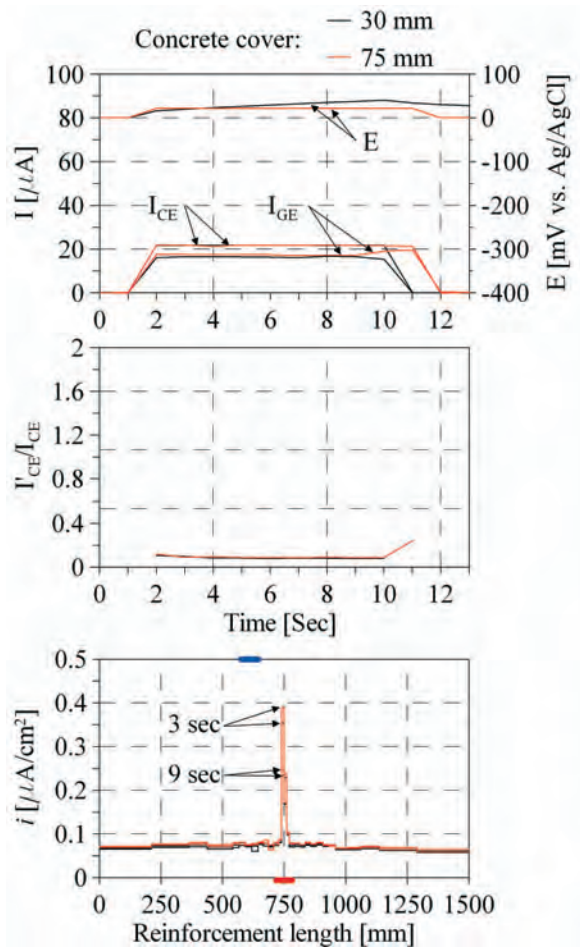


Figure 5.21 GalvaPulse measurements with use of current confinement in Position 3 on the upper reinforcement bar in Slab II. The bold blue line indicates the assumed confinement length on the segmented reinforcement bar and the red bold line the position and size of the two central anodes.

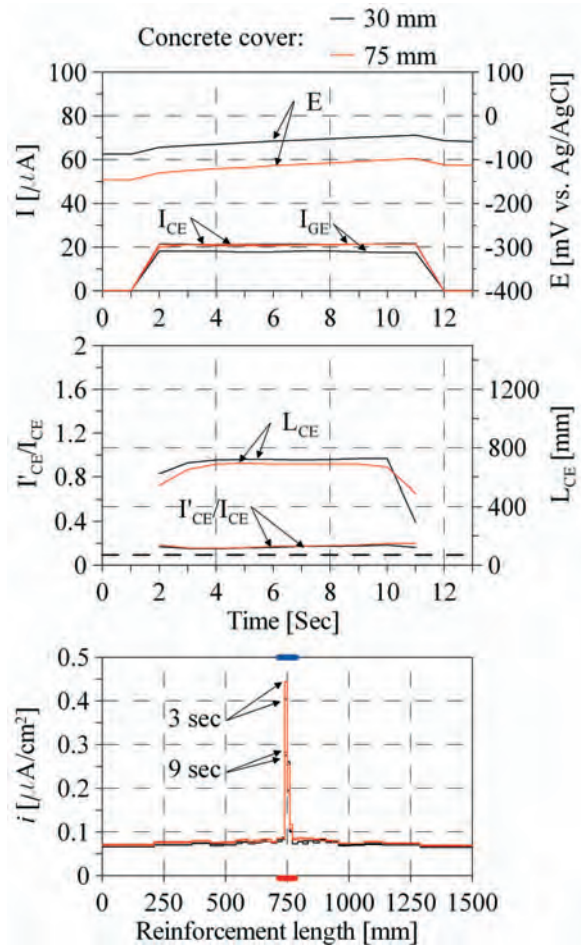


Figure 5.22 GalvaPulse measurements with use of current confinement in Position 4 on the upper reinforcement bar in Slab II. The bold blue line indicates the assumed confinement length on the segmented reinforcement bar and the red bold line the position and size of the two central anodes.

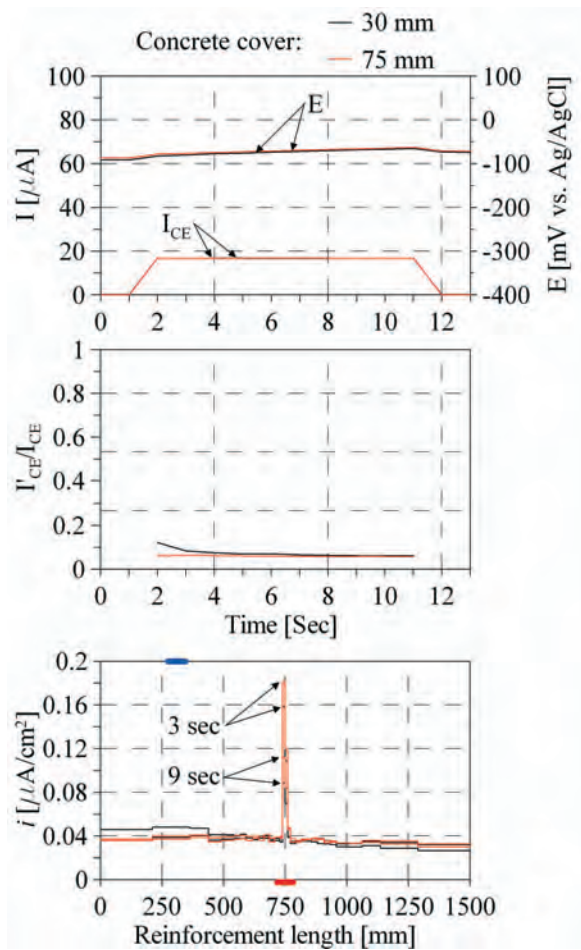


Figure 5.23 GalvaPulse measurements without use of current confinement in Position 2 on the upper reinforcement bar in Slab II. The bold blue line indicates the assumed confinement length on the segmented reinforcement bar and the red bold line the position and size of the two central anodes.

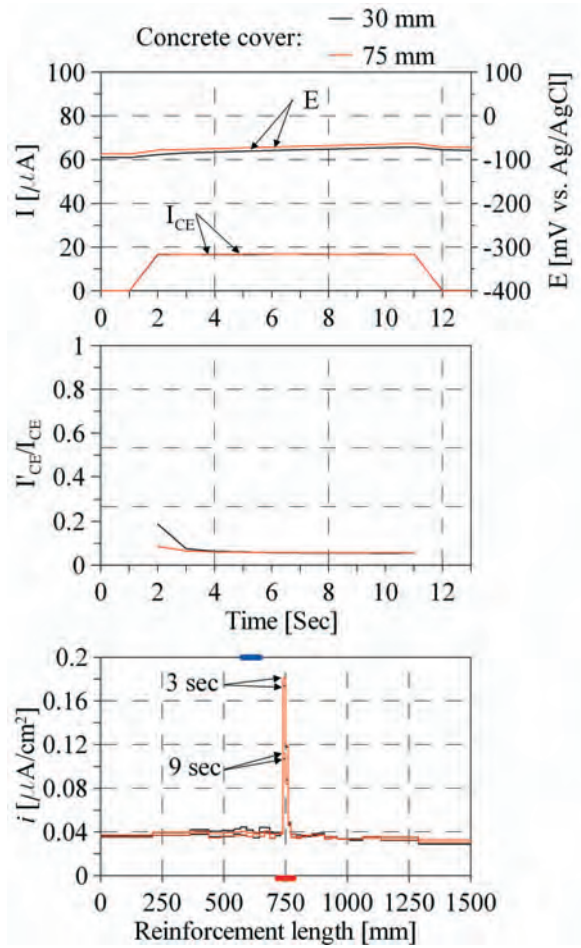


Figure 5.24 GalvaPulse measurements without use of current confinement in Position 3 on the upper reinforcement bar in Slab II. The bold blue line indicates the assumed confinement length on the segmented reinforcement bar and the red bold line the position and size of the two central anodes.

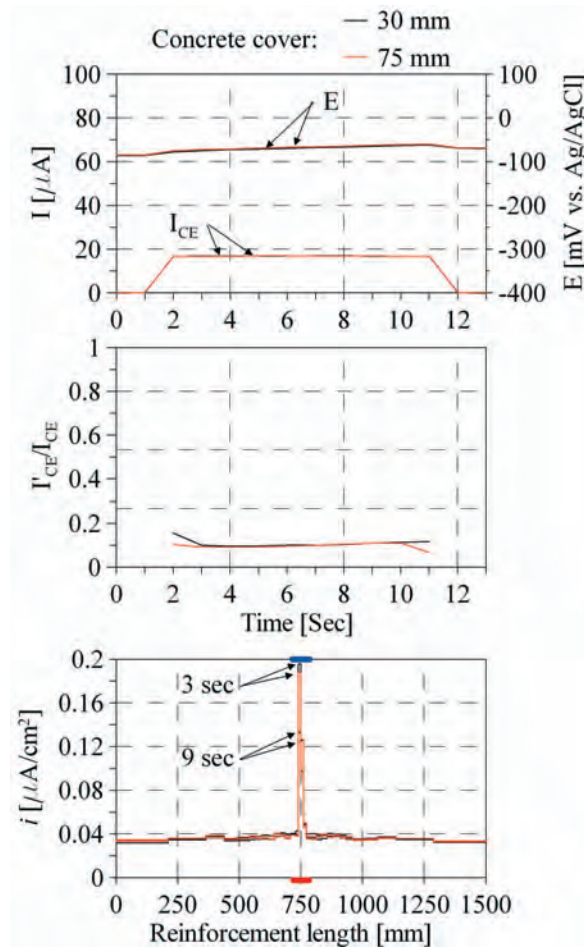


Figure 5.25 GalvaPulse measurements without use of current confinement in Position 4 on the upper reinforcement bar in Slab II. The bold blue line indicates the assumed confinement length on the segmented reinforcement bar and the red bold line the position and size of the two central anodes.

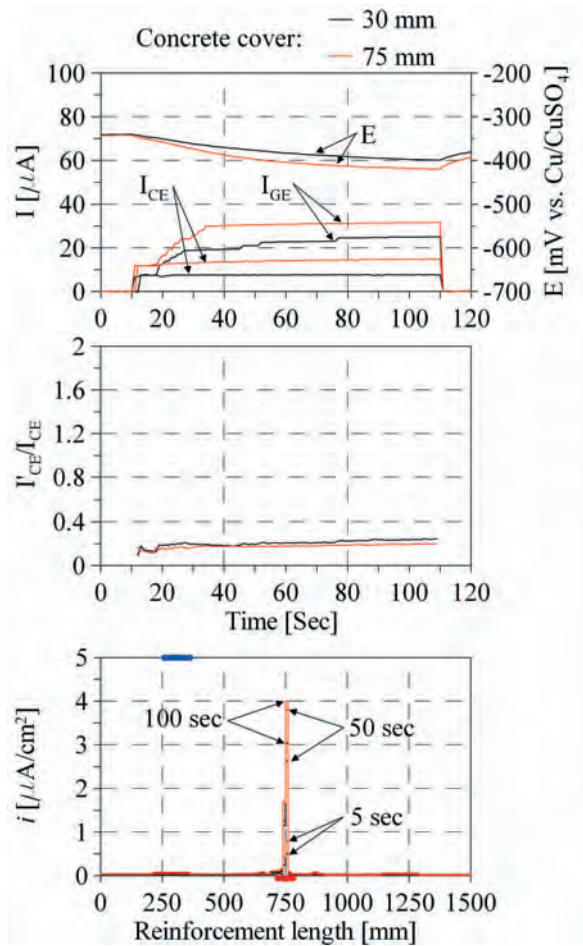


Figure 5.26 GECOR 6 measurements in Position 2 on the upper reinforcement bar in Slab III. The bold blue line indicates the assumed confinement length on the segmented reinforcement bar and the red bold line the position and size of the two central anodes.

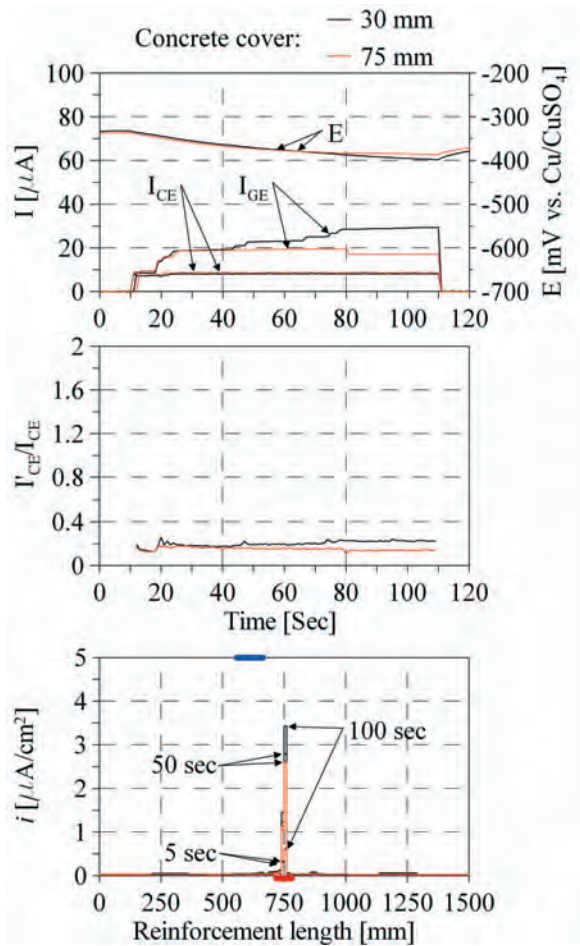


Figure 5.27 GECOR 6 measurements in Position 3 on the upper reinforcement bar in Slab III. The bold blue line indicates the assumed confinement length on the segmented reinforcement bar and the red bold line the position and size of the two central anodes.

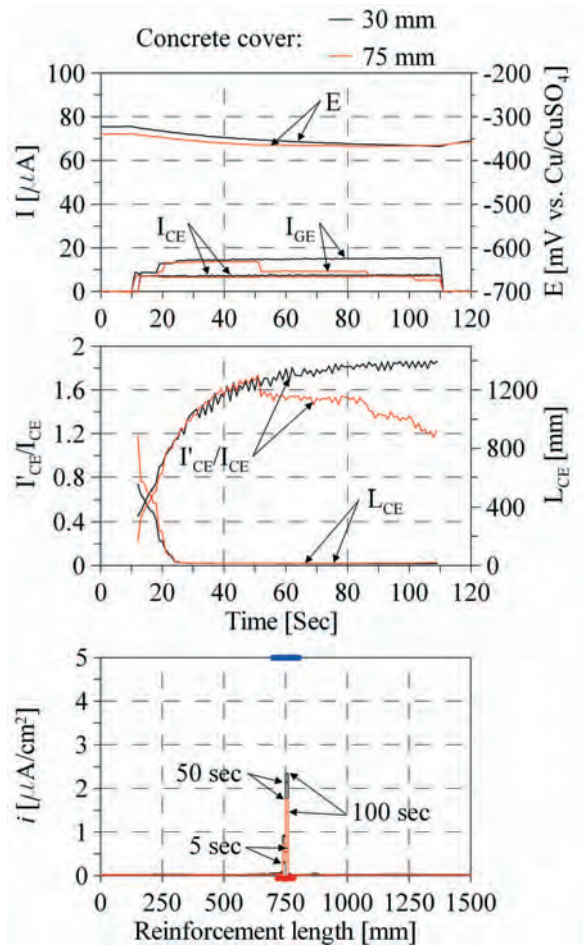


Figure 5.28 GECOR 6 measurements in Position 4 on the upper reinforcement bar in Slab III. The bold blue line indicates the assumed confinement length on the segmented reinforcement bar and the red bold line the position and size of the two central anodes.

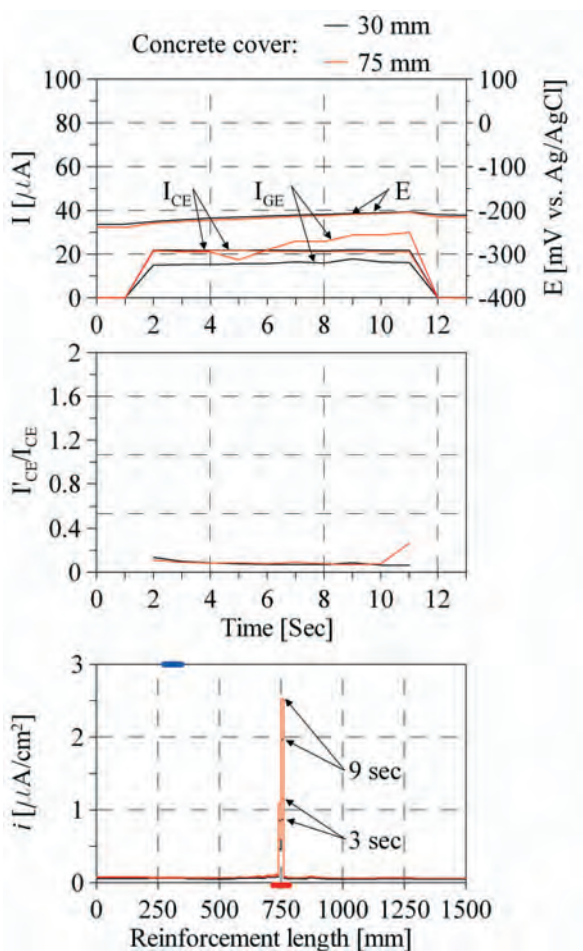


Figure 5.29 GalvaPulse measurements with use of current confinement in Position 2 on the upper reinforcement bar in Slab III. The bold blue line indicates the assumed confinement length on the segmented reinforcement bar and the red bold line the position and size of the two central anodes.

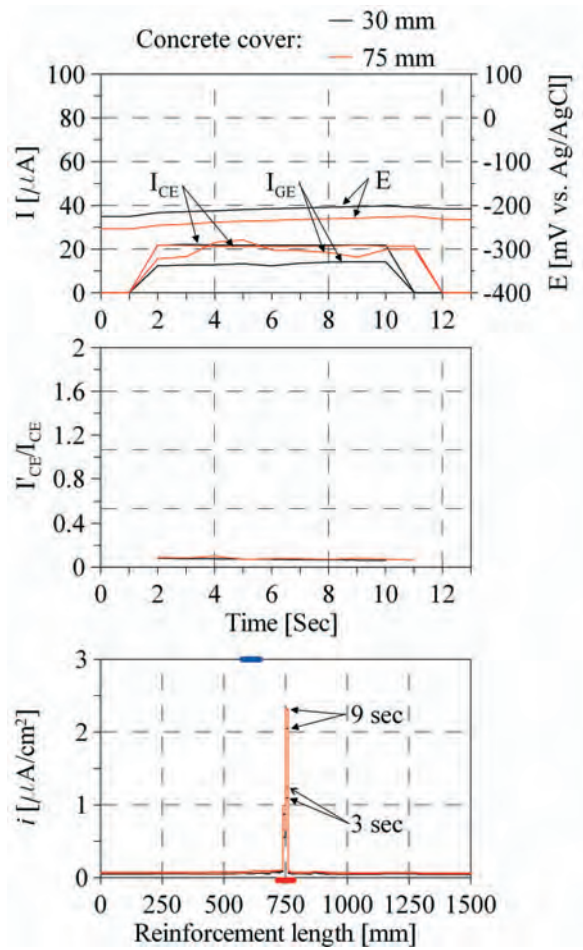


Figure 5.30 GalvaPulse measurements with use of current confinement in Position 3 on the upper reinforcement bar in Slab III. The bold blue line indicates the assumed confinement length on the segmented reinforcement bar and the red bold line the position and size of the two central anodes.

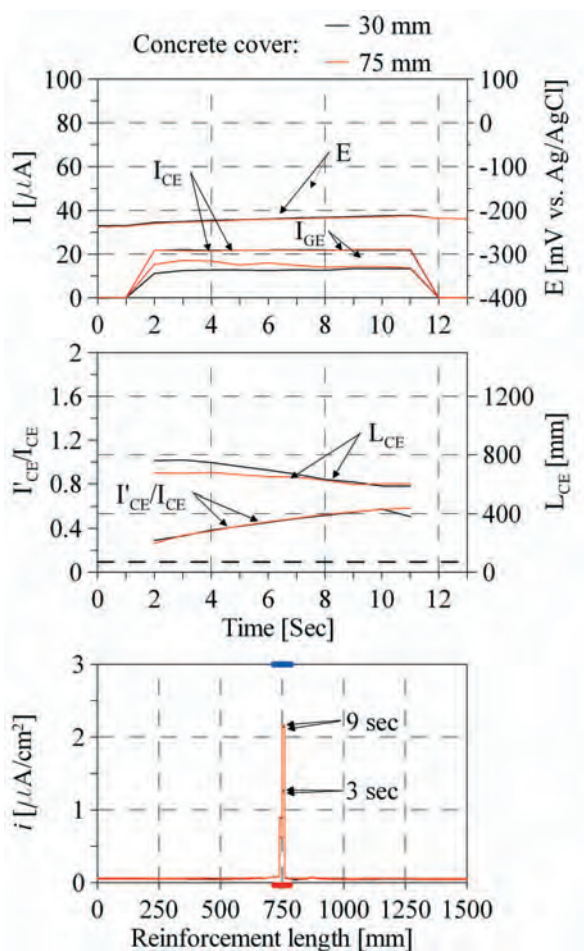


Figure 5.31 GalvaPulse measurements with use of current confinement in Position 4 on the upper reinforcement bar in Slab III. The bold blue line indicates the assumed confinement length on the segmented reinforcement bar and the red bold line the position and size of the two central anodes.

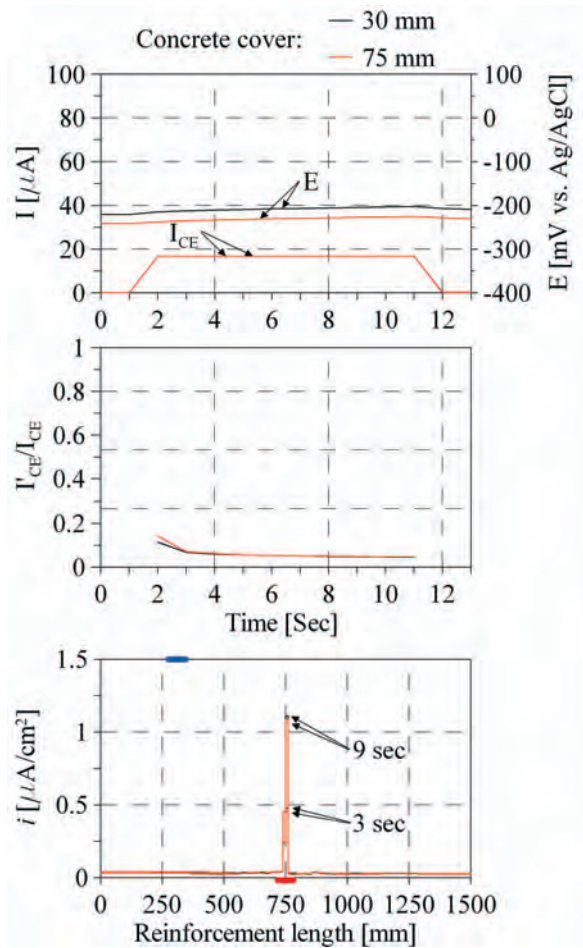


Figure 5.32 GalvaPulse measurements without use of current confinement in Position 2 on the upper reinforcement bar in Slab III. The bold blue line indicates the assumed confinement length on the segmented reinforcement bar and the red bold line the position and size of the two central anodes.

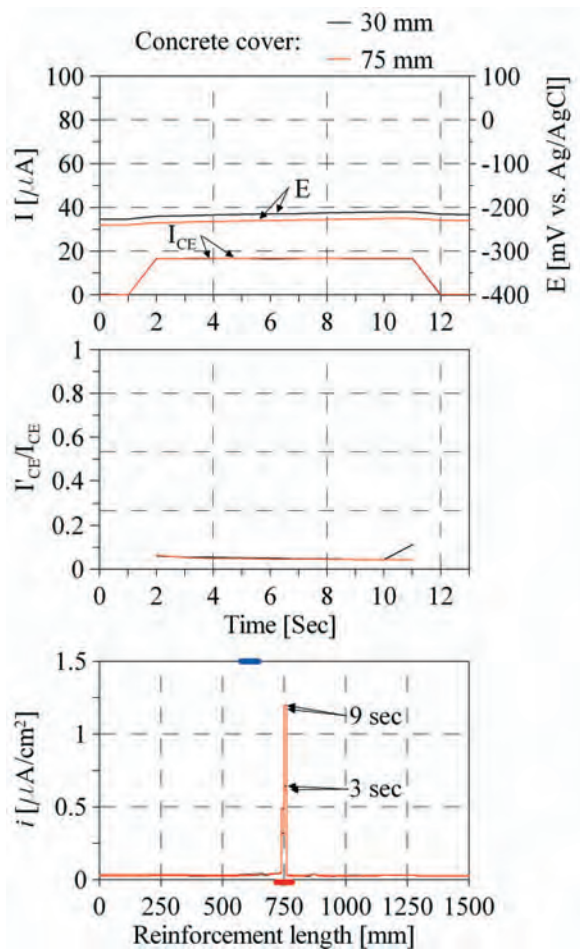


Figure 5.33 GalvaPulse measurements without use of current confinement in Position 3 on the upper reinforcement bar in Slab III. The bold blue line indicates the assumed confinement length on the segmented reinforcement bar and the red bold line the position and size of the two central anodes.

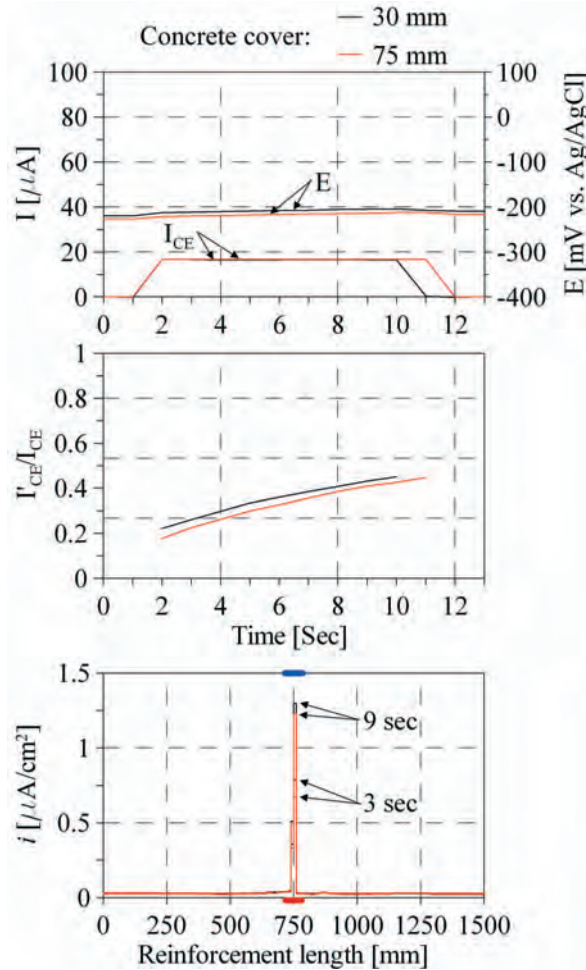


Figure 5.34 GalvaPulse measurements without use of current confinement in Position 4 on the upper reinforcement bar in Slab III. The bold blue line indicates the assumed confinement length on the segmented reinforcement bar and the red bold line the position and size of the two central anodes.

Active general corrosion

The half-cell potentials, E_{corr} , and corrosion current densities, i_{corr} , measured with the GECOR 6 and GalvaPulse (with and without current confinement) on the lower segmented reinforcement bar in Slabs II and III in Positions 1 to 7 are shown in Figures 5.35 and 5.36. On the lower reinforcement bar in Slab III corrosion current densities, i_{corr} , could not be measured with the GECOR 6, which repeatedly came up with an error message. The reason for this may be the low concrete resistivity making the guard ring control system oscillate or simply just fail. The numerical values of the measurements shown in Figures 5.35 and 5.36 are given in Appendix D together with the measured ohmic resistances, R_{Ω} , the counter-electrode currents, I_{CE} , applied during the measurements and the polarisation shifts, ΔE , obtained.

The half-cell potential values, E_{corr} , measured with the GECOR 6 have been converted from mV versus Cu/CuSO₄ to mV versus Ag/AgCl by adding 117 mV (Myrdal, 2007). No significant and systematic differences between the half-cell potentials, E_{corr} , obtained with the GECOR 6 and GalvaPulse were observed.

Similar to the measurements on the upper reinforcement bars very different corrosion current densities, i_{corr} , were obtained with the GECOR 6 and GalvaPulse instruments on the lower bar in Slab II. Also, with the GalvaPulse very different corrosion current densities, i_{corr} , were obtained with and without use of current confinement, both on Slabs II and III (Figures 5.35 and 5.36). Almost constant corrosion current densities, i_{corr} , were obtained with the GalvaPulse in all seven measurement positions on both Slabs II and III. Contrary hereto, fluctuating corrosion current densities, i_{corr} , were obtained with the GECOR 6 when measuring along the lower bar in Slab II, see Figure 5.35. However, no correlation between the measured corrosion current densities, i_{corr} , and the position of the anodes (shown with the red bold lines) was observed, see Figure 5.35.

As was the case in the previous section only selected and representative real-time recordings of the corrosion rate measurements shown in Figures 5.35 and 5.36 are included in this section: The real-time recordings of the measurements with the GECOR 6 and GalvaPulse instruments on Slab II in Positions 2 and 3, are given in Figures 5.37 to 5.42, whereas the recordings of the measurements with the GalvaPulse on Slab III in Positions 2 and 4 are given in Figures 5.43 to 5.46. A presentation of the real-time recordings and the procedure used for calculation of the ratio I'_{CE}/I_{CE} can be found in Section 5.1.3. The length L_{CE} has not been calculated for any of the real-time recordings of the measurements on the lower bars.

Considering the real-time recordings of the GECOR 6 measurements on Slab II very different guard ring currents, I_{GE} , were seen to be applied for the measurements in Positions 2 and 3, see Figures 5.37 and 5.38, top graphs. In Position 2, where the electrode assembly was positioned near an anode, guard ring currents in the range of 50 to 60 μA were seen to be applied throughout most of the polarisation period for both measurements (30 and 75 mm cover). In Position 3, over passive steel a constant guard ring current,

I_{GE} , of approximately $16 \mu A$ was applied for the measurement on the surface with a cover of 30 mm. On the surface with a cover of 75 mm the I_{GE} was seen to increase steadily to a value of approximately $38 \mu A$ at the end of the measurement. As for all other measurements the counter-electrode current, I_{CE} , was seen to be kept constant during the measurements. From the recorded current distributions it could be seen that a large part of the applied current flowed into the corroding segments independent of the electrode assembly position, see Figures 5.37 and 5.38, bottom graphs. As a result I'_{CE}/I_{CE} ratios of approximately 0.8 and 0.3 were only obtained in Positions 2 and 3, respectively. From the real-time recordings of the GalvaPulse measurements in Positions 2 and 3 on Slab II and in Positions 2 and 4 on Slab III the same phenomena was observed, see Figures 5.39, 5.40, 5.43 and 5.44. Although current confinement was used I'_{CE}/I_{CE} ratios of approximately 0.2 were only obtained during the measurements in both positions on both specimens.

The same tendencies were seen for the GalvaPulse measurements without current confinement in Positions 2 and 3 on Slab II and in Positions 2 and 4 on Slab III: Without current confinement I'_{CE}/I_{CE} ratios lower than 0.2 were obtained. The lower I'_{CE}/I_{CE} ratios were observed to be a result of generally lower current densities along the segmented reinforcement bars, rather than a result of changed current density distributions.

A thorough discussion of the results, i.e. the measured corrosion current densities, i_{corr} , and the real-time recordings is given in Chapter 6. However, before reading Chapter 6, the reader is encouraged to study Figures 5.35 to 5.46 in detail.

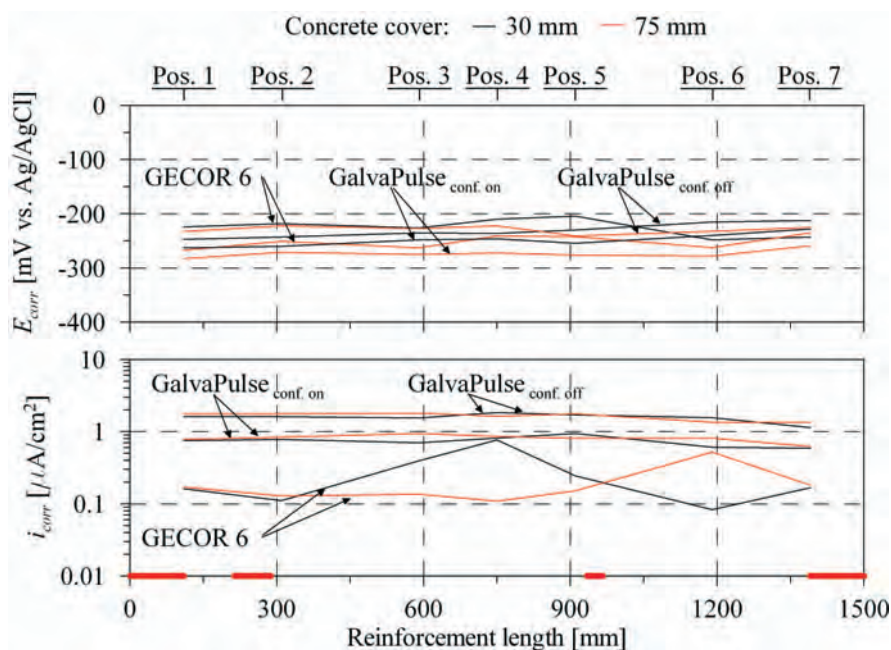


Figure 5.35 Half-cell potentials, E_{corr} , and corrosion current densities, i_{corr} , measured with the GECOR 6 and GalvaPulse instruments on the lower segmented reinforcement bar in Slab II. The positions and sizes of the anodes, i.e. the anodic segments, are shown with the bold red lines on the first axis.

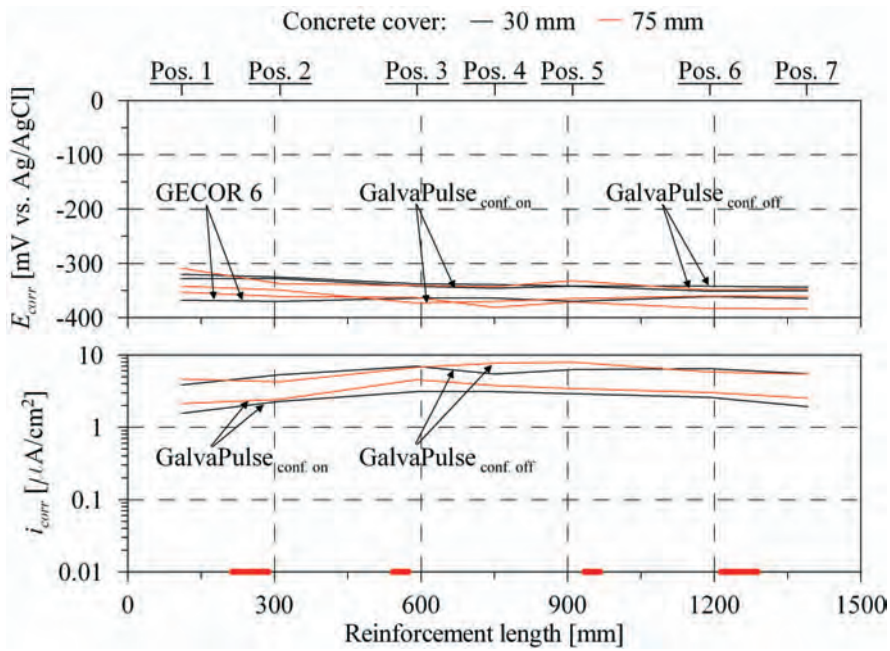


Figure 5.36 Half-cell potentials, E_{corr} , and corrosion current densities, i_{corr} , measured with the GalvaPulse instrument on the lower segmented reinforcement bar in Slab III. The positions and sizes of the anodes, i.e. the anodic segments, are shown with the red bold lines on the first axis.

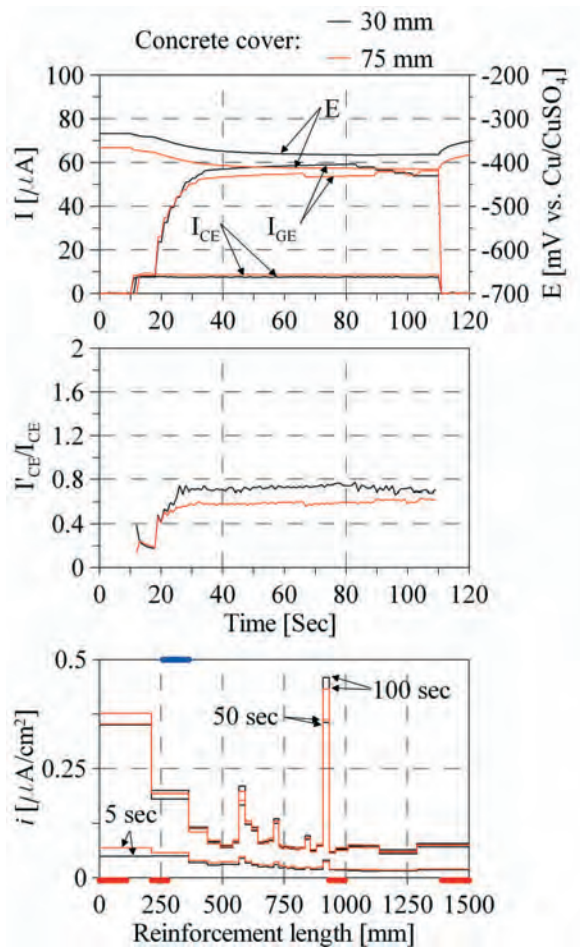


Figure 5.37 GECOR 6 measurements in Position 2 on the lower reinforcement bar in Slab II. The bold blue line indicates the assumed confinement length on the segmented reinforcement bar and the red bold lines indicate the positions and sizes of the anodes.

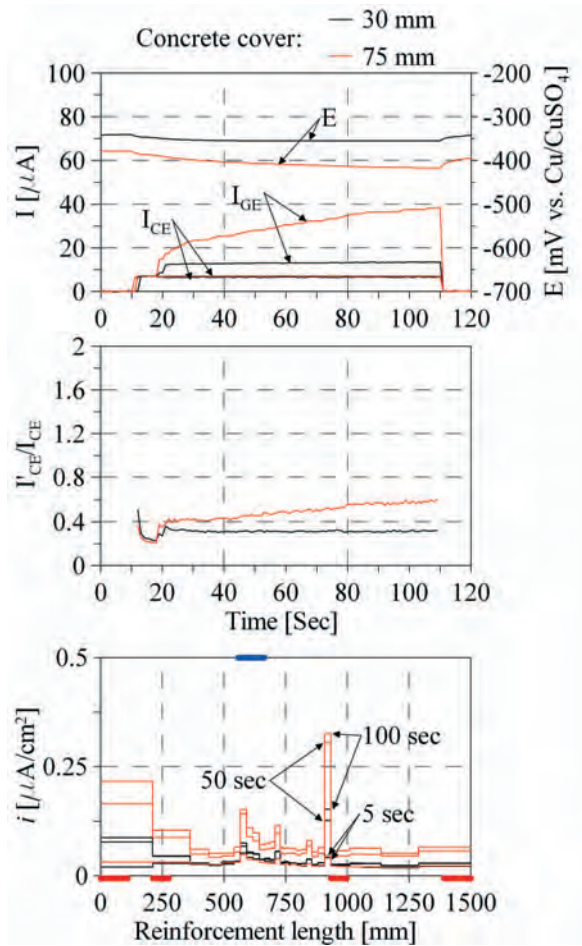


Figure 5.38 GECOR 6 measurements in Position 3 on the lower reinforcement bar in Slab II. The bold blue line indicates the assumed confinement length on the segmented reinforcement bar and the red bold lines indicate the positions and sizes of the anodes.

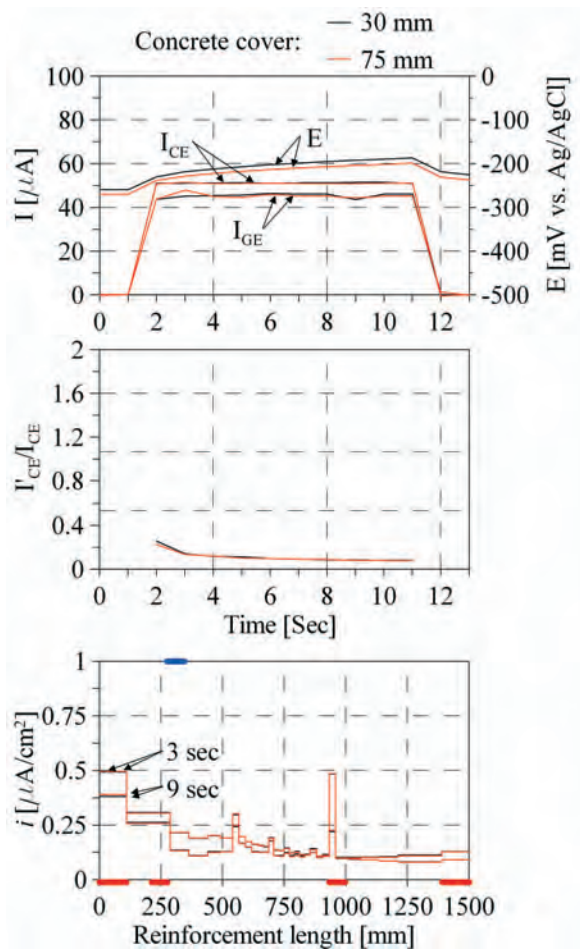


Figure 5.39 GalvaPulse measurements with use of current confinement in Position 2 on the lower reinforcement bar in Slab II. The bold blue line indicates the assumed confinement length on the segmented reinforcement bar and the red bold lines indicate the positions and sizes of the anodes.

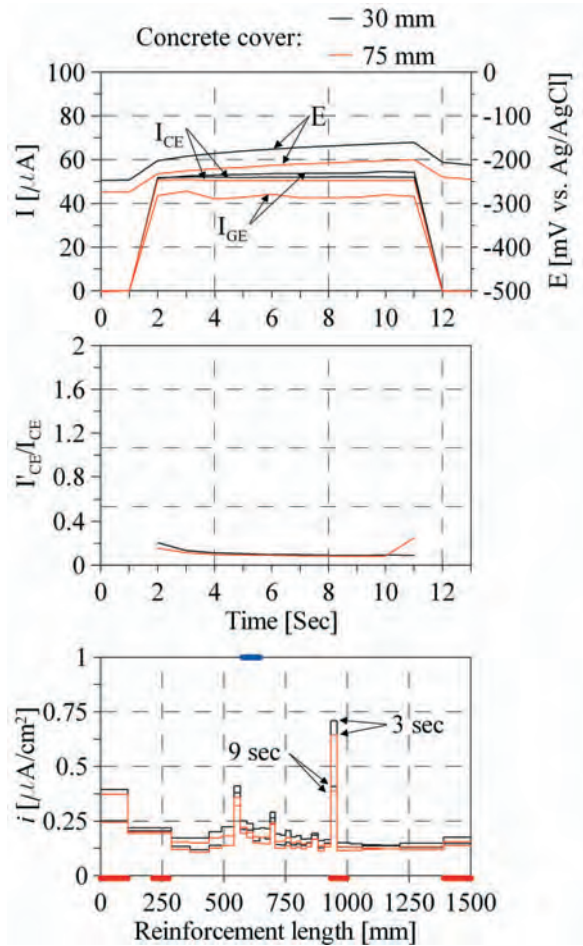


Figure 5.40 GalvaPulse measurements with use of current confinement in Position 3 on the lower reinforcement bar in Slab II. The bold blue line indicates the assumed confinement length on the segmented reinforcement bar and the red bold lines indicate the positions and sizes of the anodes.

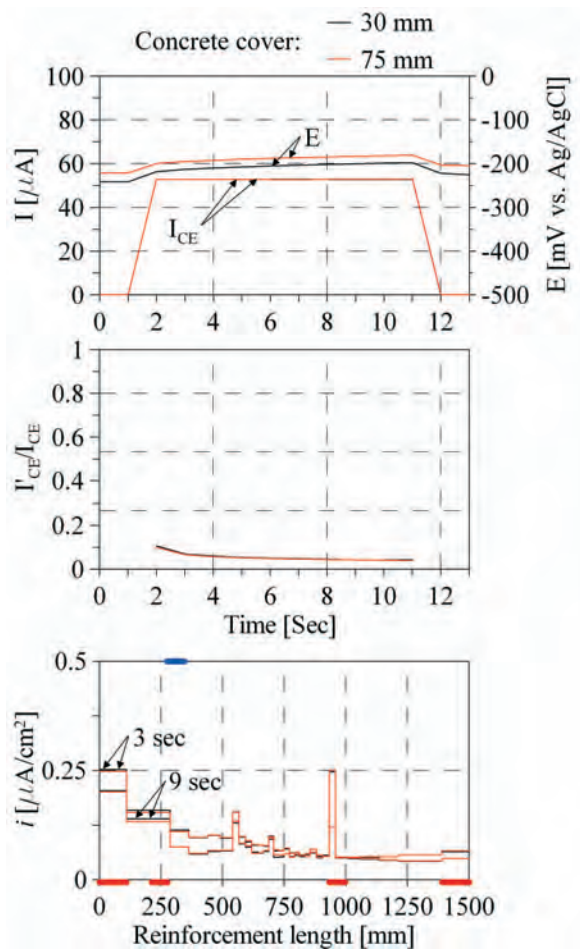


Figure 5.41 GalvaPulse measurements without use of current confinement in Position 2 on the lower reinforcement bar in Slab II. The bold blue line indicates the assumed confinement length on the segmented reinforcement bar and the red bold lines indicate the positions and sizes of the anodes.

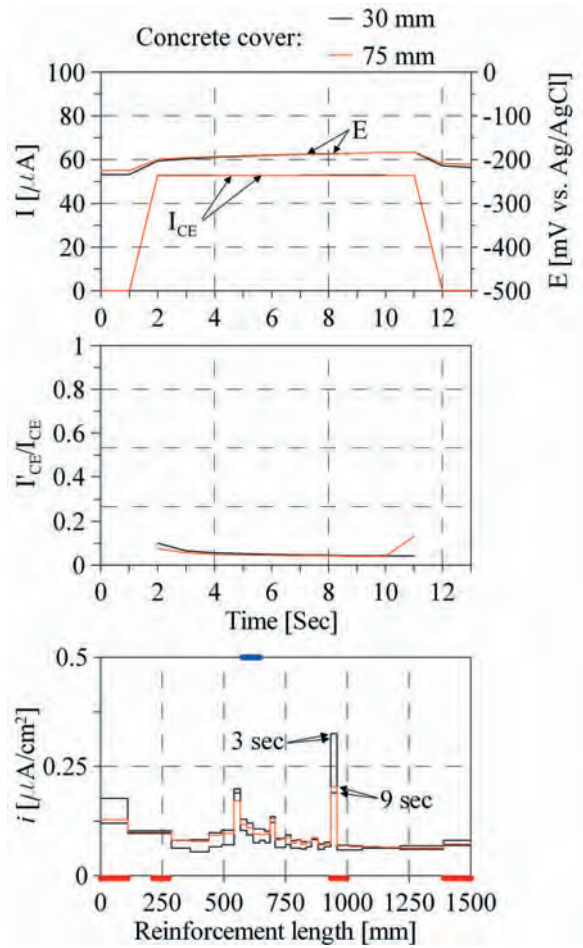


Figure 5.42 GalvaPulse measurements without use of current confinement in Position 3 on the lower reinforcement bar in Slab II. The bold blue line indicates the assumed confinement length on the segmented reinforcement bar and the red bold lines indicate the positions and sizes of the anodes.

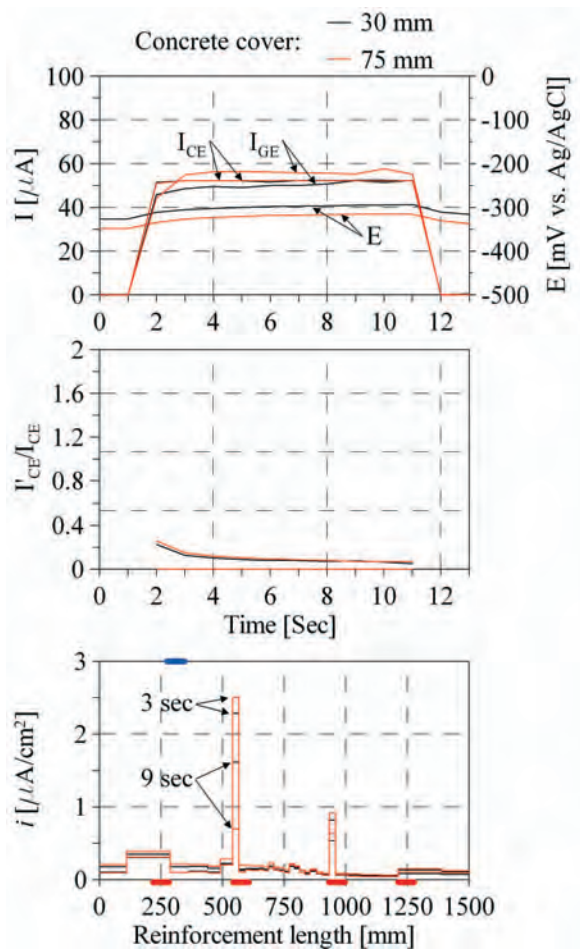


Figure 5.43 GalvaPulse measurements with use of current confinement in Position 2 on the lower reinforcement bar in Slab III. The bold blue line indicates the assumed confinement length on the segmented reinforcement bar and the red bold lines indicate the positions and sizes of the anodes.

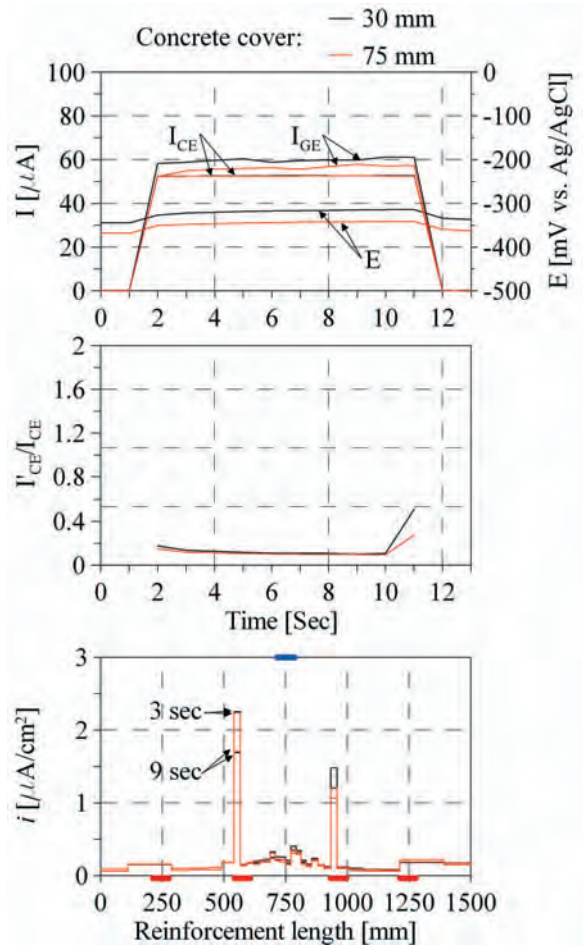


Figure 5.44 GalvaPulse measurements with use of current confinement in Position 4 on the lower reinforcement bar in Slab III. The bold blue line indicates the assumed confinement length on the segmented reinforcement bar and the red bold lines indicate the positions and sizes of the anodes.

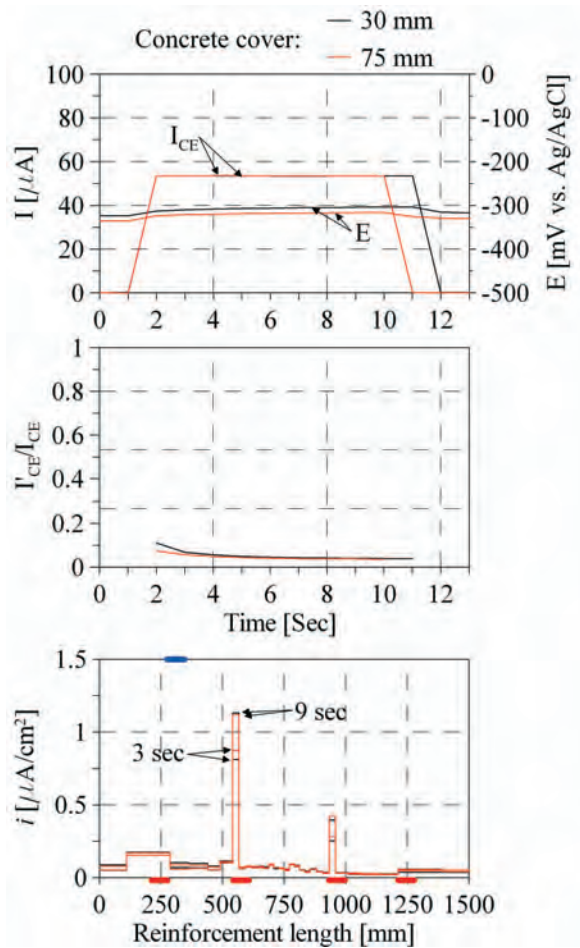


Figure 5.45 GalvaPulse measurements without use of current confinement in Position 2 on the lower reinforcement bar in Slab III. The bold blue line indicates the assumed confinement length on the segmented reinforcement bar and the red bold lines indicate the positions and sizes of the anodes.

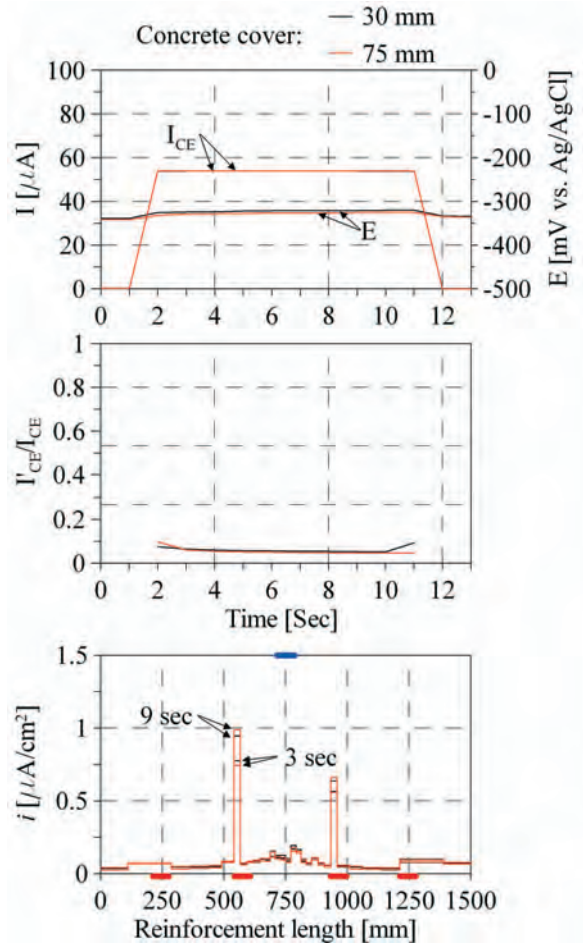


Figure 5.46 GalvaPulse measurements without use of current confinement in Position 4 on the lower reinforcement bar in Slab III. The bold blue line indicates the assumed confinement length on the segmented reinforcement bar and the red bold lines indicate the positions and sizes of the anodes.

5.2 Effect of measurement technique, procedure and exposure

In this section the results from the experimental work on the *Effect of measurement technique, procedure and exposure* (Experiment B, Figure 4.1) described in Section 4.2 are presented. As described in Section 4.2 (Table 4.7) a ten-step measurement sequence comprising one series of potentiodynamic linear polarisation resistance measurements and nine series of galvanostatic potential transient measurements (with increasing polarisation current) was used for the experimental investigations. Each series comprised measurements on all 450 steel bars (45 tests specimens each with 10 bars). During the project period the ten-step measurement sequence was repeated a number of times. Similar results were obtained from each measurement sequence. In the present section only the results from one representative measurement sequence, performed approximately 24 months after casting the specimens, are presented.

The results from the potentiodynamic linear polarisation resistance measurements are presented first. Subsequently the results from the galvanostatic potential transient measurements analysed with both the galvanostatic linear polarisation resistance technique and the galvanostatic potential transient technique are presented.

5.2.1 Potentiodynamic linear polarisation resistance measurements

The mean free corrosion potentials, E_{corr} , mean polarisation resistances, R_P , and mean corrosion current densities, i_{corr} , measured on the passive (Series I, 0 % chloride) and active generally corroding (Series II, 4 % chloride) reinforcement bars are shown in Figures 5.47, 5.48 and 5.49. The corresponding results obtained for the actively corroding partly nickel coated reinforcement bars (Series III, 4 % chloride) are shown in Figure 5.50. In all figures the results obtained at the three relative humidities, i.e. 75, 85 and 96 % RH are shown as a function of the temperature. The vertical lines above and below each data point (giving the mean value) indicate the mean value plus and minus one standard deviation. The free corrosion potentials, E_{corr} , measured versus the embedded MnO_2 reference electrodes have been converted from mV versus MnO_2 to mV versus Ag/AgCl by adding +197 mV (Figures 5.47 and 5.50) (Myrdal, 2007).

For the passive reinforcement bars (Series I, 0 % chloride) no significant effect of the temperature and relative humidity on the free corrosion potentials, E_{corr} , was observed, see Figure 5.47, top graph. The free corrosion potentials, E_{corr} , of the passive bars ranged from approximately -165 to -95 mV versus Ag/AgCl. For the active generally corroding reinforcement bars (Series II, 4 % chloride) the free corrosion potentials, E_{corr} , decreased, i.e. became more negative, with increasing relative humidity, see Figure 5.47, bottom graph. At 75 % relative humidity no significant differences between the free corrosion potentials, E_{corr} , measured at temperatures from 1 to 35 °C, were observed. At 96 % relative humidity the free corrosion potentials, E_{corr} , at 5 and 25 °C, were approximately 200 and 300 mV more negative than the potentials at 1, 15 and 35 °C.

The polarisation resistances, R_P , of the passive reinforcement bars ranged from approximately 600 to 1800 kOhm \times cm², see Figure 5.48, top graph. No clear correlation between

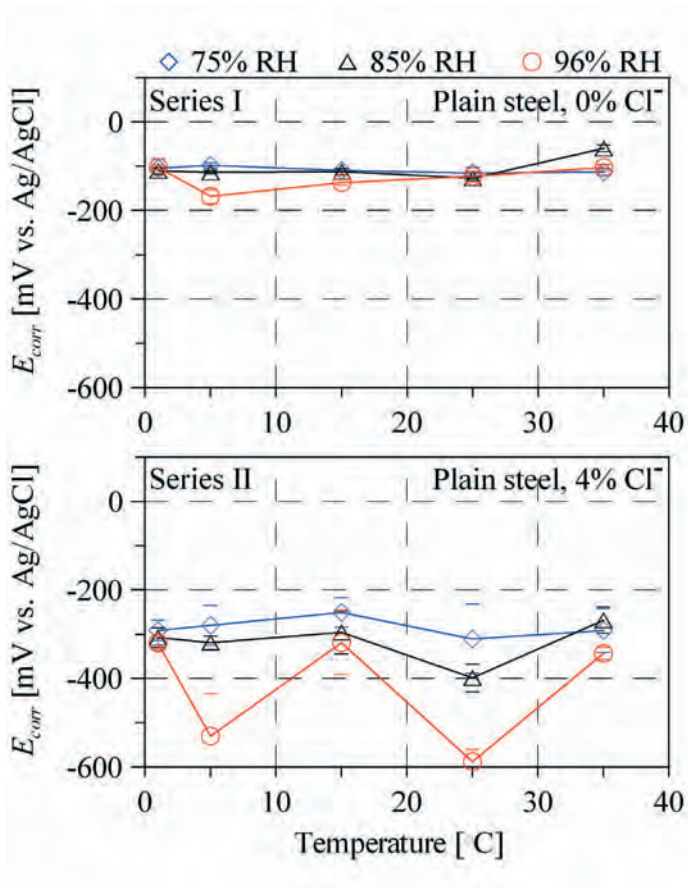


Figure 5.47 Free corrosion potentials, E_{corr} , as a function of the exposure temperature for the passive (top graph, Series I) and active generally corroding (bottom graph, Series II) reinforcement bars exposed to 75, 85 and 96 % relative humidity.

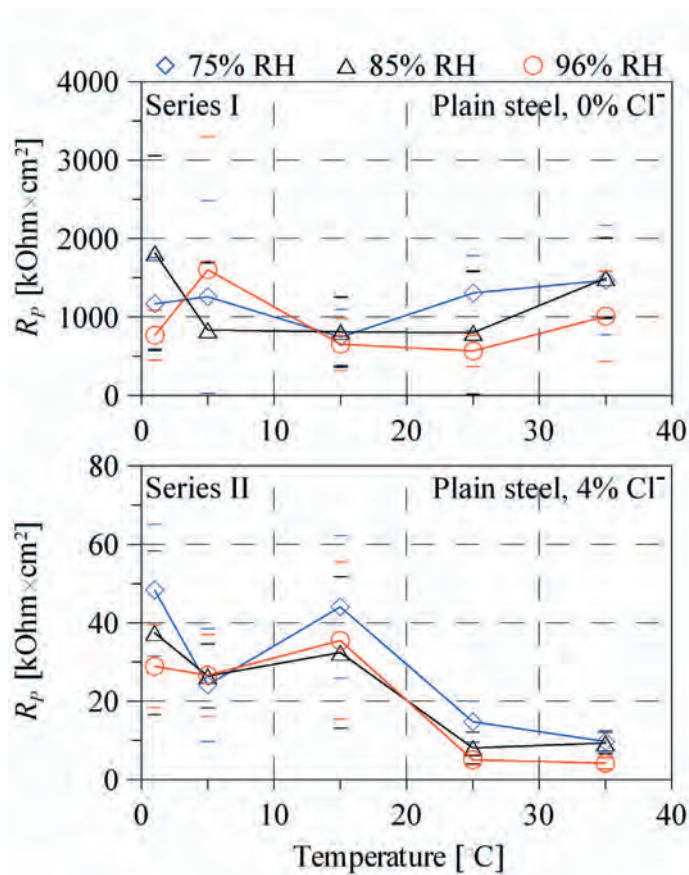


Figure 5.48 Polarisation resistances, R_p , as a function of the exposure temperature for the passive (top graph, Series I) and active generally corroding (bottom graph, Series II) reinforcement bars exposed to 75, 85 and 96 % relative humidity.

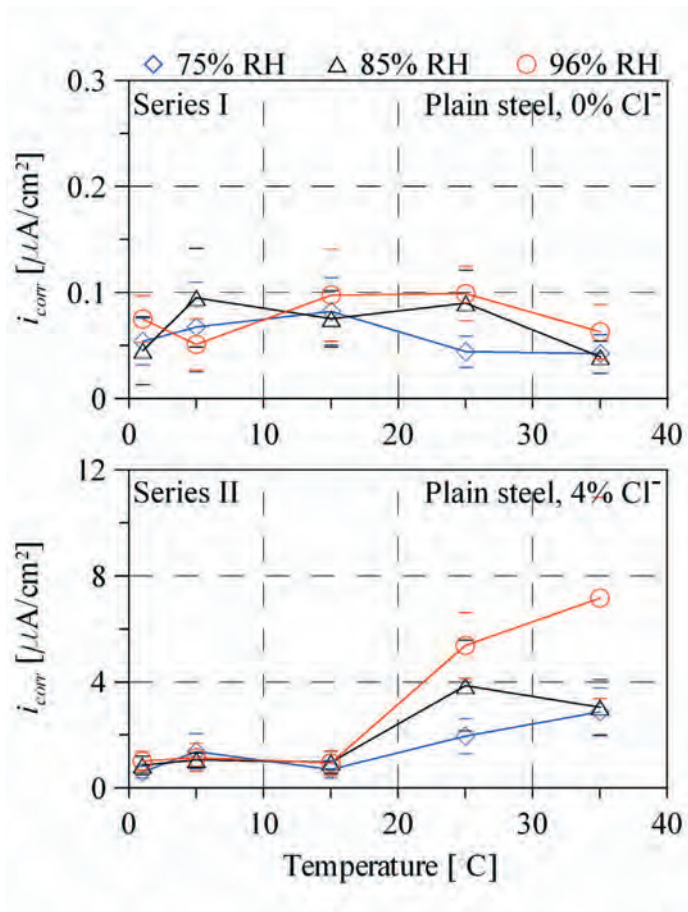


Figure 5.49 Corrosion current densities, i_{corr} , as a function of the exposure temperature for the passive (top graph, Series I) and active generally corroding (bottom graph, Series II) reinforcement bars exposed to 75, 85 and 96 % relative humidity.

the temperature and the measured polarisation resistances, R_P , was observed. However, with decreasing relative humidity a tendency to increasing polarisation resistances, R_P , was observed. The corrosion current densities, i_{corr} , for the passive reinforcement bars (Series I, 0 % chloride) ranged from approximately 0.03 to 0.1 $\mu\text{A}/\text{cm}^2$, see Figure 5.49, top graph.

As mentioned in Section 4.2.2 the potential sweep rate used for the R_P measurements on the passive reinforcement bars was higher than the intended 10 mV per minute. Analysis of the potential sweeps showed that the actual sweep rate for these measurements ranged from 15 to 18 mV per minute. The too high sweep rates were a result of the control technique used by the potentio/galvanostat: During both cathodic and anodic polarisation of the passive steel, the current change, ΔI , i.e. from start to end of each sweep was in the nA range, see Figure 4.16. In this current range an accurate control of the sweep rate was not possible as the potentio/galvanostat controlled the sweep rate by adjusting the applied current in steps of 50 nA.

On the active generally corroding reinforcement (Series II, 4 % chloride) a clear effect of both the temperature and relative humidity on the measured polarisation resistance, R_P , was observed, see Figure 5.48, lower graph: With increasing temperature and relative humidity the measured R_P values decreased: At 1 °C the measured R_P values ranged from approximately 30 to 50 $\text{k}\Omega\cdot\text{cm}^2$ whereas values in the range from approximately 5 to 10 $\text{k}\Omega\cdot\text{cm}^2$ were measured at 35 °C. Slightly deviating results were though obtained at a temperature of 5 °C. At this temperature, the measured R_P values were lower than the values obtained at both 1 and 15 °C.

Reflecting the measured R_P values, the corrosion current densities, i_{corr} , calculated for the actively corroding reinforcement bars (Series II) increased with increasing temperature and relative humidity, see Figure 5.49, bottom graph. In the range from 1 to 15 °C the calculated i_{corr} values ranged from 0.6 to 1.4 $\mu\text{A}/\text{cm}^2$ while higher values were obtained at 25 and 35 °C. At 25 °C i_{corr} values of 2, 3.9 and 5.4 $\mu\text{A}/\text{cm}^2$ were obtained at 75, 85 and 96 % relative humidity, respectively. At 35 °C almost identical i_{corr} values of approximately 3 $\mu\text{A}/\text{cm}^2$ were obtained at 75 and 85 % relative humidity whereas a value of 7.2 $\mu\text{A}/\text{cm}^2$ was obtained at 96 % relative humidity.

The effect of the relative humidity and temperature on the free corrosion potentials, E_{corr} , of the actively corroding partly nickel coated reinforcement bars (Series III) differed from that observed on the active generally corroding reinforcement bars (Series II). The free corrosion potentials, E_{corr} , of the partly nickel coated reinforcement bars are mixed potentials representing both the passive nickel layer and the actively corroding 5 mm wide uncoated carbon steel band. At a temperature of 1 °C almost identical E_{corr} values of approximately -120 mV versus Ag/AgCl were measured at 75, 85 and 96 % relative humidity. Slightly higher potential values in the range from -50 to -80 mV versus Ag/AgCl were measured at 5 °C. Above 5 °C the free corrosion potentials, E_{corr} , decreased, i.e. became more negative with increasing temperature. No significant differences between the free corrosion potentials, E_{corr} , measured at 75 and 85 % relative humidity were observed.

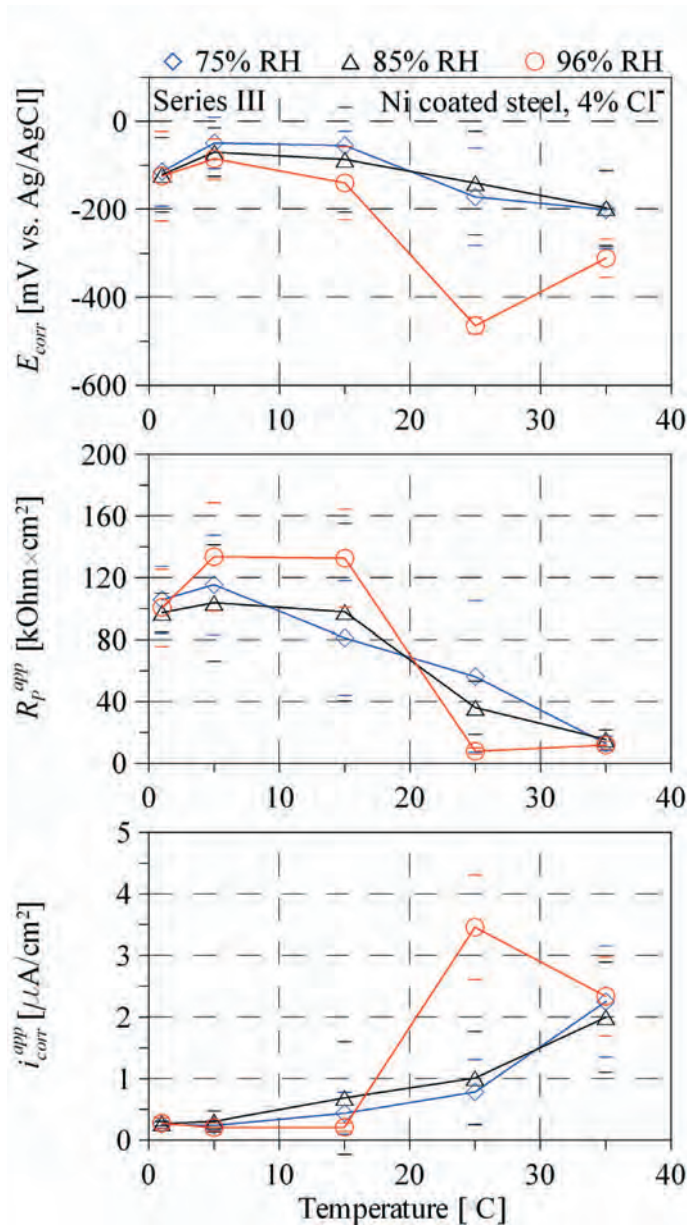


Figure 5.50 Measured free corrosion potentials, E_{corr} , polarisation resistances, R_p , and corrosion current densities, i_{corr} , as a function of the exposure temperature for the actively corroding partly nickel coated reinforcement bars (Series III) exposed to 75, 85 and 96 % relative humidity.

Much more negative potentials were recorded at 96 % relative humidity, especially at the temperature of 25 °C where E_{corr} values of approximately -460 mV versus Ag/AgCl were measured.

The polarisation resistance values measured on the partly nickel coated reinforcement bars in Series III (Figure 5.50) are apparent values, R_P^{app} , as only the mid 5 mm of the 200 mm length used for calculating the polarisation resistance were assumed actively corroding. Despite the well defined geometry (active/passive areas) calculation of the *true* R_P value for the actively corroding mid 5 mm on the otherwise passive reinforcement bars is not possible based on the results from the experiment with the segmented reinforcement bars: In this experiment it was found that a simple correction of a measured R_P^{app} value for the corroding area on an otherwise passive reinforcement bars does not give the actual R_P value due to the overlapping potential response of the passive steel (here nickel), into which a portion of the applied current flows, see Section 4.2.

The pattern observed from the free corrosion potentials, E_{corr} , of the partly nickel coated reinforcement bars was also observed from the apparent polarisation resistance values, R_P^{app} , see Figure 5.50, middle graph: At the temperature of 1 °C almost identical R_P^{app} values of approximately 100 kOhm×cm² were measured at 75, 85 and 96 % relative humidity. At 5 °C slightly higher R_P^{app} values in the range from 105 to 135 kOhm×cm² were measured. Above 5 °C the apparent polarisation resistance values, R_P^{app} , decreased with increasing temperature. Similar values were obtained at 75 and 85 % relative humidity whereas more fluctuating values were obtained at 96 % relative humidity: At both 5 and 15 °C higher R_P^{app} values were obtained at 96 % than at 75 and 85 % relative humidity. On the other hand, at 25 °C lower R_P^{app} values were obtained at 96 % relative humidity than at 75 and 85 % relative humidity.

Similar to the polarisation resistance values the corrosion current densities calculated for the partly nickel coated reinforcement bars (Figure 5.50, bottom graph) are apparent values, i_{corr}^{app} . Corresponding to the measured apparent polarisation resistances, R_P^{app} , almost identical i_{corr}^{app} values of approximately 0.3 μA/cm² were obtained at 75, 85 and 96 % relative humidity at a temperature of 1 °C, whereas values of approximately 0.2 μA/cm² were obtained at 5 °C. Above 5 °C the apparent corrosion current densities, i_{corr}^{app} , increased with increasing temperatures. At 15 and 35 °C similar i_{corr}^{app} were obtained at 75, 85 and 96 % relative humidity. On the other hand, at a temperature of 25 °C higher i_{corr}^{app} values were measured at 96 % relative humidity than at 75 and 85 % relative humidity, where similar values were obtained.

5.2.2 Galvanostatic potential transient measurements

In this section the results from the galvanostatic potential transient measurements analysed with both the galvanostatic potential transient technique and the galvanostatic linear polarisation resistance technique are presented, see Section 4.2. Only selected representative results from the measurements on the 45 test specimens are presented in order to describe the effects of the investigated parameters, i.e. the method of analysis (galvanostatic techniques), and the polarisation time and current. The results from the measurements on the passive reinforcement bars (Series I) are presented first after which the results from the measurements on the active generally corroding reinforcement bars (Series II) are presented.

Passive reinforcement

For the passive reinforcement results from the measurements on the reinforcement bars in the test specimen exposed at 25 °C and 75 % relative humidity were selected for describing the effect of the investigated parameters. This specimen was selected as a relatively high mean polarisation resistance, R_P , and rather low standard deviation was obtained from the measurements with the potentiodynamic linear polarisation resistance technique.

The mean polarisation curves, i.e. the mean curve for each polarisation current (0.25 to 100 μA) are shown in Figure 5.51. As seen from Figure 5.51 a steady state potential response within the linear potential-current range of approximately 20 mV around the free corrosion potential, E_{corr} , was not obtained during any of the measurements: With a polarisation current of 0.25 μA potential shifts in the range from -22 to -32 mV, fairly close to the linear range, were obtained at the end of the polarisation periods. However, a steady state response was not obtained during any of these measurements. For the measurements where polarisation currents of 0.5, 1, 2 and 5 μA were used steady state potential responses were also not obtained. Furthermore, the potential shifts obtained at the end of the polarisation periods of these measurements were also much higher than the 20 mV limit for the linear current-potential range. Only during the measurements with polarisation currents from 10 to 100 μA , and most pronounced for 10 μA , potential responses approximating steady state were obtained, see Figure 5.51.

The results from analysis of the polarisation curves with the galvanostatic potential transient technique, i.e. the curve fitting method, are shown in Figure 5.52, whereas the results obtained with the galvanostatic linear polarisation resistance technique are shown in Figure 5.53. For both galvanostatic techniques a significant effect of the polarisation current and time on the determined polarisation resistances, R_P , was observed, see Figures 5.52 and 5.53: With decreasing polarisation current and increasing polarisation time the measured polarisation resistances, R_P , increased. Correspondingly, the corrosion current densities, i_{corr} , calculated from the polarisation resistances, R_P , decreased with decreasing polarisation current and increasing polarisation time. The largest effect of the polarisation time on the measured polarisation resistances, R_P , was observed from the results obtained with the galvanostatic potential transient technique: For the measurements where a polarisation current of 0.25 μA was used an R_P value of approximately

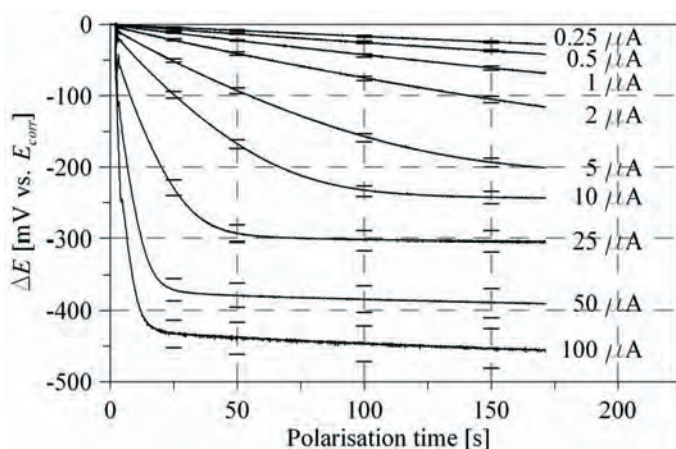


Figure 5.51 Mean polarisation curves obtained from the passive reinforcement bars in the test specimen exposed to 25 °C and 75 % relative humidity. The error bars indicate 0.5 standard deviation.

580 $\text{k}\Omega\text{m}\times\text{cm}^2$ was obtained with a polarisation time of 10 seconds, see Figure 5.52. By increasing the polarisation time to 165 seconds the measured polarisation resistance increased by a factor of approximately 120 to a value of 71200 $\text{k}\Omega\text{m}\times\text{cm}^2$. With the same parameters (0.25 μA , 10 and 165 seconds) R_P values of approximately 343 and 6680 $\text{k}\Omega\text{m}\times\text{cm}^2$ were obtained with the galvanostatic linear polarisation resistance technique, corresponding to an increase with a factor of approximately 20, see Figure 5.53. As seen from Figures 5.52 and 5.53, the increase in polarisation resistance, R_P , with increasing polarisation time decreased with increasing polarisation current and no noticeable effect of the polarisation time was observed from the measurements where a polarisation current of 100 μA was used. During these measurements almost constant R_P values of approximately 200 $\text{k}\Omega\text{m}\times\text{cm}^2$ were measured, corresponding to a corrosion current density of 0.26 $\mu\text{A}/\text{cm}^2$.

Apart from the effect of the polarisation time and current, the scatter of the R_P values determined with polarisation currents of 0.25, 0.5 and 1 μA with the galvanostatic potential transient technique should be noted, see Figure 5.52. The scatter was seen to increase with decreasing polarisation current, but decreased with increasing polarisation time. Possible explanations for the scatter are discussed in Section 6.3.2.

No systematic correlation between the ohmic resistance, R_Ω , determined as a function of the polarisation time, and the polarisation current was observed, see Figure 5.52. With a polarisation current of 0.25 μA the ohmic resistance, R_Ω , decreased slightly with the increasing polarisation time: from approximately 1.5 $\text{k}\Omega\text{m}$ for a polarisation time of 10 seconds to approximately 1 $\text{k}\Omega\text{m}$ for a polarisation time of 165 seconds. On the contrary, with polarisation currents of 0.5, 1 and 2 μA , the ohmic resistance was seen to increase

slightly with increasing polarisation time, from approximately 1.3 kOhm to 1.7 kOhm. With polarisation currents of 5, 10, 25, 50 and 100 μA varying ohmic resistances, R_{Ω} , were observed.

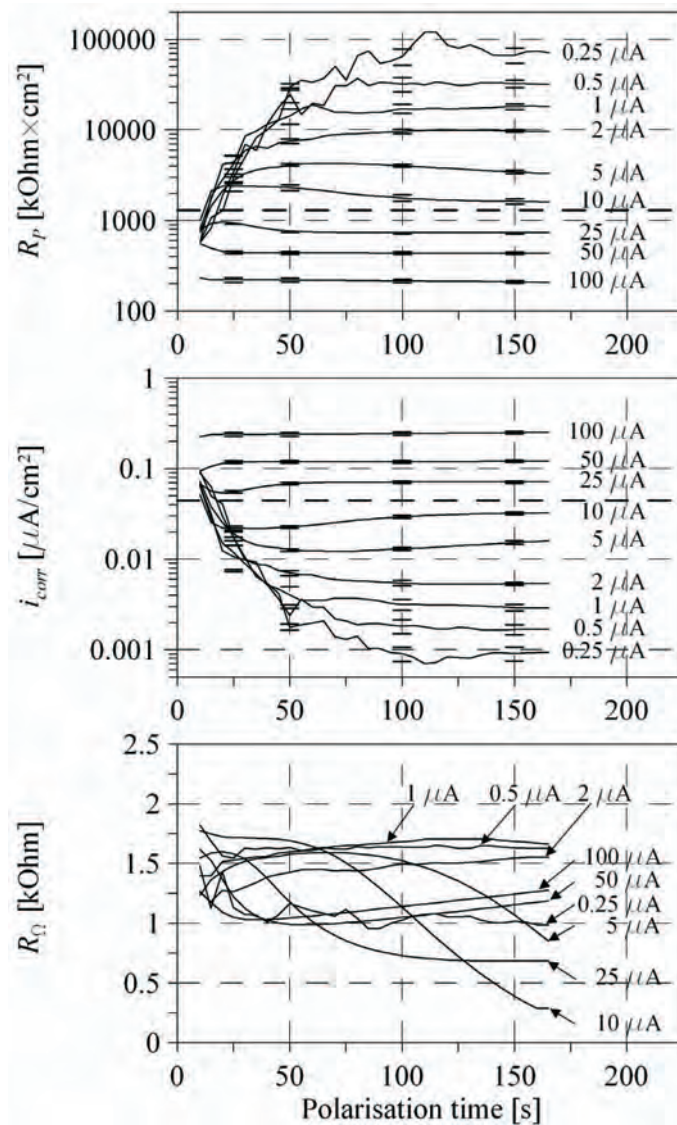


Figure 5.52 Galvanostatic potential transient technique: Mean polarisation resistances, R_p , corrosion current densities, i_{corr} , and ohmic resistances, R_Ω , as a function of the polarisation time for the passive reinforcement bars exposed to 25 °C and 75 % relative humidity. The error bars indicate 0.5 standard deviation.

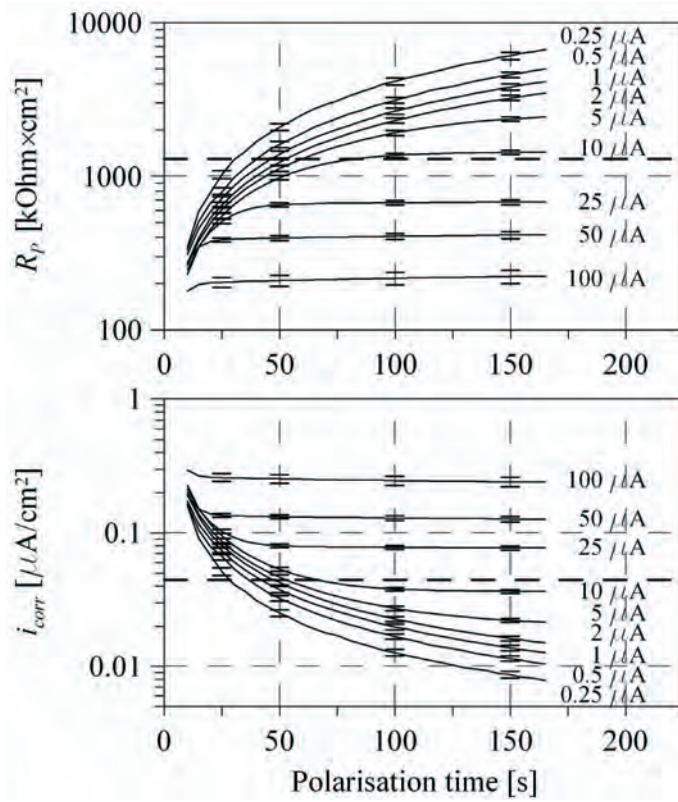


Figure 5.53 Galvanostatic linear polarisation resistance technique: Mean polarisation resistances, R_p , and corrosion current densities, i_{corr} , as a function of the polarisation time for the passive reinforcement bars exposed to 25 °C and 75 % relative humidity. The error bars indicate 0.5 standard deviation.

Table 5.5 Selected tests specimens from Series II (general corrosion): Exposure conditions, and average polarisation resistances, R_P , and corrosion current densities, i_{corr} , from the potentiodynamic linear polarisation resistance measurements (Figures 5.48 and 5.49).

Specimen	Exposure		Polarisation resistance	Corrosion current density
	T [°C]	RH [%]	R_P [kOhm \times cm ²]	i_{corr} [μ A/cm ²]
1	15	75	44.10	0.71
2	25	85	8.12	3.87
3	35	96	4.45	7.17

Active general corrosion

For the active generally corroding reinforcement (Series II) results from measurements on the reinforcement bars in three different test specimens are presented. This is done in order to describe the effect of the investigated parameters, i.e. the analysis technique and the polarisation time and current on the measured polarisation resistance, R_P , at varying corrosion rates. Three test specimens with reinforcement bars corroding at low, medium and high rates were selected. The specimens were selected by their mean corrosion current density, i_{corr} , calculated from the potentiodynamic linear polarisation resistance measurements (Figure 5.49). Details on the three selected specimens, referred to as Specimens 1, 2 and 3 in the following, are given in Table 5.5. For each specimen (Specimens 1 to 3) the results describing the effect of the analysis technique and the polarisation time and current on the measured polarisation resistance, R_P , are presented. Only the results from analysis of the potential transients obtained with polarisation currents from 5 to 100 μ A are considered, as transients with potential shifts lower than 1 mV, that could not be distinguished from the background noise, were obtained with the polarisation currents lower than 5 μ A.

The mean polarisation curves for Specimens 1, 2 and 3 are shown in Figures 5.54, 5.55 and 5.56. From these curves a clear correlation between the obtained potential shifts and the mean polarisation resistances, R_P , (and hence corrosion current densities, i_{corr}) measured with the potentiodynamic linear polarisation resistance technique (Table 5.5) was observed: With a given polarisation current (5-100 μ A) the potential shift obtained during a measurement decreased with decreasing polarisation resistance, R_P , (increasing corrosion current density, i_{corr}), see Figures 5.54, 5.55 and 5.56 and Table 5.5. For Specimen 1, with a mean i_{corr} value of 0.71 μ A/cm², polarisation curves within the linear potential-current range of approximately 50 mV that applies for actively corroding steel were only obtained with polarisation currents of 25 μ A or lower. For Specimen 2, with a mean i_{corr} value of 3.87 μ A/cm² also the polarisation curves obtained with a current of 50 μ A were within the 50 mV limit, whereas all polarisation curves from Specimen 3 with a mean i_{corr} of 7.71 μ A/cm² were within the 50 mV limit (Figures 5.54, 5.55 and 5.56).

With increasing mean corrosion current density, i_{corr} , (Specimens 1 to 3) the polarisation curves were observed to approximate a steady state potential response faster, due to the

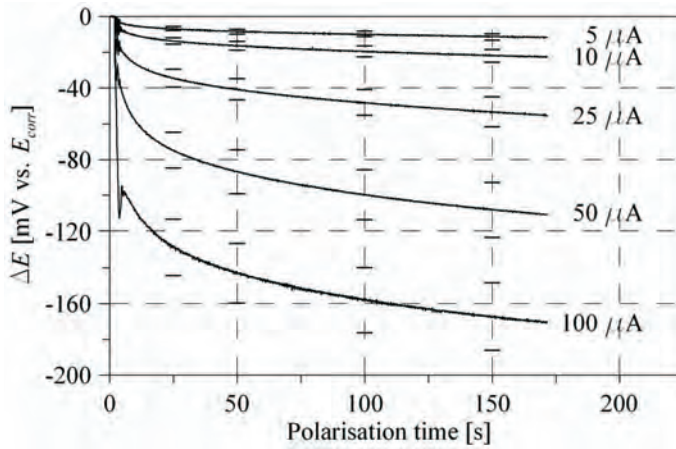


Figure 5.54 Specimen 1: Mean polarisation curves obtained from the active generally corroding reinforcement bars (Series II) exposed to 15 °C and 75 % relative humidity (Table 5.5).

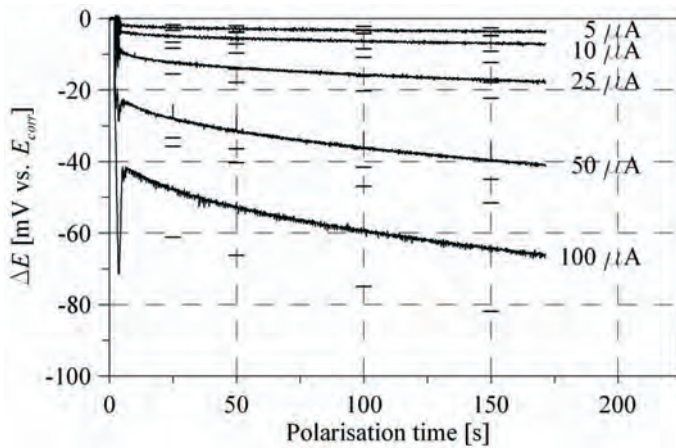


Figure 5.55 Specimen 2: Mean polarisation curves obtained from the active generally corroding reinforcement bars (Series II) exposed to 25 °C and 85 % relative humidity (Table 5.5).

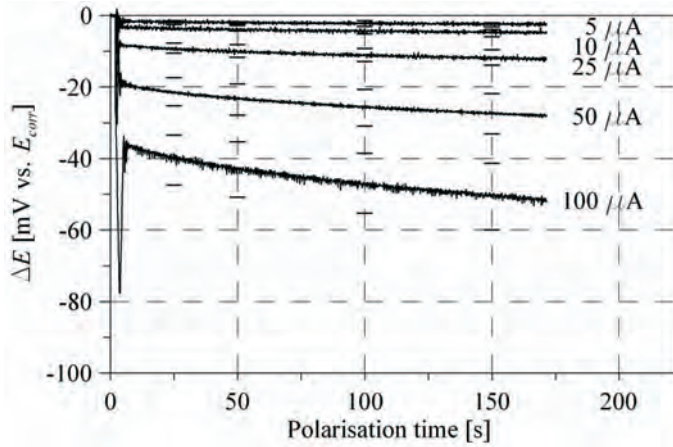


Figure 5.56 Specimen 3: Mean polarisation curves obtained from the active generally corroding reinforcement bars (Series II) exposed to 35 °C and 96 % relative humidity (Table 5.5).

lower potential transient response: For Specimens 1 and 2 only the polarisation curves measured with polarisation currents of 5 and 10 μA were seen to approximate a steady state response (Figures 5.54 and 5.55). For Specimen 3 also the polarisation curves measured with 25 μA approximated a steady state response (Figure 5.56).

As mentioned in Section 4.2.2 an initial potential *overshooting* was observed from the potential transients, see Figures 5.54, 5.55, 5.56. The potential *overshooting* was seen to increase with increasing mean corrosion current density, i_{corr} , and increasing polarisation current. The initial potential peak caused by the potential *overshooting* and the ohmic potential drop, E_{Ω} , caused by the ohmic concrete resistance, R_{Ω} , were seen to be superimposed. But unlike the almost instantaneous ohmic potential drop, E_{Ω} , the duration of the *overshooting*, i.e. the time from the initial potential rise until the potential again followed the charging curve, lasted several seconds.

As described in Section 4.2.2 the polarisation resistance, R_P , and corrosion current density, i_{corr} , were calculated as a function of the polarisation time for each recorded potential transient with both the galvanostatic potential transient technique and the galvanostatic linear polarisation resistance technique. By dividing all calculated R_P values determined for a given reinforcement bar, i.e. for all polarisation currents and times, with the (single) R_P value determined for the reinforcement bar with the potentiodynamic polarisation resistance technique (R_P^{ref}), i.e. the reference technique, relative polarisation resistances, R_P/R_P^{ref} , are obtained. This was done for all reinforcement bars in the three specimens, i.e. all measured polarisation resistances, R_P , were turned into relative polarisation resistances, R_P/R_P^{ref} . For each specimen the mean relative polarisation resistance, R_P/R_P^{ref} , as a function of the polarisation time, t , was then calculated for each polarisation current

(5-100 μA). Following the same procedure, the mean relative corrosion current densities, $i_{\text{corr}}/i_{\text{corr}}^{\text{ref}}$, as a function of the polarisation time were also calculated.

Calculation of the mean relative polarisation resistances, R_P/R_P^{ref} , and corrosion current densities, $i_{\text{corr}}/i_{\text{corr}}^{\text{ref}}$, allowed direct comparison of the results obtained for Specimens 1, 2 and 3. In addition, the correlation between the techniques, i.e. potentiodynamic linear polarisation resistance technique (reference) and the two galvanostatic techniques could easily be evaluated: In case where R_P/R_P^{ref} and $i_{\text{corr}}/i_{\text{corr}}^{\text{ref}}$ values of 1 were obtained identical results were obtained with the two techniques, i.e. the considered galvanostatic technique and the potentiodynamic linear polarisation resistance technique, whereas R_P/R_P^{ref} and $i_{\text{corr}}/i_{\text{corr}}^{\text{ref}}$ values smaller than one corresponded to lower R_P and i_{corr} values being determined with the considered galvanostatic technique and vice versa.

The mean relative polarisation resistances, R_P/R_P^{ref} , and corrosion current densities, $i_{\text{corr}}/i_{\text{corr}}^{\text{ref}}$, calculated from the results obtained with the galvanostatic potential transient technique are given in Figures 5.57, 5.58 and 5.59, whereas the mean values calculated from the results obtained with the galvanostatic linear polarisation resistance technique are given in Figures 5.60, 5.61 and 5.62. In addition, also the mean ohmic resistances, R_Ω , obtained with the galvanostatic potential transient technique are given in Figures 5.57, 5.58 and 5.59. All results are shown as a function of the polarisation time. For clarity the standard deviations are not shown together with the mean values in the graphs, but are for selected polarisation times tabularised in Appendix G.

From the mean R_P/R_P^{ref} and $i_{\text{corr}}/i_{\text{corr}}^{\text{ref}}$ values calculated from the results obtained with the galvanostatic potential transient technique (curve fitting) for Specimens 1, 2 and 3, a clear effect of the polarisation time was observed, see Figures 5.57, 5.58 and 5.59. In contrast only a very limited effect of the polarisation current was observed. For Specimen 1, mean relative polarisation resistances, R_P/R_P^{ref} , in the range from 1.2 to 1.5 were obtained with polarisation currents from 5 to 50 μA and a polarisation time of 10 seconds (Figure 5.57). By increasing the polarisation time the mean relative polarisation resistances, R_P/R_P^{ref} , increased almost linearly, and with a polarisation time of 165 seconds values in the range from 1.8 to 2.2 were obtained. Lower mean relative polarisation resistances were obtained from the measurements where polarisation currents of 100 μA were used; With a polarisation time of 10 seconds a mean R_P/R_P^{ref} value of approximately 0.8 was obtained whereas a value of approximately 1.1 was obtained with a polarisation time of 165 seconds duration (Figure 5.57). Possible explanations for the lower mean R_P/R_P^{ref} values are discussed in Section 6.3.2.

Reflecting the mean relative polarisation resistances, R_P/R_P^{ref} , the mean relative corrosion current densities, $i_{\text{corr}}/i_{\text{corr}}^{\text{ref}}$, decreased with increasing polarisation time (Figure 5.57): For measurements where polarisation currents from 5 to 50 μA were used values in the range from 0.7 to 0.9 were obtained for a polarisation time of 10 seconds, whereas values in the range from 0.5 to 0.6 were obtained when increasing the polarisation time to 165 seconds. In agreement with the lower relative polarisation resistances, R_P/R_P^{ref} , obtained for the measurements performed with polarisation currents of 100 μA , corre-

spondingly higher relative corrosion current densities, i_{corr}/i_{corr}^{ref} , were obtained.

The ohmic resistances, R_Ω , determined for Specimen 1 increased with increasing polarisation time, see Figure 5.57, bottom graph. For the measurements performed with polarisation currents from 5 to 25 μA almost identical ohmic resistances, R_Ω , were obtained: with a polarisation time of 10 seconds values from approximately 0.5 to 0.7 kOhm were obtained, whereas values of approximately 1 kOhm were obtained with a polarisation time of 165 seconds. Slightly higher ohmic resistances, R_Ω , were obtained for the measurements performed with polarisation currents of 50 and 100 μA .

As seen in Figures 5.58 and 5.59 the relative polarisation resistances, R_P/R_P^{ref} , and corrosion current densities, i_{corr}/i_{corr}^{ref} , obtained for the measurements with the galvanostatic potential transient technique for Specimens 2 and 3 were similar to the values obtained for Specimen 1 (Figure 5.57). However, a larger scatter of the calculated R_P/R_P^{ref} and i_{corr}/i_{corr}^{ref} values was observed for Specimens 2 and 3, and primarily for the values obtained for the measurements performed with polarisation currents of 5 and 10 μA . Also, lower ohmic resistances, R_Ω , were obtained for Specimens 2 and 3 than for Specimen 1: For all measurements, i.e. with polarisation currents from 5 to 100 μA , ohmic resistances, R_Ω , of approximately 0.4 kOhm were obtained, being almost independent of the polarisation time.

Similar to the results obtained with the galvanostatic potential transient technique, a clear effect of the polarisation time was also observed from the mean R_P/R_P^{ref} and i_{corr}/i_{corr}^{ref} values calculated from the results obtained with the galvanostatic linear polarisation resistance technique, see Figures 5.60, 5.61 and 5.62. Also, only a limited effect of the polarisation current was observed. For Specimen 1 relative polarisation resistances, R_P/R_P^{ref} , in the range from 0.8 to 1.0 were obtained with polarisation currents from 5 to 50 μA and a polarisation time of 10 seconds, whereas values in the range from 2.4 to 2.6 were obtained with a polarisation time of 165 seconds, see Figure 5.60. Thus, by increasing the polarisation time from 10 to 165 seconds, the measured polarisation resistances, R_P increased by a factor ranging from 2.6 to 3.0 (2.6/1 to 2.4/0.8). As also seen from the results obtained with the galvanostatic potential transient technique, lower mean relative polarisation resistances, R_P/R_P^{ref} , were obtained from the measurements with polarisation currents of 100 μA . Here, a mean R_P/R_P^{ref} value of approximately 0.4 was obtained with a polarisation time of 10 seconds, whereas a value of approximately 1.3 was obtained with a polarisation time of 165 seconds. As seen from the bottom graph in Figure 5.60 the mean relative corrosion current densities, i_{corr}/i_{corr}^{ref} , for Specimen 1 clearly reflected the mean relative polarisation resistances, R_P/R_P^{ref} , described above. However, for a polarisation time of 10 seconds very different mean relative corrosion current densities, i_{corr}/i_{corr}^{ref} , were obtained with different polarisation currents: With currents of 5 and 10 μA , i_{corr}/i_{corr}^{ref} values of approximately 2.2 were obtained, whereas values of 1.4 and 2.6 were obtained with currents of 25 and 50 μA and 100 μA , respectively (Figure 5.60, bottom graph). With increasing polarisation time the i_{corr}/i_{corr}^{ref} values obtained for the measurements performed with polarisation currents from 5 to 50 μA approximated each other, and with a polarisation time of 165 seconds almost identical values of approximately 0.5 were obtained. In

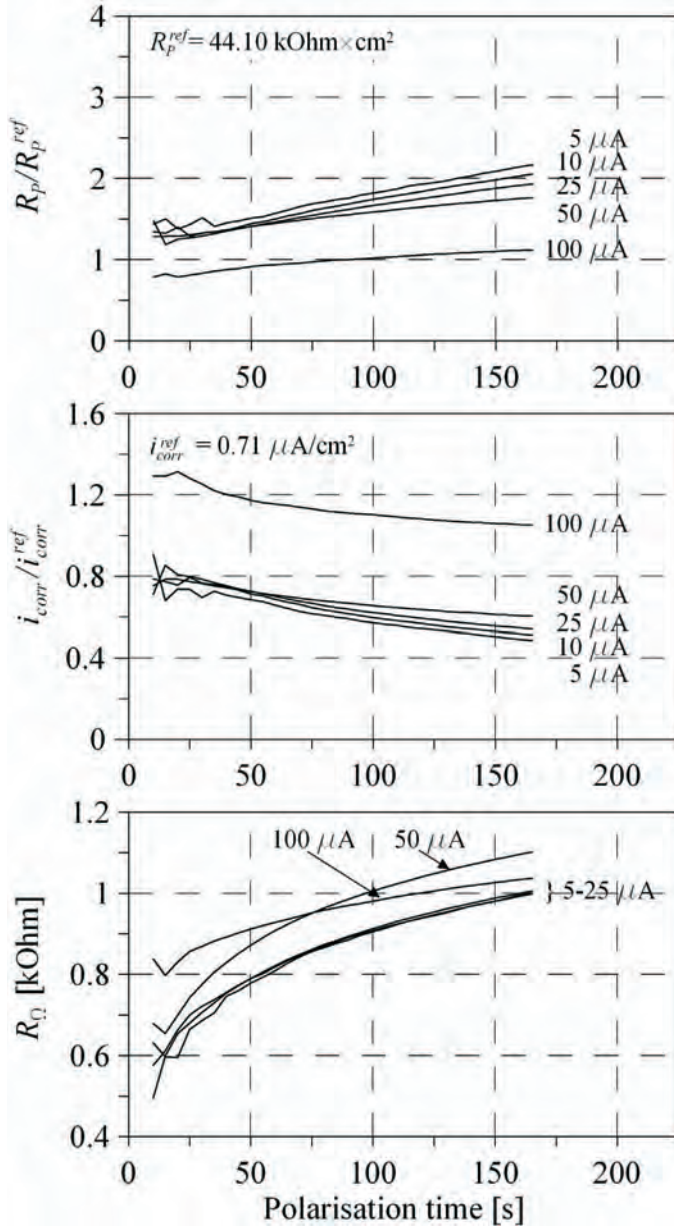


Figure 5.57 Specimen 1: Mean relative polarisation resistances, R_p/R_p^{ref} , mean corrosion current densities, i_{corr}/i_{corr}^{ref} , and (absolute) ohmic resistances, R_Ω , calculated as a function of the polarisation time from the results obtained with the galvanostatic potential transient technique.

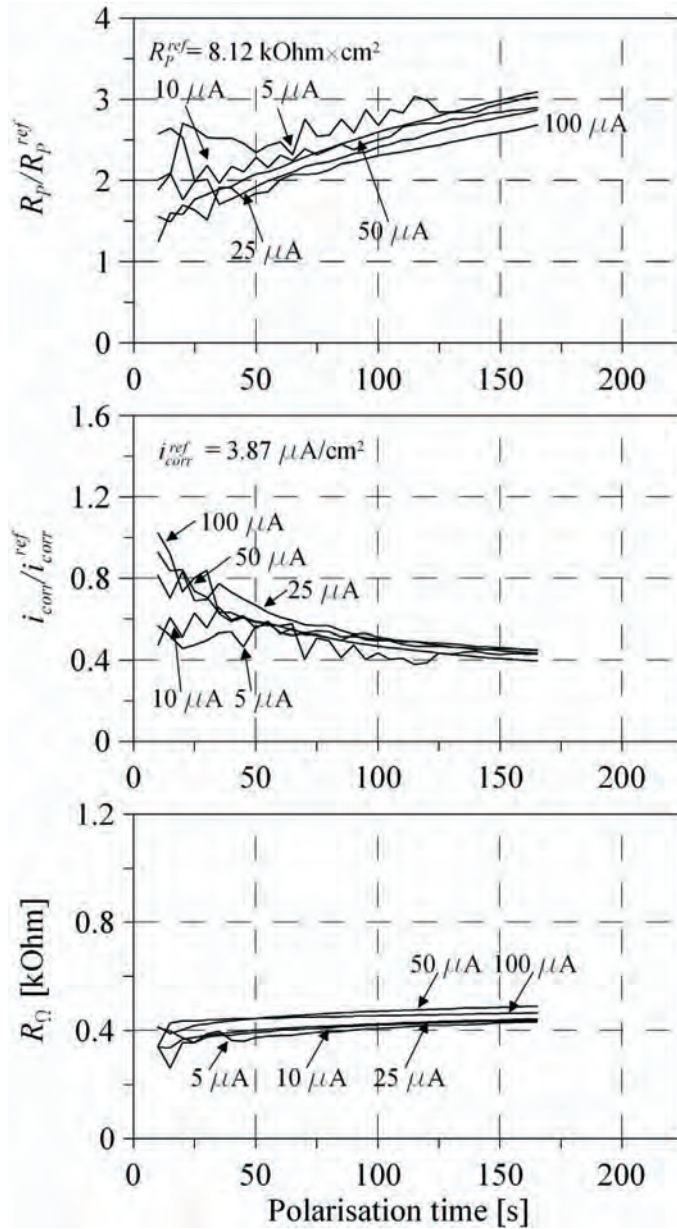


Figure 5.58 Specimen 2: Mean relative polarisation resistances, R_p/R_p^{ref} , mean corrosion current densities, i_{corr}/i_{corr}^{ref} , and (absolute) ohmic resistances, R_Ω , calculated as a function of the polarisation time from the results obtained with the galvanostatic potential transient technique.

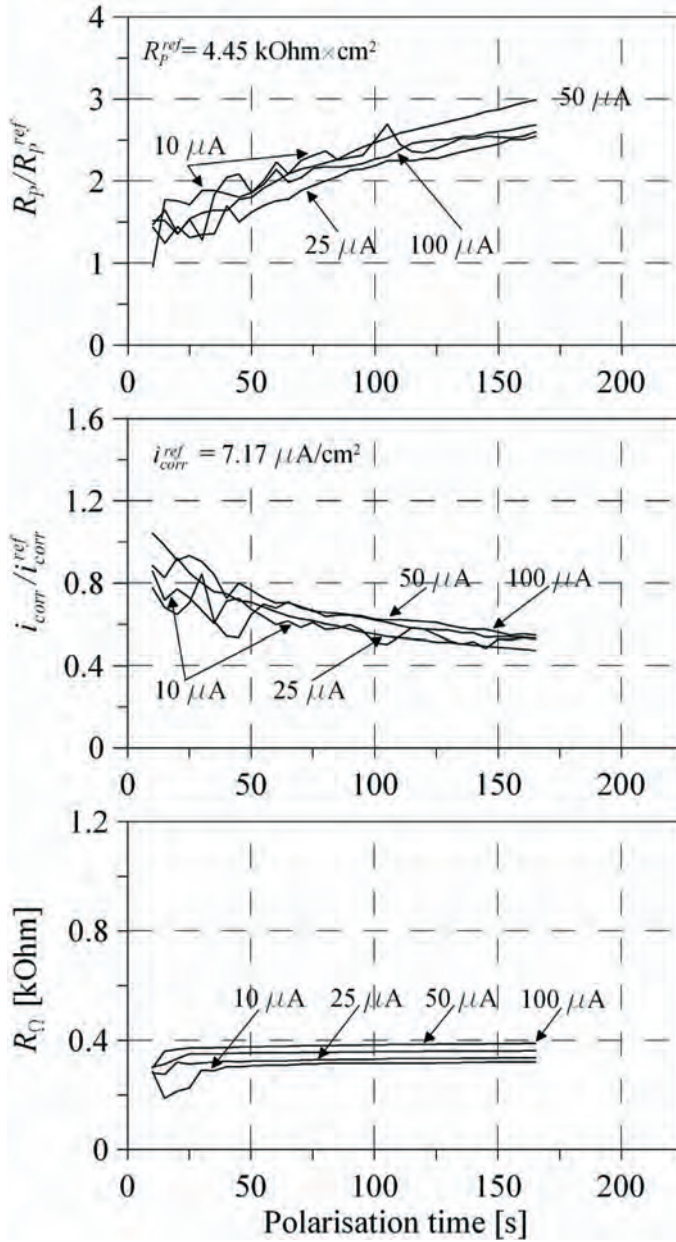


Figure 5.59 Specimen 3: Mean relative polarisation resistances, R_p/R_p^{ref} , mean corrosion current densities, i_{corr}/i_{corr}^{ref} , and (absolute) ohmic resistances, R_Ω , calculated as a function of the polarisation time from the results obtained with the galvanostatic potential transient technique.

agreement with the relative polarisation resistances, R_P/R_P^{ref} , higher relative corrosion current densities, i_{corr}/i_{corr}^{ref} , were obtained for the measurements with 100 μA . For these a mean i_{corr}/i_{corr}^{ref} value of approximately 0.8 was obtained for a polarisation time of 165 seconds.

As seen in Figures 5.61 and 5.62 the relative polarisation resistances, R_P/R_P^{ref} , and corrosion current densities, i_{corr}/i_{corr}^{ref} , obtained for the measurements with the galvanostatic linear polarisation resistance technique for Specimens 2 and 3 were similar to the values obtained for Specimen 1 (Figure 5.60). For the three specimens the same quantitative effect of the polarisation time on the R_P/R_P^{ref} and i_{corr}/i_{corr}^{ref} values was observed. A slightly varying effect of polarisation current was though observed for the three specimens. The variation was mainly seen in the R_P/R_P^{ref} and i_{corr}/i_{corr}^{ref} values obtained from the measurements performed with the low polarisation currents, i.e. 5 and 10 μA and may be a result of low potential shifts and hence low signal noise ratios. Possible explanations for the variations are discussed in Section 6.3.2.

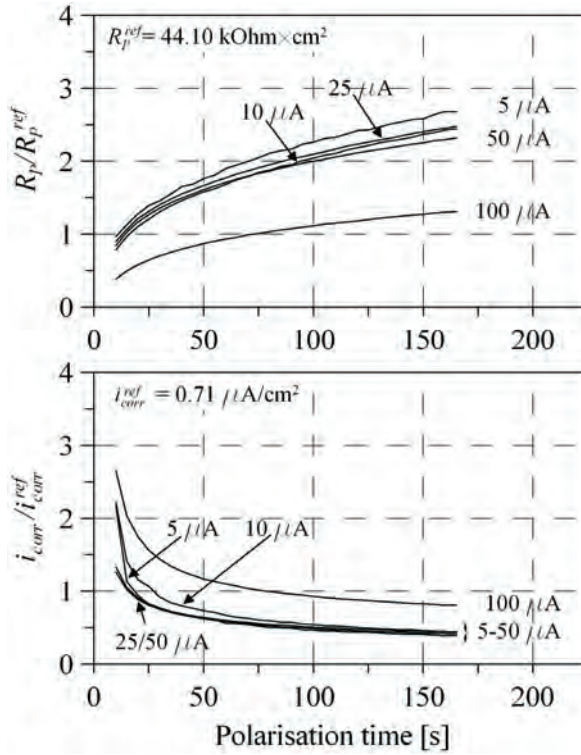


Figure 5.60 Specimen 1: Mean relative polarisation resistances, R_p/R_p^{ref} , and corrosion current densities, i_{corr}/i_{corr}^{ref} , calculated as a function of the polarisation time from the results obtained with the galvanostatic linear polarisation resistance technique.

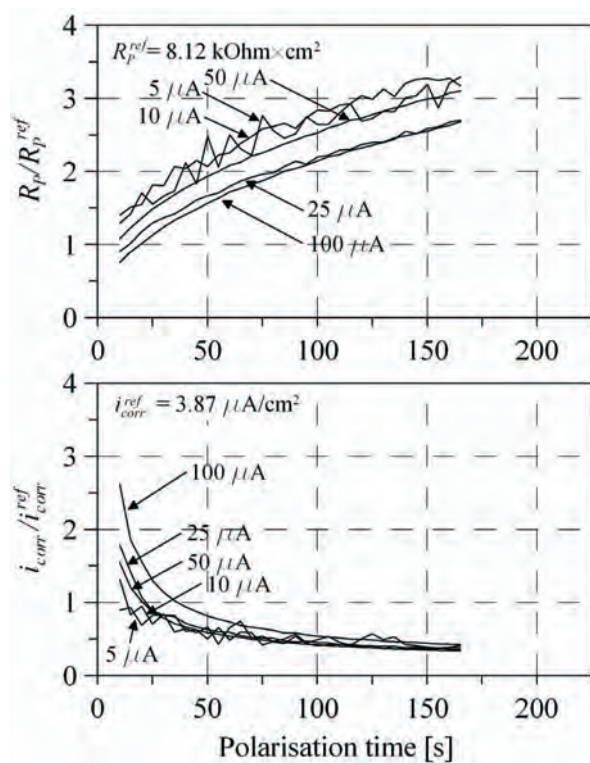


Figure 5.61 Specimen 2: Mean relative polarisation resistances, R_p/R_p^{ref} , and corrosion current densities, i_{corr}/i_{corr}^{ref} , calculated as a function of the polarisation time from the results obtained with the galvanostatic linear polarisation resistance technique.

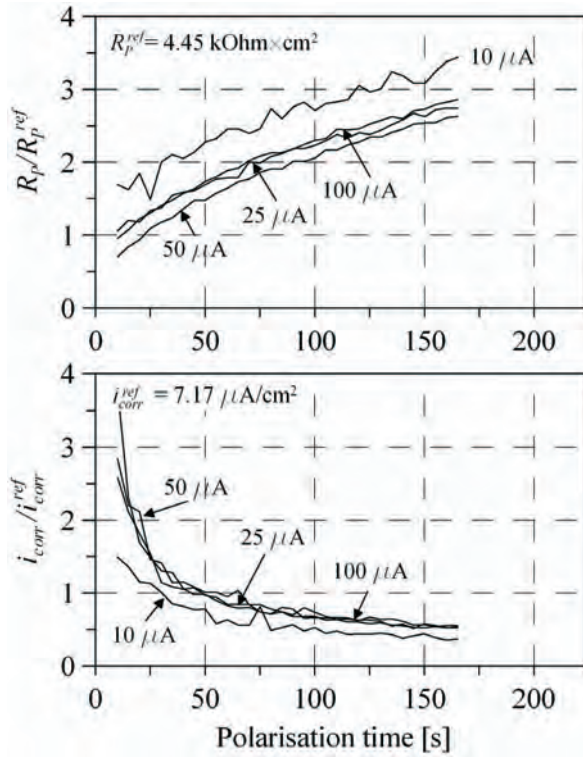


Figure 5.62 Specimen 3: Mean relative polarisation resistances, R_P/R_P^{ref} , and corrosion current densities, i_{corr}/i_{corr}^{ref} , calculated as a function of the polarisation time from the results obtained with the galvanostatic linear polarisation resistance technique.

Chapter 6

Discussion

The experimental results generated during the research project are discussed in this chapter. The chapter is divided into four main sections. In the first section half-cell potential measurements are discussed. In the second section the *effect of confinement techniques* is discussed. Both sections are based on the experimental results from *Experiment A - Effect of confinement techniques* (Table 4.1) described in Chapter 4, Section 4.1. The results are presented in Chapter 5, Section 5.1.

The third section deals with the effect of the technique and procedure used for corrosion rate measurements. Subsequently, the effect of temperature and relative humidity on the corrosion rate of steel in concrete is discussed. Sections three and four are based on the results from *Experiment B - Effect of measurement technique, procedure and exposure* (Table 4.1) described in Chapter 4, Section 4.2. The results are presented in Chapter 5, Section 5.2.

6.1 Half-cell potential measurements

The half-cell potentials, E_{corr} , measured with the laboratory potentiostat and the small unconfined electrode assembly (Figure 4.9) along the upper and lower segmented reinforcement bars in the concrete slab without chloride (Slab I) ranged from -35 to -100 mV versus Ag/AgCl, see Figure 5.5. Similar values were obtained with both the GECOR 6 and the GalvaPulse instruments, except with the GECOR 6 on the upper reinforcement bar, where values of +25 mV versus Ag/AgCl were measured, see Table 5.4. The observed differences were caused by a shift in the reinforcement bar potential, as measured versus the embedded MnO₂ reference electrode, see Table 5.4, numbers in brackets. On the concrete slabs with chloride (Slabs II and III) good agreement was also observed between the half-cell potential values measured with the small unconfined electrode assembly, the GECOR 6 and the GalvaPulse instruments, (Figures 5.6, 5.15, 5.35, and 5.7, 5.16 and 5.36). As no discrepancies between the potentials measured by the three instruments were observed (Figures 5.5 to 5.7), only the half-cell potentials measured with the laboratory potentiostat and the small unconfined electrode assembly are discussed in the following.

No differences between the half-cell potentials measured on the upper bar with two carbon

steel segments (combined with stainless segments) and the lower bar made of carbon steel segments only were observed in the slab without chloride (Slab I), see Figure 5.5. This is in agreement with expectations of no significant polarisation of either the stainless or the carbon steel in chloride free concrete (Pastore and Pedeferrrie, 1991).

The potential of stainless steel in concrete has been shown not to be affected by the chloride content, as long as the steel remains passive, i.e. below the pitting potential (Pastore and Pedeferrrie, 1991). This correlates well with the potential values recorded for the stainless segments (segments 1-16 and 19-34) on the upper reinforcement bars in Slabs II and III, see Table 5.2. The observations should not be extrapolated to other temperatures without considering that Bertolini et al. (1996) found a slight decrease in half-cell potentials with increasing chloride content at 40 °C for various types of stainless steel in simulated pore solution.

On the contrary, large potential differences were observed for the two types of bars (upper and lower) in Slabs II and III; more negative half-cell potentials were measured on the lower bars made of carbon steel segments only, see Figures 5.6 and 5.7. Also, comparing the half-cell potentials measured on the Slabs with 1.5 and 4 % chloride (Slabs II and III) a significant decrease with increasing chloride content was observed as expected.

Despite the central position of the two anodic carbon steel segments on the upper bars and the random positions of the anodic segments on the lower bars in Slabs II and III with chloride, constant half-cell potential values were measured along all the reinforcement bars (Figures 5.6 and 5.7). A slight indication of the local anodes' positions was observed as a local potential minimum when measuring on the surface with 30 mm cover on the upper bar in Slab III, only. The reason for the almost constant half-cell potentials is considered to be the low concrete resistivity enabling the few anodes to polarise the entire reinforcement bar to a potential close to that of the anodes, see Tables 4.2 and 5.1. Increasing the concrete resistivity or decreasing the cover thickness should give a clearer identification of the anodes' positions (Elsener and Böhni, 1990) (Elsener et al., 2003). In general the results indicate that unambiguous detection or accurate localisation of small corroding areas using the half-cell potential technique is difficult on wet, chloride contaminated concrete typically found in marine environments.

The expected effect of the cover thickness was only observed for the reinforcement bars with intended general corrosion (lower bars, Slabs II and III) and the reinforcement bar with the highest rate of localised corrosion (upper bar in Slab III). The increase in cover thickness from 30 to 75 mm resulted in an increase of approximately 30 mV, see Figures 5.5 to 5.7.

The positions of the anodes, i.e. the corroding segments, could not be detected as no potential gradients were observed, although measurements were made with a distance of only 50 mm. The half-cell potentials measured on the reinforcement bars with (intended) general corrosion (lower bars in Slabs II and III) are in agreement with the criteria given in the ASTM C 876-77 (1977) standard indicating 90 % probability of corrosion (< -233

mV vs. Ag/AgCl), see Table 3.2 and Figures 5.6 and 5.7. On the contrary, the localised corrosion on the upper bars could not be identified based on the ASTM C 876-77 (1977) criteria, except for the bar in the most aggressive environment when measuring on the surface with the lowest cover (upper bar in Slab III, 30 mm). The difficulty in detecting the two local anodes may be due to a more positive half-cell potential of the stainless steel increasing the mixed potential to be above the ASTM C 876-77 (1977) criteria.

The effects of cover thickness and other factors are discussed in a recent RILEM Recommendation suggesting that potential gradients rather than absolute values should be used when evaluating the *risk of corrosion* from measured half-cell potentials (Elsener et al., 2003). To assess the effect of the cover thickness and concrete resistivity half-cell potential measurements are often correlated with measurements of electrical resistance. In the present case neither half-cell potentials nor gradients indicated the localised corrosion, which was detected by macro-cell current measurements, except for the bar in the most aggressive environment. This shows that other techniques are needed for detection of corrosion in chloride contaminated structures.

6.2 Corrosion rate measurements - effect of confinement

6.2.1 Unconfined corrosion rate measurements

Although various confinement techniques have been proposed, some commercially available instruments rely on unconfined corrosion rate measurements, see e.g. Flis et al. (1993), Flis et al. (1995), Elsener et al. (1997) and Liu and Weyers (2003). Unconfined measurements provide a non-uniform current distribution between the relatively small counter-electrode on the concrete surface and the large reinforcement network. The measurements are influenced by geometrical parameters such as cover thickness and counter-electrode size in addition to concrete resistivity and corrosion state of the reinforcement, which all affect the current distribution between the counter-electrode and the reinforcement (Elsener, 2005). The use of unconfined corrosion rate measurements is discussed in the following, based on measurements with the laboratory potentiostat and the small unconfined electrode assembly and with the GalvaPulse instrument without current confinement. The measurements were undertaken on the three slabs with segmented reinforcement bars. The measurements on reinforcement in the passive state (Slab I) are discussed first, after which the measurements on actively corroding reinforcement (Slabs II and III) are considered.

Passive reinforcement

The current applied from a small counter-electrode placed on the concrete surface spreads laterally over a large length of a passive reinforcement bar due to the high polarisation resistance, R_P , (Law et al., 2001), (Andrade et al., 2004), (Elsener, 2005), see Figure 3.21. This phenomenon was observed from the real-time recordings of the GalvaPulse measurements without current confinement on the passive bars in Slab I, see Figures 5.11 and 5.14. Also, on the upper bar with both stainless and carbon steel segments the applied counter-electrode current, I_{CE} , was distributed symmetrically around the counter-electrode and

over the entire reinforcement bar length, see Figure 5.11, bottom graph. As a result of the large current spread low I'_{CE}/I_{CE} ratios of approximately 0.1 were obtained. That is, only 10 % of the applied counter-electrode current, I_{CE} , entered the assumed polarisation area below the electrode assembly. Similar observations were obtained on the lower bar in Slab I, made of carbon steel segments only: On this bar slightly higher I'_{CE}/I_{CE} ratios, starting at approximately 0.3 and decreasing during the measurements to end values of approximately 0.15, were observed, see Figure 5.14, lower graph. For both the upper and lower bars, the recorded current distributions were seen to *even out* as a function of time, i.e. the spread of the applied current increased during the measurements. This could be explained by an effect similar to that of the frequency observed from Electrochemical Impedance Spectrography measurements: At very high frequencies, corresponding to $t = 0$ for a DC measurement, only a very small area directly below the counter-electrode is polarised. When decreasing the frequency, corresponding to increasing the time for the DC measurement, the polarised area increases (Andrade et al., 2004). This is a result of the frequency depending resistance of the double layer capacitor, C_{dl} .

Similar to the observations in previous studies (Liu and Weyers, 2003) (Elsener et al., 1997), the lateral spread of the counter-electrode current, I_{CE} , resulted in much too low apparent polarisation resistances values, R_P^{app} : Using the laboratory potentiostat and the small unconfined counter-electrode a polarisation resistance of approximately 1×10^3 kOhm \times cm² was for example measured on the upper bar in Slab I, whereas a value of 23.3×10^3 kOhm \times cm² was obtained with the large counter-electrode ensuring uniform polarisation, see Table 5.2. The reason for the observed difference was the actual polarisation area being much larger than the area used for calculating the apparent polarisation resistance, R_P^{app} . Similar observations were made for the lower reinforcement bar in Slab I. For this reinforcement bar polarisation resistances, R_P , of 4.8×10^3 kOhm \times cm² and 100 kOhm \times cm² were measured with the large and small counter-electrodes, respectively, see Table 5.3 and Figure 5.5. The lower R_P values were a result of the lower bar being made of carbon steel segments only.

The relative error induced when using a small unconfined counter-electrode for measuring the R_P was investigated by Feliu et al. (1996). As seen from Figure 6.1, showing the results from their work, a relative error (R_P/R_P^{app}) exceeding a factor of 1000 should be expected for the present work where a counter-electrode with an area of 28 cm² was used (neglecting the central hole). Assuming that the true polarisation resistance was obtained with the large counter-electrode covering the entire length of the reinforcement bar and ensuring uniform polarisation, R_P/R_P^{app} ratios of approximately 20 and 50 were obtained for the upper and lower bars, respectively. The discrepancy between the observations in the present study and in Feliu et al. (1996) cannot be explained from the information given in the paper. In the work by Wojtas (2004a) increasing R_P/R_P^{app} ratios were observed from numerical simulations for increasing R_P values, see Figure 3.28 (note the reciprocal R_P/R_P^{app} ratio).

Comparing the true R_P values (large counter-electrode) measured on the upper and lower bars (23.3×10^3 and 4800 kOhm \times cm², respectively) with the R_P values given in Table 6.1

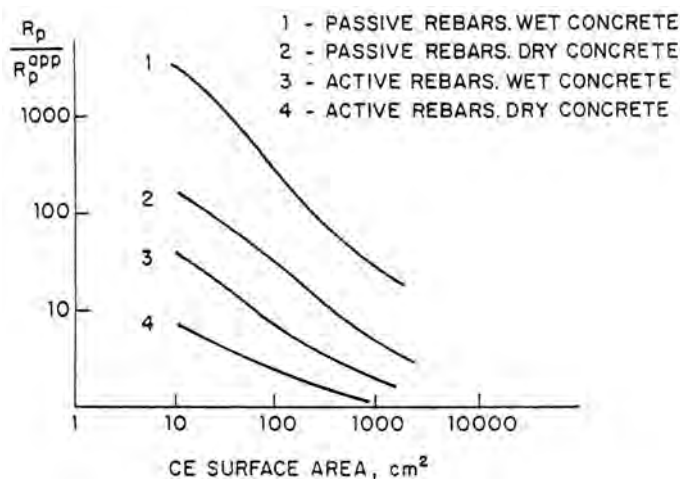


Figure 6.1 The relative error R_P/R_P^{app} as a function of the counter-electrode size (Feliu et al., 1996).

Table 6.1 Typical corrosion rates for steel in concrete (Gowers et al., 1994) (Law et al., 2001) (So and Millard, 2007).

Corrosion rate	Polarisation resistance R_P [$\text{k}\Omega \times \text{cm}^2$]	Corrosion current density i_{corr} [$\mu\text{A}/\text{cm}^2$]	Section loss* p [$\mu\text{m}/\text{year}$]
Very high	$2.5 > R_P > 0.25$	$10 < i_{corr} < 100$	$100 < p < 1000$
High	$25 > R_P > 2.5$	$1 < i_{corr} < 10$	$10 < p < 100$
Low/moderate	$250 > R_P > 25$	$0.1 < i_{corr} < 1$	$1 < p < 10$
Passive	$R_P > 250$	$i_{corr} < 0.1$	$p < 1$

* Loss of reinforcement section from Faraday's Law, assuming $\text{Fe} \rightarrow \text{Fe}^{2+}$

good agreement between the actual and predicted corrosion state, i.e. the passive state, was observed (Tables 5.2 and 5.3). This was also the case when considering the apparent polarisation resistance of the upper bar ($1000 \text{ k}\Omega \times \text{cm}^2$), see Figure 5.5. However, prediction of the corrosion state of the lower bar based on the apparent polarisation resistance ($100 \text{ k}\Omega \times \text{cm}^2$) and the R_P values in Table 6.1 would erroneously lead to the conclusion of an active bar with a low or moderate corrosion rate, see Figure 5.5.

Also, the unconfined GalvaPulse measurements provided incorrect results when interpreted using the guidelines in Table 6.1. A significant overestimation of the corrosion rate of both bars was observed: On the upper bar a corrosion current density, i_{corr} , of $0.77 \mu\text{A}/\text{cm}^2$ was measured, indicating a low/moderate corrosion rate, whereas on the lower bar i_{corr} values of 1.46 and $1.82 \mu\text{A}/\text{cm}^2$ were measured indicating a high corrosion rate, see Tables 5.4 and 6.1.

The overestimation of the corrosion rates observed from both the laboratory potentiostat

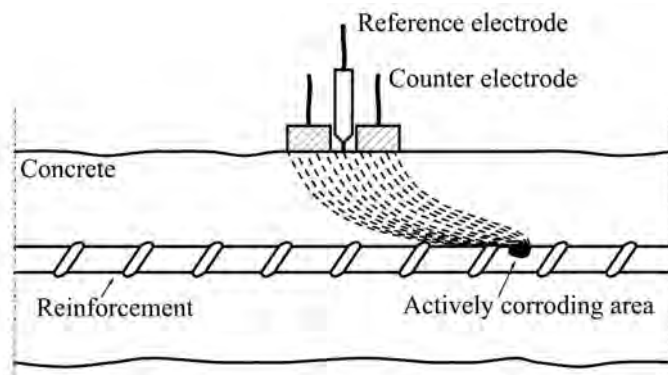


Figure 6.2 Schematic illustration of the self-confinement occurring when a small counter-electrode is used for R_P measurements on reinforcement with actively corroding areas.

with the small unconfined electrode assembly and the GalvaPulse measurements without confinement clearly demonstrate the difficulties that are associated with the use of unconfined polarisation resistance measurements. Thus clear distinction between passive and actively corroding steel with low corrosion rates seems difficult, if indeed not impossible.

Active reinforcement - general and localised corrosion

The current applied from a counter-electrode on the concrete surface follows the path of the lowest resistance to the embedded steel reinforcement (Ohms law). On actively corroding reinforcement the current from a counter-electrode flows into the active areas due to their low polarisation resistance, R_P (Elsener, 1998) (Liu and Weyers, 2003). This phenomenon, schematically illustrated in Figure 6.2, is often referred to as *self-confinement* (Elsener, 2005).

In the present work no indication of the active anodes' position was observed from the measurements on the upper reinforcement bars in the slabs with 1.5 and 4 % chloride (Slabs II and III): along the bars almost constant R_P^{app} and i_{corr}^{app} values were measured with both the laboratory potentiostat and the small unconfined electrode and the GalvaPulse instrument without current confinement, see Figures 5.6, 5.7, 5.15 and 5.16. Independent of the electrode assembly position on the concrete surface, a large portion of the current applied from the counter-electrode flowed into the two centrally positioned anodes, see Figures 5.32 to 5.34, bottom graphs. This resulted in similar R_P^{app} values being measured along the bars. The self-confinement was also observed from the I'_{CE}/I_{CE} ratios for the measurements in the three positions (Figures 5.32 to 5.34, middle graphs): in Positions 2 and 3 I'_{CE}/I_{CE} ratios of approximately 0.1 were recorded, i.e. only around 10 % of the applied counter-electrode current entered the reinforcement bar below the electrode assembly. However, in Position 4 directly over the active anodes, higher I'_{CE}/I_{CE} ratios between 0.2 and 0.45 were measured. The self-confinement was a result of the high cor-

rosion activity of the two anodes (macro-cell current densities of 0.25 and 3.24 $\mu\text{A}/\text{cm}^2$) combined with the low concrete resistivity (0.8 $\text{k}\Omega \times \text{cm}$), see Tables 5.1 and 4.2. Similar but less pronounced observations were made on the upper bar in Slab II with a lower chloride content of 1.5 %, see Figures 5.23 to 5.25. The lower self-confinement on this bar was a result of the lower corrosion activity of the centrally positioned anodes of which only one was active (macro-cell current density of 0.33 $\mu\text{A}/\text{cm}^2$) and higher concrete resistivity (1.6 $\text{k}\Omega \times \text{cm}$), see Tables 5.1 and 4.2.

To allow for comparison with the determined macro-cell current densities apparent corrosion current densities, i_{corr}^{app} , were calculated from the measured R_P^{app} values using Equation 2.19 and a B value of 26 mV . For the upper bar in Slab III the calculated apparent corrosion current densities, i_{corr}^{app} , ranged from 0.25 to 0.43 $\mu\text{A}/\text{cm}^2$ (105 to 61 $\text{k}\Omega \times \text{cm}^2$), see Figure 5.7. Comparing this with the average macro-cell current density of the two central anodes determined to 1.74 $\mu\text{A}/\text{cm}^2$ (Table 5.1), the unconfined measurements were seen to underestimate the corrosion rate. The reason for the underestimation may be the difference between the actual area of the corroding anodes (two 10 mm segments) and the area used for calculating the apparent polarisation resistance values, R_P^{app} , (22.6 cm^2). The actual area of the corroding anodes was maximum one third of the area used for calculation of the apparent polarisation resistance values. Multiplying with a factor 3 i_{corr} values in the range of 0.75 to 1.29 $\mu\text{A}/\text{cm}^2$ were obtained, still being lower than the average macro-cell current density.

On the upper bar in Slab II where the macro-cell measurements showed that only one of the two anodes was actively corroding, i_{corr}^{app} values ranging from 0.09 to 0.11 $\mu\text{A}/\text{cm}^2$ were calculated from the measured apparent polarisation resistances, R_P^{app} , ranging from 303 to 240 $\text{k}\Omega \times \text{cm}^2$, see Figures 5.6. Multiplying with a factor 6 (as only one of the two anodes was corroding) i_{corr} values in the range from 0.54 to 0.66 $\mu\text{A}/\text{cm}^2$ were obtained. These values are higher than the measured macro-cell current density of 0.33 $\mu\text{A}/\text{cm}^2$. This demonstrate that a simple correction of a measured i_{corr}^{app} value for the corroding area on an otherwise passive bar does not give the correct corrosion current density, i_{corr} .

The apparent corrosion current density depends on, among others, the measured potential response and the assumed polarised area: Despite the self-confinement, a portion of the applied counter-electrode current flows into the passive steel resulting in an increased potential response and thus a higher apparent polarisation resistance, R_P^{app} . On the other hand, using only the (small) actively corroding area for calculation of the apparent polarisation resistance a too low apparent polarisation resistance, R_P^{app} , is obtained. The net result of the two counteracting effects seems difficult, if not impossible, to determine: The contributions from the passive and actively corroding steel areas to the measured R_P^{app} is a function of the ratio between their size and the distribution of the counter-electrode current between them, which depends on their respective polarisation resistances, R_P and the electrical concrete resistivity.

The effect of the size of the corroding area on the measured apparent polarisation resistance, R_P^{app} , was investigated numerically in the work by Wojtas (2004a). From the

results in his work shown in Figure 6.3 (without confinement), it can be seen that the apparent polarisation resistance, R_P^{app} approximates the true value with the increasing size of the corroding area ($R_P^{app}/R_P=1$). However, when the corroding area is smaller than the assumed polarisation area (in his work 140 mm), the polarisation resistance is overestimated and the i_{corr} hence underestimated. This correlates well with the observations in the present work. However, a quantitative comparison between the two studies is not possible due to the very different setups (electrode assembly, concrete resistivity, polarisation resistances, etc).

Comparing the apparent corrosion current densities, i_{corr}^{app} , measured with the laboratory potentiostat and the small unconfined counter-electrode (0.9 to 0.11 $\mu\text{A}/\text{cm}^2$) with the *typical corrosion rates* given in Table 6.1, the upper bar in Slab II was at the limit between passivity and active corrosion. The i_{corr}^{app} values measured on the upper bar in Slab III (0.43 to 0.25 $\mu\text{A}/\text{cm}^2$) were in the range indicating active corrosion at a low or moderate rate.

With the GalvaPulse instrument i_{corr}^{app} values in the range from 0.65 to 0.86 $\mu\text{A}/\text{cm}^2$ were measured on the upper bar in Slab II, whereas values in the range from 1.05 to 1.59 $\mu\text{A}/\text{cm}^2$ were measured on the upper bar in Slab III, see Figures 5.15 and 5.16. Comparing the i_{corr}^{app} values with the measured macro-cell current densities, the corrosion rate was seen to be overestimated on the upper bar in Slab II, and slightly underestimated on the upper bar in Slab III. And comparing the apparent corrosion current densities, i_{corr}^{app} , with the *typical corrosion rates* in Table 6.1 the upper bar in Slab II was seen to be in the range indicating a low corrosion rate, whereas the upper bar in Slab III was in the range indicating a high corrosion rate.

Similar to the measurements on the upper bars almost constant R_P^{app} and i_{corr}^{app} values were measured along the lower reinforcement bars in Slabs II and III with the laboratory potentiostat and small unconfined counter-electrode and the GalvaPulse instrument, see Figures 5.6, 5.7, 5.35 and 5.36. Again this was a result of self-confinement. On the lower bars with several randomly positioned anodes, the current applied from the counter-electrode was distributed between the individual anodes, depending on the position of the electrode assembly on the concrete surface, the polarisation resistance of the individual anodes and the electrical concrete resistivity, see Figures 5.41, 5.42, 5.45 and 5.46. As varying macro-cell corrosion current densities were recorded for the individual anodic segments on each bar, a direct comparison with the apparent corrosion current densities, i_{corr}^{app} , calculated from the measured R_P^{app} values is not possible.

Tentatively a qualitative estimate of the corrosion state of the reinforcement bars may be obtained from the measured apparent corrosion current densities: On the lower bar in Slab II i_{corr}^{app} values in the range from 0.72 to 1 $\mu\text{A}/\text{cm}^2$ were measured with the laboratory potentiostat and unconfined electrode assembly, see Figure 5.6. Though, higher than the measured macro-cell current densities, ranging from 0.04 to 0.34 $\mu\text{A}/\text{cm}^2$ (Table 5.1), the apparent corrosion rate is in the same range (low/moderate) according to Table 6.1. With the GalvaPulse instrument apparent corrosion current densities, i_{corr}^{app} , in the

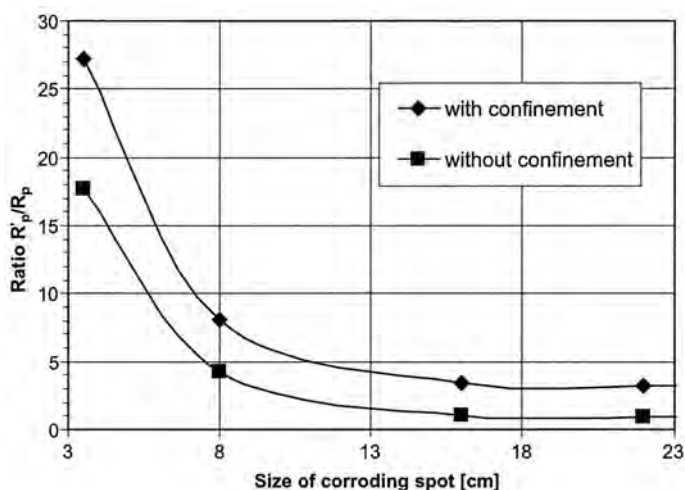


Figure 6.3 Relation between the measured apparent (R_p^{app}) and true polarisation resistance (R_p) of a corroding area on an otherwise passive reinforcement bar. The corroding spot was positioned centrally below the electrode assembly. Cover depth of 30 mm, Concrete resistivity of $20 \text{ k}\Omega \times \text{cm}$, R_p of the corroding spot $2.5 \text{ k}\Omega \times \text{cm}^2$, R_p of the passive area $600 \text{ k}\Omega \times \text{cm}^2$, Assumed polarisation length of 140 mm.

range from 1.15 to $1.84 \text{ }\mu\text{A}/\text{cm}^2$ were measured. These are also higher than the measured macro-cell current densities which correlates well with the overestimation, observed from the measurements on the upper bar in Slab II.

On the lower bar in Slab III apparent corrosion current densities, i_{corr}^{app} , in the range from 2.0 to $3.5 \text{ }\mu\text{A}/\text{cm}^2$ were obtained with the laboratory potentiostat and small unconfined electrode assembly, see Figure 5.7. On this bar the macro-cell current densities ranged from 0.2 to $6.7 \text{ }\mu\text{A}/\text{cm}^2$ with an average value of $3.2 \text{ }\mu\text{A}/\text{cm}^2$ (Table 5.1). The apparent corrosion current densities, i_{corr}^{app} , and the average macro-cell corrosion current density are comparable. Also, the corrosion current densities measured with the GalvaPulse, ranging from 3.88 to $8.03 \text{ }\mu\text{A}/\text{cm}^2$ were seen to be in good agreement with the measured macro-cell current densities.

In summary, distinction between passive and actively corroding steel with a low corrosion rate or small corroding areas seems impossible with the use of unconfined corrosion rate measurements. Also, the corrosion rate of actively corroding reinforcement cannot be accurately determined based on unconfined measurements and observations of the corroded area due to the overlapping response of the surrounding passive steel into which a portion of the applied counter-electrode current flows. Considering the results from the measurements on both the upper and lower reinforcement bars in Slabs II and III, it was found that actively corroding areas cannot be located. Also, it was observed that the ac-

curacy of the unconfined measurements increased with decreasing polarisation resistance, R_P , and increasing size of the corroding area when measuring directly over actively corroding reinforcement. This correlates well with observations and descriptions in earlier work (Liu and Weyers, 2003), (Wojtas, 2004a), (Wojtas, 2004b), (Andrade et al., 2004), (Elsener, 2005).

6.2.2 Confined corrosion rate measurements, commercial instruments

Functionality of the tested commercial instruments

In a study by Gepraegs and Hansson (2004), where three commercially available corrosion rate instruments were compared, irregular and abrupt fluctuations of the counter-electrode current, I_{GE} , were observed for the GECOR 6 during several measurements. The fluctuations were seen to result in potential shifts of the reinforcement of up to 80 mV, but no indications of any anomalies was given by the instrument. No such behaviour was observed in the present study as is described in the following.

The real-time recordings of the operation of the GECOR 6 and GalvaPulse instruments during the measurements on the segmented reinforcement bars in the passive state (Slab I), and with general and intense localised corrosion (lower and upper bars in Slabs II and III, respectively) confirmed that the confinement systems operate as anticipated with respect to the guard ring control. In all measurements with the GECOR 6, the initial potential difference between the auxiliary reference electrodes (E_{Ref2} and E_{Ref3} , see Section 4.1) was constant throughout the measurements. To maintain the initial potential difference, the I_{GE} increased steadily during the measurements on the upper passive reinforcement bar (with stainless cathodes) in Slab I, see Figure 5.9. However, on the lower passive bar, made of carbon steel segments, the I_{GE} increased only slightly when measuring at the surface with a concrete cover of 30 mm, whereas, on the surface with a cover of 75 mm a varying I_{GE} , was observed, see Figure 5.12. These observations correlate well with the observations and considerations in the work by Law et al. (2000a): When steel is passive and the polarisation resistance constant (or at least of same magnitude) along the entire reinforcement bar a symmetric current distribution, with respect to the electrode assembly, will be obtained. As a result of this, the applied guard ring current, I_{GE} , should solely be a function of the polarisation resistance, R_P , the concrete resistivity, ρ_c , and the concrete cover thickness. Considering the *true* polarisation resistances measured for the upper and lower bars in Slab I, given in Tables 5.2 and 5.3 and the real-time recordings of the guard ring currents in Figures 5.9 and 5.12 it is seen that the guard ring current increases with increasing polarisation resistance and cover thickness as expected. The effect of the concrete resistivity was not investigated for the passive steel.

For the measurements on the upper and lower reinforcement bars in Slabs II and III, the effect of self-confinement should also be considered: When measuring over passive steel near an actively corroding area a large portion of the applied current is drawn to the active area (low polarisation resistance) as the current follows the path of lowest resistance (Law et al., 2000a), see Figure 6.4.

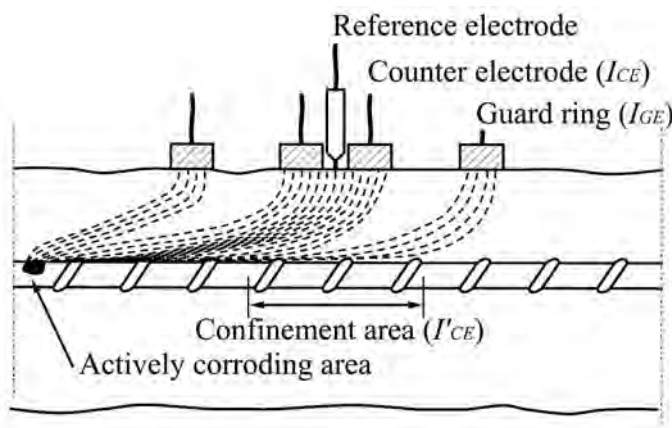


Figure 6.4 Schematic illustration of self-confinement when one active area exist: The current applied from the counter-electrode, I_{CE} , and the guard ring, I_{GE} , flows mainly into the reinforcement bar at the actively corroding area irrespective of the position of the electrode assembly on the concrete surface.

Self-confinement was observed for all measurements on the upper and lower bars in Slabs II and III (Figures 5.17 to 5.46). According to Law et al. (2000a) the orientation of the auxiliary reference electrodes in the GECOR 6 electrode assembly, with respect to the corroding area, i.e. orientated towards or away from the active area (by turning the electrode assembly 180°), to a large extent determines the applied counter-electrode current, I_{GE} : When the two electrodes are orientated in the direction in which the applied current is being drawn, i.e. towards the active area (when only one is present) they will detect the change in steel potential being induced by the current flow and the guard ring current will be adjusted, i.e. increased in order to counteract the change in potential. When the auxiliary reference electrodes are not orientated in the direction of the active area, the potential change (between the two auxiliary electrodes) will be less. A sufficiently high guard ring current that counteracts the flow to the active area will then not be supplied (Law et al., 2000a). For all measurements performed in this project the auxiliary electrodes were kept on the right hand side of the electrode assembly. Hence, higher guard ring currents should be observed when measuring in Positions 2 and 3 on the surface with a concrete cover of 30 mm, as the auxiliary electrodes in these positions were orientated towards the centrally positioned actively corroding anodes (as a result of the selected numbering). This correlates well with the guard ring currents observed when measuring on the upper reinforcement bars in Slabs II and III: In Positions 2 and 3, away from and next to the actively corroding anodes significantly higher guard ring currents were applied than when measuring directly over the active anodes (Position 4), see Figures 5.17 to 5.19 and 5.26 and 5.28. Also, as seen from these figures higher guard ring currents were in general observed when measuring on the surface with a concrete cover of 30 mm with the auxiliary electrode orientated towards the anodes.

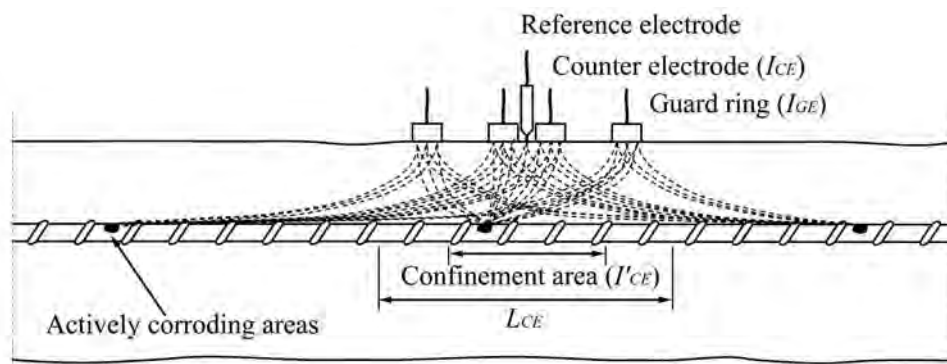


Figure 6.5 Schematic illustration of self-confinement in the case of several actively corroding anodes: The current applied from the counter-electrode, I_{CE} , and the guard ring, I_{GE} , flows mainly into the reinforcement bar at the actively corroding areas irrespective of the position of the electrode assembly on the concrete surface.

On the lower reinforcement bar in Slab II where several randomly positioned anodes with varying corrosion activities existed (see Section 5.1.1), a more complex behaviour of the GECOR 6 guard ring was observed. This was a result of several active areas, to which different amounts of the applied counter and guard currents flowed, see Figure 6.5.

When measuring in Position 2 near an actively corroding segment the guard ring current applied by the GECOR 6 increased and remained at a value of 50 to 60 μA after approximately 10 seconds, see Figure 5.37. Here, no effect of the orientation of the auxiliary reference electrodes or cover thickness was seen. However, in Position 3 over passive steel between to actively corroding segments significantly different guard ring currents were observed when measuring on each side of the specimen, i.e. with different orientations of the auxiliary reference electrodes. Again, this was a result of the active areas draining different amounts of the applied current, depending on their polarisation resistance and position with respect to the electrode assembly.

For all measurements with the GalvaPulse, the guard ring current, I_{GE} , was constant or almost constant, see e.g. Figures 5.10, 5.13, 5.20 to 5.22 and 5.43 to 5.44. This was expected as the constant I_{CE} results in a constant potential of the counter-electrode versus the reinforcement, due to an almost constant system resistance, i.e. when the potential of the reinforcement changes because of the polarisation, the counter-electrode voltage changes equivalently. Since the guard ring potential follows the counter-electrode potential (with a constant off-set), the potential difference between the guard ring and the reinforcement will be constant, resulting in a constant I_{GE} whose size is determined by the system resistance (measured through the guard ring).

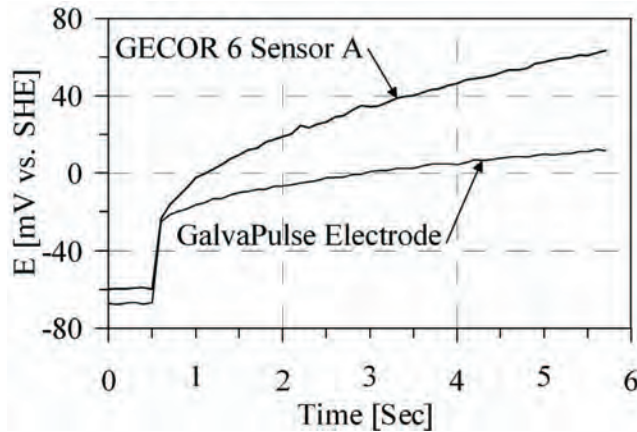


Figure 6.6 GalvaPulse polarisation curves obtained when using the GalvaPulse and the GECOR 6 electrode assemblies, respectively. A counter-electrode current, I_{CE} , of $40 \mu A$ was used for both measurements (Gepreags and Hansson, 2004).

Since the system resistance is a function of the contact area of the guard ring electrode, the I_{GE} will be a function of this, i.e. the area. This was observed in the study by Gepreags and Hansson (2004), where measurements were performed with the GalvaPulse instrument using both the GalvaPulse and the GECOR 6 electrode assembly: With the GECOR 6 electrode, a higher potential response was obtained than with the GalvaPulse electrode, which corresponds well with the GECOR 6 guard ring having a larger contact area than the GalvaPulse guard ring, see Figure 6.6.

Assessment of confinement techniques

So far only the functionality of the confinement techniques used in the selected commercial corrosion rate instruments has been considered. In the following the performance of the confinement techniques will be assessed using the results from the real-time recording of the GECOR 6 and GalvaPulse measurements on the three concrete slabs. The discussion is divided into three sections, after the intended corrosion state of the segmented reinforcement bars, i.e. *Passive reinforcement* (Slab I), *Intense localised corrosion* (upper bars in Slabs II and III) and *General corrosion* (lower bars in Slabs II and III).

As observed in experimental and numerical studies on corrosion rate instruments and confinement techniques, both the I_{CE} and I_{GE} contribute to the polarisation of the reinforcement (Gepreags and Hansson, 2004) (Wojtas, 2004a) (Wojtas, 2004b). This suggests that the I_{GE} should not be considered a current confining or encapsulating the I_{CE} , but rather a compensating current that is super-positioned with respect to the I_{CE} . However, as long as the current, I'_{CE} , flowing into the steel surface within the assumed polarisation area corresponds to the I_{CE} ($I'_{CE}/I_{CE} = 1$), the source of the current may be considered

irrelevant.

Passive reinforcement From the measurements with the GECOR 6 on the upper bar in Slab I, shown in Figure 5.9, it was seen that the continuous increase of the I_{GE} during both measurements, increased the I'_{CE}/I_{CE} ratios and decreased the L_{CE} lengths. But at the end of the measurements, when the I_{GE} currents were highest, only an I'_{CE}/I_{CE} of 0.6 and an L_{CE} of 200 mm were obtained on the surface with 30 mm cover, whereas values of 0.9 and 140 mm were obtained on the surface with 75 mm cover, respectively ($L_{CE} = 105$ mm at optimal confinement). This shows that full confinement was not achieved at any point during the measurements, resulting in an overestimation of the i_{corr} due to the lower potential response. Comparing the corrosion current densities, i_{corr} , obtained with the GECOR 6, with the *true* corrosion current density, i_{corr} , obtained from the potentiodynamic linear polarisation resistance measurement, this was seen to be true: With the GECOR 6 corrosion current densities, i_{corr} , of 0.03 and 0.02 $\mu\text{A}/\text{cm}^2$, (covers of 30 and 75 mm, respectively) were obtained, whereas the *true* corrosion rate was measured to 0.002 $\mu\text{A}/\text{cm}^2$, see Tables 5.2 and 5.4.

The increase in the I_{GE} currents during the measurements should also be taken into account, because the GECOR 6 relies on a steady state technique. As seen from Figure 5.9, the constant increase in the I_{GE} currents resulted in constantly decreasing potential responses, with no signs of steady state. Furthermore, potential shifts of -176 and -251 mV (30 and 75 mm covers, respectively) were obtained during the measurements, which put into question the use of the linear relation between potential and current around E_{corr} for calculation of the R_p . The range of linearity of the current-potential curve for passive steel embedded in concrete is, as described in Chapter 3, considered to be around or smaller than 20 mV (Stern and Geary, 1957) (Andrade and Gonzalez, 1978) (Andrade et al., 2004).

Also, from the measurements with the GECOR 6 on the lower bar, shown in Figure 5.12 a clear correlation between the variations in the I_{GE} currents and the I'_{CE}/I_{CE} ratios and L_{CE} lengths was observed. Compared to the measurements on the upper bar significantly lower I_{GE} currents were applied during the measurements on the lower bar. This was, as mentioned in Section 6.2.2, assumed to be a result of the lower polarisation resistance, R_p , of the lower bar, made of carbon steel segments only, see Tables 5.2 and 5.3. Because of the low I_{GE} currents, I'_{CE}/I_{CE} ratios and L_{CE} lengths of approximately 0.7 and 200 mm, and 0.3 and 425 mm were only obtained at the end of the measurements on the surfaces, with covers of 30 and 75 mm, respectively. Hence, full confinement was neither obtained on the lower bar. Again, a clear correlation between the obtained degree of confinement, i.e. the I'_{CE}/I_{CE} ratios, and the measured corrosion current densities, i_{corr} , was seen: On the surface with 30 mm cover where an I'_{CE}/I_{CE} ratio of 0.7 was obtained the i_{corr} was measured to 0.09 $\mu\text{A}/\text{cm}^2$, whereas on the surface with 75 mm cover, where an I'_{CE}/I_{CE} ratio of only 0.3 was obtained, an i_{corr} value of 0.016 $\mu\text{A}/\text{cm}^2$ was measured, see Table 5.4. The *true* corrosion current density, i_{corr} , was measured to 0.01 $\mu\text{A}/\text{cm}^2$, thus, similar to the measurements on the upper bar, the corrosion current density was overestimated, see Table 5.3. Potential shifts of -69 and -40 mV were obtained

Table 6.2 Guidelines for interpretation of corrosion current densities, i_{corr} , measured with the GalvaPulse instrument (with current confinement).

Corrosion rate	Corrosion current density
	i_{corr} [$\mu\text{A}/\text{cm}^2$]
High	$15 < i_{corr}$
Medium	$5 < i_{corr} < 15$
Low	$0.5 < i_{corr} < 5$
Negligible	$i_{corr} < 0.5$

during the measurements on the lower bar (30 and 75 mm covers, respectively), also far beyond the linear current-potential region around the free corrosion potential, E_{corr} .

From the measurements with the GalvaPulse on the upper bar, shown in Figure 5.10 the I'_{CE}/I_{CE} ratios and L_{CE} lengths were seen to be almost constant after a few seconds, due to the constant I_{GE} currents. However, during both measurements (covers of 30 and 75 mm, respectively) only I'_{CE}/I_{CE} ratios of approximately 0.15 and L_{CE} lengths of 600 mm were obtained, meaning that most of the current flowed away from the confinement length, L'_{CE} , assumed to be 70 mm (Figure 5.8). This way an even larger overestimation of the i_{corr} was obtained with the GalvaPulse than with the GECOR 6, which correlates well with the i_{corr} values, on both surfaces measured to $0.31 \mu\text{A}/\text{cm}^2$, see Table 5.4. On the lower bar, the I'_{CE}/I_{CE} ratios decreased and the confinement lengths, L_{CE} , increased during both measurements, despite the constant I_{GE} currents, see Figure 5.13: During both measurements the I'_{CE}/I_{CE} ratios started at approximately 0.6 and decreased to approximately 0.4 at the end of the measurements, while the confinement lengths, L_{CE} , started at approximately 150 mm and ended at approximately 800 mm. The changes correlated with the current density distributions over the segmented reinforcement bar below the electrode assembly, decreasing during the measurements, see Figure 5.13, bottom graph. This may be related to the electrical behaviour of the passive steel during charging. From the measurements corrosion current densities, i_{corr} , of 0.70 and $0.89 \mu\text{A}/\text{cm}^2$ were obtained. Similar to the measurements with the GECOR 6, higher i_{corr} values were measured on the lower bar, than on the upper bar, due to the lower R_P of this, see Table 5.3. Although smaller potential shifts, ranging from 44 to 76 mV, were obtained during the GalvaPulse measurements, due to the lower I_{GE} currents, these were also far beyond the linear current-potential region around the free corrosion potential, E_{corr} .

Comparing the i_{corr} values obtained with the two instruments on the upper and lower reinforcement bars, with the respective guidelines for interpretation of measurements, given in Tables 6.2 and 6.3, it is seen that: All i_{corr} values measured with the GECOR 6 indicated negligible corrosion i.e. passivity. With the GalvaPulse only the i_{corr} values obtained on the upper bar were in the range of negligible corrosion, whereas the i_{corr} values on the lower bar indicated a low corrosion rate, see Table 5.4.

With regard to the i_{corr} values obtained with the potentiodynamic linear polarisation

Table 6.3 Guidelines for interpretation of corrosion current densities, i_{corr} measured with the GECOR 6 instrument (Andrade et al., 2004).

Corrosion rate	Corrosion current density
	i_{corr} [$\mu\text{A}/\text{cm}^2$]
High	$1 < i_{corr}$
Moderate	$0.5 < i_{corr} < 1$
Low	$0.1 < i_{corr} < 0.5$
Negligible	$i_{corr} \leq 0.1$

resistance technique, i.e. the reference technique, the GECOR 6 and GalvaPulse overestimated the i_{corr} by a factor of approximately 10 and 100, respectively (Tables 5.2, 5.3 and 5.4. Numerically, a calibration factor 0.1 for the GECOR 6 and 0.01 for the GalvaPulse (to be multiplied) may tentatively be proposed for passive reinforcement. However, these values may change with cover thickness, concrete resistivity and polarisation resistance governing the lateral current distribution (Elsener, 1998) (Song, 2000) (Wojtas, 2004a) (Wojtas, 2004b). Similar differences were reported in the comparative study by Gepraegs and Hansson (2004).

In the numerical studies by Wojtas (2004a) and Wojtas (2004b), the GECOR 6 was found to overestimate the polarisation resistance, R_P , when measuring on passive reinforcement by a factor of up to approximately 5. This corresponds well with the experimental results found here, since the factor 10 obtained in the present study should be divided by 2 when considering the R_P instead of the i_{corr} because the GECOR 6 instrument uses a B value of 26 mV and not the 52 mV that applies for passive steel. To the authors' knowledge, no experimental or numerical results describing the accuracy of the GalvaPulse instrument, when measuring on passive reinforcement, have ever been published.

Localised corrosion Similar to the unconfined polarisation resistance measurements, discussed in Section 6.2.1, almost constant corrosion current densities, i_{corr} , were measured with the GECOR 6 and GalvaPulse instruments along the upper bars in Slabs II and III, see Figures 5.15 and 5.16. No indications of the centrally positioned anodes were observed from any of the measurements on Slab II as well as on Slab III. With respect to the GECOR 6 these observations were found contrary to the findings in earlier studies: In the work by Gonzalez et al. (1995b) (discussed in Section 3.3) the GECOR 6 was seen to be able to differentiate passive and actively corroding parts of a reinforcement bar with an accuracy of ± 10 cm. In a more recent study (also discussed in Section 3.3) Andrade and Martinez (2005) found the GECOR 6 to 'better be able to detect the localised attack because of the confinement of the current to a smaller steel area than the whole bar (compared with the use of a large counter electrode ensuring uniform polarisation). The reason for the GECOR 6 not being able to locate the local anodes in the experiments performed in this study could be related to the relatively low concrete resistivity pertaining from the use of admixed chloride for initiation of active corrosion (Table 4.2). However, admixed chloride was also used in the work by Gonzalez et al. (1995b) and Andrade and Martinez (2005), the resulting concrete resistivities were not reported in any of these publications.

From the real-time recordings of the GECOR 6 and GalvaPulse measurements on the upper bar in Slabs II and III, it was seen that for both the positioning of the electrode assembly right above, next to and away from the corroding area (Positions 4, 3 and 2, respectively) a large portion of the I_{CE} and I_{GE} flowed into the two middle segments that were actively corroding, see Figures 5.17 to 5.22 and 5.26 to 5.31 (bottom graphs). As mentioned earlier, this phenomenon, referred to as self-confinement occurs as the current follows the path of lowest resistance to the steel i.e. through the area with lowest polarisation resistance, R_P , see Section 6.2.2. The two instruments behaved differently regarding the self-confinement and a major effect of polarisation resistance, R_P , of the centrally positioned actively corroding anodes was observed: On Slab II directly over the local anodes (Position 4), full confinement ($I'_{CE}/I_{CE} = 1$) was achieved with the GECOR 6 at the end of the measurement on the surface with 30 mm cover, see Figure 5.19. However, on the surface with 75 mm cover, the measurement resulted in overconfinement with the I'_{CE}/I_{CE} approximating 1.5 at the end of the measurement. This showed that a portion of the I_{GE} flowed into the confinement area during the measurement. With the GalvaPulse (also in Position 4 on both surfaces) full confinement was far from reached during the measurements, as the I'_{CE}/I_{CE} remained constant at a value of approximately 0.2, see Figure 5.22.

In Position 3, next to the anodes (of which only one was corroding) but over passive steel, a maximum I'_{CE}/I_{CE} of approximately 0.6 was obtained with the GECOR 6, although an I_{GE} approximately 7 times the I_{CE} was applied, see Figure 5.18. The current distribution obtained in this position was almost identical to that obtained in Position 4, meaning that a large portion of the I_{CE} and I_{GE} flowed into the anodes outside the assumed confinement area. In Position 2 over passive steel further away from the anodes, I'_{CE}/I_{CE} ratios of approximately 1.2 and 0.8 (30 and 75 mm covers, respectively) were obtained at the end of the measurements, close to full confinement. During these measurements the behaviour of the GECOR 6 approximated that seen when measuring on the passive bars in Slab I, however, here a portion of the I_{CE} and I_{GE} was still seen to flow into the central anodes.

Also with the GalvaPulse almost identical current distributions were obtained when measuring in Positions 2, 3 and 4 on the upper bar in Slab II, see Figures 5.20 to 5.22. As a result of the identical current distributions and the constant I_{GE} currents, I'_{CE}/I_{CE} ratios of approximately 0.1 were obtained in Positions 3 and 2, i.e. next to and away from the central anodes, whereas I'_{CE}/I_{CE} ratios of approximately 0.2 were obtained in Position 4 directly over the anodes.

Following the guidelines for interpretation of the i_{corr} values obtained with the GECOR 6 on the upper bar in Slab II, ranging from 0.02 to 0.045 $\mu\text{A}/\text{cm}^2$ (Table D.1), the corrosion rate of the embedded steel was negligible, see Tables 6.3. In contrast the corrosion rate of the single actively corroding anode was from the macro-cell current measurement determined to 0.33 $\mu\text{A}/\text{cm}^2$ (Table 5.1). With the GalvaPulse i_{corr} values in the range from 0.34 to 0.47 $\mu\text{A}/\text{cm}^2$ were measured on the upper bar in Slab II (Table D.1). Following the guidelines for interpretation of GalvaPulse measurements, given in Table 6.2, also

these indicated a negligible corrosion rate.

On the upper bar in Slab III, directly over the local anodes (Position 4, covers of 30 and 75 mm), the measurements with the GECOR 6 resulted in overconfinement with I'_{CE}/I_{CE} ratios in excess of 1.2 during most of the measurements, see Figure 5.28. For both measurements L_{CE} lengths of approximately 12 mm were recorded, i.e. smaller than the assumed confinement length, L'_{CE} of 105 mm and in fact even smaller than the active area (20 mm). This shows that a portion of the current applied from the guard ring, I_{GE} , flowed into the local anodes. With the GalvaPulse, full confinement was not achieved during the measurements in this position; although the I'_{CE}/I_{CE} ratios increased and the L_{CE} lengths decreased during the measurements, end values of approximately 0.6 and 575 mm only were obtained as regards both measurements, see Figure 5.31.

In Positions 2 and 3, i.e. away from and next to the active segments over passive steel, I'_{CE}/I_{CE} values of approximately 0.2 and 0.1 were obtained with the GECOR 6 and GalvaPulse, respectively. This means that both instruments measured the corrosion activity of the active area and not the passive area below the electrode assembly. As a result, almost identical i_{corr} values were obtained with both instruments when measuring in Positions 2, 3 and 4, i.e. away from, next to and directly over the active area: With the GECOR 6 i_{corr} values in the range from 0.05 to 0.15 $\mu\text{A}/\text{cm}^2$ were obtained, whereas values in the range from 0.48 to 0.89 $\mu\text{A}/\text{cm}^2$ were obtained with the GalvaPulse (Table D.2). For comparison, the average macro-cell corrosion current density, i_{corr} , of the two corroding anodes was measured to 1.74 $\mu\text{A}/\text{cm}^2$. Again, considering the guidelines for interpretation of the GECOR 6 and GalvaPulse measurements, given in Tables 6.3 and 6.2, respectively, both instruments found the corrosion rate to be negligible or low. These interpretations, as well as on the upper bar in Slab II, may be critical, as the presence of such localised and rapidly corroding spots, leading to a rapid cross section reduction, will not be detected.

The underestimation of the local anodes' corrosion rates was expected, as the measured R_P in the case of localised corrosion, is related to both the active and passive areas (Wojtas, 2004b). In the work by Wojtas (2004b) it was shown that the extent of the underestimation depends on the relation between the size of the counter-electrode and guard ring, the difference between the R_P of the passive and actively corroding parts of the reinforcement, the concrete resistivity and the cover thickness. Except for the relation between the size of the counter-electrode and guard ring, this was also seen for the unconfined measurements, see Section 6.2.1.

Comparing the i_{corr} values measured with the GECOR 6 and GalvaPulse directly over the active anodes (Position 4), with the *true* values, determined from macro-cell current measurements, both instruments were underestimating the i_{corr} : the GECOR 6 by a factor of approximately ten and the GalvaPulse by a factor of approximately two. As a remedy for the low i_{corr} values obtained with the GECOR 6 when measuring on reinforcement with chloride induced corrosion, it has been suggested that the i_{corr} should be multiplied by a *pitting factor* of 4 to 8 (this is the same as a calibration factor) (Gonzalez et al., 1995a).

Introducing a factor of 8 to the GECOR 6 results obtained directly over the active areas (Position 4) in this study gave a fairly good correlation with the *true* i_{corr} values, obtained from the macro-cell current measurements (Tables D.1, D.2 and 5.1). This corresponds well with the results obtained by Andrade and Martinez (2005). However, it should be stressed that the actual 'pitting factor' depends to a great extent on the size of the corroding spot (more precisely on the ratio between the size of the corroding spot and the concrete cover thickness (Elsener, 1998), the concrete cover and the concrete resistivity (Gonzalez et al., 1995b)).

General corrosion Similar to the measurements on the upper reinforcement bars, almost constant i_{corr} values were recorded along the lower reinforcement bars in Slabs II and III with the GalvaPulse instrument, see Figures 5.35 and 5.36. With the GECOR 6 measurements could only be performed on the lower bar in Slab II, where varying results were obtained, see Figure 5.35. Measurements on the lower bar in Slab III could not be performed because of the confinement technique used in the GECOR 6 instrument.

For the lower bars, the same fundamental situation prevailed as for the upper bars: the current applied from the electrode assembly, (I_{CE} and I_{GE}) was drawn to the actively corroding segments, however, instead of only being drawn to the central anodes as on the upper bars, the current was distributed among the randomly positioned anodes, see Figures 5.37 to 5.40 and 5.43 to 5.44. A schematic illustration of the *self-confinement* phenomenon in the case of several actively corroding anodes is shown in Figure 6.5. Comparing the current distributions recorded during the measurements on the lower bars in Slabs II and III, the highest degree of self-confinement was observed on the lower bar in Slab III, see Figures 5.39, 5.40, 5.43 and 5.44. This was expected due to the low concrete resistivity combined with the low R_P of the corroding segments in this slab (Tables 4.2 and 5.1, respectively).

From the attempted measurements with the GECOR 6 on the lower bar in Slab III, it was seen that the high lateral current flow from the electrode assembly to the randomly positioned anodes, made the I_{GE} current oscillate ($\pm 200\mu A$). This was a result of the instrument not being able to change the potential difference between the auxiliary reference electrode and hence the current distribution by adjusting the guard ring current. As mentioned, no difficulties were encountered when measuring with the GalvaPulse on the lower bars, this was because of the more *simple* guard ring control which was only affected by the system resistance, see Section 6.2.2.

In both Positions 2 and 3 on the lower bar in Slab II, full confinement was not obtained with the GECOR 6, see Figures 5.37 and 5.38: In Position 2, near a corroding segment an I_{GE} of approximately 7 times the I_{CE} was applied during both measurements (30 and 75 mm covers). However, I'_{CE}/I_{CE} ratios of approximately 0.7 were only obtained at the end of the measurements, i.e. after 100 seconds. In Position 3, over passive reinforcement between two corroding segments, slightly lower I'_{CE}/I_{CE} ratios were obtained: at the end of the measurements values of approximately 0.3 and 0.6 were obtained on the surfaces with covers of 30 and 75 mm, respectively. This means that, independent of the position

of the electrode assembly, the measured R_P is a *mixed value* representing both the several corroding anodes and the passive steel. Hence, similar to the unconfined measurements, direct comparison with the *true* corrosion rate of the individual anodes is not possible. With the GECOR 6 i_{corr} values in the range from approximately 0.08 to 0.80 $\mu\text{A}/\text{cm}^2$ were measured, indicating low to moderate corrosion rate, see Tables D.3 and 6.3. For comparison the corrosion current densities of the actively corroding segments were from the macro-cell current measurement seen to range from 0.04 to 0.34 $\mu\text{A}/\text{cm}^2$ (Table 5.1).

The same phenomena, i.e. self-confinement was also observed from the measurements with the GalvaPulse on the lower bar in Slab II, however, as a result of the constant I_{GE} with approximately same size as the I_{CE} , I'_{CE}/I_{CE} ratios of approximately 0.2 to 0.1 were obtained in both Positions 2 and 3. The corrosion current densities were in the range from 0.61 to 0.94 $\mu\text{A}/\text{cm}^2$, corresponding to a low corrosion rate following the guidelines for interpretation of the GalvaPulse measurements (Tables D.3 and 6.2). On the lower bar in Slab III, I'_{CE}/I_{CE} ratios of approximately 0.1 to 0.2 were obtained when measuring with the GalvaPulse in Positions 2 and 3. However, i_{corr} values in the range from 1.6 to 4.6 $\mu\text{A}/\text{cm}^2$ were obtained from the measurements, corresponding well to the i_{corr} values of the corroding anodes (macro-cell measurements) found to range from 0.2 to 6.7 $\mu\text{A}/\text{cm}^2$ with an average value of 3.2 $\mu\text{A}/\text{cm}^2$ (Tables D.4 and 5.1).

To the author's knowledge no information on the performance of the GECOR 6 and GalvaPulse in the case of reinforcement with several randomly positioned anodes, with well defined geometry has previously been published. From the experiments in this work it seems that the i_{corr} values, and especially those obtained with the GalvaPulse, approximate the true i_{corr} values with increasing corrosion current density, i_{corr} , and increasing size of the corroding area (total corroding area). However, accurate localisation of the corroding areas seems impossible due to the lateral current flow from the electrode assembly to the actively corroding areas with both the GECOR 6 and the GalvaPulse. This is in contrast to a recent RILEM Recommendation where it is stated that the method of modulated confinement (as used by the GECOR 6) is the most suitable for cases of localised attack, because it delimitates the area polarised and therefore, it is able to reduce the inherent error due to the relative area sizes. Moreover it is the only method which is able to minimize the effect of macro-cells or to notice active/passive region transition' (Andrade et al., 2004).

Testing confinement techniques - general considerations As seen from the results discussed in the previous sections, very different current distributions between the electrode assembly placed on the concrete surface and the embedded segmented reinforcement bars were observed for passive and actively corroding reinforcement. In the case of passive reinforcement almost symmetrical current distributions, with respect to the electrode assembly, were observed. Whereas in the case of active corrosion the randomly distributed active and passive areas on the lower bars (Slabs II and III) resulted in highly asymmetrical current distributions governed by the positions and sizes of the active areas. The situation with randomly positioned passive and active areas is often seen in practice, even long time after initiation of corrosion by carbonation or chlorides, see e.g. Luping

(2002) and Andrade and Martinez (2005). This should be taken into consideration when testing and using confinement techniques.

From the measurements discussed in the previous sections it was seen that in the case of passive reinforcement the lateral current spread from the electrode assembly can easily exceed a length of 1.5 metres (0.75 metres on each side of the electrode assembly), see Figures 5.9 to 5.14, bottom graphs. Hence, when confinement systems are tested on passive reinforcement embedded in concrete, the test specimens should have a length of at least 1.5 metres. With decreasing concrete resistivity the length of the test specimens should be increased. This is in good agreement with the suggestions in a recent RILEM Recommendation: here, a size of $150 \times 150 \times 15$ cm is suggested for both test specimens without - and with - admixed chloride, i.e. passive and actively corroding reinforcement, respectively (Andrade et al., 2004).

Compared to passive reinforcement the case of actively corroding reinforcement is much more complex. Ideal general corrosion, with a constant R_P over the entire length and circumference of the reinforcement bar, is rarely seen (Luping, 2002) (Liu and Weyers, 2003). This has not been taken into account in earlier studies where commercial corrosion rate instruments with different confinements techniques were tested, see e.g. Luping (2002), Liu and Weyers (2003), Gepraegs and Hansson (2004) and Andrade and Martinez (2005). In those studies i_{corr} values are typically given as average values (over the length) of a single or several bars in a test specimen, not considering the likely effect of self-confinement. Without knowing the true corrosion state of the embedded reinforcement bars, i.e. the number, size and positioning of the active/passive areas, the apparent constant i_{corr} values may erroneously be assumed to reflect ideal general corrosion. However, as seen from the discussion in the previous sections, the i_{corr} measured with a laboratory potentiostat and a small unconfined electrode assembly or the two commercial instruments, GECOR 6 and GalvaPulse using current confinement, seldom correlate with the actual i_{corr} of the reinforcement directly below the electrode assembly.

From the experimental results it was also seen that, although a good correlation between i_{corr} values measured with a commercial instrument and the true i_{corr} was observed, this was not necessarily a result of the instrument being able to confine the applied current, I_{CE} . This questions the use of comparative measurements, i.e. electrochemical and gravimetric, for evaluation of confinement systems as suggested in the recent RILEM recommendation (Luping, 2002), (Liu and Weyers, 2003), (Andrade et al., 2004), (Andrade and Martinez, 2005). Instead, a more direct method, e.g. based on segmented reinforcement bars, measuring the actual current distribution between the electrode assembly on the concrete surface and the embedded reinforcement bar together with the operation of the instrument, as suggested in the present work, could be used.

6.3 Corrosion rate measurements - effect of technique and procedure

The effect of the polarisation time and current on the determined polarisation resistance, R_P , and thus the corrosion current density, i_{corr} , is discussed in this section. The discussion is based on the results from the measured galvanostatic potential transients analysed using either the galvanostatic transient technique or the galvanostatic linear polarisation resistance technique (Table 4.1, Experiment B). The discussion is divided into two sections covering passive (Series I) and active generally corroding reinforcement (Series II), respectively.

The results obtained from the partly nickel coated reinforcement bars (Series III) are not considered in this section as observations from the segmented reinforcement bars showed that a simple correction of a measured i_{corr}^{app} value for the corroding area on an otherwise passive bar does not give the actual i_{corr} value, see Section 6.2.

6.3.1 Passive reinforcement

On passive reinforcement the polarisation resistances, R_P , obtained with both the galvanostatic transient technique and the galvanostatic linear polarisation resistance technique were observed to be highly affected by the polarisation time and current used for the measurements, see Figures 5.52 and 5.53. Similar trends were observed for both techniques: With increasing polarisation time and decreasing current the obtained polarisation resistance, R_P , increased. However, the extent of the effects, i.e. the increase in polarisation resistance, R_P , with increasing polarisation time and decreasing current, differed up to a factor of 10 for the two techniques. As a result different polarisation times and currents should be used with the two techniques for obtaining an estimate for the *actual* corrosion rate, i.e. corrosion current density, i_{corr} .

From Figure 3.7 it can be seen that the polarisation resistance, R_P , measured on passive steel with the potentiodynamic linear polarisation resistance technique - in contrast to measurements on actively corroding steel - is a function of the sweep rate used and does not converge to a constant value with decreasing sweep rate. Thus, possible reference R_P and i_{corr} values obtained with the potentiodynamic linear polarisation resistance technique can only be used as a qualitative indicator for passive reinforcement.

The corrosion rate of passive steel in concrete has been suggested as being approximately $0.1 \mu\text{m}/\text{year}$ ($\approx 0.009 \mu\text{A}/\text{cm}^2$), which is in good agreement with the values ranging from approximately 0.006 to $0.03 \mu\text{A}/\text{cm}^2$ reported in experimental studies where different electrochemical techniques have been used, see e.g. Arup (1983), Gonzalez et al. (1985a) and Millard et al. (1992). For comparison, the upper and lower i_{corr} values reported in literature from measurements on passive steel in concrete are shown in Figures 6.7 and 6.8, together with the results obtained with two galvanostatic techniques (from Figures 5.52 and 5.53). Corrosion current densities, i_{corr} , in the range associated with passivity, i.e. lower than $0.03 \mu\text{A}/\text{cm}^2$, were only obtained with the two techniques when a combination of a sufficiently low polarisation current and a sufficiently long polarisation time were used.

With the galvanostatic linear polarisation resistance technique (Figure 6.7) corrosion current densities, i_{corr} , below $0.03 \mu\text{A}/\text{cm}^2$ were only obtained when a polarisation current of $5 \mu\text{A}$ or less was used. With the current of $5 \mu\text{A}$ a polarisation time of 85 seconds was required to obtain an i_{corr} value of $0.03 \mu\text{A}/\text{cm}^2$, whereas a polarisation time of 40 seconds was required when a current of $0.25 \mu\text{A}$ was used, see Figure 6.7. The polarisation times required to obtain a corrosion current density, i_{corr} , of $0.03 \mu\text{A}/\text{cm}^2$ with the polarisation currents from 0.25 to $5 \mu\text{A}$ are summarised in Table 6.4 together with the potential shifts, ΔE , obtained at the given times.

It is interesting to see that stationary potential responses were not achieved during any of these measurements (0.25 to $5 \mu\text{A}$) even after a polarisation time of 170 seconds, see Figure 5.52. Also, only the non-stationary potential transients obtained with polarisation currents of 0.25 and $0.5 \mu\text{A}$ were within or near the linear potential-current range of approximately 20 mV around the free corrosion potential, E_{corr} (Andrade et al., 2004). This is in good agreement with the findings reported by Videm and Myrdal (1997) and Luping (2002). Hence, currents below $0.5 \mu\text{A}$ and polarisation times of several minutes should be used for obtaining a stationary potential response within the linear current-potential range when measuring on passive steel. For on-site corrosion rate measurements this is highly impractical as the electrode assembly placed on the concrete surface (counter and reference electrode) is hand-held and a large number of measurements are often made, typically in a grid, for *mapping* the condition of a reinforced concrete structure.

However as seen from the results, a clear indication of passivity can be obtained even though stationary conditions are not achieved and the obtained potential shift, ΔE , is outside the linear current-potential range around the free corrosion potential, E_{corr} . However, a sufficiently long polarisation time, t_P , should be used to decrease the influence of the selected polarisation current on the measured corrosion current density, i_{corr} , see Figure 6.7. As seen from Figure 6.7 a polarisation time of 100 seconds seems to be a good compromise between a *sufficiently long* polarisation time and a reasonable measuring time. With a polarisation time of 100 seconds the corrosion current density, i_{corr} , measured with polarisation currents from 0.25 to $5 \mu\text{A}$ ranged from 0.012 to $0.027 \mu\text{A}/\text{cm}^2$, all clearly showing the reinforcement bars to be in the passive state, see Table 6.5. It is interesting to see that the mean corrosion current density, i_{corr} , obtained with a polarisation current of $5 \mu\text{A}$ ($0.027 \mu\text{A}/\text{cm}^2$), resulting in a potential shift of -156 mV was only a factor of approximately 2.25 higher than the mean i_{corr} value obtained with $0.25 \mu\text{A}$ ($0.012 \mu\text{A}/\text{cm}^2$), where a potential shift, ΔE , of only -17 mV was obtained.

It should also be mentioned that the polarisation time of 100 seconds found appropriate for galvanostatic linear polarisation resistance measurements on passive steel is significantly longer than the 15-60 seconds suggested for the potentiostatic linear polarisation resistance technique in the literature (Millard et al., 1992) (Andrade et al., 2004). This correlates well with the mathematical derivations given in work by Gabrielli et al. (1979) showing that potentiostatic measurements of the corrosion current density, i_{corr} , on passive steel approaches a constant value much quicker than galvanostatic measurements, see

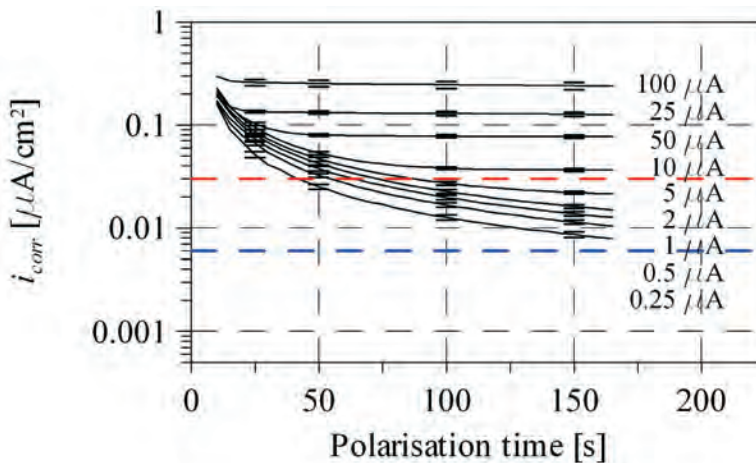


Figure 6.7 Galvanostatic linear polarisation resistance technique: Mean corrosion current densities, i_{corr} , obtained with polarisation currents from 0.25 to 100 μA as a function of the polarisation time for the passive reinforcement bars exposed at 25 °C and 75 % relative humidity (from Figure 5.53). The red and blue punctuated lines indicate a corrosion current density, i_{corr} , of 0.03 and 0.006 $\mu\text{A}/\text{cm}^2$, respectively.

Section 3.2.1.

With the galvanostatic potential transient technique, corrosion current densities, i_{corr} , below 0.03 $\mu\text{A}/\text{cm}^2$ were not only obtained with polarisation currents from 0.25 to 5 μA but also 10 μA , see Figure 6.8. With these currents (0.25 to 10 μA) polarisation times from 15 to 25 seconds were required to obtain a corrosion current density of 0.03 $\mu\text{A}/\text{cm}^2$, see Table 6.6. As seen from Table 6.6 and Figure 6.8 no effect of the polarisation current on the required polarisation time to obtain a corrosion current density, i_{corr} , of 0.03 $\mu\text{A}/\text{cm}^2$ was observed for polarisation times up till approximately 20 seconds. For longer polarisation times the difference between the corrosion current densities, i_{corr} , measured with the different polarisation currents increased with increasing polarisation time until approximately 100 seconds after which almost constant i_{corr} values were obtained, see Figure 6.8. From these results it seems that a polarisation time of 20 seconds and a polarisation current giving a potential response lower than approximately 80 mV (here 10 μA) should be used for practical measurements with the galvanostatic potential transient technique.

A huge effect of the polarisation time on the measured corrosion current density, i_{corr} , was also observed in the work by Luping (2002). In contrast to the present work Luping (2002) did not observe any effect of the polarisation current on the measured corrosion current density, i_{corr} , see Figure 6.9. The reason for the discrepancy is not known but could be related to the much higher corrosion current densities, i_{corr} , obtained in the work

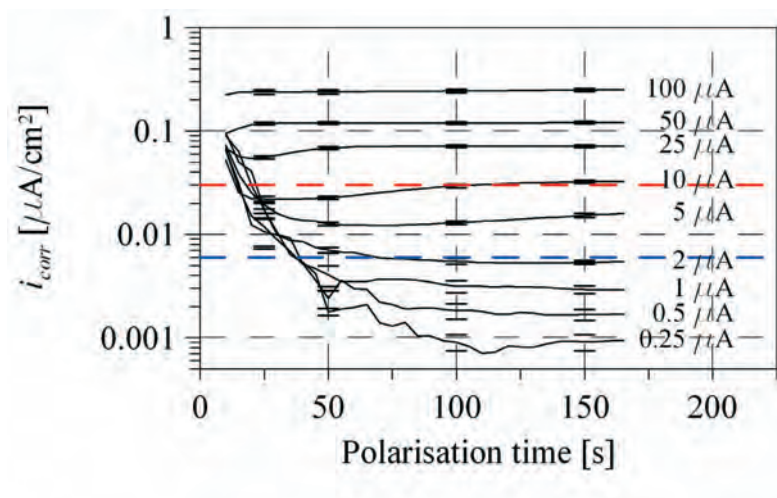


Figure 6.8 Galvanostatic potential transient technique: Mean corrosion current densities, i_{corr} , obtained with polarisation currents from 0.25 to 100 μA as a function of the polarisation time for the passive reinforcement bars exposed at 25 °C and 75 % relative humidity (from Figure 5.52). The red and blue punctuated lines indicate a corrosion current density, i_{corr} , of 0.03 and 0.006 $\mu\text{A}/\text{cm}^2$, respectively.

Table 6.4 The polarisation time, t , (to the nearest 5 seconds) required to obtain a corrosion current density, i_{corr} , of 0.03 $\mu\text{A}/\text{cm}^2$ with the galvanostatic linear polarisation resistance technique on the passive reinforcement bars (Figure 6.7.)

Polarisation current	Polarisation time	Mean potential shift
I_{CE} [μA]	t [sec]	ΔE [mV]
0.25	40	-7
0.5	55	-14
1	65	-29
2	75	-58
5	85	-140

Table 6.5 Mean corrosion current densities, i_{corr} , and potential shifts, ΔE , determined with the galvanostatic linear polarisation resistance technique on the passive reinforcement using a polarisation time 100 seconds.

Polarisation current I_{CE} [μA]	Mean corrosion current density i_{corr} [$\mu\text{A}/\text{cm}^2$]	Mean potential shift ΔE [mV]
0.25	0.012	-17
0.5	0.017	-27
1	0.020	-42
2	0.023	-75
5	0.027	-156

Table 6.6 The polarisation time, t , (to the nearest 5 seconds) required to obtain a corrosion current density, i_{corr} , of $0.03 \mu\text{A}/\text{cm}^2$ with the galvanostatic transient technique on the passive reinforcement bars (Figure 6.8.)

Polarisation current I_{CE} [μA]	Polarisation time t [sec]	Potential shift ΔE [mV]
0.25	25	-4
0.5	20	-5
1	15	-8
2	15	-14
5	20	-42
10	15	-64

by Luping (2002) (Figures 6.8 and 6.9).

When considering the effect of the polarisation current on the measured corrosion current density the work by Pruckner (2002) should also be mentioned. In his work the effect of the polarisation time and current on the corrosion current density, i_{corr} , measured with a GalvaPulse instrument (using current confinement) was investigated. The results from the measurements on laboratory specimens with passive and actively corroding reinforcement are shown in Figures 6.10 and 6.11, respectively. Pruckner (2002) also concluded that the measured corrosion current density depends on the polarisation current and time. These findings should however not be used without considering the effect of current confinement.

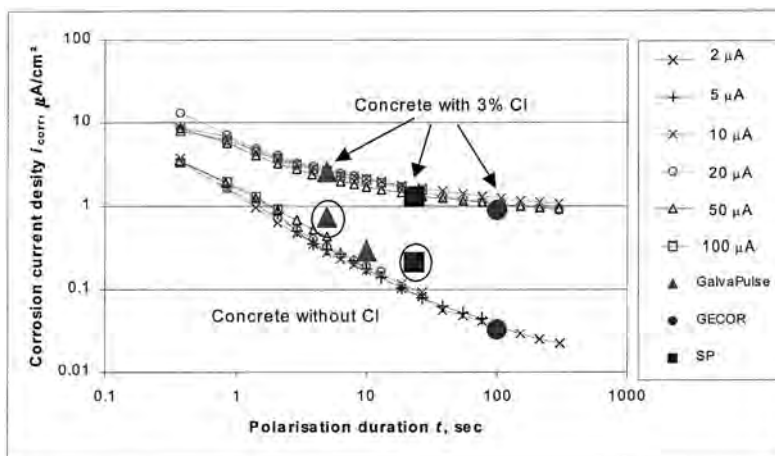


Figure 6.9 Corrosion current densities, i_{corr} , determined with the galvanostatic transient technique (curve-fitting) as a function of the polarisation duration for passive (without chloride) and actively corroding (with 3% chloride) steel in concrete (Luping, 2002).

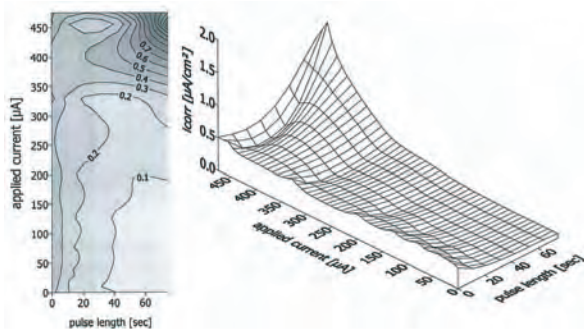


Figure 6.10 Corrosion current density, i_{corr} , measured with the GalvaPulse instrument on passive reinforcement, as a function of the polarisation time, t , and the applied current, I_{CE} (Pruckner, 2002).

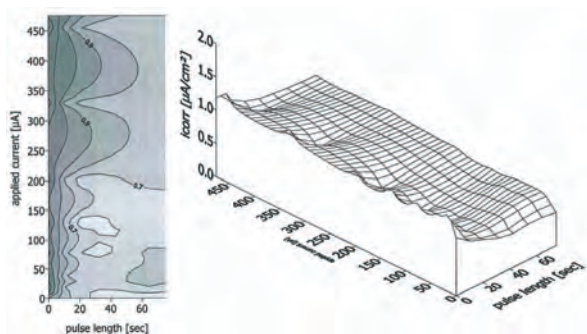


Figure 6.11 Corrosion current density, i_{corr} , measured with the GalvaPulse instrument on actively corroding reinforcement, as a function of the polarisation time, t , and the applied current, I_{CE} (Pruckner, 2002).

6.3.2 Actively corroding reinforcement

For assessment of the effect of the polarisation current and time at various corrosion rates results from three test specimens with reinforcement corroding at low, medium and high rates are used. As described in Section 5.2.2 the three tests specimens were selected from their mean corrosion current densities calculated from the potentiodynamic linear polarisation resistance measurements, see Figure 5.49.

Before going into the discussion it should be remembered that the R_P and i_{corr} values determined as a function of the polarisation time with the galvanostatic potential transient technique and the galvanostatic linear polarisation resistance technique are given as relative mean values, i.e. R_P/R_P^{ref} and i_{corr}/i_{corr}^{ref} . The reference values, R_P^{ref} and i_{corr}^{ref} were determined using the potentiodynamic linear polarisation resistance technique, see Section 5.2.2.

The data from the potentiodynamic linear polarisation resistance technique, used as reference technique, showed that the sweep rates used for the measurements on the actively corroding reinforcement had varied from 10.0 to 5.4 mV per minute. The lowest sweep rates were observed for the reinforcement bars with highest corrosion rate. For the three selected specimens (Specimens 1, 2 and 3, Table 5.5) mean sweep rates of 9.9, 6.3 and 5.4 mV per minutes had been used. As seen from Figure 3.7 lower sweep rates result in lower polarisation resistances, R_P , and hence higher corrosion current densities, i_{corr} , being measured. This is supported by Gonzalez et al. (2005) who, similarly to Millard et al. (1992), investigated the effect of the sweep rate on the measured polarisation resistance, R_P , for passive and actively corroding steel in mortar. The above indicates that the varying sweep rates only to a limited extent affected the relative polarisation resistances, R_P/R_P^{ref} , and corrosion current densities, i_{corr}/i_{corr}^{ref} , calculated from the R_P and i_{corr} values obtained with the two galvanostatic techniques for the three test specimens.

For all three test specimens a huge effect of the polarisation time on the R_P/R_P^{ref} and i_{corr}/i_{corr}^{ref} values was observed for both the galvanostatic potential transient technique and the galvanostatic linear polarisation resistance technique, see Figures 5.57 to 5.62. In contrast only a minor effect of the polarisation current on the R_P/R_P^{ref} and i_{corr}/i_{corr}^{ref} values was observed for the two galvanostatic techniques. With respect to the galvanostatic potential transient technique this is in good agreement with the results reported in the work by Pruckner (2002) and Luping (2002) shown in Figures 6.11 and 6.9, respectively. For the galvanostatic potential transient technique the effect of the polarisation time found in this study agree well with the results reported in the work by Millard et al. (1992) shown in Figure 3.6.

For both galvanostatic techniques slightly deviating results were observed for Specimen 1 (lowest corrosion rate) where the mean R_P/R_P^{ref} values for the measurements with 100 μA were approximately a factor of 2 lower (and the i_{corr}/i_{corr}^{ref} values higher) than the values obtained with polarisation currents from 5 to 50 μA , see Figures 5.57 and 5.60. The reason for this seems to be the potential overshooting (see Section 4.2.2) observed

for the potential transients measured with the polarisation current of $100 \mu\text{A}$, see Figure 5.54. The overshooting superimposes the first steep part of the charging curve making the vertical potential drop, E_Ω , appear larger and the transient potential response, ΔE , smaller, with the result of too high ohmic resistances, R_Ω , and too low polarisation resistances, R_P , being determined. No effect of the potential overshooting was observed on the measured R_P/R_P^{ref} and i_{corr}/i_{corr}^{ref} values for Specimens 2 and 3. This is probably due to the much more *flat* polarisation curves, being a result of the lower polarisation resistances, R_P , i.e. higher corrosion rates, see Figures 5.55 and 5.56.

Excluding the measurements on Specimen 1 affected by the potential overshooting ($100 \mu\text{A}$), no major differences between the relative polarisation resistances, R_P/R_P^{ref} , as well as corrosion current densities, i_{corr}/i_{corr}^{ref} , determined from the measurements with the galvanostatic linear polarisation resistance technique for Specimens 1, 2 and 3 were observed, see Figures 5.60 to 5.62. This also applied for the galvanostatic potential transient technique for Specimens 2 and 3, whereas a slightly lower effect of the polarisation time, i.e. lower increase in relative polarisation resistances, R_P/R_P^{ref} , with increasing polarisation time, was observed for Specimen 1, see Figures 5.55 to 5.56. This could be explained by the applied method of analysis (curve fitting) resulting in an apparent time dependent ohmic resistance, see Figure 5.56. Similar observations were not made for Specimens 2 and 3 where the determined ohmic resistances, R_Ω , were almost constant or only slightly increasing with increasing polarisation time, see Figures 5.55 and 5.56.

Thus, the results obtained by the galvanostatic linear polarisation resistance technique show that the effect of the polarisation time on the measured polarisation resistance, R_P , and hence corrosion current density, i_{corr} , is independent of the corrosion rate of the steel. Also, for the galvanostatic potential transient technique the effect of the polarisation time on the measured polarisation resistance changes only slightly with the corrosion rate. This means that the same polarisation time can be used for R_P measurements with both the galvanostatic techniques on actively corroding reinforcement irrespective of the corrosion rate. To the author's knowledge, no experimental results describing the effect of the polarisation time on the measured R_P values at varying corrosion rates have earlier been published for either of the two galvanostatic techniques.

For the galvanostatic linear polarisation resistance technique R_P and i_{corr} values comparable to those ($R_P/R_P^{ref} \approx 1$) obtained with the potentiodynamic linear polarisation resistance technique, i.e. the reference technique were obtained with polarisation times in the range from approximately 20 to 50 seconds, see Figures 5.60 to 5.62. As illustrated in Figure 6.12 this correlate well with the results obtained by Millard et al. (1992).

In general, with the galvanostatic potential transient technique R_P values higher than those obtained with the potentiodynamic linear polarisation resistance technique, i.e. the reference technique were obtained, see Figures 5.57 to 5.59. With a polarisation time of 10 seconds R_P/R_P^{ref} values of approximately 1.5 were obtained, i.e. the R_P values determined with the galvanostatic potential transient technique were approximately 50 % higher than those determined with the potentiodynamic linear polarisation resistance technique. To

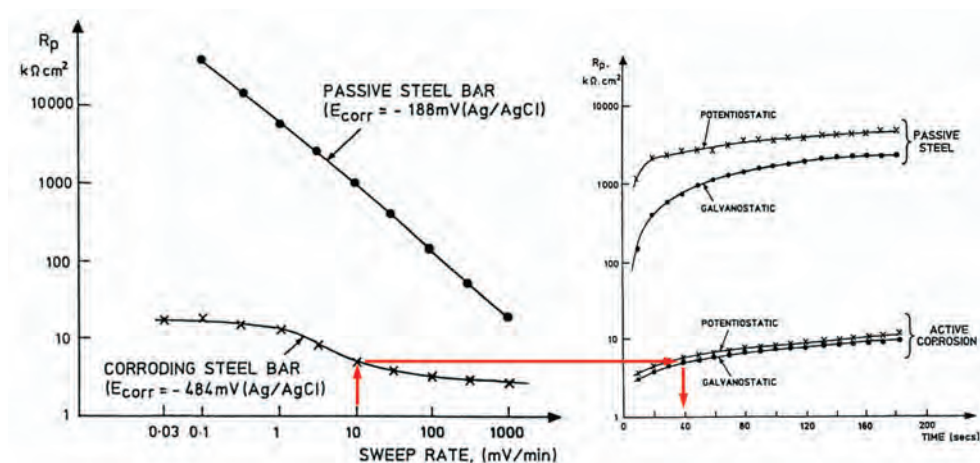


Figure 6.12 Polarisation resistance, R_P , as a function of the potential sweep rate when measured with the potentiodynamic polarisation resistance technique (left), and as a function of the polarisation time when measured with the galvanostatic linear polarisation resistance technique (right) for passive and actively corroding steel. As indicated with the red arrows comparable R_P values are obtained with a sweep rate of 10 mV per minute (left) and a polarisation time of approximately 40 seconds (right). After (Millard et al., 1992).

the author's knowledge no experimental results describing the correlation between R_P measurements with the (classic) potentiodynamic linear polarisation resistance technique and the galvanostatic potential transient technique have earlier been published.

As mentioned earlier, only a very limited effect of the polarisation current on the measured R_P values was observed for both galvanostatic techniques. However, the general scatter of the R_P/R_P^{ref} values determined as a function of time with both galvanostatic techniques increased with increasing corrosion rate, i.e. decreasing polarisation resistance, R_P , (Specimens 1 to 3), and decreasing polarisation current (5-100 μA), see Figures 5.57 to 5.62. This indicates that the scatter was correlated with the ratio between the obtained potential shift, ΔE , and the background noise, i.e. the signal-noise ratio. Therefore, in order to minimise the scatter and increase the accuracy, a polarisation current resulting in the highest potential shift within the linear current-potential region around the free corrosion potential, E_{corr} , should ideally be used. For actively corroding steel embedded in concrete the range of linearity of the current-potential curve is considered to be around 50 mV (Stern and Geary, 1957), (Andrade and Gonzalez, 1978). Hence, a target potential shift, ΔE , in the range from 40 to 50 mV (excluding potential drop) should be used for polarisation resistance measurements on actively corroding steel. However, with galvanostatic polarisation techniques, where the potential is the uncontrolled parameter this can only be obtained by repetitive measurements where the polarisation current is adjusted

until the target potential shift is obtained.

As for the analysis of the measured data, the large effect of the polarisation time on the corrosion current densities, i_{corr} , obtained with the galvanostatic potential transient technique basically show that the simple Randles circuit (Figure 3.4 and Equation 3.8) does not describe the potential response of a steel-concrete system accurately. As discussed in Section 3.2.2, this has been demonstrated earlier in a number of experimental studies (Videm and Myrdal, 1997), (Luping, 2002), (Feliu et al., 2005). In the work by Videm (1997) several series coupled parallel Resistor-Capacitor pairs (RC pairs) were used to describe the potential response as a function of the polarisation time. With an increasing polarisation time an increasing number of RC-pairs were found necessary, see Figure 3.15. As an alternative to the simple Randles circuit Luping (2002) suggested an exponential relationship for describing the potential response of a steel-concrete system. However this includes two constants without any physical meaning. Based on the obtained correlation between model and experimental data, what seems to be a promising approach is found in the work by Feliu et al. (2005) where an equivalent Randles circuit modified with a Constant Phase Element (CPE) and a Warburg diffusion element (Z_d) was proposed for describing the potential response of steel concrete systems, see Figures 3.18 and 3.19. The present documentation of the model does, however, not allow for comparison to other data. Also, it should still be remembered that corrosion current densities, i_{corr} , clearly indicating the passive or active state of the steel can be obtained assuming a simple Randles circuit as demonstrated in the present work.

6.4 Corrosion rate - effect of exposure

In the following the effect of relative humidity and temperature on the corrosion rate of passive and active generally corroding reinforcement is discussed. The discussion is based on the results obtained from the measurements with the potentiodynamic linear polarisation resistance technique on the passive (Series I) and active generally corroding (Series II) reinforcement bars in Experiment B (Table 4.1). The results are presented in Section 5.2.1.

6.4.1 Relative humidity

For the passive reinforcement no effect of the relative humidity on the free corrosion potentials, E_{corr} , was observed, see Figure 5.47. This shows that although the oxygen diffusion coefficient decreases with increasing moisture content the potential of the passive reinforcement bars were not affected by a restricted oxygen availability, i.e. concentration polarisation, see Figure 2.6. Hence, the factors controlling the corrosion process of the passive bars may have been a combination of activation and resistance polarisation (see Section 2.3). This is in agreement with results obtained by Tuutti (1982) showing that concentration polarisation due to lack of oxygen only becomes noticeable at relative humidities in excess of approximately 95 % on steel in concrete with w/c-ratios above approximately 0.5. No data were given for 'low' w/c-ratios.

On the actively corroding reinforcement with general corrosion, an effect of the relative humidity on the free corrosion potentials, E_{corr} , was observed, see Figure 5.47. In general the free corrosion potentials, E_{corr} , were seen to decrease, i.e. become more negative, with increasing relative humidity.

No correlation between the free corrosion potentials, E_{corr} , and the polarisation resistances, R_P , (and thus the corrosion current densities, i_{corr}) was observed, see Figures 5.47 and 5.49). This is in accordance with the theory and suggests that the corrosion rate was under resistance control, i.e. resistance polarisation, see Figure 6.14. Contrary to the observations in the present study, Glass et al. (1991) found an almost exponential correlation between the corrosion current density, i_{corr} , and the corrosion potential, E_{corr} , in an experimental study where mild steel probes were embedded in carbonated chloride containing mortar, see Figure 6.13. Glass et al. (1991) stated that the only explanation for the more negative corrosion potentials being associated with higher corrosion rates was a decrease in anodic polarisation, see Figure 6.14. From this Glass et al. (1991) suggested, in conflict with earlier work by among others Arup (1983), Alonso et al. (1988) and Tuutti (1982) that the corrosion rate is under anodic control rather than resistance control. The different observations indicate that one or more of the polarisation types (activation, resistance and/or concentration) will act depending on the steel-concrete system, i.e. the concrete resistivity, moisture content, chloride content, steel composition, etc.

From the polarisation resistances, R_P , (and corrosion current densities, i_{corr}) obtained from the actively corroding bars with general corrosion a clear and systematic effect of the relative humidity was observed at 25 and 35 °C, whereas no effect of the relative

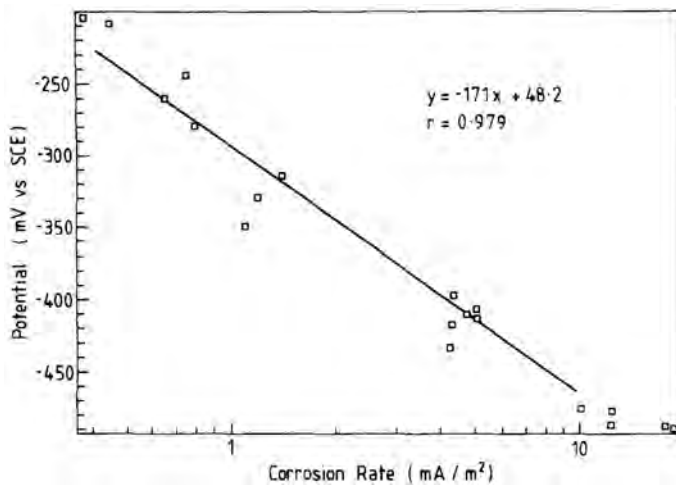


Figure 6.13 The relationship between corrosion potential and corrosion rate obtained by Glass et al. (1991) from polarisation resistance probes (mild steel) embedded in carbonated mortar containing 0.4 % chloride by mass of mortar.

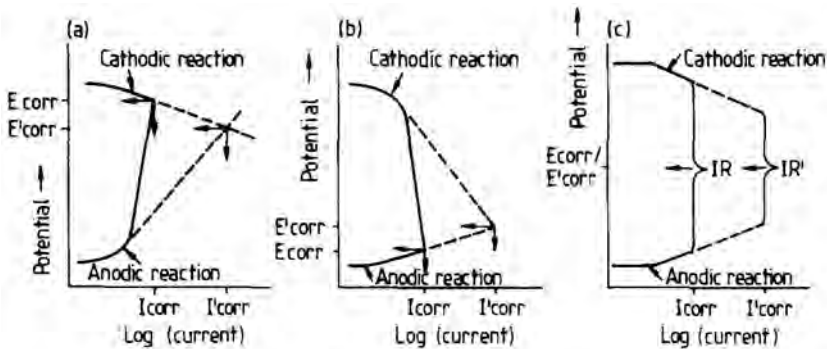


Figure 6.14 Evans diagram showing the increase in corrosion rate from i_{corr} to i'_{corr} and the corresponding changes in the corrosion potential from E_{corr} to E'_{corr} resulting from (a) a process under anodic control and subject to decreased anodic polarisation, (b) a process under cathodic control and subject to decreased cathodic polarisation and (c) a process under resistance control and subject to a fall in resistance (Glass et al., 1991).

humidity - and temperature - was observed in the temperature range from 1 to 15 °C, see Figures 5.48 and 5.49. At the lower temperatures corrosion current densities, i_{corr} , in the range from 0.8 to 1.2 $\mu\text{A}/\text{cm}^2$ were obtained.

The most likely explanation for the constant corrosion rates is that the corrosion rate of the active bars was under a combination of resistance and anodic control as suggested earlier. This means that the constant corrosion current densities, i_{corr} , obtained in the temperature range from 1 to 15 °C could be considered as a *lower bound* for the corrosion rate for the specimens with admixed chloride. A *lower bound* for the corrosion rate of approximately 1 $\mu\text{A}/\text{cm}^2$ was also observed by Tuutti (1982) (see Figure 6.15) as well as by Glass et al. (1991), who studied carbonated specimens with a chloride content of 1 % by mass of cement.

In the study by Tuutti (1982) the effect of the relative humidity on the corrosion rate was investigated for both carbonation and chloride initiated reinforcement corrosion, see Figure 6.15. All experiments were made at a constant temperature of 20 °C and the corrosion rates were determined from gravimetric measurements. Comparing the results obtained by Tuutti (1982) for chloride initiated corrosion with the results obtained in the present work for the actively corroding reinforcement bars with general corrosion exposed to 25 °C good correlation was observed, see Figures 6.15 and 5.49: Slightly higher corrosion current densities, i_{corr} , were obtained for the actively corroding reinforcement bars exposed to 25 °C in this work reflecting the 5 °C higher exposure temperature and the slightly higher chloride content of the specimens: For the specimens in this work 4 % chloride by mass of cement was added to the concrete, whereas Tuutti (1982) used 5 % calcium chloride by mass of cement, corresponding to 3.2 % chloride by mass of cement.

6.4.2 Temperature

In the following, the results obtained for the actively corroding reinforcement bars with general corrosion (Series II) are discussed. For the passive reinforcement no effect of the temperature on the free corrosion potentials, E_{corr} , and corrosion current densities, i_{corr} , was observed, see Figures 5.47 and 5.49. For the actively corroding reinforcement bars no systematic effect of the temperature on the free corrosion potentials, E_{corr} , was observed, see Figure 5.47. In contrast a clear effect of the temperature on the corrosion current densities, i_{corr} , was observed: In the temperature range from 1 to 15 °C the corrosion current densities, i_{corr} , were in the range from 0.8 to 1.2 $\mu\text{A}/\text{cm}^2$, see Figure 5.49. Above 15 °C the corrosion current densities, i_{corr} , increased with increasing temperature - and increasing relative humidity. Except for the reinforcement bars exposed to 85 % relative humidity where a slight deviation was observed; the corrosion current density at 35 °C was lower than that at 25 °C.

As described in Section 2.3.4 the Arrhenius Equation (Equation 2.21) has in many studies been found suitable for describing the effect of the temperature on the corrosion current density, i_{corr} , for actively corroding steel in concrete, see e.g. Raupach (1997a), Bertolini

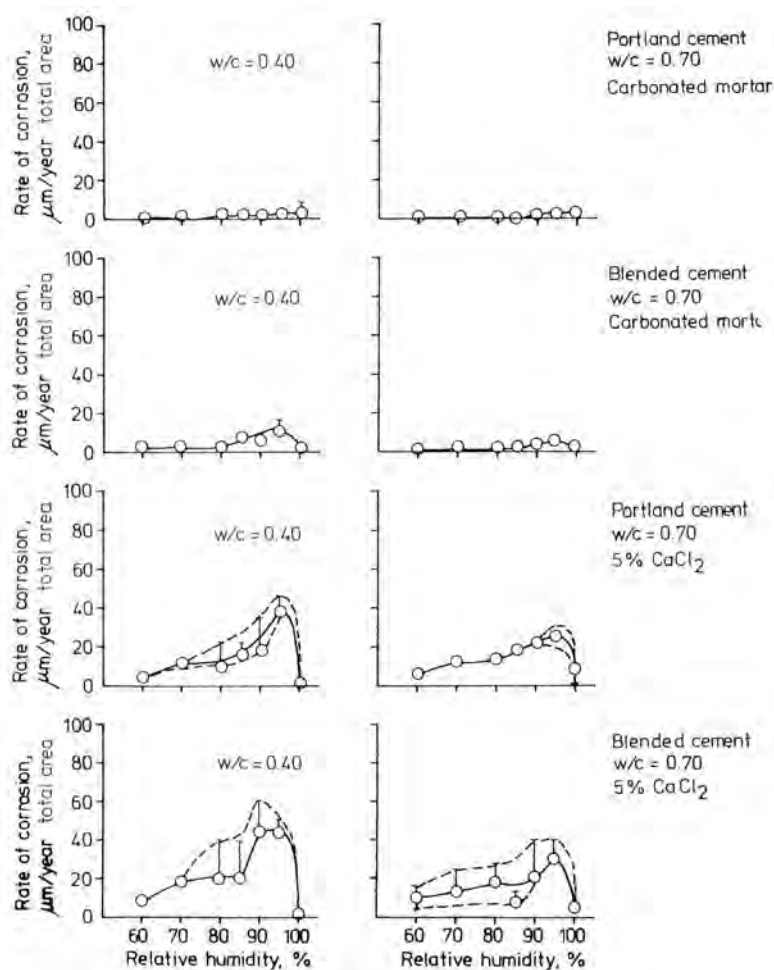


Figure 6.15 Measured rate of corrosion ($1 \mu\text{A}/\text{cm}^2 \approx 11.6 \mu\text{m}/\text{year}$) as a function of the relative humidity for carbonation and chloride initiated corrosion (Tuutti, 1982).

and Polder (1997), Jäggi et al. (2005) and the literature cited herein. Data from Jäggi et al. (2005) showing the effect of the temperature on the corrosion rate in the temperature range from -20 to +50 °C are given in Figure 2.13.

In conflict with the studies mentioned above, the Arrhenius equation did not describe the temperature dependency of the corrosion current density, i_{corr} , of the actively corroding reinforcement bars in the present study. The reason for the discrepancies may be related to the methodology used for determining the effect of the temperature: In all the studies where the Arrhenius equation has been found suitable for describing the effect of the temperature on the corrosion current density, i_{corr} , it appears that the same methodology has been used for the experiments: In the studies by Raupach (1997a), Bertolini and Polder (1997) and Jäggi et al. (2005) the effect of the temperature has been investigated by subjecting a test specimen to a number of different temperature steps, while measuring the corrosion current density, i_{corr} , of the embedded actively corroding steel. Depending on the duration of each temperature step such measurements will to a large extent only reflect the *short-term effect* of the temperature on the corrosion current density. The corrosion rate changes during the propagation phase, although the environment around the steel is constant (Tuutti, 1982). This is because the corrosion products are impermeable and form diffusion barriers, which lead to a reduction in the corrosion rate with time, see Figure 6.16. However, the initial corrosion products are exposed to stresses when new products are formed and consequently crack. As a result the diffusion barrier is damaged, and it may be assumed that the corrosion rate is practically constant after a few years (Tuutti, 1982). In this study where measurements were made on a number of identical test specimens exposed to different but constant environments over a period of two years, an estimate for the *long-term effect* of the temperature - and relative humidity - on the corrosion rate has been obtained.

The practically constant corrosion current densities obtained after years of exposure under constant conditions may be considered to represent the *long-term effect* of the exposure conditions, deviating from the *short-term effect*.

Cracks in the concrete cover were only observed on the two test specimens with active generally corroding reinforcement (Series II) exposed to 25 °C and 85 % relative humidity and to 35 °C and 96 % relative humidity. Crack widths up to 0.5 mm were observed on the test specimen exposed to 25 °C and 85 % relative humidity, where a mean corrosion current density, i_{corr} , of 3.9 $\mu\text{A}/\text{cm}^2$ was measured, see Figure 6.17. The test specimen exposed to 35 °C and 96 % relative humidity with a mean i_{corr} value of 7.2 $\mu\text{A}/\text{cm}^2$ had crack widths larger than 10 mm and the concrete on the surface had started to spall, see Figure 6.18. These observations are interesting as it shows that reinforcement corroding with a corrosion current density, i_{corr} , of approximately 4 $\mu\text{A}/\text{cm}^2$ may cause cracking and spalling after less than 2 years at atmospheric exposure. It should be mentioned that the corrosion rate measurements presented in the present work were performed prior to the severe cracking on the two test specimens. The photos of the test specimens shown in Figures 6.17 and 6.18 were taken after the test period had ended.

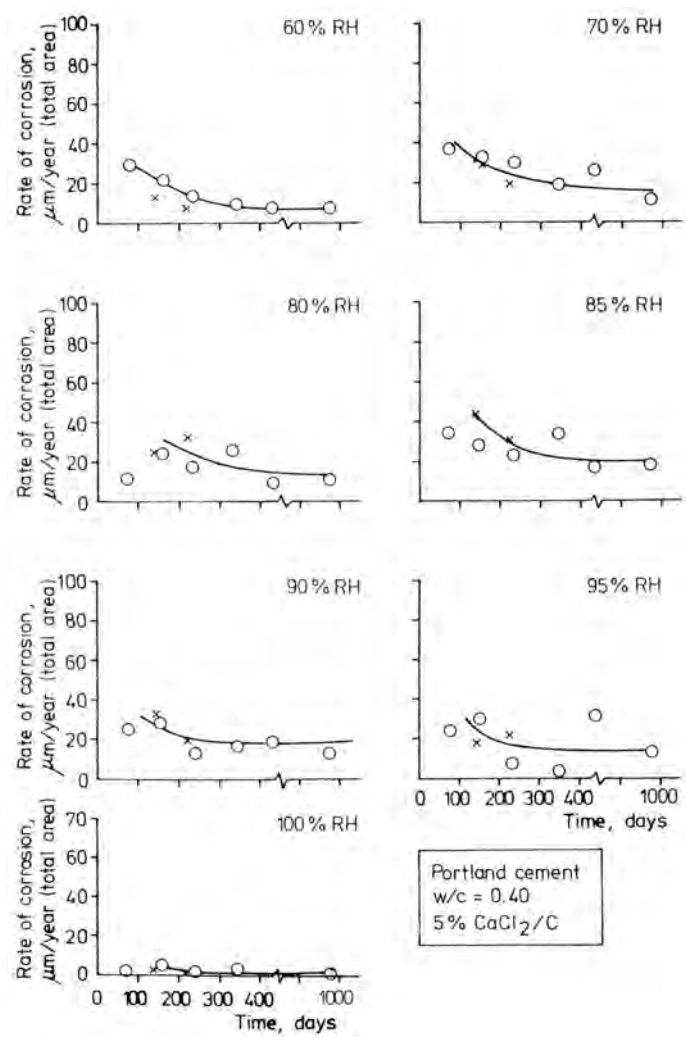


Figure 6.16 Measured rate of corrosion ($1 \mu\text{A}/\text{cm}^2 \approx 11.6 \mu\text{m}/\text{year}$) as a function of the time for different relative humidities (Tuutti, 1982).

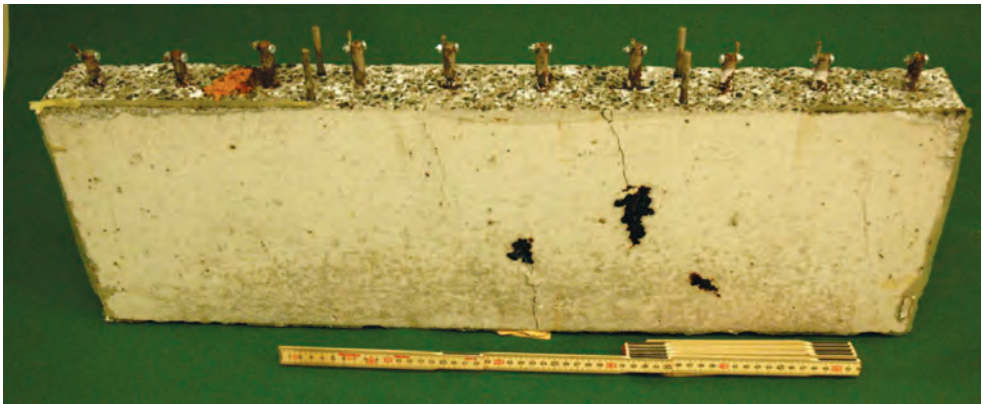


Figure 6.17 Test specimen with active generally corroding reinforcement exposed at 25°C and 85 % relative humidity for approximately 2 years. Cracks with a width of up to approximately 0.5 mm were observed on the surface together with corrosion products.

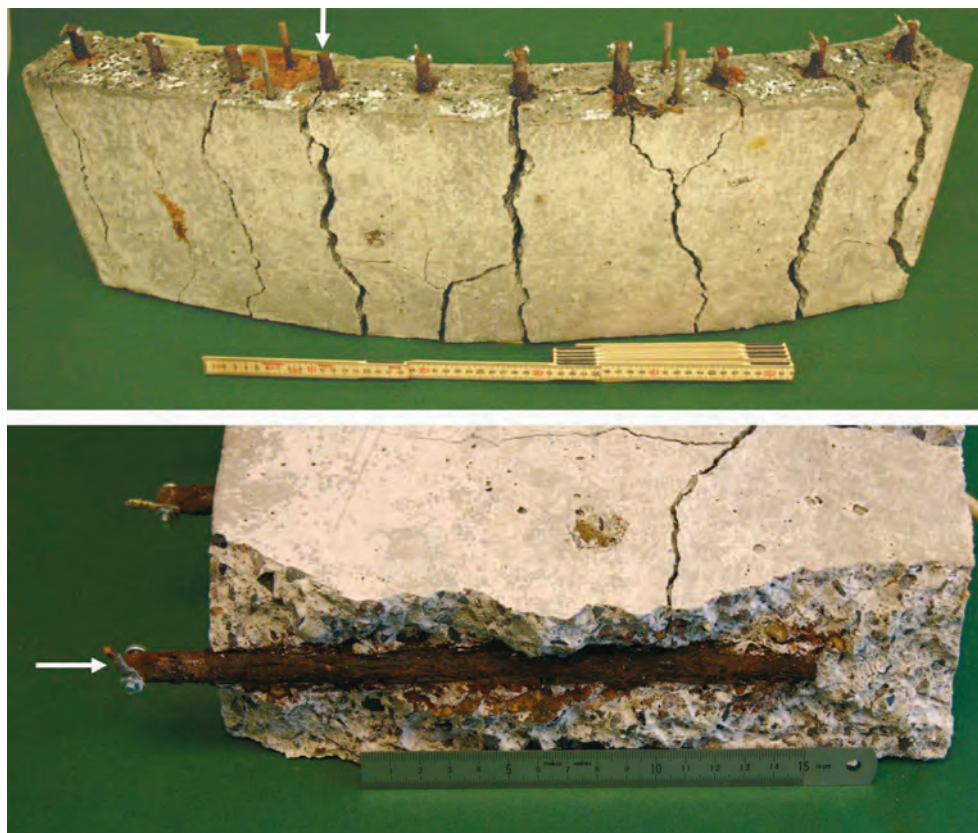


Figure 6.18 Test specimen with active generally corroding reinforcement exposed at 35 °C and 96 % relative humidity for approximately 2 years. The expansive corrosion products have bent the specimen due to the reinforcing properties of the mmo-titanium mesh positioned below the surface on the rear side of the specimen. The white arrow on the top figure indicates the position of the exposed bar shown in the bottom figure.

Chapter 7

Conclusion

The purpose of the present study was to provide background information for future development of instruments for on-site corrosion rate measurements and assessment of reinforced concrete structures. The functionality and efficiency of various current confinement techniques and the effect of the electrochemical techniques and the polarisation time and current on the measured polarisation resistance were investigated. Based on this, the performance of the GECOR 6 and GalvaPulse instruments were evaluated. Also, the effect of temperature and relative humidity on the corrosion rate of actively corroding steel in concrete was investigated.

Based on the investigations in the present thesis the following conclusions can be drawn:

Effect of confinement techniques

On passive reinforcement neither of the instrument, i.e. GECOR 6 and GalvaPulse were able to effectively confine (or compensate) for the lateral spread-out of the counter-electrode current. As a result, both instruments overestimated the corrosion rate of the passive steel. During measurements on passive reinforcement, the GECOR 6 increased the guard ring current steadily with a rate depending on the polarisation resistance, R_P , of the embedded steel and the concrete cover thickness. The increasing guard ring current resulted in a constantly decreasing potential response with no signs of steady state, bringing into question the use of the galvanostatic linear polarisation resistance technique relying on a steady-state potential response. Also, both instruments polarised the passive reinforcement far beyond the linear potential-current region around the free corrosion potential, E_{corr} , bringing into question the whole basis of the measurements.

For reinforcement with one or several actively corroding areas on an otherwise passive reinforcement bar, it was found that neither of the instruments could locate the actively corroding areas due to *self-confinement* of the active areas. In the presence of a single small area with a high corrosion rate, both instruments underestimated the corrosion rate. This is a critical issue as the presence of such localised and rapidly corroding spots, leading to rapid cross section reduction, will not be detected. The underestimation was due to a combination of the constant confinement length, here considerably bigger than the

actively corroding area, and the obtained confinement. With increasing size of the corroding area(s) and increasing corrosion rate, the measured corrosion rates, and especially those measured with the GalvaPulse, were found to approximate the actual corrosion rate.

It should be kept in mind that, although a good correlation between the corrosion rate measured with a commercial instrument using current confinement and the actual corrosion rate is obtained, this is not necessarily a result of the instrument being able to confine the applied counter-electrode current. This questions the use of comparative measurements, i.e. electrochemical versus gravimetric, for evaluation of confinement systems as suggested in e.g. a recent RILEM Recommendation (Andrade et al., 2004).

To accommodate this, a method for quantitative assessment of confinement techniques based on monitoring the operation of the instrument and the current distribution between the electrode assembly on the concrete surface and a segmented reinforcement bar embedded in the concrete was developed as part of the present work. The applicability of the method was demonstrated using two commercially available corrosion rate instruments based on different confinement techniques and different electrochemical techniques: the GECOR 6 and the GalvaPulse.

The use of unconfined corrosion rate measurement was also investigated. For these it was found that distinction between passive and actively corroding steel with a low corrosion rate or small corroding areas is almost impossible. This is due to the overestimation of the corrosion rate of passive steel caused by the lateral current flow from the counter-electrode. Similar to the confined corrosion rate measurements (GECOR 6 and GalvaPulse) it was found that the accuracy of the unconfined measurements increased with increased corroding area and corrosion rate. From this study it was also demonstrated that the actual corrosion rate of actively corroding reinforcement cannot be determined based on unconfined measurements and observations of the corroded area due to the overlapping response of the surrounding passive steel into which a portion of the applied polarisation current flows.

The conclusions regarding current confinement are based on investigations on concrete slabs with cover thickness of 30 and 75 mm representing most chloride exposed structures. However, the concrete had a relatively high w/c-ratio (0.5) and therefore a relatively low electrical resistivity, facilitating the distribution of current and thus proving a conservative assessment of the efficiency of the confinement techniques. For modern concretes with lower w/c-ratios and supplementary cementitious materials, which have higher resistivity, improved efficiency of the current confinement techniques may be expected.

Effect of measurement technique and procedure

In addition to the effect of the confinement techniques, the effect of the polarisation time and current on the measured polarisation resistance, R_P , and thus the corrosion current density, i_{corr} , was investigated. Two electrochemical techniques were considered in the study; the galvanostatic linear polarisation resistance technique and the galvano-

static potential transient technique used in the GECOR 6 and GalvaPulse instruments, respectively. On passive reinforcement the measured polarisation resistance, R_P , was for both electrochemical techniques found to be highly affected by the polarisation time and current and no plateau at either short or long polarisation times or high or low currents were identified. However, it was shown that a qualitative estimate clearly showing the passive state of the reinforcement can be obtained even though stationary conditions are not achieved and the obtained potential response is outside the linear current-potential range around the free corrosion potential.

For practical measurements, a polarisation time of 100 seconds was found to be appropriate when using the galvanostatic linear polarisation resistance technique, whereas a polarisation time of 20 seconds was found appropriate for the galvanostatic potential transient technique. With these polarisation times corrosion current densities, i_{corr} , clearly indicating passivity ($i_{corr} < 0.03 \mu A/cm^2$) were obtained with potential shifts (excluding ohmic potential drop) as high as 150 mV for the galvanostatic linear polarisation resistance technique and 80 mV for the galvanostatic potential transient technique.

On actively corroding reinforcement a large effect of the polarisation time on the measured polarisation resistance, R_P , was found for both electrochemical techniques. In contrast only a minor effect of the polarisation current was observed. For the galvanostatic linear polarisation resistance technique it was shown that the effect of the polarisation time on the measured polarisation resistance, R_P , and hence corrosion current density, i_{corr} , is independent of the corrosion rate of the steel. Also, for the galvanostatic potential transient technique the effect of the polarisation time on the measured polarisation resistance, R_P , changes only slightly with the corrosion rate. This means that the same polarisation time can be used for R_P measurements with both the galvanostatic linear polarisation resistance technique and the galvanostatic potential transient technique on actively corroding reinforcement irrespective of the corrosion rate.

Similar polarisation resistances, R_P , were obtained with the galvanostatic and potentiodynamic linear polarisation resistance techniques when polarisation times from 20 to 50 seconds and sweep rates from 5 to 10 mV per minute were used. But higher polarisation resistances, R_P , were in general measured with the galvanostatic potential transient technique: With a polarisation time of only 10 seconds R_P values approximately 50 % higher were obtained with the galvanostatic potential transient technique than with the potentiodynamic linear polarisation resistance technique when using a sweep rate in the range of 5 to 10 mV per minute. For both the galvanostatic linear polarisation resistance technique and the galvanostatic potential transient technique it was found that a polarisation current resulting in the highest potential response within the linear current-potential range around the free corrosion potential, E_{corr} , i.e. 40 to 50 mV (excluding ohmic potential drop) should be used, in order to maximise the signal-noise ratio and thus increase the accuracy.

Effect of exposure

In contrast to a number of short term studies the Arrhenius equation was found inadequate for describing the temperature dependency of the corrosion rate in this study. Here measurements were made after approximately two years of constant exposure and a combined effect of temperature and time is expected to influence the corrosion rate.

Based on repetitive measurements on reinforcement bars in chloride contaminated concrete a constant corrosion current density, i_{corr} , of approximately $1 \mu A/cm^2$ was found in the temperature range from 1 to 15 °C with relative humidities from 75 to 96 %. Above 15 °C the corrosion current density increased with increasing temperature and relative humidity, as expected.

Chapter 8

Recommendations for further work

The present research project has contributed to the understanding of corrosion rate measurements on steel reinforcement in concrete and the effect of exposure on the corrosion rate of steel in concrete. During the project a number of questions that calls for further clarification were identified.

Effect of confinement techniques

In the present project, the performance of two commercially available corrosion rate instruments was investigated and the variations in measured corrosion rates explained from measurements on slabs with segmented reinforcement bars prepared from concrete with and without admixed chloride. The cover thickness varied from 30 to 75 mm representing most chloride exposed structures. However, the concrete had a relatively high w/c-ratio (0.5) and therefore a relatively low electrical resistivity, facilitating the distribution of current and thus proving a conservative assessment of the efficiency of the confinement techniques. The limited efficiency of the confinement techniques may be less pronounced in modern concretes with lower w/c-ratios and supplementary cementitious materials, which have higher resistivity. Using the same approach the performance of the instruments should be investigated in case of higher resistivity than in the present study.

A standard test method based on the use of segmented reinforcement bars should be developed as an alternative to the test method for evaluating confinement techniques suggested in a recent RILEM Recommendation relying on comparative measurements, i.e. electrochemical and gravimetric (Andrade et al., 2004).

Effect of measuring technique and procedure

Assuming the Randles circuit modified with a Constant Phase Element and a Warburg diffusion element as proposed by Feliu et al. (2005) to describe the time dependent potential response, E_t , of steel-concrete systems accurate (and thus the polarisation resistance, R_P , being independent of the polarisation time) an algorithm applicable in hand-held instruments for analysis of potential transients should be established.

Additionally the applicability of the modified Randles circuit should be documented.

Effect of temperature and relative humidity

In contrast to short-term studies, the Arrhenius equation was in the present study found inadequate for describing the long-term effect of temperature on the corrosion rate of steel in concrete as the corrosion rate changes over time despite a constant exposure. It is proposed to determine the short-term effect of temperature (the activation energy) at different stages of the corrosion process as well as the reversibility of the kinetics of the corrosion process. A long-term study with constant reference exposure and relatively short intermediate periods with varying exposure (returning to the reference exposure) should be conducted. Polarisation resistance measurements should be performed at short time intervals during the entire exposure period.

Bibliography

- Alekseev, S. N. (1993). Corrosion of steel reinforcement. In Mallick, S. K., editor, *Durability of reinforced concrete in aggressive media*, pages 305–349. A.A. Balkema/Rotterdam/Brookfield. Russian Translation Series 96.
- Alonso, C., Andrade, C., and Gonzalez, J. (1988). Relation between resistivity and corrosion rate of reinforcements in carbonated mortar made with several cement types. *Cement and Concrete Research*, 8(5):687–698.
- Andrade, C. (1973). *New electrochemical technique for the corrosion measurement in reinforced and prestressed concretes*. PhD thesis, University of Madrid.
- Andrade, C. and Alonso, C. (1995). Corrosion rate monitoring in the laboratory and on-site. *Construction and Building Materials*, 10(5):315–328.
- Andrade, C., Alonso, C., Gulikers, J., Polder, R., Cigna, R., Vennesland, Ø., Salta, M., Raharinaivo, R., and Elsener, B. (2004). Test methods for on-site corrosion rate measurement of steel reinforcement in concrete by means of the polarization resistance method. *Materials and Structures*, 37:623–643.
- Andrade, C., Alonso, C., and Sarria, J. (2002). Corrosion rate evolution in concrete structures exposed to the atmosphere. *Cement and Concrete Composites*, 24:55–64.
- Andrade, C., Castelo, V., Alonso, C., and Gonzalez, J. A. (1984). The determination of the corrosion rate of steel embedded in concrete by the polarization resistance and ac impedance methods. In Chaker, V., editor, *Corrosion effect of stray currents and the techniques for evaluating corrosion of rebars in concrete*, STP 906. ASTM International.
- Andrade, C. and Castillo, A. (2003). Evolution of reinforcement corrosion due to climatic variations. *Materials and Corrosion*, 54:379–386.
- Andrade, C. and Gonzalez, J. A. (1978). Quantitative measurements of corrosion rate of reinforcing steels embedded in concrete using polarization resistance measurements. *Werkstoffe und Korrosion*, 29(8):515–519.
- Andrade, C., Keddad, M., Nóvoa, X. R., Pérez, M. C., Rangel, C. M., and Takenouti, H. (2001). Electrochemical behaviour of steel rebars in concrete: influence of environmental factors and cement chemistry. *Electrochemical Acta*, 46:3905–3912.

- Andrade, C. and Martinez, I. (2005). Calibration by gravimetric losses of electrochemical corrosion rate measurement using modulated confinement of current. *Materials and Structures*, 38:833–841.
- APM 219 (1996). Concrete testing - hardened concrete, electrical resistivity. *AEC laboratory, Denmark*.
- APM 506 (1993). Prøvning af tilslagsmaterialer - bestemmelse af egenpakningsgrad. *AEC laboratory, Denmark*. In Danish.
- Arup, H. (1967). *Metallernes Korrosion*. Akademisk Forlag. In Danish.
- Arup, H. (1983). The mechanisms of protection of steel by concrete. In Crane, A. P., editor, *Corrosion of Reinforcement in Concrete Construction*, pages 151–157. Society of chemical industry, Ellis Horwood Limited.
- Arup, H. (1985). Electrochemical monitoring of the corrosion state of steel in concrete. In *First International Conference on Deterioration & Repair of Reinforced Concrete in the Arabian Gulf*.
- Arya, C. and Vassie, P. R. W. (1995). Influence of cathode-to-anode area ratio and separation distance on galvanic corrosion currents of steel in concrete containing chlorides. *Cement and Concrete Research*, 25(5):989–998.
- ASTM C 876-77 (1977). Standard test method for half-cell potentials of uncoated reinforced steel in concrete. *ASTM International*.
- ASTM E415-99a (2005). Standard test method for optical emission vacuum spectrometric analysis of carbon and low-alloy steel. *ASTM International*.
- ASTM G 1-90 (1990). Standard practice for preparing, cleaning and evaluating corrosion test specimens. *ASTM International*.
- Baccay, M. A., Otsuki, N., Nishida, T., and Maruyama, S. (2006). Influence of cement type and temperature on the rate of corrosion of steel in concrete exposed to carbonation. *Corrosion*, 62(9):811–821.
- Bardal, E. (1994). *Korrosjon og korrosjonsvern*. Tapir Akademisk Forlag, 2 edition. In Norwegian.
- Bässler, R., Burkert, A., Frølund, T., and Klinghoffer, O. (2007). Use of portable equipment to determine the corrosion rate of concrete structures. In Raupach, M., Elsener, B., Polder, R., and Mietz, J., editors, *Corrosion of reinforcement in concrete, Mechanisms, monitoring, inhibitors and rehabilitation techniques*. Woodhead Publishing.
- Bažant, Z. P. (1978). Physical model for corrosion of steel in concrete. Technical report, CBI.
- Bertolini, L., Bolzoni, F., Pastore, T., and Pedferri, P. (1996). Behaviour of stainless steel in simulated concrete pore solution. *British Corrosion Journal*, 31(3):218–222.

- Bertolini, L. and Polder, R. (1997). Concrete Resistivity and Reinforcement Corrosion Rate as a Function of Temperature and Humidity of the Environment, TNO report-97-bt-R 0574. Technical report, TNO Building and Construction Research.
- Bonhoeffer, K. and Jena, W. (1951). *Zeitschrift fr Elektrochemie*, 59.
- Brem, M. (2004). *Numerische Modellierung der Korrosion an Stahlbetonbauten*. PhD thesis, ETH Zürich. In German.
- Britz, D. and Brocke, W. A. (1975). Elimination of ir-drop in electrochemical cells by the use of a current-interruption potentiostat. *Electroanalytical Chemistry and Interfacial Electrochemistry*, 58:301–311.
- Broomfield, J. P. (1997a). *Corosion of Steel in Concrete*. E & FN Spon.
- Broomfield, J. P. (1997b). Rebar corrosion - what do we know for sure? In Blankvoll, A., editor, *Repair of concrete structures, From theory to practice in a marine environment*.
- Butler, J. A. V. and Armstrong, G. (1934). Electrolytic properties of hydrogen. *Journal of the Chemical Society*, pages 743–750.
- Chao, C. Y., Lin, L. F., and Macdonald, D. D. (1981). A point defect model for anodic passive films - ii. chemical breakdown and pit initiation. *Electrochemical Society*, 128(6):1194–1198.
- Clear, K. C. (1989). Measuring rate of corrosion of steel in field concrete structures. Technical report, Transportation Research Record 1211.
- DS 2426 (2004). Concrete - materials - rules for application of EN 206-1 in denmark. Technical report, Danish Standards Association.
- DS/EN 1097-6 (2000). Tests for mechanical and physical properties of aggregates - part 7: Determination of the particle density and water absorption. *European Committee for Standardization*.
- DS/EN 12350-2 (2002). Testing fresh concrete - part 2: Slump test. *European Committee for Standardization*.
- DS/EN 12350-6 (2002). Testing fresh concrete - part 2: Density. *European Committee for Standardization*.
- DS/EN 12350-7 (2002). Testing fresh concrete - part 2: Air content - pressure methods. *European Committee for Standardization*.
- DS/EN 12390-3 (2002). Testing hardened concrete - part 3: Compressive strength of test specimens. *European Committee for Standardization*.
- DS/EN 12390-7 (2002). Testing hardened concrete - part 3: Density of hardened concrete. *European Committee for Standardization*.

- DS/EN 933-1 (1997). Tests for geometrical properties of aggregates - part 1: Determination of particle size distribution - sieving method. *European Committee for Standardization*.
- Elsener, B. (1995). Corrosion rate of reinforced concrete structures determined by electrochemical methods. *Materials Science Forum*, 192-194:857–866.
- Elsener, B. (1998). Corrosion rate of steel in concrete - from laboratory to reinforced concrete structures. In Mietz, J., Elsener, B., and Polder, R., editors, *Corrosion of Reinforcement in Concrete - Monitoring, Prevention and Rehabilitation*, EFC Publication No. 25, pages 92–103. Woodhead Publishing.
- Elsener, B. (2005). Corrosion rate of steel in concrete - measurements beyond the tafel law. *Corrosion Science*, 47:3019–3033.
- Elsener, B., Andrade, C., Gulikers, J., Polder, R., and Raupach, M. (2003). Half-cell potential measurements - potential mapping on reinforced concrete structures. *Materials and Structures*, 36:461–471.
- Elsener, B. and Böhni, H. (1982). Untersuchungen zum aktiv/passiv-übergang von nichtrostenden chromnickelstählen in organisch wässrigen medien. *Werkstoffe und Korrosion*, 33:207–212. In German.
- Elsener, B. and Böhni, H. (1983). Computer-assisted d.c. and a.c techniques in electrochemical investigations of the active-passive transition. *Corrosion Science*, 23(4):341–352.
- Elsener, B. and Böhni, H. (1990). Potential mapping and corrosion of steel in concrete. In Berke, N., Chaker, V., and Whiting, D., editors, *Corrosion rates of steel in concrete*, STP 1065. ASTM International.
- Elsener, B., Flükiger, D., Wojtas, H., and Böhni, H. (1996a). Methoden zur erfassung der korrosion von stahl in beton. Technical report, Eidengenössisches Verkehrs- und Energiewirtschaftsdepartement, Bundesamt für Strassenbau, Zürich. In German.
- Elsener, B., Hug, A., Burchler, D., and Böhni, H. (1996b). Evaluation of localized corrosion rate on steel in concrete by galvanostatic pulse technique. In Page, C. L., Bamforth, P. B., and Figg, J. W., editors, *Corrosion of Reinforcement in Concrete Construction*. Royal Society of Chemistry SCI.
- Elsener, B., Klinghoffer, O., Frølund, T., Rislund, E., Schiegg, Y., and Böhni, H. (1997). Assessment of reinforcement corrosion by means of galvanostatic pulse technique. In Blankvoll, A., editor, *Proceedings of International Conference on Repair of Concrete Structures-From Theory to Practice in a Marine Environment*, pages 391–400, Svovlvær, Norway.
- Enevoldsen, J. N., Hansson, C. M., and Hope, B. B. (1994). The influence of internal relative humidity on the rate of corrosion of steel embedded in concrete and mortar. *Cement and concrete research*, 24(7):1373–1382.

- Escalante, E. and Ito, S. (1990). Measuring the rate of corrosion of steel in concrete. In Berke, N. S., Chaker, V., and Whittings, D., editors, *Corrosion Rates of Steel in Concrete, ASTM STP 1065*. ASTM International.
- Escalante, E., Ito, S., and Cohen, M. (1980). Measuring the corrosion rate of reinforcing steel in concrete. Technical report, National Bureau of standards.
- Feliu, S., Gonzalez, J. A., and Andrade, C. (1996). Electrochemical methods for on-site determination of corrosion rates of rebars. In Berke, N. S., Escalante, E., Nmai, C. K., and Whiting, D., editors, *Techniques to assess the corrosion activity of steel reinforced concrete structures, ASTM STP 1276*. ASTM International.
- Feliu, S., Gonzalez, J. A., Andrade, C., and Feliu, V. (1988). On-site determination of the polarization resistance in a reinforced concrete beam. *Corrosion Engineering*, 44(10):761–765.
- Feliu, S., Gonzalez, J. A., Andrade, M. C., and Feliu, V. (1987). On-site determination of the polarization resistance in a reinforced concrete beam, paper no. 145. In *Corrosion 87 - The NACE Annual Conference and Corrosion Show*.
- Feliu, S., Gonzalez, J. A., Andrade, M. C., and Feliu, V. (1989a). Determining polarisation resistance in reinforced concrete slabs. *Corrosion Science*, 29(1):105–113.
- Feliu, S., Gonzalez, J. A., Andrade, M. C., and Feliu, V. (1989b). Polarization resistance measurements in large concrete specimens: mathematical solution for a unidirectional current distribution. *Materials and Structures*, 22:199–205.
- Feliu, S., Gonzalez, J. A., and Escudero, M. L. (1990a). Influence of counter electrode size on the on-site measurement of polarization resistance in concrete structures, paper no. 142. In *CORROSION/90 The NACE International Annual Conference and Corrosion Show*.
- Feliu, S., Gonzalez, J. A., Escudero, M. L., Feliu, S., and Andrade, M. C. (1989c). Possibilities of the "guard ring" for the confinement of the electrical signal in polarization measurements of reinforcement, paper no. 623. In *CORROSION 89 The NACE International Annual Conference and Corrosion Show*.
- Feliu, S., Gonzalez, J. A., Escudero, M. L., Feliu, S., and Andrade, M. C. (1990b). Possibilities of the guard ring for electrical signal confinement in polarization measurements of reinforcements. *Corrosion*, 46(12):1015–1020.
- Feliu, S., Gonzalez, J. A., Feliu, V., Feliu, S., Escudero, M. L., Rodriguez-Maribona, I. A., Austin, V., Andrade, M. C., Bolano, J. A., and Jimenez, F. (1993). Corrosion detecting probes for use with a corrosion-rate meter for electrochemically determining the corrosion rate of reinforced concrete structures. United States Patent 5259944.
- Feliu, V., Gonzalez, J., and Feliu, S. (2005). Modelling of the steel-concrete interface to obtain information on reinforcement bar corrosion. *Journal of Applied Electrochemistry*, 35:429–436.

- Feliu, V., Gonzalez, J. A., Andrade, C., and Feliu, S. (1998). Equivalent circuit for modelling the steel-concrete interface. i. experimental evidence and theoretical predictions. *Corrosion Science*, 40(6):975–993.
- Feliu, V., Gonzalez, J. A., and Feliu, S. (2004). Algorithm for extracting corrosion parameters from the response of the steel-concrete system to a current pulse. *Journal of The Electrochemical Society*, 151(3):134–140.
- Fidjestol, P. and Nielsen, N. (1980). Field test of reinforcement corrosion in concrete. In *Performance of concrete in marine environment, ACI SP-65*, pages 205–221.
- Flis, J., Pickering, H. W., and Osseo-Asare, K. (1995). Assessment of data from three electrochemical instruments for evaluation of reinforcement corrosion rates in concrete bridge components. *Corrosion*, 51(8):601–609.
- Flis, J., Sabol, S., Pickering, H. W., Sehgal, A., Osseo-Asare, K., and Cady, P. (1993). Electrochemical measurements on concrete bridges for evaluation of reinforcement corrosion rates. *Corrosion*, 49(7):601–612.
- Fontana, M. G. and Greene, N. D. (1978). *Corrosion engineering*. McGraw-Hill.
- Gabrielli, C., Keddam, K., and Takenouti, H. (1979). The relationship between the impedance of corroding electrode and its polarization resistance determined by a linear voltage sweep technique. *Electrochimica Acta*, 24:61–65.
- Garces, P., Andrade, M. C., Saez, A., and Alonso, M. C. (2005). Corrosion of reinforcing steel in neutral and acid solutions simulating the electrolytic environments in the micropores of concrete in the propagation period. *Corrosion Science*, 47:289–306.
- Gepreags, O. K. and Hansson, C. M. (2004). A comparative evaluation of three commercial instruments for field measurements of reinforcing steel corrosion rates. In Berke, N. S., Thomas, M., Yunping, X., and Veleva, L. L., editors, *Electrochemical Techniques for Evaluating Corrosion Performance and Estimating Service-Life of Reinforced Concrete, ASTM STP 1457*. ASTM International.
- Gjørv, O. E., Vennesland, Ø., and El-Busaidy, A. H. S. (1977). Electrical resistivity of concrete in the oceans. In *9th Annual Offshore Technology Conference, paper 2803, Houston*.
- Glass, G. K., Page, C. L., and Short, N. R. (1991). Factors affecting the corrosion rate of steel in carbonated mortars. *Corrosion Science*, 32(12):1283–1294.
- Glass, G. K., Page, C. L., Short, N. R., and Zhang, J. Z. (1997). The analysis of potentiostatic transients applied to the corrosion of steel in concrete. *Corrosion Science*, 39(9):1657–1663.
- Gonzalez, J., Algaba, S., and Andrade, C. (1980). Corrosion of reinforcing bars in carbonated concrete. *British Corrosion Journal*, 15(3):135–139.

- Gonzalez, J. A., Andrade, C., Alonso, C., and Feliu, S. (1995a). Comparison of rates of general corrosion and maximum pitting penetration of concrete embedded steel reinforcement. *Cement and Concrete Research*, 25(2):257–264.
- Gonzalez, J. A., Benito, M., Feliu, S., Rodriguez, P., and Andrade, C. (1995b). Suitability of assessment methods for identifying active and passive zones in reinforced concrete. *Corrosion*, 51(2):145–152.
- Gonzalez, J. A., Miranda, J. M., Biribilis, B., and Feliu, S. (2005). Electrochemical techniques for studying corrosion of reinforcing steel: Limitations and advantages. *Corrosion*, 61(1):37–50.
- Gonzalez, J. A., Miranda, J. M., and Feliu, S. (2004). Considerations on reproducibility of potential and corrosion rate measurements in reinforced concrete. *Corrosion Science*, 46:2467–2485.
- Gonzalez, J. A., Molina, A., Escudero, M. L., and Andrade, C. (1985a). Errors in the electrochemical evaluation of very small corrosion rates - i. polarisation resistance method applied to corrosion of steel in concrete. *Corrosion Science*, 25(10):917–930.
- Gonzalez, J. A., Molina, A., Escudero, M. L., and Andrade, C. (1985b). Errors in the electrochemical evaluation of very small corrosion rates - ii. other electrochemical techniques applied to corrosion of steel in concrete. *Corrosion Science*, 25(7):519–530.
- Gowers, K. R., Bungey, J. H., and Millard, S. G. (1996). Galvanostatic pulse transient analysis for determining concrete reinforcement corrosion rates. In Page, C. L., Ramforth, P. B., and Figg, J. W., editors, *Corrosion of reinforcement in concrete construction*. Society of Chemical Industry, Construction Materials Group.
- Gowers, K. R. and Millard, S. G. (1993). On-site linear polarization resistance mapping of reinforced concrete structures. *Corrosion Science*, 35(5-8):1593–1600.
- Gowers, K. R., Millard, S. G., Gill, J. S., and Gill, R. P. (1994). Programmable linear polarisation meter for determination of corrosion rate of reinforcement in concrete structures. *British Corrosion Journal*, 29(1):25–32.
- Gulikers, J. (2005). Theoretical considerations on the supposed linear relationship between concrete resistivity and corrosion rate of steel reinforcement. *Materials and Corrosion*, 56(5):393–403.
- Hope, B. B., Ip, A. K., and Manning, D. G. (1985). Corrosion and electrical impedance in concrete. *Cement and concrete research*, 15(3):525–534.
- Hunkeler, F. (1996). The resistivity of pore water solution - a decisive parameter of rebar corrosion and repair methods. *Construction and Building Materials*, 10(5):381–389.
- Hunkeler, F. (2005). *Corrosion in reinforced concrete structures*, chapter 1, Corrosion in reinforced concrete: processes and mechanisms. Woodhead Publishing.

- Ijsseling, F. P. (1986). Application of electrochemical methods of corrosion rate determination to systems involving corrosion products layers. *British Corrosion Journal*, 21(2):95–101.
- Jäggi, S. (2001). *Experimentelle und numerische Modellierung der lokalen Korrosion von Stahl in Beton*. PhD thesis, ETH Zürich. In German.
- Jäggi, S., Böhni, H., and Elsener, B. (2001). Macrocell corrosion of steel in concrete - experiments and numerical modelling. European Federation of Corrosion. Proceedings on CD.
- Jäggi, S., Bürchler, D., Elsener, B., and Böhni, H. (2005). Chloride induced corrosion of steel in concrete - influence of temperature and electrical resistance of concrete. Technical report, ETH, Zürich.
- Jäggi, S., Elsener, B., and Böhni, H. (2000). Oxygen reduction on mild steel and stainless steel in alkaline solutions. In j. Mietz, Polder, R., and Elsener, B., editors, *Corrosion of Reinforcement in Concrete - Corrosion Mechanisms and Corrosion Protection*, European Federation of Corrosion publications, 31, pages 3–12. IOM Communications.
- John, D. G., Searson, P. C., and Dawson, J. L. (1981). Use of ac impedance in studies on steel in concrete in immersed conditions. *British Corrosion Journal*, 16(2):102–106.
- Jones, D. A. and Greene, N. D. (1966). Electrochemical measurement of low corrosion rates. *Corrosion*, 22:198–205.
- Koryta, J., Dvořák, J., and Boháčková, V. (1970). *Electrochemistry*. Methuen & CO Ltd.
- Kouřil, M., Novák, P., and Bojko, M. (2006). Limitations of the linear polarization method to determine stainless steel corrosion rate in concrete environment. *Cement & Concrete Composites*, 28:220–225.
- Kranc, S. C. and Sagües, A. A. (1993). Polarization current distribution and electrochemical impedance response of reinforced concrete when using guard ring electrodes. *Electrochimica Acta*, 38(14):2055–2061.
- Küter, A., Möller, P., and Geiker, M. (2004). Corrosion of steel in concrete - thermodynamical aspects. In *Nordic Corrosion Congress 13, Reykjavik, Iceland*.
- Law, D. W., Millard, S. G., and Bungey, J. H. (2000a). Effect of electrode orientation on linear polarisation measurements using sensor controlled guard ring. *British Corrosion Journal*, 35(2):136–140.
- Law, D. W., Millard, S. G., and Bungey, J. H. (2000b). Galvanostatic pulse measurements of passive and active reinforcing steel in concrete. *Corrosion*, 56(1):48–56.
- Law, D. W., Millard, S. G., and Bungey, J. H. (2001). Use of galvanostatic pulse measurements on active reinforcing steel in concrete to assess corrosion rates. *British Corrosion Journal*, 36(1):75–80.

- Leek, D. S. and Poole, A. B. (1990). The breakdown of the passive film on high yield mild steel by chloride ions. In Page, C. L., Treadaway, K. W. J., and Bamforth, P. B., editors, *Corrosion of Reinforcement in Concrete*. Society of Chemical Industry, Elsevier Applied Science.
- Liu, T. and Weyers, R. W. (1998). Modeling the dynamic corrosion process in chloride contaminated structures. *Cement and Concrete Research*, 28(3):365–379.
- Liu, Y. and Weyers, R. E. (2003). Comparison of guarded and unguarded linear polarization ccd devices with weight loss measurements. *Cement and Concrete Research*, 33:1093–1101.
- Lopez, W. and Gonzalez, J. A. (1993). Influence of the degree of pore saturation on the resistivity of concrete and the corrosion rate of steel reinforcement. *Cement and concrete research*, 23(2):368–376.
- Lopez, W., Gonzalez, J. A., and Andrade, C. (1993). Influence of temperature on the service life of rebars. *Cement and Concrete Research*, 23(5):1130–1140.
- Luping, T. (2002). Calibration of the electrochemical methods for the corrosion rate measurements of steel in concrete, nordtest project no. 1531-01. Technical report, SP Swedish National Testing and Research Institute, Building Technology.
- MathWorks, T. (2006). *Curve Fitting Toolbox, For Use with MATLAB, User's Guide*, version 1 edition.
- Millard, S. G., Gowers, K. R., and Bungey, J. H. (1995). Galvanostatic pulse techniques: A rapid method of assessing corrosion rates of steel in concrete structures, paper no. 525. In *Corrosion 95 - The NACE International Annual Conference and Corrosion Show*.
- Millard, S. G., Gowers, K. R., and Gill, R. P. (1992). Practical field measurement of reinforcement corrosion in concrete using linear polarisation methods. *British Journal of NDT*, 34(9):444–452.
- Millard, S. G., Law, D., Bungey, J., and Cairns, J. (2001). Environmental influences on linear polarisation corrosion rate measurement in reinforced concrete. *NDT&E International*, 34:409–417.
- Monfore, G. E. (1968). The electrical resistivity of concrete. *Journal of the PCA Research and Development Laboratories*, pages 35–48.
- Myrdal, R. (2007). *The electrochemistry and characteristics of embeddable reference electrodes for concrete*. Woodhead Publishing.
- Neville, A. M. (1999). *Properties of concrete*, volume Fourth. Longman.
- Newton, C. J. and Sykes, J. M. (1988). A galvanostatic pulse technique for investigation of steel corrosion in concrete. *Corrosion Science*, 28(11):1051–1074.

- Nygaard, P. V., Geiker, M., Møller, P., Sørensen, H. E., and Klinghoffer, O. (2005). Corrosion rate measurements, modelling and testing of the effect of a guard ring on current confinement. Published at: Eurocorr 2005, 4-8 September 2005. Lisbon, Portugal.
- Oelssner, W., Berthold, F., and Guth, U. (2006). The ir drop - well known but often underestimated in electrochemical polarization measurements and corrosion testing. *Materials and Corrosion*, 57(6):455–466.
- O'Grady, W. E. (1980). Mössbauer study of the passive oxide film on iron. *Journal of the Electrochemical Society*, 127(3):555–563.
- Okada, T. (1990). A two-step initiation hypothesis of pitting corrosion in passive metals. In Sato, N. and Hashimoto, K., editors, *Passivity of metals - Proceedings of the Sixth International Symposium on Passivity - PART I*, volume 31, pages 453–458. PERGA-MON PRESS.
- Page, C. L. (1988). *Corrosion of steel in concrete*, chapter 2. Chapman and Hall.
- Pastore, T. and Pedferrie, P. (1991). Corrosion behaviour of a duplex stainless steel in chloride contaminated concrete. In *Proceedings of International Conference of Stainless Steels*, volume 1, pages 351–358. The Iron and Steel Institute of Japan.
- Polder, R., Andrade, C., Elsener, B., Vennesland, O., Gulikers, J., Weidert, R., and Raupach, M. (2000). Test methods for on-site measurement of resistivity of concrete. *Materials and Structures*, 33:603–611.
- Polder, R., Tondi, A., and Cigna, R. (1993). Concrete resistivity and corrosion rate of reinforcement, TNO Report 93-BT-r0170.
- Polder, R. B. (2001). Test methods for on site measurement of resistivity of concrete - a RILEM TC-154 technical recommendation. *Construction and building materials*, 15:125–131.
- Polder, R. B., Bamforth, P. B., Basheer, M., Chapman-Andrews, J., Cigna, R., Jafar, M. I., Mazzoni, A., Nolan, E., and Wojtas, H. (1994). Reinforcement corrosion and concrete resistivity - state of the art, laboratory and field results. In *International Conference on Corrosion and Corrosion Protection of Steel in Concrete*, University of Sheffield.
- Pourbaix, M. (1974). Applications of electrochemistry in corrosion science and practice. *Corrosion Science*, 14(1):25–82.
- Pruckner, F. (2002). *Diagnosis and protection of corroding steel in concrete*. PhD thesis, Department of Structural Engineering, Norwegian University of Science and Technology.
- Raupach, M. (1997a). Effect of temperature on chloride induced steel corrosion in concrete. In Bardal, E., editor, *EUROCORR 97, The European Corrosion Congress, Event No. 208*, volume I, pages 431–438. European Federation of Corrosion, Tapir.

- Raupach, M. (1997b). Results from laboratory tests and evaluation of literature on the influence of temperature on reinforcement corrosion. In Mietz, J., Elsener, B., and Polder, R., editors, *Corrosion of Reinforcement in Concrete - Monitoring, Prevention and Rehabilitation*. IOM Communications.
- Rodriguez, J., Ortega, L. M., Garcia, M., Johansson, L., and Petterson, K. (1994). On site corrosion rate measurements in concrete structures using a device developed under the eureka project eu-401. In *International Conference - 'Concrete Across the Borders*.
- Sagoe-Crentsil, K. K. and Glasser, F. P. (1989). Steel in concrete: Part I A review of the electrochemical and thermodynamic aspects. *Magazine of Concrete Research*, 41(149):205–212.
- Sagoe-Crentsil, K. K. and Glasser, F. P. (1990). Analysis of the steel:concrete interface. In Page, C. L., Treadaway, K. W. J., and Bamforth, P. B., editors, *Corrosion of Reinforcement in Concrete*. Society of Chemical Industry, Elsevier Applied Science.
- Sagoe-Crentsil, K. K. and Glasser, F. P. (1993a). Constitution of green rust and its significance to the corrosion of steel in portland cement. *Corrosion*, 49(6):457–463.
- Sagoe-Crentsil, K. K. and Glasser, F. P. (1993b). "Green Rust, Iron solubility and the role of chloride in the corrosion of steel at high pH". *Cement and concrete research*, 23(4):785–791.
- Sagoe-Crentsil, K. K., Glasser, F. P., and Irvine, J. T. S. (1992). Electrochemical characteristics of reinforced concrete corrosion as determined by impedance spectroscopy. *British Corrosion Journal*, 27(2):113–118.
- Sagües, A. A., Kranc, S. C., and I.Moreno, E. (1996). Evaluation of electrochemical impedance with constant phase angle component from the galvanostatic step response of steel in concrete. *Electrochimica Acta*, 41(7/8):1239–1243.
- Sandberg, P. (1998). Chloride initiated reinforcement corrosion in marine concrete, Report TVBM-1015. Technical report, Lund Institute of Technology, Lund, Sweden.
- Sato, N. (1971). A theory for breakdown of anodic oxide films on metals. *Electrochimica Acta*, 16:1683–1692.
- Schiessl, P. and Raupach, M. (1990). Influence of concrete composition and microclimate on the critical chloride content in concrete. In Page, C. L., Treadaway, K. W. J., and Bamforth, P. B., editors, *Corrosion of Reinforcement in Concrete*. Society of Chemical Industry, Elsevier Applied Science.
- Scully, J. R. (2000). Polarization resistance method for determination of instantaneous corrosion rates. *Corrosion*, 56(2):199–220.
- Sehgal, A., Li, D., Kho, Y. T., Osseo-Asare, K., and Pickering, H. W. (1992). Reproducibility of polarization resistance measurements in steel-in-concrete systems. *Corrosion*, 48:706–712.

- So, H.-S. and Millard, S. G. (2007). Electrochemical transient techniques for the evaluation of reinforcement corrosion in concrete. *Insight: Non-destructive testing and condition monitoring*, 47(7):390–396.
- Song, G. (2000). Theoretical analysis of the measurement of polarisation resistance in reinforced concrete. *Cement and Concrete Composites*, 22:407–415.
- Spellman, D. L. and Stratfull, R. F. (1973). Concrete variables and corrosion testing. *Highway Research Records* 423.
- Stern, M. and Geary, A. L. (1957). Electrochemical polarization, i. a theoretical analysis of the shape of polarization curves. *Journal of the Electrochemical Society*, 104(1):56–63.
- Stratfull, R. F. (1957). The corrosion of steel in a reinforced concrete bridge. *Corrosion*, 13:173–178.
- Stratfull, R. F., Jurkovich, W. J., and Spellman, D. L. (1975). Corrosion testing of bridge decks. *Transportation research records*.
- Suzuki, M., Kanno, K., and Sato, Y. (1980). Application of the coulometric method to corrosion rate measurements. *Werkstoffe und Korrosion*, 31(5):364–370.
- Tuutti, K. (1982). *Corrosion of steel in concrete*. Number 4:82. Swedish Cement and Concrete Research Institute, Stockholm.
- Van Daveer, J. R. (1975). Techniques for evaluating reinforced concrete bridge decks. *Journal of the American Concrete Institute*, 72(12):697–704.
- Vassie, R. P. W. (1978). Evaluation of techniques for investigating the corrosion of steel in concrete. *TRRL Supplementary Report 39*.
- Videm, K. (1997). Experience with galvanostatic pulse technique and other methods to assess rebar corrosion, paper no. 279. In *Corrosion 97 - The NACE Annual Conference and Corrosion Show*.
- Videm, K. (1998). Field and laboratory experience with potentiostatic polarization and potentiokinetic scans to assess the severity of corrosion of steel in concrete. In Mietz, J., Elsener, B., and Polder, R., editors, *Corrosion of Reinforcement in Concrete - Monitoring, Prevention and Rehabilitation*. IOM Communications.
- Videm, K. and Myrdal, R. (1997). Electrochemical behavior of steel in concrete and evaluation of the corrosion rate. *Corrosion*, 53(9):734–742.
- Walter, G. W. (1977). Problems arising in the determination of accurate corrosion rates from polarization resistance measurements. *Corrosion Science*, 17:983–993.
- Whiting, D. A. and Nagi, M. A. (2003). Electrical resistivity of concrete - a literature review. Technical report, Portland Cement Association. Serial no. 2457.

- Wojtas, H. (2004a). Determination of corrosion rate of reinforcement with a modulated guard ring electrode; analysis of errors due to lateral current distribution. *Corrosion Science*, 46(7):1621–1632.
- Wojtas, H. (2004b). Determination of polarization resistance of reinforcement with a sensorized guard ring: Analysis of errors. *Corrosion*, 60(4):414–420.
- Yonezawa, T., Ashworth, V., and Procter, R. P. M. (1988). Pore solution composition and chloride effects on the corrosion of steel in concrete. *Corrosion*, 44(7):489–499.
- Żakowski, K. and Sokółski, W. (1999). Numeric method of ir elimination from measurement results of potential of underground pipelines in the zone of interaction of stray currents. *Corrosion Science*, 41:2213–2222.
- Zivica, V. (2002). Significance and influence of the ambient temperature as a rate factor of steel reinforcement corrosion. *Bulletin of Materials Science*, 25(5):375–380.

Appendix A

Concrete composition

This appendix describes in detail the constituent concrete materials and the concrete mix design used for all test specimens and slabs in the experimental work. First, a detailed description of the constituent materials is given. Following this, the concrete mix design and the procedure used for mixing the concretes are given.

A.1 Constituent materials

The constituents for the concretes used were ordinary materials used for concrete production in Denmark. Essential properties have been determined and are presented together with declared material properties below.

A.1.1 Cement

As cement white Portland cement "AALBORG WHITE ©" type CEM I 52.5 R from Aalborg Portland in Denmark was used. All concrete mixes were made with cement from the same batch (TUN no. 8919599). A sample of the cement was sent to Aalborg Portland for analysis. Results from the analysis are shown in Table A.1.

A.1.2 Water

The water used was ordinary potable tap water. No analysis of the water was made.

A.1.3 Fine aggregate

The fine aggregate used was class E sea-sand (in accordance with DS 2426 (2004)) in the fraction 0-4 mm. The fine aggregate was purchased from RN Sten og Grus in Denmark. The properties determined by testing are shown in Table A.2. The test results are shown together with declared values for the chemical properties in Table A.3.

A.1.4 Coarse aggregate

The coarse aggregate used was sea-material, class A (in accordance with DS 2426 (2004)) in the fraction 4-8 mm. The coarse aggregate was purchased from RN Sten og Grus in

Table A.1 *Cement composition.*

Property	Value	
	mass%	
Oxides:	SiO ₂	24.39
	Al ₂ O ₃	2.06
	Fe ₂ O ₃	0.34
	CaO	68.42
	MgO	0.59
	SO ₃	2.09
Loss of ignition		0.71
Cl ⁻		0.009
Alkalies:	K ₂ O	0.022
	Na ₂ O	0.176
	Eqv. Na ₂ O	0.191

Table A.2 *Test methods used to determine the physical properties of the fine and coarse aggregates.*

Property	Method
Absorption and density	DS/EN 1097-6 (2000)
Grading	DS/EN 933-1 (1997)
Eigen packing	APM 506 (1993)

Denmark. The properties determined by testing are shown in Table A.2. The test results are shown together with declared values for the chemical properties in Table A.3.

A.2 Concrete

A.2.1 Concrete mix design

A w/c ratio of 0.5 was selected for the experiments. A target paste content of approximately 27 % was chosen as the paste content in 'ordinary' concrete ranges from 26 to 28 % by volume of concrete. The grading of the aggregate was determined from theoretical packing calculations using the commercial program '4C Packing' from the Danish Technological Institute. The result of the packing calculation for the two phase system is shown in Figure A.1. A combination of 43 % fine aggregate and 57 % coarse aggregate was chosen for the concretes. The grading curve resulting from combining the two aggregate fractions (43 %/57 %) is shown in Figure A.2. From the selected w/c ratio and the target paste content the cement content was determined to 325 kg/m³ concrete. A natural air content of 2.0 vol % was assumed. The mix design calculated from the selected parameters is shown in Table A.4.

Table A.3 *Essential properties for the aggregates used in the concrete.*

Properties of aggregates		Fine aggregate 0-4 mm	Coarse aggregate 4-8 mm	
Sieve analysis	Sieve size [mm]	Percentage passing		
	31.5	100	100	mass%
	16	100	100	mass%
	8	100	100	mass%
	4	98.4	4.4	mass%
	2	88.0	0.4	mass%
	1	71.9	0.2	mass%
	0.5	49.5	0.2	mass%
	0.25	19.8	0.2	mass%
	0.125	1.8	0.2	mass%
	0.075	0.4	0.2	mass%
Density, saturated surface dry		2643	2623	kg/m ³
Absorption		0.36	1.0	mass%
Eigen-packing		0.70	0.62	-
Cl ⁻ content		0.012	0.007	mass%
Equivalent Na ₂ O		0.011	0.006	mass%

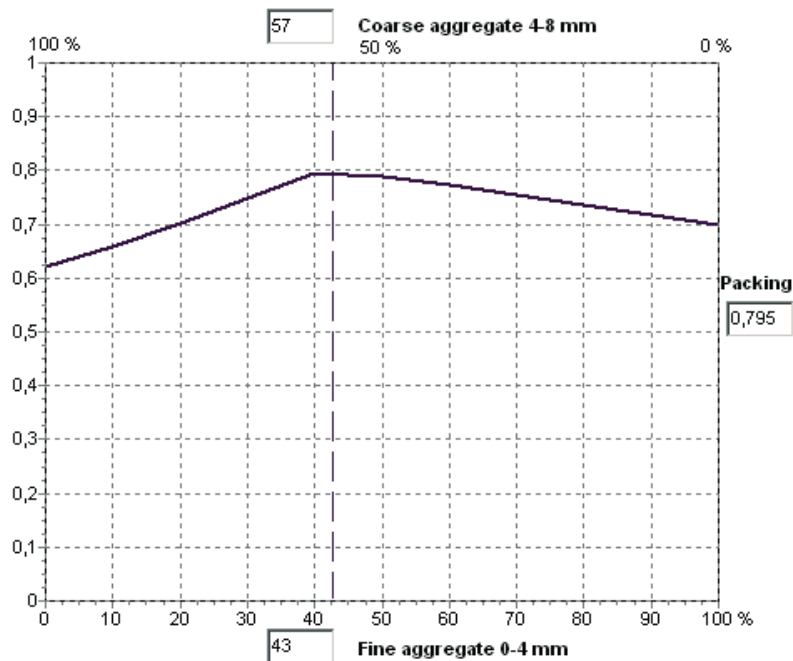


Figure A.1 The packing diagram resulting from the theoretical calculation. The selected composition is indicated with the vertical dashed line.



Figure A.2 Grading of the combined aggregate.

Table A.4 Concrete mix design

Constituents	Type		Unit
Cement	Aalborg White®	325	kg/m ³
Water	Tap water	162.5	kg/m ³
Paste content	-	26.6	vol%
Cement matrix	-	281	dm ³ /m ³
Aggregate	0-4 mm	814	kg/m ³
Aggregate	4-8 mm	1079	kg/m ³

A.2.2 Mixing

The mixing was done by use of a 120 litre laboratory pan mixer from Zyklos. Before mixing, all constituent were weighed out to the nearest 20 grams. The aggregates were first mixed for approximately one minute after which half of the water was added while the mixer was rotating. After mixing for another minute the mixer was stopped. After a two minute pause, allowing the aggregates to absorb a part of the added water, the cement was added and the mixing continued. The remaining water was subsequently added while the mixer was rotating. The total mixing time from adding the cement was approximately 5 minutes.

After mixing the slump, density and air content of the fresh concrete was measured. Besides the test specimens for the given experiment, 12 Ø100×200 mm cylinders for testing the hardened properties of the concrete were cast. Casting and curing of the test specimens is described in Chapter 4 - Experimental. All test cylinders were sealed in plastic and cured at 20 C° until testing. The fresh and hardened properties of the individual concrete batches as well as the test methods used are described in Appendices B and C.

Appendix B

Concrete properties I

In this Appendix the fresh and hardened properties of the three concretes batches used for casting the three test slabs (Slabs I to III) described in Section 4.1 are given. One batch was used for each slab. The mix design and mixing of the concretes are described in Appendix A. The fresh and hardened properties determined for each concrete batch are given in Table B.1 together with the test methods used. The compressive strength and electrical resistivity at a given age was determined as the average value of three $\varnothing 100 \times 200$ mm cylinders. The density of the hardened concrete was calculated as the average of all cylinders tested for each batch.

The electrical resistivity determined at the time of testing (last row in Table B.1) was measured on the slabs with segmented reinforcement bars. A measurement was performed by placing two 80 mm diameter stainless steel discs on the surface of a test specimen, i.e. one disc on each side of the specimen exactly opposite to each other on a moist sponge. The electrical resistance between the discs was measured by applying a stable alternating current of 40 mA at a frequency of 128 HZ. The resistivity was calculated from the obtained resistance by multiplying with the contact area of the discs (50.3 cm^2) and dividing with the thickness of the specimen (11.7 cm). The value for each concrete, i.e. each specimen was calculated as the average of three measurements performed at different positions on the specimen.

Table B.1 *Fresh and hardened properties of the three concretes used for the slabs described in Section 4.1.*

		Slab			Unit	Test method
		I	II	III		
Fresh properties						
Slump		20	50	50	mm	DS/EN 12350-2 (2002)
Air content		2.0	2.2	2.0	vol%	DS/EN 12350-7 (2002)
Density		2370	2400	2380	kg/m ³	DS/EN 12350-6 (2002)
Hardened properties						
Density		2370	2340	2330	kg/m ³	DS/EN 12390-7 (2002)
Compressive strength	1-day	27.5	30	24.5	MPa	DS/EN 12390-3 (2002)
	3-day	36	36.5	35	MPa	
	28-day	-	-	-	MPa	
Resistivity	1-day	4.7	2.5	0.8	kΩ×cm	APM 219 (1996)
	3-day	6.3	2.8	1.0	kΩ×cm	
	28-day	-	-	-	kΩ×cm	
	Testing*	3.4	1.6	0.8	kΩ×cm	Explained in the text.

*: Determined at the time of testing, i.e. when performing the experiments described in Section 4.1.

Appendix C

Concrete properties II

In this Appendix the fresh and hardened properties of the nine concrete batches used for casting the three series (I-III) of test specimens described in Section 4.2 are given. Five test specimens and 12 Ø100×200 mm cylinders were cast from each batch. The mix design and mixing of the concretes are described in Appendix A. The fresh and hardened properties of the three batches used for casting the test specimens in each series (I to III) are given in Tables C.1 to C.3, together with the test methods used. The compressive strength and electrical resistivity at a given age was determined as the average value of three Ø100×200 mm cylinders. The density of the hardened concrete was calculated as the average of all cylinders tested for each batch.

Table C.1 *Fresh and hardened properties of the three concrete batches used for casting the test specimens in Series I (0 % chloride, plain uncoated steel bars).*

		Series I (0 % Cl ⁻)				
		Batch 1	Batch 2	Batch 3	Unit	Test method
Fresh properties						
Slump		70	30	20	mm	DS/EN 12350-2 (2002)
Air content		2.1	1.5	2.2	vol%	DS/EN 12350-7 (2002)
Density		2280	2330	2280	kg/m ³	DS/EN 12350-6 (2002)
Hardened properties						
Density		2340	2380	2350	kg/m ³	DS/EN 12390-7 (2002)
Compressive strength	1-day	16.5	18.5	16.0	MPa	DS/EN 12390-3 (2002)
	3-day	31.0	34.0	38.0	MPa	
	28-day	40.0	44.5	45	MPa	
Resistivity	1-day	-	3.8	3.3	kΩ×cm	APM 219 (1996)
	3-day	6.5	5.7	6.0	kΩ×cm	
	28-day	7.6	-	-	kΩ×cm	

Table C.2 *Fresh and hardened properties of the three concrete batches used for casting the test specimens in Series II (4 % chloride, plain uncoated steel bars).*

Series II (4 % Cl ⁻)						
		Batch 1	Batch 2	Batch 3	Unit	Test method
Fresh properties						
Slump		50	50	80	mm	DS/EN 12350-2 (2002)
Air content		2.0	2.5	1.5	vol%	DS/EN 12350-7 (2002)
Density		2310	2310	2330	kg/m ³	DS/EN 12350-6 (2002)
Hardened properties						
Density		2380	2370	2350	kg/m ³	DS/EN 12390-7 (2002)
Compressive strength	1-day	19.5	21.0	19.0	MPa	DS/EN 12390-3 (2002)
	3-day	27.0	29.0	28.0	MPa	
	28-day	34.5	35.5	33.0	MPa	
Resistivity	1-day	1.4	1.4	-	kΩ×cm	APM 219 (1996)
	3-day	2.6	-	-	kΩ×cm	
	28-day	4.0	4.4	4.5	kΩ×cm	

Table C.3 *Fresh and hardened properties of the three concrete batches used for casting the test specimens in Series III (4 % chloride, partly nickel coated steel bars).*

Series III (4 % Cl ⁻)						
		Batch 1	Batch 2	Batch 3	Unit	Test method
Fresh properties						
Slump		70	90	60	mm	DS/EN 12350-2 (2002)
Air content		2.0	2.2	2.5	vol%	DS/EN 12350-7 (2002)
Density		2300	2310	2300	kg/m ³	DS/EN 12350-6 (2002)
Hardened properties						
Density		2350	2350	2350	kg/m ³	DS/EN 12390-7 (2002)
Compressive strength	1-day	20.5	19.0	20.5	MPa	DS/EN 12390-3 (2002)
	3-day	27.0	27.5	27.0	MPa	
	28-day	35.0	34.5	35.5	MPa	
Resistivity	1-day	1.5	1.5	1.5	kΩ×cm	APM 219 (1996)
	3-day	2.3	2.6	2.6	kΩ×cm	
	28-day	4.0	4.3	4.1	kΩ×cm	

Appendix D

GECOR 6 and GalvaPulse measurements, numerical values

In this Appendix the numerical values of the results obtained from the GECOR 6 and GalvaPulse measurements on the upper and lower segmented reinforcement bars in Slabs II and III shown in Figures 5.15, 5.16, 5.35 and 5.36 are given, together with the counter-electrode currents, I_{CE} , applied during the measurements and the potential shifts, ΔE , obtained.

Table D.1 Measurement data from the GECOR 6 and GalvaPulse measurements on the upper segmented reinforcement bar in Slab II, see also Figure 5.15.

		Measurement position							
		Unit	1	2	3	4	5	6	7
GECOR 6									
Cover:									
30 mm	E_{corr}	mV vs. Ag/AgCl	-132	-124	-124	-122	-119	-123	-118
	i_{corr}	$\mu\text{A}/\text{cm}^2$	0.023	0.020	0.023	0.038	0.035	0.030	0.045
	R_{Ω}	kOhm	0.32	0.18	0.30	0.18	0.35	0.30	0.31
	I_{CE}	μA	7	5	6	6	6	5	7
	ΔE	mV	178	165	167	105	115	120	116
75 mm	E_{corr}	mV vs. Ag/AgCl	-146	-145	-139	-135	-128	-135	-124
	i_{corr}	$\mu\text{A}/\text{cm}^2$	0.033	0.025	0.030	0.025	0.030	0.058	0.038
	R_{Ω}	kOhm	0.27	0.45	0.31	0.43	0.32	0.41	0.34
	I_{CE}	μA	7	5	5	5	5	8	8
	ΔE	mV	161	135	101	128	128	97	149
GalvaPulse <small>conf. on</small>									
Cover:									
30 mm	E_{corr}	mV vs. Ag/AgCl	-131	-112	-97	-89	-68	-76	-68
	i_{corr}	$\mu\text{A}/\text{cm}^2$	0.346	0.366	0.468	0.435	0.414	0.365	0.385
	R_{Ω}	kOhm	1	1	1	1	1	1	1
	I_{CE}	μA	20	20	20	20	20	20	20
	ΔE	mV	55	46	28	29	40	43	50
75 mm	E_{corr}	mV vs. Ag/AgCl	-127	-134	-137	-147	-131	-145	-157
	i_{corr}	$\mu\text{A}/\text{cm}^2$	0.409	0.374	0.442	0.380	0.395	0.424	0.340
	R_{Ω}	kOhm	1	1	1	1	1	1	1
	I_{CE}	μA	20	20	20	20	20	20	20
	ΔE	mV	49	36	31	32	44	49	54
GalvaPulse <small>conf. off</small>									
Cover:									
30 mm	E_{corr}	mV vs. Ag/AgCl	-124	-93	-96	-87	-76	-86	-72
	i_{corr}	$\mu\text{A}/\text{cm}^2$	0.648	0.671	0.784	0.751	0.858	0.780	0.695
	R_{Ω}	kOhm	0	0	0	0	0	0	0
	I_{CE}	μA	20	20	20	20	20	20	20
	ΔE	mV	32	18	16	16	24	25	28
75 mm	E_{corr}	mV vs. Ag/AgCl	-102	-106	-89	-86	-88	-103	-97
	i_{corr}	$\mu\text{A}/\text{cm}^2$	0.733	0.739	0.811	0.813	0.725	0.834	0.656
	R_{Ω}	kOhm	0	0	0	0	0	0	0
	I_{CE}	μA	20	20	20	20	20	20	20
	ΔE	mV	27	16	16	16	25	28	28

Table D.2 Measurement data from the GECOR 6 and GalvaPulse measurements on the upper segmented reinforcement bar in Slab III, see also Figure 5.16.

		Measurement position							
Unit		1	2	3	4	5	6	7	
GECOR 6									
Cover:									
30 mm	E_{corr}	mV vs. Ag/AgCl	-211	-225	-216	-206	-218	-221	-221
	i_{corr}	$\mu\text{A}/\text{cm}^2$	0.149	0.088	0.088	0.124	0.073	0.063	0.061
	R_{Ω}	kOhm	0.08	0.17	0.20	0.10	0.25	0.25	0.13
	I_{CE}	μA	7	8	9	9	8	8	7
	ΔE	mV	33	57	60	44	31	78	76
75 mm	E_{corr}	mV vs. Ag/AgCl	-204	-227	-222	-224	-228	-221	-224
	i_{corr}	$\mu\text{A}/\text{cm}^2$	0.045	0.139	0.124	0.190	0.159	0.303	0.202
	R_{Ω}	kOhm	0.14	0.16	0.09	0.1	0.09	0.15	0.13
	I_{CE}	μA	8		9	8	8		9
	ΔE	mV	108	78	49	26	33	19	143
GalvaPulse <small>conf. on</small>									
Cover:									
30 mm	E_{corr}	mV vs. Ag/AgCl	-219	-233	-226	-237	-229	-232	-225
	i_{corr}	$\mu\text{A}/\text{cm}^2$	0.541	0.578	0.703	0.852	0.643	0.528	0.675
	R_{Ω}	kOhm	0	0	0	0	0	0	0
	I_{CE}	μA	20	20	20	20	20	20	20
	ΔE	mV	32	29	25	23	26	30	31
75 mm	E_{corr}	mV vs. Ag/AgCl	-231	-240	-254	-238	-248	-250	-253
	i_{corr}	$\mu\text{A}/\text{cm}^2$	0.613	0.482	0.701	0.737	0.930	0.604	0.888
	R_{Ω}	kOhm	0	0	0	0	0	0	0
	I_{CE}	μA	20	20	20	20	20	20	20
	ΔE	mV	31	22	21	24	26	30	31
GalvaPulse <small>conf. off</small>									
Cover:									
30 mm	E_{corr}	mV vs. Ag/AgCl	-212	-222	-228	-220	-221	-235	-235
	i_{corr}	$\mu\text{A}/\text{cm}^2$	1.137	1.238	1.208	1.414	1.231	1.113	1.092
	R_{Ω}	kOhm	0	0	0	0	0	0	0
	I_{CE}	μA	20	20	20	20	20	20	20
	ΔE	mV	19	18	17	16	16	18	20
75 mm	E_{corr}	mV vs. Ag/AgCl	-227	-242	-241	-227	-260	-253	-251
	i_{corr}	$\mu\text{A}/\text{cm}^2$	1.051	1.201	1.334	1.589	1.462	1.131	1.236
	R_{Ω}	kOhm	0	0	0	0	0	0	0
	I_{CE}	μA	20	20	20	20	20	20	20
	ΔE	mV	18	16	14	15	16	16	18

Table D.3 Measurement data from the GECOR 6 and GalvaPulse measurements on the lower segmented reinforcement bar in Slab II, see also Figure 5.35.

		Measurement position							
Unit		1	2	3	4	5	6	7	
GECOR 6									
Cover:									
30 mm	E_{corr}	mV vs. Ag/AgCl	-244	-218	-226	-210	-204	-248	-243
	i_{corr}	$\mu\text{A}/\text{cm}^2$	0.162	0.111	0.394	0.768	0.245	0.083	0.167
	R_{Ω}	kOhm	0.36	0.28	0.32	0.29	0.30	0.27	0.34
	I_{CE}	μA	8	8	7	8	9		6
	ΔE	mV	35	48	14	7	22	77	27
75 mm	E_{corr}	mV vs. Ag/AgCl	-267	-251	-263	-241	-242	-262	-235
	i_{corr}	$\mu\text{A}/\text{cm}^2$	0.172	0.129	0.136	0.109	0.152	0.52	0.182
	R_{Ω}	kOhm	0.35	0.29	0.45	0.38	0.44	0.44	0.45
	I_{CE}	μA	8	9	7	9	10		8
	ΔE	mV	34	48	39	52	46	13	34
GalvaPulse <small>conf. on</small>									
Cover:									
30 mm	E_{corr}	mV vs. Ag/AgCl	-263	-260	-248	-246	-254	-240	-228
	i_{corr}	$\mu\text{A}/\text{cm}^2$	0.751	0.780	0.704	0.818	0.944	0.612	0.589
	R_{Ω}	kOhm	1	1	1	1	1	1	1
	I_{CE}	μA	50	50	50	50	50	50	50
	ΔE	mV	83	43	86	68	73	77	82
75 mm	E_{corr}	mV vs. Ag/AgCl	-283	-271	-275	-272	-276	-278	-259
	i_{corr}	$\mu\text{A}/\text{cm}^2$	0.780	0.847	0.9421	0.864	0.809	0.817	0.629
	R_{Ω}	kOhm	1	1	1	1	1	1	1
	I_{CE}	μA	50	50	50	50	50	50	50
	ΔE	mV	72	71	74	79	84	73	87
GalvaPulse <small>conf. off</small>									
Cover:									
30 mm	E_{corr}	mV vs. Ag/AgCl	-247	-243	-235	-236	-230	-215	-212
	i_{corr}	$\mu\text{A}/\text{cm}^2$	1.613	1.619	1.552	1.842	1.703	1.567	1.145
	R_{Ω}	kOhm	0	0	1	0	0	0	0
	I_{CE}	μA	50	50	50	50	50	50	50
	ΔE	mV	46	43	51	42	42	44	48
75 mm	E_{corr}	mV vs. Ag/AgCl	-233	-222	-227	-222	-241	-232	-225
	i_{corr}	$\mu\text{A}/\text{cm}^2$	1.747	1.771	1.806	1.636	1.765	1.361	1.354
	R_{Ω}	kOhm	0	0	1	0	0	0	0
	I_{CE}	μA	50	50	50	50	50	50	50
	ΔE	mV	39	40	43	42	45	42	50

Table D.4 Measurement data from the GECOR 6 and GalvaPulse measurements on the lower segmented reinforcement bar in Slab III, see also Figure 5.36.

		Measurement position							
Unit		1	2	3	4	5	6	7	
GECOR 6									
Cover:									
30 mm	E_{corr}	mV vs. Ag/AgCl	-368	-370	-364	-364	-	-361	-
	i_{corr}	$\mu\text{A}/\text{cm}^2$	-	-	-	-	-	-	-
	R_Ω	kOhm	0.18	0.15	0.12	0.14	-	0.09	-
	I_{CE}	μA	11	21	25	24	22	16	17
	ΔE	mV	-	-	-	-	-	-	-
75 mm	E_{corr}	mV vs. Ag/AgCl	-353	-361	-363	-381	-371	-383	-384
	i_{corr}	$\mu\text{A}/\text{cm}^2$	-	-	-	-	-	-	-
	R_Ω	kOhm	0.31	0.14	0.13	0.13	0.15	0.13	0.14
	I_{CE}	μA	15	24	34	43	39	34	23
	ΔE	mV	-	-	-	-	-	-	-
GalvaPulse <small>conf. on</small>									
Cover:									
30 mm	E_{corr}	mV vs. Ag/AgCl	-328	-328	-342	-346	-342	-351	-350
	i_{corr}	$\mu\text{A}/\text{cm}^2$	1.559	2.284	3.126	3.124	2.92	2.59	1.94
	R_Ω	kOhm	0	0	0	0	0	0	0
	I_{CE}	μA	50	50	50	50	50	50	50
	ΔE	mV	39	34	29	31	31	30	38
75 mm	E_{corr}	mV vs. Ag/AgCl	-342	-349	-373	-370	-365	-360	-361
	i_{corr}	$\mu\text{A}/\text{cm}^2$	2.141	2.434	4.554	3.797	3.462	3.055	2.525
	R_Ω	kOhm	0	0	0	0	0	0	0
	I_{CE}	μA	50	50	50	50	50	50	50
	ΔE	mV	39	32	25	27	27	29	33
GalvaPulse <small>conf. off</small>									
Cover:									
30 mm	E_{corr}	mV vs. Ag/AgCl	-320	-325	-338	-339	-342	-342	-344
	i_{corr}	$\mu\text{A}/\text{cm}^2$	3.88	5.345	6.979	5.473	6.283	6.507	5.495
	R_Ω	kOhm	0	0	0	0	0	0	0
	I_{CE}	μA	50	50	50	50	50	50	50
	ΔE	mV	24	20	18	19	20	19	21
75 mm	E_{corr}	mV vs. Ag/AgCl	-309	-337	-341	-343	-332	-349	-348
	i_{corr}	$\mu\text{A}/\text{cm}^2$	4.677	4.266	6.766	7.738	8.029	5.828	5.461
	R_Ω	kOhm	0	0	0	0	0	0	0
	I_{CE}	μA	50	50	50	50	50	50	50
	ΔE	mV	21	19	16	16	16	18	20

Appendix E

MatLab code, Potentiodynamic polarisation resistance

In this Appendix the code for the MatLab program used for calculating the polarisation resistances, R_P , and corrosion current densities, i_{corr} , from the potential sweeps measured in the experiment described in Section 4.2.2 is given:

```
clear all

G=textread('IR_d.txt');

A=textread('LPR_071203_lpr.txt');

z=size(A);

for j=1:45;

    for k=1:10;

        c=1;

    for i=1:z(1);

        B=A(i,:);

        if B(1,3)== j && B(1,4)==k;
            C(c,:) = B;
            clear B
            c=c+1;
        else
        end
    end
end
```

```
end

%The IR drop fro the measurement is taken from IR_d

for d=1:450;

    D=G(d,:);

    if D(1)==j && D(2)==k;

        if j<=15

            Ecorr=D(3);
            IR=0;

            elseif j>15
            Ecorr=D(3);
            IR=D(4);
            end
        end
    end
end

%In the following all measurements from each rebar are collected in C

%Reinforcemet bar nr. is calculated:
%
Line=(j-1)*10+k;

%Ecorr=IR_d(Rbar,3);
%IR=IR_d(Rbar,4);

f=fittype('Rp1*x+K');

lng=length(C(:,8));

t_sw=lng/(C(lng,5))*60;

%Analysis of data where the cathodic curve is only avaiailable
if lng<=16

    Eu1=-C(2:13,8);
    I1=-C(2:13,7)*50/1000; % One current unit is 50 nA

    for w=1:length(Eu1)
```

```

    E1(w)=Eu1(w)-IR*I1(w)/1000; %Ohmic drop compensation
end

%t_sw= abs((C(13,8)-C(7,8))/(C(13,5)-C(7,5)));

f1=fit(I1,E1',f,'StartPoint',[1 1]);

coeff1=coeffvalues(f1);

Rp1=abs(coeff1(2))*2*pi*0.5*20; %kOhm*cm^2

end

%end of cathodic curve analysis

%Analysis of the anodic curves

if lng > 17
    Eu2=-C(16:lng,8);
    I2=-C(16:lng,7)*50/1000; % One current unit is 50 nA

    for w3=1:length(Eu2)

        E2(w3)=Eu2(w3)-I2(w3)*IR/1000;
    end

    f2=fit(I2,E2',f,'StartPoint',[1 1]);

    coeff2=coeffvalues(f2);

    Rp1=abs(coeff2(2))*2*pi*0.5*20; %kOhm*cm^2

end

%Calculation of corrosion current density (microA/cm^2)

if j <= 15;

    icorr=(52/Rp1);

elseif j>15

    icorr=(26/Rp1);

end

```

%A matrix with Rp and Icorr is created:

```
lpr_rp_i(Line,1)=j;  
lpr_rp_i(Line,2)=k;  
lpr_rp_i(Line,3)=Ecorr;  
lpr_rp_i(Line,4)=Rp1;  
lpr_rp_i(Line,5)=icorr;  
lpr_rp_i(Line,6)=t_sw;
```

%swep rate is given in mV/min.

```
clear Rbar icorr Rp1 Ecorr E2 I2 E1 I1 t_sw lng C B  
end  
end dlmwrite('lpr_rp_i.txt',lpr_rp_i,'delimiter','\t',...  
    'precision','%.4f','newline','pc')
```

Appendix F

MatLab code, Potential transient measurements

In this Appendix the code for the MatLab program used for calculating the polarisation resistances, R_P , corrosion current densities, i_{corr} , and ohmic resistances, R_Ω , with the galvanostatic linear polarisation resistance technique and the galvanostatic potential transient technique from the potential transients measured in the experiment described in Section 4.2.2 is given:

```
clear

A=textread('071203.TXT_converted.txt');

z=size(A); %Size of data matrix

l1=z(1); w=z(2);

for i=1:l1;

%Parameters are taken from the row
%(containing all information from the measurement):

B=A(i,:); %one line is taken from A and analyzed.

l2=length(B); Date=B(1); Day=B(2); Block=B(3);
Reinf=B(4);

%The corrosion potential [mV] is calculated from
%the first 20 measurements, i.e. before any current is applied.

Ecorr=-(sum(B(6:25))/20000);
% The CE current is set:

    if Day == 2;
```



```
        Ice=-5;
    elseif Day == 3
        Ice=-10;
    elseif Day == 4
        Ice=-25;
    elseif Day == 5
        Ice=-50;
    elseif Day == 6
        Ice=-100;
    end

%All potential readings are put in M

M=-B(6:12)/1000;

%Data from M is taken for analysis:
Start =[1 1 0.5];

for j=1671:-50:121;

    clear xfit
    clear yfit

%A vector with Y values is created

if Block >= 16 && Block <=30

    z=1;
    for r=71:j
        yfit(z)=(M(r)-Ecorr);
        z=z+1;
    end

%A vector with X-values is created:

t=5; for h=1:length(yfit);
    xfit(h)=t;
    t=t+0.1;
end

else z=1; for r=31:j
    yfit(z)=(M(r)-Ecorr);
    z=z+1;
end
```

```
%A vector with X-values is created:

t=1; for h=1:length(yfit);
    xfit(h)=t;
    t=t+0.1;
end
end

f=fittype('n*Rw+n*Rp*(1-exp(-x/(Rp*Cd)))','problem','n');

f1=fit(xfit,yfit,f,'problem',Ice,'StartPoint',Start,'MaxFunEvals',...
5000,'Lower',[0,0,0]);

Start=coeffvalues(f1);

Cd=Start(1)*1000/2*pi*0.5*20; %Capacitance in microFarad/cm2
Rp=Start(2)*2*pi*0.5*20; %Polarisation resistance in kOhmcm^2
Rw=Start(3) %IR drop in kOhm

% Corrosion current density is calculated for the curve fit

if Block >=16;
    icorr=(0.026/Rp)*1000
else
    icorr=(0.052/Rp)*1000;
end

%The polarisation resistance is calculated after the
%linear polarisation resistance technique - all
%'end values' from each yfit array are placed in
%a vector

e=length(yfit);

%Counter

cou=((j-121)/50)+1;

E_end(cou)=mean(yfit(e-10:e));

%The calculated parameters are placed in separate matrices:

%Counter that calculates the column number, ie. the
%measurements are placed in columns with increasing
%polarisation time: 5, 10, 15,... sec.
```

```
v=((j-121)/50)+4;

%A vector with measurements times corresponding to the
%data in the matrices below is created:

x_time(v)=(((j-31)/10)+1);

%Polarisation resistance from curve fitting:

puls_rp(i,1)=Block; puls_rp(i,2)=Reinf; puls_rp(i,3)=Ice; puls_rp(i,v)=Rp;

%Corrosion current densities:

puls_icorr(i,1)=Block; puls_icorr(i,2)=Reinf;
puls_icorr(i,3)=Ice; puls_icorr(i,v)=icorr;

%Double layer capacitance

puls_cd(i,1)=Block; puls_cd(i,2)=Reinf; puls_cd(i,3)=Ice; puls_cd(i,v)=Cd;

%Ohmic resistance

puls_rw(i,1)=Block; puls_rw(i,2)=Reinf; puls_rw(i,3)=Ice; puls_rw(i,v)=Rw;

clear Rp icorr Cd Rw Rp2 Icorr2 dE

end

Idrop=puls_rw(i,4);

%Polarisation resistance in kOhm*cm2:

Rp2(1,:)=((E_end(1,:)/Ice)-Idrop)*2*pi*0.5*20;

%corrosion current density is calculated for Rp2

if Block >= 16;

    for sa=1:32;
        icorr2(sa)=26/Rp2(sa);
    end

elseif Block<16
```

```

        for sa=1:32;
            icorr2(sa)=52/Rp2(sa);
        end
    end

    %Polarisation resistance from lin polarisation resistance meas:

    lin_rp(i,1)=Block;
    lin_rp(i,2)=Reinf;
    lin_rp(i,3)=Ice;
    lin_icorr(i,1)=Block;
    lin_icorr(i,2)=Reinf;
    lin_icorr(i,3)=Ice;

    for se=1:32

        lin_rp(i,se+3)=Rp2(se);

        lin_icorr(i,se+3)=icorr2(se);

    end

    clear Block Reinf Ice Rp2 icorr2
end

dlmwrite('puls_rp.txt',puls_rp,'delimiter','\t',...
'precision','%.6f','newline','pc')

dlmwrite('puls_icorr.txt',puls_icorr,'delimiter',...
'\t','precision','%.6f','newline','pc')

dlmwrite('puls_cd.txt',puls_cd,'delimiter','\t',...
'precision','%.6f','newline','pc')

dlmwrite('puls_rw.txt',puls_rw,'delimiter','\t',...
'precision','%.6f','newline','pc')

dlmwrite('lin_rp.txt',lin_rp,'delimiter','\t',...
'precision','%.6f','newline','pc')

dlmwrite('lin_icorr.txt',lin_icorr,'delimiter',...
'\t','precision','%.6f','newline','pc')

```


Appendix G

Mean values and Standard deviations for Section 5.2.2

In this Appendix the mean values and standard deviations for the relative polarisation resistances, R_P/R_P^{ref} , and corrosion current densities, i_{corr}/i_{corr}^{ref} , shown in Figures 5.54 to 5.59 are given. The values are tabularised for polarisation times of 25, 50, 100 and 150 seconds.

Table G.1 Mean relative polarisation resistances, R_P/R_P^{ref} , and standard deviations calculated from the results obtained with the galvanostatic linear polarisation resistance technique.

		Polarisation time [s]							
Current		25		50		100		150	
[μA]		Mean	Std	Mean	Std	Mean	Std	Mean	Std
Specimen 1	5	2.4	0.5	1.8	0.6	2.3	0.5	2.6	0.6
	10	1.2	0.7	1.6	0.7	2.1	0.8	2.4	0.9
	25	1.3	0.4	1.7	0.4	2.1	0.4	2.4	0.4
	50	1.3	0.3	1.6	0.3	2.0	0.3	2.3	0.3
	100	0.7	0.1	0.9	0.1	1.1	0.2	1.3	0.3
Specimen 2	5	1.6	1.0	2.5	1.4	2.6	1.5	3.2	1.6
	10	1.8	1.4	2.1	1.6	2.8	1.8	3.3	2.0
	25	1.3	1.1	1.7	1.1	2.2	1.1	2.6	1.0
	50	1.5	1.2	1.9	1.2	2.5	1.1	3.0	1.1
	100	1.1	1.2	1.6	1.2	2.2	1.3	2.6	1.4
Specimen 3	10	1.5	1.1	2.3	1.6	2.7	1.6	3.1	1.5
	25	1.3	1.8	1.7	2.0	2.2	2.3	2.6	2.6
	50	1.1	1.0	1.5	1.1	2.1	1.3	2.5	1.6
	100	1.3	1.1	1.7	1.3	2.3	1.4	2.7	1.6

Table G.2 Mean relative corrosion current densities, i_{corr}/i_{corr}^{ref} , and standard deviations calculated from the results obtained with the galvanostatic linear polarisation resistance technique.

		Polarisation time [s]							
Current		25		50		100		150	
[μA]		Mean	Std	Mean	Std	Mean	Std	Mean	Std
Specimen 1	5	0.8	0.3	0.6	0.2	0.5	0.1	0.4	0.1
	10	1.1	0.5	0.7	0.3	0.6	0.2	0.5	0.1
	25	0.8	0.2	0.6	0.1	0.5	0.1	0.4	0.1
	50	0.8	0.2	0.6	0.1	0.5	0.1	0.5	0.1
	100	1.6	0.2	1.2	0.2	0.9	0.2	0.8	0.2
Specimen 2	5	0.8	0.4	0.5	0.2	0.5	0.3	0.4	0.2
	10	0.7	0.5	0.7	0.5	0.4	0.3	0.4	0.2
	25	0.9	0.6	0.6	0.4	0.5	0.3	0.4	0.2
	50	0.9	0.5	0.6	0.3	0.4	0.2	0.4	0.2
	100	1.3	0.8	0.8	0.5	0.5	0.3	0.4	0.2
Specimen 3	10	1.1	0.8	0.8	0.7	0.5	0.4	0.4	0.3
	25	1.5	0.9	1.0	0.5	0.7	0.5	0.6	0.3
	50	1.5	1.0	1.0	0.6	0.7	0.4	0.5	0.3
	100	1.5	1.8	1.0	0.9	0.7	0.6	0.6	0.6

Table G.3 Mean relative polarisation resistances, R_P/R_P^{ref} , and standard deviations calculated from the results obtained with the galvanostatic potential transient technique.

	Current [μ A]	Polarisation time [s]							
		25		50		100		150	
		Mean	Std	Mean	Std	Mean	Std	Mean	Std
Specimen 1	5	1.4	0.4	1.5	0.3	1.8	0.4	2.1	0.5
	10	1.3	0.2	1.4	0.3	1.7	0.4	2.0	0.5
	25	1.3	0.2	1.4	0.2	1.7	0.3	1.9	0.4
	50	1.3	0.2	1.4	0.2	1.6	0.4	1.7	0.4
	100	0.8	0.2	0.9	0.3	1.0	0.4	1.1	0.4
Specimen 2	5	2.6	1.7	2.4	1.3	2.7	1.3	2.9	1.4
	10	2.0	1.2	2.3	1.2	2.5	1.2	2.8	1.4
	25	2.0	1.3	1.9	1.1	2.4	1.2	2.8	1.3
	50	1.8	1.1	2.1	1.0	2.6	1.2	3.0	1.3
	100	1.6	0.8	1.8	0.5	2.3	0.9	2.6	1.1
Specimen 3	10	1.7	1.0	1.9	0.8	2.5	1.3	2.5	1.6
	25	1.3	0.6	1.6	0.9	2.2	1.3	2.5	1.5
	50	1.5	0.9	1.8	1.0	2.5	1.6	2.9	1.9
	100	1.5	0.4	1.9	1.0	2.3	1.4	2.6	1.7

Table G.4 Mean relative corrosion current densities, i_{corr}/i_{corr}^{ref} , and standard deviations calculated from the results obtained with the galvanostatic potential transient technique.

	Current [μ A]	Polarisation time [s]							
		25		50		100		150	
		Mean	Std	Mean	Std	Mean	Std	Mean	Std
Specimen 1	5	0.7	0.2	0.7	0.1	0.6	0.1	0.5	0.1
	10	0.8	0.1	0.7	0.1	0.6	0.1	0.5	0.1
	25	0.8	0.1	0.7	0.1	0.6	0.1	0.6	0.1
	50	0.8	0.1	0.7	0.1	0.7	0.1	0.6	0.2
	100	1.3	0.3	1.2	0.3	1.1	0.4	1.1	0.5
Specimen 2	5	0.5	0.2	0.6	0.3	0.4	0.2	0.4	0.2
	10	0.6	0.3	0.6	0.3	0.5	0.3	0.5	0.3
	25	0.7	0.4	0.7	0.3	0.5	0.3	0.5	0.2
	50	0.7	0.4	0.6	0.3	0.5	0.2	0.4	0.2
	100	0.8	0.5	0.6	0.2	0.5	0.2	0.5	0.2
Specimen 3	10	0.7	0.4	0.7	0.4	0.5	0.3	0.5	0.3
	25	0.9	0.5	0.8	0.4	0.6	0.4	0.6	0.4
	50	0.9	0.5	0.7	0.4	0.6	0.4	0.5	0.3
	100	0.7	0.2	0.7	0.3	0.6	0.4	0.5	0.4

List of Symbols

Latin letters

A	Area [m ²]
A_F	Frequency factor [-]
a	Constant combining E_a and R ($a = \frac{E_a}{R}$) [K]
B	Proportionality factor [V]
b	Constant combining E_a and R ($b = \frac{E_a}{R}$) [K]
C_{dl}	Double layer capacitance [F/m ²]
E	Potential [V]
E_a	Activation energy [J mol ⁻¹]
E_{corr}	Free corrosion potential [V]
E_{max}	Steady state potential response [V]
E_P	Polarisation potential [V]
E_{Ref1}	Potential measured versus reference electrode no. 1 [V]
E_{Ref2}	Potential measured versus reference electrode no. 2 [V]
E_{Ref3}	Potential measured versus reference electrode no. 3 [V]
E_t	Time dependent potential response [V]
E_Ω	Ohmic potential drop [V]
F	Faraday constant [96485 Coulomb/mol e ⁻]
I	Current [A]
I_{CE}	Counter-electrode current [A]
I'_{CE}	Current entering the reinforcement steel over the assumed confinement area [A]
I_{corr}	Corrosion current [A]
I_{GE}	Guard ring current [A]
I_t	Time dependent current response [A]
I_{tr}	Transitory current response [A]
i	Current density [A/m ²]
i_a	Anodic current density [A/m ²]
$i_c, i_{cathode}$	Cathodic current density [A/m ²]
i_{corr}	Corrosion current density [A/m ²]
i_{corr}^{app}	Apparent corrosion current density [A/m ²]
i_{corr}^{ref}	Reference corrosion current density [A/m ²]
i_x	Corrosion current density at temperature T_x [A/m ²]
i_y	Corrosion current density at temperature T_y [A/m ²]
i_0	Corrosion current density at E_{corr} [A/m ²]

Latin letters

k	Potential sweep rate [V/s]
k_F	Rate constant (Arrhenius equation) [-]
L_{CE}	Reinforcement length over which the I_{CE} is distributed [m]
L'_{CE}	Assumed confinement length [m]
M	Molar mass [kg mol ⁻¹]
R	Ideal gas constant [J mol ⁻¹ K ⁻¹]
R_P	Polarisation resistance [Ohm×m ²]
R_P^{app}	Apparent corrosion current density [Ohm×m ²]
R_P^{ref}	Reference polarisation resistance [Ohm×m ²]
R_Ω	Ohmic concrete resistance [Ohm]
S	Slope [V s ^{-1/2}]
T	Temperature [K]
t	Time [s]
U_{CE}	Counter-electrode voltage [V]
U_{GE}	Guard ring voltage [V]
x_1	Distance from counter-electrode [m]
x_2	Distance from counter-electrode [m]
z	Number of ionic charges [-]
z_d	Warburg diffusion element [-]

Greek letters

β_a	Anodic Tafel constant [V/dec]
β_c	Cathodic Tafel constant [V/dec]
η	Overpotential [V]
η_a	Anodic overpotential [V]
η_c	Cathodic Overpotential [V]
ρ	Specific density [kg/m ³]
ρ_c	Electrical concrete resistivity [Ohm×m]
ρ_x	Electrical concrete resistivity at Temperature T_x [Ohm×m]
ρ_y	Electrical concrete resistivity at Temperature T_y [Ohm×m]
σ	Warburg coefficient [Ohm m ² s ^{-1/2}]
τ	Time constant [s, Ohm×F]
τ_E	Time constant, potentiostatic polarisation [s, Ohm×F]
τ_I	Time constant, galvanostatic polarisation [s, Ohm×F]

Abbreviations

Ag/AgCl	Silver-silver chloride (reference electrode)
CE	Counter-electrode
CPE	Constant phase element
CSE	Copper-copper sulfate (reference electrode)
EIS	Electrochemical impedance spectrography
GE	Guard ring
LPR	Linear polarisation resistance
RH	Relative humidity
SCE	Saturated Calomel electrode (reference electrode)
SHE	Standard hydrogen electrode (reference electrode)
Std	Standard deviation
w/c	Water/cement-ratio

List of Figures

2.1	Simplified Pourbaix diagram for a Fe-H ₂ O system at 25 °C and iron molality of 10 ⁻⁶ Fe mol/kg H ₂ O (Page, 1988).	8
2.2	Schematic illustration of the basic corrosion mechanism, i.e. anodic dissolution of iron and cathodic reduction of oxygen (Sandberg, 1998).	9
2.3	Typical example of a severe general corrosion attack in uncarbonated concrete, caused by excessive amounts of chloride.	11
2.4	Simplified electrochemical corrosion process around a corrosion pit on steel in concrete (Arup, 1983).	12
2.5	Partial and sum polarisation curves of a corroding metal (Elsener, 2005).	14
2.6	Pourbaix diagrams illustrating the effect of moisture and correlated oxygen content on the steel potential (Sandberg, 1998).	14
2.7	Schematic illustration of the oxygen concentration as a function of depth below the concrete cover for concrete submerged in sea water (Fidjestol and Nielsen, 1980).	15
2.8	Polarisation curves for an electrode process. The relationship between polarisation potential, η , and current density, i , is given by the Tafel equations (Equations 2.16 and 2.17) (Page, 1988).	17
2.9	Stern diagram for active and passive polarisation curves (Sandberg, 1998).	18
2.10	Linear correlation between polarising potential and current around the free corrosion potential, E_{corr} (Bardal, 1994).	19
2.11	Linear relationship between overpotential (measured potential minus the free corrosion potential) and applied current for single electrode systems (Stern and Geary, 1957).	21
2.12	Corrosion current density as a function of the temperature for steel in carbonated concrete (Tuutti, 1982).	22
2.13	Macro-cell current as a function of the temperature for steel in mortar. The macro-cell current is given in % of the current recorded at 20 °C. Results obtained by Jäggi et al. (2001) are shown together with results reported in the literature by Schiessl and Raupach (1990), Arya and Vassie (1995), Raupach (1997b) and Liu and Weyers (1998). Reprint from (Jäggi et al., 2001).	23
2.14	Electrical concrete conductivity as a function of the relative humidity in the concrete (Tuutti, 1982).	25

2.15	Corrosion current density, i_{corr} , as a function of ohmic resistance, R_Ω for steel in mortar. The slope of the straight tendency line was found to be about -1 (Alonso et al., 1988).	26
2.16	The relationship between corrosion potential, concrete resistance and corrosion current density obtained from a polarisation resistance probe in carbonated mortar with 0.4 % chloride (Glass et al., 1991).	27
2.17	Corrosion current density as a function of the internal relative humidity (Tuutti, 1982).	27
3.1	Schematic illustration of half-cell potential measurement of steel in concrete ASTM C 876-77 (1977).	30
3.2	Effect of concrete cover thickness on the depth of potential field above a local anode (reference electrode type not given) (Elsener and Böhni, 1990).	32
3.3	Potentiostatic, galvanostatic and potentiodynamic polarisation methods illustrated by the applied input and response. After (Millard et al., 1992).	34
3.4	Simple modified Randles circuit over which a polarising potential, ΔE , is applied. ΔE_Ω represents the potential drop caused by the ohmic resistance, R_Ω , and ΔE_P the polarising potential over the double layer. C_{dl} is the double layer capacitance. After Gonzalez et al. (1985a).	35
3.5	Corrosion current density, i_{corr} , as a function of sweep rate (potentiodynamic method, \square) and delay time (potentiostatic method, \circ) for passive steel in mortar exposed to ≈ 100 % RH (Gonzalez et al., 1985a).	37
3.6	Polarisation resistance, R_P , as a function of delay time obtained with potentiostatic and galvanostatic polarisation measurements on passive and actively corroding reinforcement (Millard et al., 1992).	38
3.7	Effect of potentiodynamic sweep rate on the measured polarisation resistance, R_P , for passive and actively corroding reinforcement (Millard et al., 1992).	39
3.8	Potentiodynamic polarisation curves for stainless steel in an alkaline solution (pH 12.5) with a chloride content of 15 g/litre at various sweep rates (Kouřil et al., 2006).	40
3.9	Schematic potential sweep illustrating the difference between the applied and the polarising potential due to the ohmic resistance, R_Ω	41
3.10	Schematic illustration of the current interrupt technique. The parameters are explained in the text. After (Oelssner et al., 2006).	42
3.11	Schematic illustration of the galvanostatic pulse ohmic resistance compensation method. Parameters are explained in the text.	43
3.12	Schematic galvanostatic polarisation obtained from a simple Randles circuit. a: Potential transient as a function of the time, t . b: $\ln(E_{max} - E_t)$ as a function of time ($\Delta\eta = E_{max} - E_t$) Newton and Sykes (1988).	45
3.13	Schematic illustration of $\ln(E_{max} - E_t)$ as a function of time, t , for a system with two resistance-capacitor pairs. Note that potentials are given by V instead for E . Also, \ln is shown as \log_e . Reprint from (Law et al., 2001).	46

3.14	Equivalent circuits obtained from potential transient analysis. a) Steel in solution, b) steel in gel, c) passive steel in concrete, d) active steel in concrete (Newton and Sykes, 1988).	48
3.15	Potential transient for passive steel in mortar obtained with a galvanostatic current density of $0.022 \mu A/cm^2$. Two resistance-capacitor pairs are used to fit the recorded transient (Videm, 1997).	49
3.16	Equivalent Randles circuit modified with a Constant Phase Element (CPE). Parameters are explained in the text. After (Sagües et al., 1996).	50
3.17	Measured (circles) and modelled (solid line) potential response (without ohmic resistance, R_Ω) to a current pulse of $0.25 \mu A$ as a function of the polarisation time (Sagües et al., 1996).	50
3.18	Equivalent Randles circuit modified with a Constant Phase Element (CPE) and a Warburg diffusion element (Z_d).	51
3.19	Comparison of experimental (full line) and CPE-Warburg Randles circuit model fit (circles). Reprint from (Feliu et al., 2005).	52
3.20	Schematic illustration of the current flow from a small counter-electrode placed on the concrete surface to a reinforcement bar with uniform general corrosion.	53
3.21	Schematic illustration of the lateral current spread occurring when a small counter-electrode is used for R_P measurements on passive steel.	54
3.22	Model circuit for interpreting the lateral signal spreading. a) Transmission line model. b, c) Flow of current through an infinitesimally small element of the beam shown in d) (Andrade and Alonso, 1995).	55
3.23	Graphical extrapolation of apparent polarisation resistances, R_P^{app} , in order to determine the true polarisation resistance, R_P . Reference values (methods A-C) were obtained using the two approaches from the transmission line model and a large counter-electrode ensuring a uniform polarisation (Feliu et al., 1990a).	57
3.24	Schematic illustration of the guard ring (external CE) in the ideal case where the current lines (dashed lines) from the central counter-electrode are directed to the reinforcement directly below it (Feliu et al., 1989c).	58
3.25	Sensorised guard ring: schematic illustration of the electrode assembly with counter-electrode (central CE), guard ring (external CE), central reference electrode (RE) and sensors (S_1 and S_2). The punctuated circle with diameter D indicate the area to which the current applied from the counter-electrode is confined (Feliu et al., 1990a).	59
3.26	Variation of the corrosion current density, i_{corr} , along the continuous and discontinuous reinforcement bars, measured with a small unconfined counter-electrode (left), and the GECOR instrument using the sensorised guard ring (right) (Gonzalez et al., 1995b).	61
3.27	Schematic illustration of the current distribution between the GECOR electrode assembly and a reinforcement bar with a small corroding area (Liu and Weyers, 2003).	62

3.28	Relation between the measured and true polarisation resistance (R'_P/R_P ratio) as a function of the polarisation resistance, R_P , for measurements without confinement and with the sensorised guard ring (Wojtas, 2004a).	63
3.29	Relation between the measured and true polarisation resistance (R'_P/R_P ratio) as a function of the size of the corroding area for measurements without confinement and with the sensorised guard ring (directly over the active area) (Wojtas, 2004a).	64
3.30	Comparison between electrochemical and gravimetric weight losses (Andrade and Martinez, 2005).	65
4.1	Approach, experimental variations and methods used in the two experiments performed in the research project.	68
4.2	The GECOR 6 Corrosion Rate Meter from Geocisa, Spain (shown without connecting cables).	69
4.3	Real-time recording of a GECOR 6 measurement on passive reinforcement showing the reinforcement potential against the three reference electrodes ($E_{Ref\ 1}$ to $E_{Ref\ 3}$) and the current applied from the counter-electrode, I_{CE} , and the guard ring, I_{GE} . The default polarisation time of 100 seconds was used for the measurement.	70
4.4	The GalvaPulse instrument from FORCE Technology, Denmark.	71
4.5	Real-time recording of a GalvaPulse measurement on passive reinforcement using current confinement. A current pulse of $20\ \mu A$ and 10 second's duration was used for the measurement. The current applied from and the voltage of the counter-electrode and guard ring, I_{CE} , U_{CE} and I_{GE} , U_{GE} , respectively, are shown in the upper graph, whereas the potential of the reinforcement versus the reference electrode, E , is shown in the lower graph.	72
4.6	Geometry of the test slabs. Measurements positions (Positions 1-7) for the GECOR 6 and GalvaPulse are shown with large and smaller dashed circles, respectively. All measures are given in mm.	73
4.7	Manufacture of test slabs. a: Segmented reinforcement bars, reference electrodes, chloride sensors and lifting frames mounted in the mould (mould side removed for better view). b: All reinforcement segments are isolated with silicone rings. c: The fibreglass bar with the connecting wires and a part of the 160 mm end segment protruding from the slab. d: The three test slabs - ready for testing.	74
4.8	A wire is soldered to the inside of each segment, here with lengths of 20, 25 and 50 mm, respectively (from right). The silicone rings are placed between the segments when mounted on the fibreglass bar.	76
4.9	The laboratory potentiostat and the <i>small unconfined electrode assembly</i> consisting of a 60 mm diameter zinc counter-electrode (with a 30 mm diameter hole) with a centrally positioned Ag/AgCl reference electrode.	79

4.10	Schematic illustration of the system used for real-time monitoring of the operation of the corrosion rate instruments and current distribution. In addition to the zero-resistance ammeters and voltmeters shown with full lines, voltmeters shown with dotted lines were used with the GalvaPulse and the reference electrodes with dotted lines with the GECOR 6. Not all segments and zero-resistance ammeters used are shown.	81
4.11	Geometry of the test specimens. All measures are given in mm.	83
4.12	Production of test specimens: a, b: Side and end views of the five specimen mould (side and end wall removed). c: The mould is placed on a vibration table and the specimens cast. d: The specimens are demoulded after one day.	84
4.13	The two types of reinforcement bars prepared for the experiment. Lower: A cleaned and uncoated bar as used in Series I and II. Upper: A partly nickel coated bar as used in Series III. Only the length to the left of the vertical line was embedded in the test specimen.	86
4.14	A test specimen from each series (I-III) is placed in each climate chamber maintained at a constant temperature and relative humidity.	87
4.15	Schematical illustration of the test setup used for the potentiodynamic and galvanostatic measurements. Only two of the 45 test specimens are shown. All specimens were connected to the measurement setup as these two. . . .	88
4.16	Potentiodynamic linear polarisation resistance measurement on passive steel (Series I). Upper graph: Potential as a function of time. Lower graph: The responding current as a function of the potential. The bold line indicate the free corrosion potential, E_{corr} , and the blue and red arrows the cathodic and anodic polarisation, respectively.	90
4.17	Potentiodynamic linear polarisation resistance measurement on actively corroding steel (Series II). Upper graph: Potential as a function of time. Lower graph: The responding current as a function of the potential. The bold line indicate the free corrosion potential, E_{corr} , and the blue and red arrows the cathodic and anodic polarisation, respectively.	91
4.18	Equivalent circuits of a corroding electrode (upper) and the potential-voltage response to a triangular potential sweep (lower). Left and right figure shows the systems without and with ohmic resistance, R_Ω , respectively (shown on the figure as R_e). The polarisation resistance, R_P is equal to the slope of the parallelogram, i.e. $R_P = dE/dI$ (Gabrielli et al., 1979). . . .	93
4.19	Potential transients obtained with varying counter-electrode currents from passive steel in a concrete specimen with 0 % chloride (Series I) exposed to 15 °C and 85 % relative humidity.	94
4.20	Potential transients obtained with varying counter electrode currents from actively corroding steel (general corrosion) in a concrete specimen with 4 % chloride (Series II) exposed to 15 °C and 85 % relative humidity.	95

5.1	Macro-cell current density distribution on the upper segmented reinforcement bar in Slab II with 1.5 % chloride. The current densities of the anodic and cathodic segments, i.e. i_{corr} and $i_{cathode}$ are shown in the top and bottom diagrams, respectively.	98
5.2	Macro-cell current density distribution on the upper segmented reinforcement bar in Slab III with 4 % chloride. The current densities of the anodic and cathodic segments, i.e. i_{corr} and $i_{cathode}$ are shown in the top and bottom diagrams, respectively.	99
5.3	Macro-cell current density distribution on the lower reinforcement bar in Slab II with 1.5 % chloride. Segments 1, 3, 25 and 32 are seen to be anodic (positive current densities).	99
5.4	Macro-cell current density distribution on the lower reinforcement bar in Slab III with 4 % chloride. Segments 3, 8, 25 and 30 are seen to be anodic (positive current densities).	100
5.5	Slab I (0 % chloride): Half-cell potentials, E_{corr} , (top), apparent polarisation resistances, R_P^{app} , (middle) and ohmic resistances, R_Ω , (bottom) measured on both surfaces (30 and 75 mm cover) along the upper and lower segmented reinforcement bars at intervals of 50 mm with the small unconfined electrode assembly and the laboratory potentiostat.	102
5.6	Slab II (1.5 % chloride): Half-cell potentials, E_{corr} , (top), apparent polarisation resistances, R_P^{app} , (middle) and ohmic resistances, R_Ω (bottom) measured on both surfaces (30 and 75 mm cover) along the upper and lower segmented reinforcement bars at intervals of 50 mm with the small unconfined electrode assembly and the laboratory potentiostat. The uppermost red bold line indicates the position and size of the two central anodes on the upper segmented bar, whereas the red bold lines on the first axis indicate the positions and sizes of the anodes on the lower segmented bar.	103
5.7	Slab III (4 % chloride): Half-cell potentials, E_{corr} , (top), apparent polarisation resistances, R_P^{app} , (middle) and ohmic resistances, R_Ω (bottom) measured on both surfaces (30 and 75 mm cover) along the upper and lower segmented reinforcement bars at intervals of 50 mm with the small unconfined electrode assembly and the laboratory potentiostat. The uppermost red bold line indicates the position and size of the two central anodes on the upper segmented bar, whereas the red bold lines on the first axis indicate the positions and sizes of the anodes on the lower segmented bar.	104
5.8	Schematic illustration of the current, I'_{CE} , flowing into the reinforcement over the assumed confinement length, L'_{CE} , and the length L_{CE} over which the applied counter-electrode current, I_{CE} , is distributed. A current I_{GE} is applied from the guard ring for confining the counter-electrode current, I_{CE}	108
5.9	GECOR 6 measurements on the upper reinforcement bar in Slab I, Position 4. The bold blue line indicates the assumed confinement length on the segmented reinforcement bar.	109
5.10	GalvaPulse measurements with use of current confinement on the upper reinforcement bar in Slab I, Position 4. The bold blue line indicates the assumed confinement length on the segmented reinforcement bar.	110

5.11	GalvaPulse measurements without use of current confinement on the upper reinforcement bar in Slab I, Position 4. The bold blue line indicates the assumed confinement length on the segmented reinforcement bar.	111
5.12	GECOR 6 measurements on the lower reinforcement bar in Slab I, Position 4. The bold blue line indicates the assumed confinement length on the segmented reinforcement bar.	112
5.13	GalvaPulse measurements with use of current confinement on the lower reinforcement bar in Slab I, Position 4. The bold blue line indicates the assumed confinement length on the segmented reinforcement bar.	113
5.14	GalvaPulse measurements without use of current confinement on the lower reinforcement bar in Slab I, Position 4. The bold blue line indicates the assumed confinement length on the segmented reinforcement bar.	114
5.15	Half-cell potentials, E_{corr} , (top) and corrosion current densities, i_{corr} , (bottom) measured with the GECOR 6 and GalvaPulse instruments along the upper segmented reinforcement bar in Slab II. The position and size of the two central anodes is indicated by the red bold line on the first axis.	117
5.16	Half-cell potentials, E_{corr} , (top) and corrosion current densities, i_{corr} , (bottom) measured with the GECOR 6 and GalvaPulse instruments along the upper segmented reinforcement bar in Slab III. The position and size of the two central anodes is indicated by the red bold line on the first axis.	118
5.17	GECOR 6 measurements in Position 2 on the upper reinforcement bar in Slab II. The bold blue line indicates the assumed confinement length on the segmented reinforcement bar and the red bold line the position and size of the two central anodes.	119
5.18	GECOR 6 measurements in Position 3 on the upper reinforcement bar in Slab II. The bold blue line indicates the assumed confinement length on the segmented reinforcement bar and the red bold line the position and size of the two central anodes.	120
5.19	GECOR 6 measurements in Position 4 on the upper reinforcement bar in Slab II. The bold blue line indicates the assumed confinement length on the segmented reinforcement bar and the red bold line the position and size of the two central anodes.	121
5.20	GalvaPulse measurements with use of current confinement in Position 2 on the upper reinforcement bar in Slab II. The bold blue line indicates the assumed confinement length on the segmented reinforcement bar and the red bold line the position and size of the two central anodes.	122
5.21	GalvaPulse measurements with use of current confinement in Position 3 on the upper reinforcement bar in Slab II. The bold blue line indicates the assumed confinement length on the segmented reinforcement bar and the red bold line the position and size of the two central anodes.	123
5.22	GalvaPulse measurements with use of current confinement in Position 4 on the upper reinforcement bar in Slab II. The bold blue line indicates the assumed confinement length on the segmented reinforcement bar and the red bold line the position and size of the two central anodes.	124

5.23	GalvaPulse measurements without use of current confinement in Position 2 on the upper reinforcement bar in Slab II. The bold blue line indicates the assumed confinement length on the segmented reinforcement bar and the red bold line the position and size of the two central anodes.	125
5.24	GalvaPulse measurements without use of current confinement in Position 3 on the upper reinforcement bar in Slab II. The bold blue line indicates the assumed confinement length on the segmented reinforcement bar and the red bold line the position and size of the two central anodes.	126
5.25	GalvaPulse measurements without use of current confinement in Position 4 on the upper reinforcement bar in Slab II. The bold blue line indicates the assumed confinement length on the segmented reinforcement bar and the red bold line the position and size of the two central anodes.	127
5.26	GECOR 6 measurements in Position 2 on the upper reinforcement bar in Slab III. The bold blue line indicates the assumed confinement length on the segmented reinforcement bar and the red bold line the position and size of the two central anodes.	128
5.27	GECOR 6 measurements in Position 3 on the upper reinforcement bar in Slab III. The bold blue line indicates the assumed confinement length on the segmented reinforcement bar and the red bold line the position and size of the two central anodes.	129
5.28	GECOR 6 measurements in Position 4 on the upper reinforcement bar in Slab III. The bold blue line indicates the assumed confinement length on the segmented reinforcement bar and the red bold line the position and size of the two central anodes.	130
5.29	GalvaPulse measurements with use of current confinement in Position 2 on the upper reinforcement bar in Slab III. The bold blue line indicates the assumed confinement length on the segmented reinforcement bar and the red bold line the position and size of the two central anodes.	131
5.30	GalvaPulse measurements with use of current confinement in Position 3 on the upper reinforcement bar in Slab III. The bold blue line indicates the assumed confinement length on the segmented reinforcement bar and the red bold line the position and size of the two central anodes.	132
5.31	GalvaPulse measurements with use of current confinement in Position 4 on the upper reinforcement bar in Slab III. The bold blue line indicates the assumed confinement length on the segmented reinforcement bar and the red bold line the position and size of the two central anodes.	133
5.32	GalvaPulse measurements without use of current confinement in Position 2 on the upper reinforcement bar in Slab III. The bold blue line indicates the assumed confinement length on the segmented reinforcement bar and the red bold line the position and size of the two central anodes.	134
5.33	GalvaPulse measurements without use of current confinement in Position 3 on the upper reinforcement bar in Slab III. The bold blue line indicates the assumed confinement length on the segmented reinforcement bar and the red bold line the position and size of the two central anodes.	135

5.34	GalvaPulse measurements without use of current confinement in Position 4 on the upper reinforcement bar in Slab III. The bold blue line indicates the assumed confinement length on the segmented reinforcement bar and the red bold line the position and size of the two central anodes.	136
5.35	Half-cell potentials, E_{corr} , and corrosion current densities, i_{corr} , measured with the GECOR 6 and GalvaPulse instruments on the lower segmented reinforcement bar in Slab II. The positions and sizes of the anodes, i.e. the anodic segments, are shown with the bold red lines on the first axis.	139
5.36	Half-cell potentials, E_{corr} , and corrosion current densities, i_{corr} , measured with the GalvaPulse instrument on the lower segmented reinforcement bar in Slab III. The positions and sizes of the anodes, i.e. the anodic segments, are shown with the red bold lines on the first axis.	140
5.37	GECOR 6 measurements in Position 2 on the lower reinforcement bar in Slab II. The bold blue line indicates the assumed confinement length on the segmented reinforcement bar and the red bold lines indicate the positions and sizes of the anodes.	141
5.38	GECOR 6 measurements in Position 3 on the lower reinforcement bar in Slab II. The bold blue line indicates the assumed confinement length on the segmented reinforcement bar and the red bold lines indicate the positions and sizes of the anodes.	142
5.39	GalvaPulse measurements with use of current confinement in Position 2 on the lower reinforcement bar in Slab II. The bold blue line indicates the assumed confinement length on the segmented reinforcement bar and the red bold lines indicate the positions and sizes of the anodes.	143
5.40	GalvaPulse measurements with use of current confinement in Position 3 on the lower reinforcement bar in Slab II. The bold blue line indicates the assumed confinement length on the segmented reinforcement bar and the red bold lines indicate the positions and sizes of the anodes.	144
5.41	GalvaPulse measurements without use of current confinement in Position 2 on the lower reinforcement bar in Slab II. The bold blue line indicates the assumed confinement length on the segmented reinforcement bar and the red bold lines indicate the positions and sizes of the anodes.	145
5.42	GalvaPulse measurements without use of current confinement in Position 3 on the lower reinforcement bar in Slab II. The bold blue line indicates the assumed confinement length on the segmented reinforcement bar and the red bold lines indicate the positions and sizes of the anodes.	146
5.43	GalvaPulse measurements with use of current confinement in Position 2 on the lower reinforcement bar in Slab III. The bold blue line indicates the assumed confinement length on the segmented reinforcement bar and the red bold lines indicate the positions and sizes of the anodes.	147
5.44	GalvaPulse measurements with use of current confinement in Position 4 on the lower reinforcement bar in Slab III. The bold blue line indicates the assumed confinement length on the segmented reinforcement bar and the red bold lines indicate the positions and sizes of the anodes.	148

5.45	GalvaPulse measurements without use of current confinement in Position 2 on the lower reinforcement bar in Slab III. The bold blue line indicates the assumed confinement length on the segmented reinforcement bar and the red bold lines indicate the positions and sizes of the anodes.	149
5.46	GalvaPulse measurements without use of current confinement in Position 4 on the lower reinforcement bar in Slab III. The bold blue line indicates the assumed confinement length on the segmented reinforcement bar and the red bold lines indicate the positions and sizes of the anodes.	150
5.47	Free corrosion potentials, E_{corr} , as a function of the exposure temperature for the passive (top graph, Series I) and active generally corroding (bottom graph, Series II) reinforcement bars exposed to 75, 85 and 96 % relative humidity.	152
5.48	Polarisation resistances, R_P , as a function of the exposure temperature for the passive (top graph, Series I) and active generally corroding (bottom graph, Series II) reinforcement bars exposed to 75, 85 and 96 % relative humidity.	153
5.49	Corrosion current densities, i_{corr} , as a function of the exposure temperature for the passive (top graph, Series I) and active generally corroding (bottom graph, Series II) reinforcement bars exposed to 75, 85 and 96 % relative humidity.	154
5.50	Measured free corrosion potentials, E_{corr} , polarisation resistances, R_P , and corrosion current densities, i_{corr} , as a function of the exposure temperature for the actively corroding partly nickel coated reinforcement bars (Series III) exposed to 75, 85 and 96 % relative humidity.	156
5.51	Mean polarisation curves obtained from the passive reinforcement bars in the test specimen exposed to 25 °C and 75 % relative humidity. The error bars indicate 0.5 standard deviation.	159
5.52	Galvanostatic potential transient technique: Mean polarisation resistances, R_P , corrosion current densities, i_{corr} , and ohmic resistances, R_Ω , as a function of the polarisation time for the passive reinforcement bars exposed to 25 °C and 75 % relative humidity. The error bars indicate 0.5 standard deviation.	161
5.53	Galvanostatic linear polarisation resistance technique: Mean polarisation resistances, R_P , and corrosion current densities, i_{corr} , as a function of the polarisation time for the passive reinforcement bars exposed to 25 °C and 75 % relative humidity. The error bars indicate 0.5 standard deviation. . .	162
5.54	Specimen 1: Mean polarisation curves obtained from the active generally corroding reinforcement bars (Series II) exposed to 15 °C and 75 % relative humidity (Table 5.5).	164
5.55	Specimen 2: Mean polarisation curves obtained from the active generally corroding reinforcement bars (Series II) exposed to 25 °C and 85 % relative humidity (Table 5.5).	164
5.56	Specimen 3: Mean polarisation curves obtained from the active generally corroding reinforcement bars (Series II) exposed to 35 °C and 96 % relative humidity (Table 5.5).	165

5.57	Specimen 1: Mean relative polarisation resistances, R_P/R_P^{ref} , mean corrosion current densities, i_{corr}/i_{corr}^{ref} , and (absolute) ohmic resistances, R_Ω , calculated as a function of the polarisation time from the results obtained with the galvanostatic potential transient technique.	168
5.58	Specimen 2: Mean relative polarisation resistances, R_P/R_P^{ref} , mean corrosion current densities, i_{corr}/i_{corr}^{ref} , and (absolute) ohmic resistances, R_Ω , calculated as a function of the polarisation time from the results obtained with the galvanostatic potential transient technique.	169
5.59	Specimen 3: Mean relative polarisation resistances, R_P/R_P^{ref} , mean corrosion current densities, i_{corr}/i_{corr}^{ref} , and (absolute) ohmic resistances, R_Ω , calculated as a function of the polarisation time from the results obtained with the galvanostatic potential transient technique.	170
5.60	Specimen 1: Mean relative polarisation resistances, R_P/R_P^{ref} , and corrosion current densities, i_{corr}/i_{corr}^{ref} , calculated as a function of the polarisation time from the results obtained with the galvanostatic linear polarisation resistance technique.	172
5.61	Specimen 2: Mean relative polarisation resistances, R_P/R_P^{ref} , and corrosion current densities, i_{corr}/i_{corr}^{ref} , calculated as a function of the polarisation time from the results obtained with the galvanostatic linear polarisation resistance technique.	173
5.62	Specimen 3: Mean relative polarisation resistances, R_P/R_P^{ref} , and corrosion current densities, i_{corr}/i_{corr}^{ref} , calculated as a function of the polarisation time from the results obtained with the galvanostatic linear polarisation resistance technique.	174
6.1	The relative error R_P/R_P^{app} as a function of the counter-electrode size (Feliu et al., 1996).	179
6.2	Schematic illustration of the self-confinement occurring when a small counter-electrode is used for R_P measurements on reinforcement with actively corroding areas.	180
6.3	Relation between the measured apparent (R_P^{app}) and true polarisation resistance (R_P) of a corroding area on an otherwise passive reinforcement bar. The corroding spot was positioned centrally below the electrode assembly. Cover depth of 30 mm, Concrete resistivity of $20 \text{ k}\Omega \times \text{cm}$, R_P of the corroding spot $2.5 \text{ k}\Omega \times \text{cm}^2$, R_P of the passive area $600 \text{ k}\Omega \times \text{cm}^2$, Assumed polarisation length of 140 mm.	183
6.4	Schematic illustration of <i>self-confinement</i> when one active area exist: The current applied from the counter-electrode, I_{CE} , and the guard ring, I_{GE} , flows mainly into the reinforcement bar at the actively corroding area irrespective of the position of the electrode assembly on the concrete surface.	185
6.5	Schematic illustration of <i>self-confinement</i> in the case of several actively corroding anodes: The current applied from the counter-electrode, I_{CE} , and the guard ring, I_{GE} , flows mainly into the reinforcement bar at the actively corroding areas irrespective of the position of the electrode assembly on the concrete surface.	186

6.6	GalvaPulse polarisation curves obtained when using the GalvaPulse and the GECOR 6 electrode assemblies, respectively. A counter-electrode current, I_{CE} , of 40 μA was used for both measurements (Gepreags and Hansson, 2004).	187
6.7	Galvanostatic linear polarisation resistance technique: Mean corrosion current densities, i_{corr} , obtained with polarisation currents from 0.25 to 100 μA as a function of the polarisation time for the passive reinforcement bars exposed at 25 °C and 75 % relative humidity (from Figure 5.53). The red and blue punctuated lines indicate a corrosion current density, i_{corr} , of 0.03 and 0.006 $\mu A/cm^2$, respectively.	198
6.8	Galvanostatic potential transient technique: Mean corrosion current densities, i_{corr} , obtained with polarisation currents from 0.25 to 100 μA as a function of the polarisation time for the passive reinforcement bars exposed at 25 °C and 75 % relative humidity (from Figure 5.52). The red and blue punctuated lines indicate a corrosion current density, i_{corr} , of 0.03 and 0.006 $\mu A/cm^2$, respectively.	199
6.9	Corrosion current densities, i_{corr} , determined with the galvanostatic transient technique (curve-fitting) as a function of the polarisation duration for passive (without chloride) and actively corroding (with 3% chloride) steel in concrete (Luping, 2002).	201
6.10	Corrosion current density, i_{corr} , measured with the GalvaPulse instrument on passive reinforcement, as a function of the polarisation time, t , and the applied current, I_{CE} (Pruckner, 2002).	201
6.11	Corrosion current density, i_{corr} , measured with the GalvaPulse instrument on actively corroding reinforcement, as a function of the polarisation time, t , and the applied current, I_{CE} (Pruckner, 2002).	202
6.12	Polarisation resistance, R_P , as a function of the potential sweep rate when measured with the potentiodynamic polarisation resistance technique (left), and as a function of the polarisation time when measured with the galvanostatic linear polarisation resistance technique (right) for passive and actively corroding steel. As indicated with the red arrows comparable R_P values are obtained with a sweep rate of 10 mV per minute (left) and a polarisation time of approximately 40 seconds (right). After (Millard et al., 1992).	205
6.13	The relationship between corrosion potential and corrosion rate obtained by Glass et al. (1991) from polarisation resistance probes (mild steel) embedded in carbonated mortar containing 0.4 % chloride by mass of mortar.	208
6.14	Evans diagram showing the increase in corrosion rate from i_{corr} to i'_{corr} and the corresponding changes in the corrosion potential from E_{corr} to E'_{corr} resulting from (a) a process under anodic control and subject to decreased anodic polarisation, (b) a process under cathodic control and subject to decreased cathodic polarisation and (c) a process under resistance control and subject to a fall in resistance (Glass et al., 1991).	208
6.15	Measured rate of corrosion ($1 \mu A/cm^2 \approx 11.6 \mu m/year$) as a function of the relative humidity for carbonation and chloride initiated corrosion (Tuutti, 1982).	210

6.16	Measured rate of corrosion ($1 \mu\text{A}/\text{cm}^2 \approx 11.6 \mu\text{m}/\text{year}$) as a function of the time for different relative humidities (Tuutti, 1982).	212
6.17	Test specimen with active generally corroding reinforcement exposed at 25 °C and 85 % relative humidity for approximately 2 years. Cracks with a width of up to approximately 0.5 mm were observed on the surface together with corrosion products.	213
6.18	Test specimen with active generally corroding reinforcement exposed at 35 °C and 96 % relative humidity for approximately 2 years. The expansive corrosion products have bent the specimen due to the reinforcing properties of the mmo-titanium mesh positioned below the surface on the rear side of the specimen. The white arrow on the top figure indicates the position of the exposed bar shown in the bottom figure.	214
A.1	The packing diagram resulting from the theoretical calculation. The selected composition is indicated with the vertical dashed line.	238
A.2	Grading of the combined aggregate.	238

List of Figures

List of Tables

3.1	Selected half-cell electrodes used in practice, their potentials, given versus the Standard Hydrogen Electrode (SHE) at 25 °C and temperature coefficients (Myrdal, 2007).	30
3.2	Interpretation guidelines for half-cell potentials, E_{corr} , as stated in ASTM C 876-77 (1977).	31
3.3	Typical range of potentials of ordinary steel in concrete (Elsener et al., 2003).	31
4.1	Mix design of concretes.	75
4.2	Selected properties of the concretes used for the three slabs.	75
4.3	Composition of the carbon steel and stainless steel [mass%]. Tested in accordance with ASTM E415-99a (2005).	77
4.5	Composition of the carbon steel used as reinforcement [mass%]. Tested in accordance with ASTM E415-99a (2005). Only selected components are given.	85
4.4	Mix design of concretes.	85
4.6	Properties of the test specimens in the three series (I-III). Each series contained 15 geometrically identical test specimens - each with 10 reinforcement bars.	86
4.7	Measurement sequence and parameters used for the individual measurement steps where the same type of measurements was made on all 450 reinforcement bars.	89
5.1	Macro-cell currents, I_{corr} , and calculated current densities, i_{corr} , for the anodic segments on the upper and lower segmented reinforcement bars in Slabs II and III.	100
5.2	Slabs I to III, upper bars: Half-cell potentials, E_{corr} , polarisation resistances, R_P , and ohmic resistances, R_Ω , measured with the large counter-electrode ensuring uniform polarisation and the laboratory potentiostat.	105
5.3	Slabs I to III, lower bars: Half-cell potentials, E_{corr} , polarisation resistances, R_P , and ohmic resistances, R_Ω , measured with the large counter-electrode ensuring uniform polarisation and the laboratory potentiostat.	105

5.4	Results from measurements with the GECOR 6 and GalvaPulse with and without current confinement (conf. on and conf. off, respectively) in Position 4 on the upper and lower segmented reinforcement bars in Slab I. The numbers in brackets are the half-cell potentials measured versus the embedded MnO_2 reference electrode (mV versus MnO_2).	108
5.5	Selected tests specimens from Series II (general corrosion): Exposure conditions, and average polarisation resistances, R_P , and corrosion current densities, i_{corr} , from the potentiodynamic linear polarisation resistance measurements (Figures 5.48 and 5.49).	163
6.1	Typical corrosion rates for steel in concrete (Gowers et al., 1994) (Law et al., 2001) (So and Millard, 2007).	179
6.2	Guidelines for interpretation of corrosion current densities, i_{corr} , measured with the GalvaPulse instrument (with current confinement).	189
6.3	Guidelines for interpretation of corrosion current densities, i_{corr} measured with the GECOR 6 instrument (Andrade et al., 2004).	190
6.4	The polarisation time, t , (to the nearest 5 seconds) required to obtain a corrosion current density, i_{corr} , of $0.03 \mu\text{A}/\text{cm}^2$ with the galvanostatic linear polarisation resistance technique on the passive reinforcement bars (Figure 6.7.)	199
6.5	Mean corrosion current densities, i_{corr} , and potential shifts, ΔE , determined with the galvanostatic linear polarisation resistance technique on the passive reinforcement using a polarisation time 100 seconds.	200
6.6	The polarisation time, t , (to the nearest 5 seconds) required to obtain a corrosion current density, i_{corr} , of $0.03 \mu\text{A}/\text{cm}^2$ with the galvanostatic transient technique on the passive reinforcement bars (Figure 6.8.)	200
A.1	Cement composition.	236
A.2	Test methods used to determine the physical properties of the fine and coarse aggregates.	236
A.3	Essential properties for the aggregates used in the concrete.	237
A.4	Concrete mix design	239
B.1	Fresh and hardened properties of the three concretes used for the slabs described in Section 4.1.	242
C.1	Fresh and hardened properties of the three concrete batches used for casting the test specimens in Series I (0 % chloride, plain uncoated steel bars). . .	244
C.2	Fresh and hardened properties of the three concrete batches used for casting the test specimens in Series II (4 % chloride, plain uncoated steel bars). . .	244
C.3	Fresh and hardened properties of the three concrete batches used for casting the test specimens in Series III (4 % chloride, partly nickel coated steel bars). .	245
D.1	Measurement data from the GECOR 6 and GalvaPulse measurements on the upper segmented reinforcement bar in Slab II, see also Figure 5.15. . .	248

D.2	Measurement data from the GECOR 6 and GalvaPulse measurements on the upper segmented reinforcement bar in Slab III, see also Figure 5.16.	249
D.3	Measurement data from the GECOR 6 and GalvaPulse measurements on the lower segmented reinforcement bar in Slab II, see also Figure 5.35.	250
D.4	Measurement data from the GECOR 6 and GalvaPulse measurements on the lower segmented reinforcement bar in Slab III, see also Figure 5.36.	251
G.1	Mean relative polarisation resistances, R_P/R_P^{ref} , and standard deviations calculated from the results obtained with the galvanostatic linear polarisation resistance technique.	264
G.2	Mean relative corrosion current densities, i_{corr}/i_{corr}^{ref} , and standard deviations calculated from the results obtained with the galvanostatic linear polarisation resistance technique.	264
G.3	Mean relative polarisation resistances, R_P/R_P^{ref} , and standard deviations calculated from the results obtained with the galvanostatic potential transient technique.	265
G.4	Mean relative corrosion current densities, i_{corr}/i_{corr}^{ref} , and standard deviations calculated from the results obtained with the galvanostatic potential transient technique.	265

Condition assessment of reinforced concrete structures is facilitated by non-destructive techniques. Over the last decade the trend in corrosion monitoring has moved from half-cell potential mapping towards non-destructive corrosion rate measurements. However, the measured corrosion rate depends on the instrument as well as the measuring procedure, and furthermore corroding areas on the reinforcement cannot be accurately located.

In the first part of the thesis the confinement and electrochemical techniques used in the commercial instruments for on-site corrosion rate measurements are investigated and the variations in measured corrosion rates are explained. The second part of the thesis presents a study on the long-term combined effect of temperature and relative humidity on the corrosion rate of steel in concrete.

DTU Civil Engineering
Department of Civil Engineering
Technical University of Denmark

Brovej, Building 118
2800 Kgs. Lyngby
Telephone 45 25 17 00

www.byg.dtu.dk